



National Library  
of Canada

Bibliothèque nationale  
du Canada

CANADIAN THESES  
ON MICROFICHE

THÈSES CANADIENNES  
SUR MICROFICHE

0-315-09162-2

104

57079

MITROVIC

NAME OF AUTHOR/NOM DE L'AUTEUR Vesna Scepanovic

TITLE OF THESIS/TITRE DE LA THÈSE "Anodic Films on Single-Phase Ni-Mo Alloys in  
Acid Solution"

UNIVERSITY/UNIVERSITÉ McMaster

DEGREE FOR WHICH THESIS WAS PRESENTED/  
GRADE POUR LEQUEL CETTE THÈSE FUT PRÉSENTÉE Ph.D.

YEAR THIS DEGREE CONFERRED/ANNÉE D'OBTENTION DE CE DEGRÉ 1982

NAME OF SUPERVISOR/NOM DU DIRECTEUR DE THÈSE Dr. M.B. Ives

Permission is hereby granted to the NATIONAL LIBRARY OF CANADA to microfilm this thesis and to lend or sell copies of the film. *L'autorisation est, par la présente, accordée à la BIBLIOTHÈQUE NATIONALE DU CANADA de microfilmer cette thèse et de prêter ou de vendre des exemplaires du film.*

The author reserves other publication rights, and neither the thesis nor extensive extracts from it may be printed or otherwise reproduced without the author's written permission. *L'auteur se réserve les autres droits de publication; ni la thèse ni de longs extraits de celle-ci ne doivent être imprimés ou autrement reproduits sans l'autorisation écrite de l'auteur.*

DATED/DATÉ September 3, 1982. SIGNED/SIGNÉ V. Scepanovic

PERMANENT ADDRESS/RÉSIDENCE FIXE NATIONAL RESEARCH COUNCIL  
(CHEM. DIVISION) MONTREAL RD  
OTTAWA, ONT

ANODIC FILMS ON SINGLE PHASE Ni-MO  
ALLOYS IN ACID SOLUTION

By



VESNA MITROVIC-SCEPANOVIC, Dipl.Eng.Tech., M.Eng.

A Thesis

Submitted to the School of Graduate Studies  
in Partial Fulfilment of the Requirements  
for the Degree  
Doctor of Philosophy

McMaster University

June 1982

ANODIC FILMS ON Ni-Mo ALLOYS

DOCTOR OF PHILOSOPHY (1982)  
(Metallurgy and Materials Science)

MCMASTER UNIVERSITY

TITLE: Anodic Films on Single Phase Ni-Mo Alloys in Acid  
Solution

AUTHOR: Vesna Mitrovic-Scepanovic, Dipl. Eng. Techn., Belgrade  
M.Eng., McMaster

SUPERVISOR: Professor M.B. Ives

NUMBER OF PAGES: xvi, 192

## ABSTRACT

The anodic oxide films of single phase Ni-Mo alloys (5 - 15 wt % Mo) formed in 0.15 N  $\text{Na}_2\text{SO}_4$  (pH 2.8) have been investigated using electrochemical techniques, atomic absorption spectroscopy, Auger electron spectroscopy and X-ray photoelectron spectroscopy. The anodic oxide film of Ni formed under the same condition has been used as a reference in order to study the effect of molybdenum addition on the nature of the passive film of nickel.

The electrochemical studies have indicated a negative effect of molybdenum addition to stability of the passive film and a different mechanism of the film growth on the alloys with respect to that on nickel.

Dissolution of nickel and molybdenum during the film formation has been found to proceed in proportions other than their ratio in the alloy and which was also time dependent. Selective dissolution of molybdenum has been found during the initial stages of anodization and its enrichment in the film at longer anodization times. Chronoamperometric measurements combined with dissolution analysis suggested an increase of the film thicknesses with anodization time.

Auger electron spectroscopy with ion sputtering confirmed the anodization time dependence of the film thickness

and an enrichment of the film-solution interface in molybdenum. The thickness of the passive film of nickel has not been found to change significantly with anodization time.

Characterization of nickel and molybdenum species in the film has been based on the findings of X-ray photoelectron spectroscopy, which combined with the evidence offered by structure analysis (RHEED), suggested the passive film to be a two-phase oxide film containing defective or hydrated NiO and probably amorphous  $\text{MoO}_3$ . A model which explains the growth of two-phase oxide coverage on Ni-Mo alloys has been proposed.

## ACKNOWLEDGEMENTS

My sincere thanks to Professor Brian Ives for his guidance, constant encouragement and patient counsel in the course of this project.

Gratitude is also expressed to the members of my supervisory committee, Professor W.W. Smeltzer and Professor O.E. Hileman.

I am grateful to Dr. M.J. Graham of the National Research Council of Canada for providing the surface analysis and to Mr. G.I. Sproule for carrying out the measurements.

I have benefited from the discussions with Dr. B. MacDougall and Dr. D. Mitchell of the National Research Council of Canada and Dr. M. Moriya of Hokkaido University.

I owe many thanks to the technical staff of both the Department of Metallurgy and Materials Science and the Institute of Materials Research, in particular to Mr. D.S. Hodgson, Mr. J.D. Garret and Mr. J. Hudak.

I would like to thank Miss Estelle Vincent for typing the manuscript.

Finally I gratefully acknowledge the financial support from McMaster University in the form of a graduate assistantship and from the National Research Council in the form of research grants to Dr. Ives.

## TABLE OF CONTENTS

CHAPTER I	INTRODUCTION	<u>PAGE</u>
1.1	PASSIVITY OF METALS AND ALLOYS	1
1.2	PASSIVITY OF NICKEL	10
1.3	PASSIVITY OF MOLYBDENUM	14
1.4	EFFECT OF Mo AS AN ALLOYING ELEMENT ON THE PROPERTIES OF PASSIVE FILMS	20
1.5	STATEMENT OF THE PROBLEM	26
CHAPTER II	EXPERIMENTAL TECHNIQUES	
2.1	MATERIALS AND SPECIMEN PREPARATION	27
2.2	ELECTROLYTIC SOLUTION	35
2.3	DESCRIPTION OF APPARATUS FOR ELECTROCHEMICAL MEASUREMENTS	36
2.4	ELECTROCHEMICAL TECHNIQUES	40
2.4.1	POTENTIOSTATIC POLARIZATION	40
2.4.2	OPEN CIRCUIT POTENTIAL DECAY, GALVANOSTATIC CHARGING AND SURFACE REACTIVITY MEASUREMENTS	40
2.5	SURFACE ANALYSIS	42



	<u>PAGE</u>
2.5.1 AUGER ELECTRON SPECTROSCOPY AND ION SPUTTERING	42
2.5.2 X-RAY PHOTOELECTRON SPECTROSCOPY	45
2.6 DISSOLUTION MEASUREMENTS BY ATOMIC ABSORPTION SPECTROSCOPY (AAS)	46

### CHAPTER III

### RESULTS AND DISCUSSION

3.1.1 POLARIZATION CHARACTERISTICS OF Ni AND Mo	50
3.1.2 ANODIC POTENTIOSTATIC POLARIZATION OF Ni-Mo ALLOYS	53
3.1.3 POTENTIOSTATIC FILM FORMATION	58
3.2 OPEN CIRCUIT DECAY AND SURFACE MEASUREMENTS	63
3.2.1 OPEN CIRCUIT POTENTIAL DECAY OF PASSIVE Ni	65
3.2.2 OPEN CIRCUIT POTENTIAL DECAY OF Ni-Mo ALLOYS	71
3.3 CATHODIC REDUCTION OF ANODIZED Ni-Mo ALLOY	76
3.3.1 CATHODIC REDUCTION OF Ni-13Mo ALLOY	77

	<u>PAGE</u>
3.4 DISSOLUTION DURING ANODIC POLARIZATION AT A FIXED POTENTIAL IN THE PASSIVE REGION	79
3.5 AUGER ELECTRON SPECTROSCOPY AND DEPTH PROFILING	86
3.5.1 AES ANALYSIS OF THE PASSIVE FILM ON Ni	87
3.5.2 AES ANALYSIS OF THE FILMS ON Ni-13Mo ALLOY	94
3.5.2.1 THE EFFECT OF SAMPLE PREPARATION ON THE COMPOSITION OF THE SURFACE OF Ni-13Mo	95
3.5.2.2 FILM THICKNESS AS A FUNCTION OF ANODIZATION TIME	100
3.5.2.3 ANODIC FILM CHARACTERIZATION AFTER OPEN CIRCUIT POTENTIAL DECAY (OCPD) OF ANODIZED Ni-13Mo	108
3.5.2.4 SURFACE COMPOSITION OF Ni-13Mo POLARIZED IN THE ACTIVE REGION	112
3.5.2.5 THE EFFECT OF SOLUTION pH ON THE COMPOSITION AND THICKNESS OF ANODIZED Ni-13Mo	115
3.5.3 QUANTITATIVE ASPECTS OF AES ANALYSIS OF Ni-Mo ALLOYS	120

	<u>PAGE</u>
3.5.4 X-RAY PHOTOELECTRON SPECTROSCOPY (XPS) OF ANODIZED Ni-13Mo	130
3.5.4.1 Ni(2p) ELECTRON SPECTRUM OF Ni-13Mo	131
3.5.4.2 Mo(3d) ELECTRON SPECTRUM OF Ni-13Mo	142
3.5.4.3 O(1s) ELECTRON SPECTRUM OF Ni-13Mo	155
3.5.4.4 REFLECTION HIGH ENERGY ELECTRON DIFFRACTION (RHEED) OF ANODIZED Ni-13Mo	169
CHAPTER IV SUMMARY AND CONCLUSIONS	173
REFERENCES	181

## FIGURE CAPTIONS

<u>FIG</u>		<u>PAGE</u>
2-1	Ni-Mo CONSTITUTIONAL DIAGRAM	28
2-2	MICROSTRUCTURE OF Ni-13Mo (HOT ROLLED)	34
2-3	THE ELECTROCHEMICAL CELL	37
2-4	THE ELECTROCHEMICAL SETUP	38
2-5	THE ELECTRICAL CIRCUIT	39
3-1	POTENTIOSTATIC POLARIZATION OF Ni	51
3-2	POTENTIOSTATIC POLARIZATION OF Mo	52
3-3	POTENTIOSTATIC POLARIZATION OF Ni AND Ni-Mo ALLOYS (1%, 3%, 5% Mo)	55
3-4	POTENTIOSTATIC POLARIZATION OF Ni, Mo AND Ni-Mo ALLOYS (5%, 10%, 15%, 22% Mo)	56
3-5	ANODIC CURRENT TRANSIENTS AT +300 AND +500 mv (Ni)	60
3-6	ANODIC CURRENT TRANSIENTS AT +300, +500, +700 mV (Ni-10Mo)	61
3-7	OPEN CIRCUIT DECAY OF POTENTIAL AS A FUNCTION OF ANODIZATION TIME (Ni)	67
3-8	OPEN CIRCUIT DECAY OF POTENTIAL AS A FUNCTION OF ANODIZATION POTENTIAL (Ni)	68
3-9	OPEN CIRCUIT DECAY OF POTENTIAL AS A FUNCTION OF Mo CONTENT (5%, 10%, 15% Mo)	74

<u>FIG.</u>		<u>PAGE</u>
3-10	OPEN CIRCUIT DECAY PROFILE AND CHANGE OF SURFACE REACTIVITY FOR Ni AND Ni-10Mo ALLOY	75
3-11	GALVANOSTATIC CATHODIC CHARGING OF ANODIZED Ni-13Mo	78
3-12	DISSOLUTION RATE OF Ni and Mo AS A FUNCTION OF ANODIZATION TIME (Ni-13Mo)	81
3-13	SELECTIVITY COEFFICIENT OF Mo AS A FUNCTION OF ANODIZATION TIME (Ni-13Mo)	82
3-14	CALCULATED AND MEASURED DISSOLVED AMOUNTS OF Ni and Mo AS A FUNCTION OF ANODIZATION TIME	83
3-15	AES SPECTRUM OF PASSIVE FILM ON Ni	90
3-16	AES PROFILE OF PASSIVE FILM ON Ni(500 mV, 4h.)	91
3-17	AES PROFILE OF PASSIVE FILM ON Ni(500 mV, 48 h.)	92
3-18	AES PROFILE OF PASSIVE FILM ON Ni(500 mV, 48 h., C-LINE REMOVED)	93
3-19	AES PROFILE OF Ni-13Mo FOLLOWING ELECTRO-POLISHING	97
3-20	AES PROFILE OF Ni-13Mo FOLLOWING ELECTRO-POLISHING AND CATHODIC REDUCTION	98
3-21	AES PROFILE OF Ni-13Mo FOLLOWING CATHODIC REDUCTION	99

<u>FIG.</u>		<u>PAGE</u>
3-22	AES PROFILE OF Ni-13Mo FOLLOWING ANODIZATION (+500 mV, 1 h.)	101
3-23	AES PROFILE OF Ni-13Mo FOLLOWING ANODIZATION (+500 mV, 2 h.)	102
3-24	AES PROFILE OF Ni-13Mo FOLLOWING ANODIZATION (+500 mV, 4 h.)	103
3-25	AES PROFILE OF Ni-13Mo FOLLOWING ANODIZATION (+500 mV, 48 h.)	104
3-26	RELATIVE CHANGE OF FILM THICKNESS WITH ANODIZATION TIME (Ni, Ni-13Mo)	105
3-27	AES PROFILE OF Ni-13Mo FOLLOWING ANODIZATION (2 h.)	109
3-28	AES PROFILE OF Ni-13Mo FOLLOWING ANODIZATION (2 h.) AND OCPD (3 min)	110
3-29	AES PROFILE OF Ni-13Mo FOLLOWING ANODIZATION (2 h.) and OCPD (30 min)	111
3-30	AES SPECTRUM OF Ni-13Mo FOLLOWING POLARIZATION IN THE ACTIVE REGION (30 min)	113
3-31	AES PROFILE OF Ni-13Mo FOLLOWING POLARIZATION IN THE ACTIVE REGION (30 min)	114
3-32	AES PROFILE OF Ni-13Mo FOLLOWING ANODIZATION (pH 10.2)	117

FIG.PAGE

3-33	AES PROFILE OF Ni-13Mo FOLLOWING ANODIZATION (pH 2.8)	118
3-34	AES PROFILE OF Ni-13Mo FOLLOWING ANODIZATION (pH 1.5)	119
3-35	AES PROFILE OF Ni-13Mo (91.6 at% Ni, 8.4 at% Mo) FOLLOWING ANODIZATION	122
3-36	VARIATION OF Mo AUGER MNN SPECTRA WITH SPUTTERING TIME (1 KeV Xe <sup>+</sup> ), (AIR FORMED FILM ON Mo)	123
3-37	VARIATION OF Mo AUGER MNN SPECTRA WITH SPUTTERING TIME (1 KeV Xe <sup>+</sup> ), (ANODIZED Ni-13Mo)	124
3-38	VARIATION OF Mo IMM AUGER SPECTRA WITH SPUTTERING TIME (1 KeV Xe <sup>+</sup> ), (AIR FORMED FILM ON Mo)	125
3-39	AES PROFILE ON THE AIR FORMED FILM ON Mo. CONCENTRATION CHANGE OF Mo AS A FUNCTION OF THE TYPE OF AUGER TRANSITION CONSIDERED	126
3-40	AES SPECTRUM OF OXYGEN AFTER 2.3 min OF SPUTTERING (1 KeV Xe <sup>+</sup> )	127
3-41	AES SPECTRUM OF OXYGEN AFTER ~ 10 min OF SPUTTERING (1 KeV Xe <sup>+</sup> )	128

<u>FIG.</u>		<u>PAGE</u>
3-42	VARIATION OF Ni(848 eV) AUGER SPECTRUM WITH TIME OF ELECTRON BEAM IRRADIATION (5 KeV)	129
3-43	Ni(2p) ELECTRON SPECTRUM OF Ni-13Mo FOLLOWING MECHANICAL POLISHING AND ELECTROPOLISHING	132
3-44	Ni(2p) ELECTRON SPECTRUM OF Ni-13Mo FOLLOWING ELECTROPOLISHING AND CATHODIC REDUCTION	133
3-45	Ni(2p) ELECTRON SPECTRUM OF Ni-13Mo FOLLOWING MECHANICAL POLISHING AND CATHODIC REDUCTION	134
3-46	Ni(2p) ELECTRON SPECTRUM OF Ni-13Mo FOLLOWING POLARIZATION IN THE ACTIVE POTENTIAL RANGE	135
3-47	Ni(2p) ELECTRON SPECTRUM OF Ni-13Mo FOLLOWING ANODIZATION (+500 mV, 2 h., pH 2.8)	136
3-48	Ni(2p) ELECTRON SPECTRUM OF Ni-13Mo FOLLOWING ANODIZATION (2 h.) and OCPD (3 min)	137
3-49	Ni(2p) ELECTRON SPECTRUM OF Ni-13Mo FOLLOWING ANODIZATION (2 h.) and OCPD (30 min)	138
3-50	Ni(2p) ELECTRON SPECTRUM OF Ni-13Mo FOLLOWING ANODIZATION (pH 10.2)	139
3-51	Ni(2p) ELECTRON SPECTRUM OF Ni-13Mo FOLLOWING ANODIZATION (pH 1.5)	
3-52	Mo(3d) ELECTRON SPECTRUM OF Ni-13Mo FOLLOWING MECHANICAL POLISHING AND ELECTROPOLISHING	144



<u>FIG.</u>		<u>PAGE</u>
3-53	Mo(3d) ELECTRON SPECTRUM OF Ni-13Mo FOLLOWING ELECTROPOLISHING AND CATHODIC REDUCTION	145
3-54	Mo(3d) ELECTRON SPECTRUM OF Ni-13Mo FOLLOWING MECHANICAL POLISHING AND CATHODIC REDUCTION	146
3-55	Mo(3d) ELECTRON SPECTRUM OF Ni-13Mo FOLLOWING POLARIZATION IN THE ACTIVE RANGE (30 min)	147
3-56	Mo(3d) ELECTRON SPECTRUM OF Ni-13Mo FOLLOWING ANODIZATION (+500 mV, 2 h., pH 2.8)	148
3-57	Mo(3d) ELECTRON SPECTRUM OF Ni-13Mo FOLLOWING ANODIZATION (2 h.) and OCPD (3 min)	149
3-58	Mo(3d) ELECTRON SPECTRUM OF Ni-13Mo FOLLOWING ANODIZATION (2 h.) and OCPD (30 min)	150
3-59	Mo(3d) ELECTRON SPECTRUM OF Ni-13Mo FOLLOWING ANODIZATION (pH 10.2)	151
3-60	Mo(3d) ELECTRON SPECTRUM OF Ni-13Mo FOLLOWING ANODIZATION (pH 1.5)	152
3-61	Mo(3d) SPECTRUM OF AIR FORMED FILM ON Mo	153
3-62	DECONVOLUTED Mo(3d) PEAK FOR ANODIZED Ni-13Mo	154
3-63	O(1s) ELECTRON SPECTRUM OF Ni-13Mo FOLLOWING MECHANICAL POLISHING AND ELECTROPOLISHING	157
3-64	O(1s) ELECTRON SPECTRUM OF Ni-13Mo FOLLOWING ELECTROPOLISHING AND CATHODIC REDUCTION	158

<u>FIG.</u>		<u>PAGE</u>
3-65	O(1s) ELECTRON SPECTRUM OF Ni-13Mo FOLLOWING MECHANICAL POLISHING AND CATHODIC REDUCTION	159
3-66	O(1s) ELECTRON SPECTRUM OF Ni-13Mo FOLLOWING POLARIZATION IN THE ACTIVE POTENTIAL RANGE	160
3-67	O(1s) ELECTRON SPECTRUM OF Ni-13Mo FOLLOWING ANODIZATION (+500 mV, 2 h., pH 2.8)	161
3-68	O(1s) ELECTRON SPECTRUM OF Ni-13Mo FOLLOWING ANODIZATION (2 h.) and OCPD (3 min)	162
3-69	O(1s) ELECTRON SPECTRUM OF Ni-13Mo FOLLOWING ANODIZATION (2 h.) and OCPD (30 min)	163
3-70	O(1s) ELECTRON SPECTRUM OF Ni-13Mo FOLLOWING ANODIZATION (pH 10.2)	164
3-71	O(1s) ELECTRON SPECTRUM OF Ni-13Mo FOLLOWING ANODIZATION (pH 1.5)	165
3-72	O(1s) ELECTRON SPECTRUM OF AIR FORMED FILM ON Mo	166
3-73	DECONVOLUTION OF O(1s) PEAK FOR ANODIZED Ni-13Mo	168
3-74	REFLECTION HIGH ENERGY ELECTRON DIFFRACTION PATTERN OF ANODIZED Ni-13Mo	172
4-1	SCHEMATIC ILLUSTRATION OF A TWO PHASE ANODIC OXIDE FILM ON SINGLE PHASE Ni-Mo ALLOYS IN ACID SOLUTIONS	178

## CHAPTER 1

### INTRODUCTION

#### 1.1 PASSIVITY OF METALS AND ALLOYS

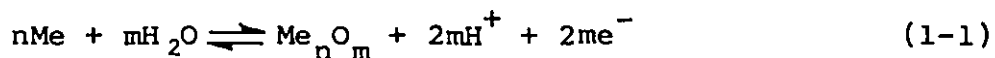
Some of the most important and interesting methods for upgrading the corrosion resistance of metals and alloys deal with the phenomenon of passivity. From a technological point of view an understanding of the mechanism of passivity is essential because the breakdown of passivity is the principal reason for corrosion failures. An enormous number of papers relating to various aspects of passivity have been published. Such widespread interest is provoked not only by the practical importance but also by the complexity of the phenomena.

Since the rate of any thermodynamically probable electrochemical corrosion process depends on the degree of thermodynamic instability and cathodic and anodic polarization as the principal resistive factors, it seems most logical to define passivity on the basis of these controlling factors. Numerous examples of passivity show that in all cases of improved corrosion resistance there is a sharp increase in inhibition of the anodic process. Therefore passivity can be defined [1] as a state of improved corrosion resistance (under conditions where, from a thermodynamic point of view, the metal or the alloy is active) accounted for by inhibition of the anodic process of metal dissolution.

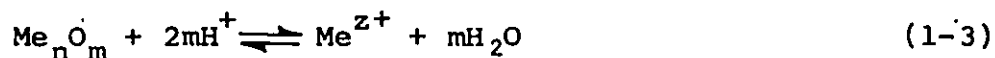
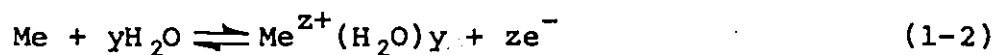
The phenomenon of passivity is associated with a decrease of the rate of anodic dissolution to very low values

with increasing oxidizing conditions of the electrolyte. This is generally due to the formation of oxide films by anodic reactions in aqueous electrolytes. The formation of a passive film is governed by the potential and pH conditions in the case of a stable surface oxide layer, and by the relative reaction rates when the oxide film is metastable [2].

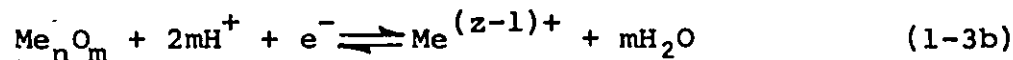
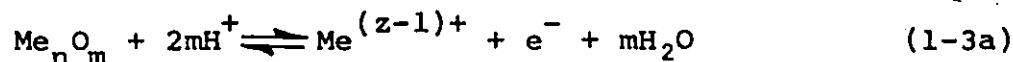
For most metals the formation of an anodic oxide film is possible in aqueous solutions according to the reaction



In concurrence with (1-1), the anodic dissolution of the metal, (1-2), and chemical dissolution of the oxide, (1-3), take place



Under certain conditions, oxidative, (1-3a), or reductive, (1-3b) dissolution of the oxide should be taken into account as well:



From a phenomenological standpoint, the equilibrium potential-pH

diagram [3] shows the range of pH values and potentials (with reference to the standard hydrogen potential) where the reactants participating in reactions (1-1), (1-2) and (1-3) are the most stable ones. However, the formation of metastable oxide phases is possible in certain ranges of pH and potential, even if they are less stable than the metal ions, if the rate of oxide growth according to (1-1) exceeds the rate of dissolution by (1-3), (1-3a) or (1-3b). The rate of oxide dissolution depends on the pH value of the electrolyte and on the potential difference at the interface [4]. The potential at which the rate of dissolution drops because the reaction (1-2) is blocked by the anodic oxide film is called passivation potential. The well known N-shaped current density-potential curve (e.g. fig. 3-1) is indicative of passivation of a metal. Hoar [5] pointed out that the behaviour of an anode above the passivation potential depends largely on the electrical, mechanical and chemical properties of the film. If it is a good electronic conductor and if the anode potential is allowed to rise, so that anodic oxidation of electrolyte (e.g.  $\text{OH}^-$  or  $\text{H}_2\text{O}$  to  $\text{O}_2$ ) at the film/solution interface becomes possible, this process may account for practically all the charge passing; little further change of metal takes place and the metal is anodically passivated. If the film is a very poor electronic conductor, passage of charge across it can take place only by ion movement from the metal/film or the film/solution interface. In this case more metal is converted into oxide, i.e., anodic

oxidation or film growth occurs, and the metal cannot be said to be passive. When the film is not mechanically stable it becomes disrupted during growth and further growth is stimulated at points where solution enters the defects in the film. If the film substance is not the only thermodynamically possible product it may be dissolved by the electrolyte and become porous, and thus more easily thickened. Combinations of the above phenomena are often observed.

The oxide film theory in the modern form, due primarily to Evans [6], has been challenged by proponents of the theories of change of the metallic surface involving not film formation but electronic modifications [7-12] or adsorption of ions or molecules [13-18]. Many passivity theories that have been presented in the literature fall into the categories of adsorption theory and three-dimensional oxide theory. Relatively recently, Sato [19] presented a generalized theory in which the passivity of transition metals is attributed to a thin oxide film which in the initial stages of formation might involve adsorption of oxygen or  $\text{OH}^-$  ions.

Within the framework of the general theory, which is rather phenomenological, there are three mechanisms that have been proposed:

- (i) electron configuration induced adsorption passivity [20-21]
- (ii) ionic space charge induced passivity [22-23]
- (iii) ion selective fixed charge induced passivity [24]

The first one, proposed by Uhlig, stated the importance of chemisorption of oxygen in the occurrence of passivity of metals and alloys. The adsorbed oxygen film is favoured by the transition metals with uncoupled d-electrons with which adsorbed oxygen interacts. In the case of alloys, the more passive component is the electron acceptor and the other component is a donor. The critical composition of a binary alloy corresponds to a percent of acceptor at which the number of available uncoupled electrons in it is equal to the number of available electrons in the donor.

The second theory proposes the space charge induced passivity model according to which the ionic current in the barrier layer can be greatly reduced by the ionic space charge within the layer, as compared to the corresponding rate expected in the absence of the space charge. This approach is based on field assisted ionic conduction.

The first model does not consider the kinetic stability of a passive film and the second one is not concerned with dissolution rate of the barrier layer which eventually determines the dissolution rate of the passive metal.

Sakashita and Sato [25] have proposed that the ion selectivity due to the fixed charge in hydrated oxide membranes on metals plays an important role in producing passivity. In this model a bipolar film consisting of an anion selective layer on the metal side and a cation selective layer on the solution

side might retard the ionic current in the anodic direction. The role of hydrated metal oxide membranes could provide the explanation for the effect of various electrolytes on passivity.

According to Sato [25] the passive films on metals may be classified into the five types:

- the adsorption film
- the barrier film of a three-dimensional oxide
- the film consisting of a barrier layer covering less protective layer
- the film composed of a barrier layer covered with a hydrated deposit layer
- the film with a barrier layer with a porous layer of the composition on top of it.

The adsorbed film consists of a monoatomic or multi-molecular layer of oxygen or other species. Frankenthal [27] reported  $10^6 - 10^7$  C/cm field slightly above the passivation potential of Fe-26 Cr alloy due to an adsorbed layer of oxygen or oxyhydroxide ("primary" film  $0.35 \text{ mC/cm}^2$  thick, reduces uniformly and completely).

The three dimensional oxide film generally has the steady state thickness which is a linear function of potential if the passive current is independent of potential. (This is not the case if the passive current is potential dependent [29].) A typical example of a barrier type passive film is that on Fe [28]. This type of film sustains  $\sim 10^6 - 10^7$  V/cm. However, it



is often difficult to draw a line between an adsorbed film and a thin three-dimensional barrier film.


The passive films on Co [30] and Cu [31] in neutral solutions are examples of a barrier film formed on a less protective layer: the barrier  $\text{Co}_3\text{O}_4$  film is formed on an inner layer of CoO and similarly for copper, of CuO on  $\text{Cu}_2\text{O}$ .

The passive film on Fe in neutral solutions is composed of a barrier oxide film covered with a hydrated deposit layer [32]. A similar type of passive film was found on Ti in acid solutions [33].

The anodic oxide films on Al are typical examples of passive films consisting of a compact layer in contact with the metal and a porous layer of the same composition in contact with the electrolyte.

The composition of barrier films often changes with the potential. Changes in the film composition induce changes in the electronic band structure of the films. According to some reports [34] the passive film on Ni is  $\text{Ni}_{1-x}\text{O}$  (p-type semiconductor). Its composition changes over a wide range of potentials and its passive dissolution current increases continuously with potential.

For alloys, the degree of enrichment or depletion of the film is generally a function of potential [35]. In some cases an enrichment or depletion of some components is found in the substrate layer [36].



The presence of water in the passive films has been reported for some metals and alloys [37-42]. Since the presence of water affects the structure of the film and consequently influences its physical and chemical properties, its role should not be ignored. Okamoto [40] suggested the necessity for the presence of water in the passive film. However, experimentally it is difficult to distinguish between the incorporated, adsorbed and water of hydration of metal compounds in the passive film.

The mechanism of electronic conductivity in the passive layers has a great influence on their corrosion resistance, e.g., high electronic conductivity favours the anodic oxidation of anions in the solution instead of metal dissolution. Generally, for most metals the passive film is a poor electronic conductor with properties ranging from those of a semiconductor to those of an insulator. Redox reactions (e.g. oxygen evolution) can occur if the film is sufficiently thin [43]. On the other hand, for metals to dissolve, the transport of cations or anions through the oxide layer is necessary. The ionic current in a passive film follows either the field-assisted ionic conduction [44] or the place-exchange mechanism [45], probably depending on the film thickness. Experimentally, it is difficult to differentiate between these two mechanisms. An alternative model, the validity of which has been demonstrated by use of experimental data for Fe, has been recently proposed [46].

When a metal enters the passive state, where the

dissolution of metal is inhibited by the presence of a surface film, the maintenance of such a passive state depends upon the electrical characteristics of the film and the stability of the film to the environment. In the steady state, the ionic current through the film is equal to the film dissolution current across the double layer at the film/solution interface. The rate of film dissolution is controlled by the double layer potential difference. Vetter [47] assumed that potential difference to be determined by the oxygen reaction at the film/solution interface in the steady state. An alternative approach has been made by Sato [19] where the double layer potential difference is related to the electric field in the film in the absence of surface charge at the interface. It has been pointed out that dissolution rates of a passive film under non-steady state and steady state conditions are not equal [28,48,49], but whatever the mechanism is in each case, the dissolution rate is always a function of the potential difference in the double layer.

Although passivity is quite a general phenomenon, not being restricted to a specific metal or alloy or to a specific passivating solution, it is possible to conclude that a general framework of passivity has been established. The problems of fundamental and practical interest that have been proposed for further study [25] are the mechanism of dissolution of passive metals and alloys, the role of anions in growth and dissolution of passive layers, the effect of alloying elements on the

composition and properties of the passive films and the effect of various environments on the stability of passive films on metals and alloys.

## 1.2 PASSIVITY OF NICKEL

The electrochemical behaviour of Ni has been the subject of intensive investigation in a variety of electrolytes. Models for the passive film and the experimental data on which the models are based have often contradicted each other, mostly due to differences in experimental techniques and often due to different interpretations.

Well established experimental results exist for the steady state polarization curve of Ni in different electrolytes. The anodic polarization of Ni shows typical current density - potential profile with the active, passive and transpassive regions. The oxide film is believed to inhibit Ni-dissolution by forming a physical barrier between the metal and solution [50-53].

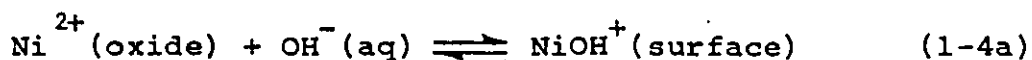
In acid solutions the current density drops until a minimum is reached and increases again towards oxygen evolution region, i.e., Ni does not show a potential region with constant current density [50,54,55]. Wagner [56] explains the potential dependent dissolution of Ni in the passive state with the low density of electronic defects in NiO which, therefore, behaves like a dielectric. The potential gradient in the oxide is caused by the

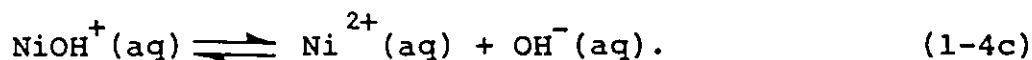
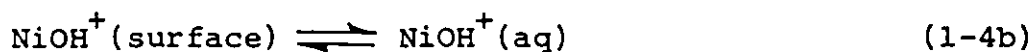
surface charge, not by the space charge, which leads to the potential dependent dissolution current.

Dissolution of passive Ni yields  $\text{Ni}^{2+}$  ions up to the potential region where oxygen starts to be evolved simultaneously [57] although some authors [58] propose that  $\text{Ni}^{3+}$  goes into solution in the oxygen evolution potential region. It was found that the dissolution rate in the passive region is pH dependent [54, 58-62, 89, 90]. The pH dependence of passive Ni dissolution as given by Vetter [54] is similar to that found by others [58, 89, 90]. Within a certain potential range the dissolution current density seems to be independent of pH because the change of oxide composition with potential and the change of potential difference at the oxide/electrolyte interface, due to the pH of electrolyte, compensate each other.

The change of dissolution current density with the potential is related to a corresponding change in the degree of oxidation. Sato and Okamoto [58-62] found the dissolution current density in the passive region to be independent of potential and dependent on pH in the acid solutions, with no effect of  $\text{Ni}^{2+}$  and  $\text{SO}_4^{2-}$  ion concentration.

The formation and dissolution of the passive film proceed simultaneously and the rates of those reactions at steady state are exactly the same so as to keep the film thickness constant. The dissolution reaction may be expressed as follows:



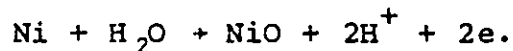


The thickness of the passive film on Ni has been determined by coulometry [63], ellipsometry [64-68] and nuclear microanalysis [69,70]. The composition of the passive film formed in neutral and acid solutions is generally thought to be NiO with maximum thickness reported from 12 Å [71-76] to 18 Å [77,78]. In contrast, Bochrís et al. [65] have reported 60-100 Å film formed on Ni in the sulphate electrolyte of pH ~ 3. In a borate electrolyte a considerably thicker, porous film could be grown the thickness of which changes with the potential [63,67,80-84]. The current efficiency for the film formation is rather small [63,83,84] and therefore coulometry can be used for the film thickness determination only by taking into account the charge that corresponds to Ni dissolution. On the other hand certain assumptions about the optical constants must be made in ellipsometry.

The two main mechanisms suggested for the oxide formation on Ni are:

- (i) dissolution-precipitation mechanism [64-66]
- (ii) direct oxidation of the metal surface [51,52,85,86]

In the first case it is postulated that oxide can form when the solubility of a species such as  $\text{Ni}(\text{OH})_2$  in the vicinity of the electrode is exceeded, resulting in precipitation of  $\text{Ni}(\text{OH})_2$  onto the electrode surface. The second mechanism would involve an electrochemical reaction such as



The most probable mechanism of film formation assumes that in the early stages of Ni-anodization the surface is covered with chemisorbed oxygen which is converted to Ni-oxide with continued oxidation [71-75,80,81]. The stability of different oxygen species on anodized Ni was characterized in relation to their cathodic reduction behaviour and the open-circuit potential decay. The surface-analytical techniques (RHEED, Oxygen  $K_{\alpha}$  X-ray emission spectroscopy, AES and replica electron microscopy) were employed to study the film structure, composition, thickness and morphology. These are probably the most comprehensive studies of the nature of passive film on Ni. It appears that 9 - 12 Å NiO with a defect character is the passive film on Ni in acid sulfate solutions. The overall film thickness seems to be independent of the anodic formation conditions but the defect character of the film and consequently its stability changes as a function of both the time and the potential of anodization. The defect character of the film was found to depend also on the epitaxy between the metal and the oxide. In the case of borate solutions (pH ~ 8) a distinctly different oxide film is formed. It is believed to be NiOOH with the thickness going up to 1000 Å [80,82]. The growth kinetics of this film are interpreted in terms of an outer porous film growing on top of an inner, compact, passive film, i.e., the measured corrosion current determines the rate of growth of the porous film.

According to some earlier reports [52,53,58-62,87], the passivation potential of Ni corresponds to the NiO/Ni<sub>3</sub>O<sub>4</sub> equilibrium potential and polarization to higher potentials leads to conversion of the oxide to Ni<sub>2</sub>O<sub>3</sub>. Different oxidation states as a function of pH and the potential could be expected for Ni on the basis of equilibrium potential - pH diagram [3]. Thus the passive film on Ni was thought to be either simple Ni<sub>3</sub>O<sub>4</sub> or a duplex oxide of NiO and Ni<sub>3</sub>O<sub>4</sub>. In another view [88] the direct oxidation to Ni<sub>3</sub>O<sub>4</sub> and Ni<sub>2</sub>O<sub>3</sub> has been proposed to take place in the active region which can lead to the formation of solid solutions of Ni<sub>2</sub>O<sub>3</sub> in NiO. This means an increase in Ni<sup>3+</sup> ion concentration (3d holes) in the oxide. If the oxidation rate is determined by the concentration of 3d holes, an increase of their concentrations should cause an acceleration in oxidation.

### 1.3 PASSIVITY OF MOLYBDENUM

Reports concerning the corrosion characteristics and anodic dissolution of Mo have appeared in the literature sporadically. The variety of oxidation states and the complex chemistry exhibited by Mo have led to some confusion and seemingly contradictory information concerning its behaviour.

Latimer [91], Pourbaix [3], Pozdeeva et al. [92] and Markovic [94] calculated the standard potentials for systems of Mo and its oxides in aqueous solutions from thermodynamic data taken from the literature. The potential - pH diagram was



constructed [3] taking the following species into account: Mo,  $\text{MoO}_2$ ,  $\text{MoO}_3$ ,  $\text{Mo}^{3+}$  and  $\text{MoO}_4^{2-}$ . The diagram is valid only in the absence of substances which form complexes or insoluble salts with Mo.

According to the published work on the dissolution of Mo in aqueous electrolytes, the metal goes into solution in the hexavalent state whereby a dark, amorphous and porous layer is formed. The composition of this layer has not yet been established. Heumann and Hauck [95,96] have reported that layer to be composed of  $\text{MoO}_2$  and that the anodic oxidation of that oxide determines the course of the current-potential curve. The work of Wikstrom and Nobe [97] agrees with these findings.

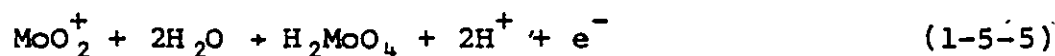
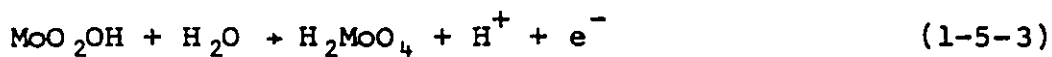
Pozdeeva et al. [93] studied oxidation of Mo in  $1\text{N H}_2\text{SO}_4$  and in KOH solutions by taking potentiostatic polarization curves and comparing the results with the curves taken with various Mo-oxides and with the standard potentials of formation of the oxides, calculated from thermodynamic data. From the potentials of formation it was concluded that only  $\delta$ - and  $\gamma$ -phases could be the passivating species in acid solutions. These phases were synthesized. They had the compositions  $\text{MoO}_{2.08}$  and  $\text{MoO}_{2.70}$ , respectively. From the electrochemical behaviour of the synthesized oxide phases it was concluded that Mo is passivated by a film of  $\gamma$ -phases ( $\text{MoO}_{2.65} - \text{MoO}_{2.75}$ ). On anodic polarization of Mo in  $1\text{N H}_2\text{SO}_4$  the authors found that Mo did not dissolve at potentials more negative than  $-0.15\text{ V (NHE)}$ . Since the value of

standard potential for reaction



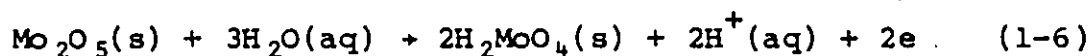
is -0.20 V (NHE) they concluded that Mo has no active region in its solution, i.e., the region of immunity borders with the passive region. (These results do not agree with those of Wikstrom and Nobe [97].) The interpretation of polarization curves was as follows: Metallic Mo is passive in 1N H<sub>2</sub>SO<sub>4</sub> in the potential range of -0.15 V to 0.4 V (NHE). At potentials of 0.4 - 0.7 V it dissolves by passing through the formation of δ- and γ-oxides and subsequent oxidation of these oxides to H<sub>2</sub>MoO<sub>4</sub>. At higher potentials the process is slowed down by the formation of β- and β'-phases mixed with MoO<sub>3</sub>. At potentials higher than 1 V (NHE) the rate of oxidation is independent of potential. The process of formation, oxidation and chemical dissolution of the multilayer film determines the anodic behaviour of Mo at potentials higher than 0.75 V. No oxygen evolution was found in 1NH<sub>2</sub>SO<sub>4</sub>. Mo goes into solution as MoO<sub>4</sub><sup>2-</sup> ions. At ~ -0.15 V a film appears on the electrode surface. The authors claim that Mo cannot be passivated in alkaline solutions because δ- and γ-phases form at -0.9 V but these species are oxidized at -0.96 to -1.0 V so they cannot exist at -0.9 V. The β and β' phases (MoO<sub>2.87</sub> and MoO<sub>2.89</sub> respectively) are stable at the potentials of interest but dissolve chemically in alkaline solutions making passivation impossible. These conclusions are in disagreement with the findings

of other authors [95,96,98] who consider Mo to be in the passive state in alkaline solutions and find that the anodic dissolution curve overlaps with the transpassive region. Studies of the dissolution of Mo in a broad range of pH (0.28 - 14) by galvanostatic methods [98] led the authors to propose at least five steps for the transpassive dissolution of Mo:

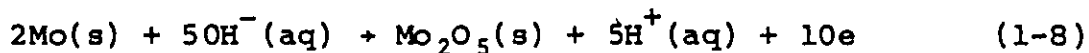
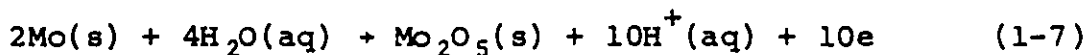


The authors suggest that some of these steps take place simultaneously. The sequence (1) + (2) + (3) agrees with the mechanism proposed elsewhere [95,96] whereby it was found by means of chemical and X-ray analysis that the surface film is  $\text{MoO}_2$ . Anodic polarization of Mo in 1N  $\text{H}_2\text{SO}_4$ , as investigated by differential capacitance measurements and open circuit potential decay [97], indicated that  $\text{MoO}_2$  was always present on the electrode surface and that anodic dissolution of Mo involves  $\text{MoO}_2$ . Johnson et al. [99] studied anodic polarization of Mo in

acid and alkaline solutions and reported that Mo dissolves as  $\text{Mo}^{6+}$  and forms a dark blue film in acid electrolytes and a black one in alkaline electrolytes. X-ray studies showed that films were generally amorphous except those formed in alkaline solutions which exhibited a certain degree of crystallinity. The films were found to be  $\gamma\text{-(MoO}_{2.65\text{-}2.75})$  and  $\beta\text{-(MoO}_{2.87})$  for pH 13.6, depending on the current density, and  $\alpha\text{-(MoO}_3)$  for pH 9.5. In alkaline electrolytes the authors found an active dissolution range followed by a transpassive range. In acid electrolytes the active and transpassive regions were separated by a "secondary passivation" region where current fluctuations were found. This effect was considered to be due to the film growth on the surface. By comparing the open circuit potentials with those of possible equilibria, it was concluded that the reaction at open circuit was:



$\text{Mo}_2\text{O}_5$  is formed by one of the following reactions both of which are rapid:



In the transpassive dissolution the overall rate is determined by a slow dissolution of  $H_2MoO_4$ .

The anodic dissolution of Mo in 2N  $H_2SO_4$  and 1N HCl [100], investigated by the potential sweep method and rotating electrode, gave five current maxima independent of the sweep rate, indicating that the corresponding potentials were reversible. Those potentials were dependent on pH and one of the five current maxima was sensitive to addition of  $Mo^{6+}$  to the solution. The same authors performed impedance measurements in nonaqueous electrolytes [101] in order to obtain information on the oxidation of Mo to the states lower than +6. It was concluded that there are many conceivable dissolution mechanisms.

The electrochemical behaviour of thin surface films on Mo in 1N  $H_2SO_4$  and 1N  $Na_2SO_4$  [102] investigated by galvanostatic and potentiostatic polarization showed that the thickness of the film increased with the potential. The film thickness was constant up to 100 min of polarization and increased sharply after that. A critical value of current was found at which the film reached its maximum thickness (300 - 500 A); thereafter the thickness decreased with increasing current. It was also found that cathodic reduction did not cause Mo to become active but the film thickness decreased with time to a certain extent.

Ikonopisov [103] found that very thin anodic films on Mo are semiconducting and believed that they consisted of a lower oxide. Beyond a critical thickness, this semiconducting film was

argued to be converted to  $\text{MoO}_3$ , since the latter is the only known oxide of Mo which has low enough conductivity to permit film growth.

Daly and Keil [104] have found, by measuring the charge and comparing it to chemical analysis of dissolved films, that Mo in anodic films has an average oxidation state of 5.5.

Thermal oxide formed on Mo was shown by Hickman and Gulbransen [105] to exist in layers such that  $\text{MoO}_2$  was next to the metal and  $\text{MoO}_3$  on the outside. In other work [106] only  $\text{MoO}_2$  was identified, while ion-implanting Mo with  $\text{O}_2^+$  also led to  $\text{MoO}_2$  [107].

Arora and Kelly [108] found that anodic films on Mo are crystalline below a critical thickness of 90 - 300 Å (6-10 V) and amorphous beyond that thickness. The diffraction patterns suggested the thin film to be  $\text{MoO}_2 \cdot \text{H}_2\text{O}$ .

Judging from the results, an elucidation of the mechanism of anodic dissolution of Mo in aqueous solutions seems very difficult.

#### 1.4 EFFECT OF Mo AS AN ALLOYING ELEMENT ON THE PROPERTIES OF PASSIVE FILMS

In recent years corrosion research has been increasingly concentrating attention on elucidating the role played by alloying components in the formation of passivating layers on alloys and on ensuring the increased stability of these layers.

The effect of Mo has been dealt with mostly in the case of stainless steels where it has been known for a long time that it reduces pitting susceptibility. The quantitative analyses have been done relatively recently but a few consistent conclusions were obtained. Some information also exist about the corrosion characteristics of Ni-Mo-Cr alloys (Hastelloys) [109-111] and a number of reports concerning binary Fe-Mo alloys [112-117] and Ni-Mo alloys [118-122].

Uhlig [109] believed that the alloys of Ni-Mo system are not passive in the sense that their electrochemical behaviour does not approach that of less active metal. The electrochemical studies of Greene [118] have shown this to be untrue; all single phase alloys exhibit typical active-passive behaviour. By means of electrochemical and dissolution measurements [121] it was found that Mo accumulates in the passive film accelerating the film growth. ESCA results suggested the existence of Ni- and Mo-oxides in the form of a solid solution in the passive region and as separate phases in the transpassive region. It was also pointed out that small amounts of Cr added to single phase Ni-Mo alloys lowered the passive current density. The electrochemical measurements on Ni and single phase Ni-Mo alloys [122] suggested a negative effect of Mo on the stability of passive film on Ni.

According to the polarization behaviour [113] when Mo alone is added to Fe, there are no beneficial effects in the solutions of pH 3, although that pH lies in the middle of MoO<sub>2</sub> stability zone on the potential-pH diagram [3].

Kodama and Ambrose [116] have studied the effect of  $\text{MoO}_4^{2-}$  ion on the repassivation kinetics of Fe in aerated solutions containing  $\text{Cl}^-$  ions and  $\text{MoO}_4^{2-}$  ions. Their results demonstrated that dissolved molybdate ion is effective in repassivating Fe undergoing pitting corrosion in borate-buffer solutions containing 0.01 M NaCl and 0.01 M  $\text{Na}_2\text{MoO}_4$ . Thermodynamic data suggested that Mo improves localized corrosion resistance by forming an insoluble molybdate compound which inhibits propagation of pits but not their initiation. Ambrose [117] has also investigated the effect of Mo on the repassivation kinetics of Fe on a series of Fe-Mo alloys with the intention of comparing the results with those obtained when  $\text{MoO}_4^{2-}$  was added directly into the solution. It was found that a critical concentration of Mo (~ 5%), whether present in the metal or in the solution, was necessary to provide a film of critical thickness which determines whether the localized corrosion process will propagate or not.

Composition profiles in depth of passive films on Fe-5Mo and pure Fe [115] in deaerated borate-buffer solution (pH 8.4) have shown that there was no Mo in the outer layer of the passive film. The thickness of the inner layer was about one half of that on pure Fe and it increased linearly with anodic potential of the film formation. The estimated electric field of the inner layer was two times as high as that for pure Fe. The diffusion coefficient of migrating ions in the inner layer of the passive film on Fe-Mo alloy suggested that ionic current of



$\text{Fe}^{3+}$  ion migration is predominant as opposed to the case of pure Fe where the ionic current is carried by oxygen ions in the barrier layer. It was concluded that Mo was incorporated into the inner layer to form a stable oxide with high resistivity to ionic conduction.

There have been numerous studies concerning the beneficial effect of Mo on the corrosion properties of stainless steels, due both to the complexity of the passive state of steels and its practical importance. Recently, more detailed studies have investigated the relationship between the electrochemical properties of passive films and the results of physical measurements of thin surface layers. From potentiostatic polarization Mo is known to decrease the critical and the passive current density in  $\text{H}_2\text{SO}_4$  solutions [123-126]. In addition, the pitting potential in the chloride containing solutions increases remarkably with Mo content [123,127-129]. AES and ESCA have suggested that no or exceedingly small quantities of Mo are present in the passive films on stainless steels in acid and neutral solution, independent of chloride ions in the solution [113,130,131].

It has been proposed [116,117,132] that the effectiveness of Mo alloying against pitting is achieved through the adsorption of  $\text{MoO}_4^{2-}$  rather than through Mo incorporation into the passive film. Some ESCA measurements, however, demonstrated that Mo is incorporated into the passive film as  $\text{Mo}^{6+}$  ( $\text{MoO}_3$ ),

playing an important role in the pitting corrosion resistance [114,133].

According to some investigators [114,121,125,126,128] the beneficial effect of Mo was dependent on the Cr level, with a higher Cr level exhibiting the greater effect. In order to clarify the influence of Mo on the electrochemical characteristics of Cr Klimmeck [134] carried out electrochemical measurements on Cr-Mo alloys (with up to 20% Mo) in the active and passive region. It was shown that the behaviour in the active region was determined mainly by Mo. The active state, easily obtained for Cr, appears for 10% Mo and does not appear at all for 20% Mo in 5N HCl solution. In contrast to this no specific effect of Mo could be found in the passive and transpassive region.

In spite of the fact that addition of Mo to Fe decreases the passivation tendency of Fe in  $H_2SO_4$  solutions and does not allow Fe to passivate in 1N HCl [12], Hashimoto and coworkers have found that amorphous Fe-Mo-13P-C [135] passivates in 1N HCl as well as Fe-Mo-18C alloy [136], as long as the amount of Mo does not exceed some critical value beyond which the anodic current density increases in both the active and the passive regions.

It is evident that there is no definite explanation of the role of Mo in improving the corrosion properties. The explanations made to date can be summarized as follows:

- (1) Mo once dissolved as molybdate ion into solution is adsorbed on the break-down sites of passive films and acts as an anodic inhibitor [116-137].
- (2) Mo in the alloy substrate promotes the repassivation of microbreakdown sites and enhances the corrosion resistance [138].
- (3) Mo stabilizes the inner layer of passive films [139-140] by improving the quality of the bonding at the metal oxide surface.
- (4) Mo produces passive films with non-defective structure.

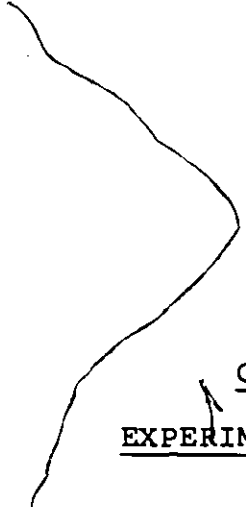
Thus, serious contradictions have been found, even when the same experimental techniques were used. The available evidence to support various ideas explaining the critical role of Mo are rather limited. Further studies are required in order to elucidate the presence of Mo and its state in the passive film.

### 1.5 STATEMENT OF THE PROBLEM

To understand the role played by the surface oxide film in determining the corrosion susceptibility of metals and alloys, it is necessary to understand the nature of the oxide film itself, e.g., its thickness, composition, structure and stability.

Many of these film properties cannot be obtained by the exclusive use of electrochemical methods but require complementary information from surface analytical techniques, e.g., Auger electron spectroscopy (AES) to give the atomic composition and thickness, X-ray photoelectron spectroscopy (XPS) to give the chemical composition of the film, reflection high energy electron diffraction (RHEED) to give the structure of the film. Additional information on the role played by alloying components in the formation, growth and stability of passive layers on alloys can be obtained from the dissolution behaviour of an alloy and its components under the conditions of passivation.

The purpose of this work was to study the nature and character of the anodic film formed on single phase Ni-Mo alloys in an acid solution. A combination of electrochemical measurements and the above noted surface analytical techniques with dissolution measurements would provide needed experimental information for better understanding of the effect of Mo as an alloying element on the properties of the passive film on Ni.



CHAPTER II  
EXPERIMENTAL TECHNIQUES

2.1 MATERIALS AND SPECIMEN PREPARATION

The materials used were Ni and Ni-Mo alloys containing 1 - 22 wt % Mo. The preliminary electrochemical investigation was performed on Ni and Ni-Mo alloys supplied by Metallurgical Laboratories, Falconbridge Nickel Mines Ltd., Thornhill, Ont. The characterization of the alloys has been based on the phase diagram of Ni-Mo system, Fig. 2.1 [141]. All the alloy samples except 22% Mo belong to the  $\alpha$ -phase, i.e. solid solution of Mo in Ni and have the FCC structure. The Ni was "low oxygen Ni" received as cold-rolled sheets prepared from cathode material. The composition of Ni and Mo used for preparation of the alloys is given in Tables 2-1 and 2-2 respectively. Samples were cut from sheets rolled from arc-melted buttons, heat treated in accordance with the schedule given in Table 2-3. These heat treatments produced the average grain size 50 - 100  $\mu\text{m}$ . The major part of the work was done on Ni-13% Mo alloy, supplied as hot rolled, 0.8 cm. sheet by Cabot Corporation, Kokomo, Indiana. The composition of Ni-13% Mo alloys is given in Table 2-4. The material was checked for segregation by means of electron microprobe analysis. No segregation of Mo was detected.

Fig. 2-1

Ni-Mo Constitutional diagram

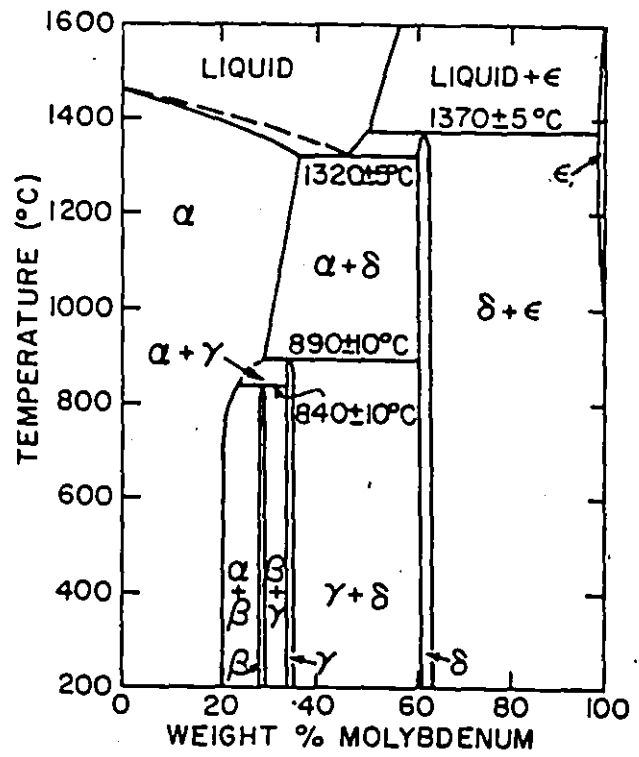


TABLE 2-1

Analysis of cold-rolled sheets of Ni prepared  
directly from cathode material

<u>Element</u>	<u>Analysis in ppm by weight</u>
Al	1
Ca	3
C	15
Cr	<0.6
Co	6
Cu	8
Fe	4
PC	8
Mg	<1
Mn	<0.7
P	<2
Si	5
S	5
Ti	<1
H	1.5
N	2
O	1.4

TABLE 2-2

Qualitative spectrographic analysis of Ni and Mo  
used for preparation of Ni-Mo alloys

Element

Al	0.01 - 0.10	0.003 - 0.003
Ca	0.0003 - 0.003	0.001 - 0.01
Cr	-	0.001 - 0.01
Co	0.001 - 0.01	0.003 - 0.03
Cu	0.0001 - 0.001	-
Fe	0.003 - 0.03	0.01 - 0.1
Mg	0.001 - 0.01	0.001 - 0.01
Mo	-	MC
Ni	MC	0.1 - 1
Si	0.001 - 0.01	0.003 - 0.03

MC - Main Component



TABLE 2-3

Heat treatment schedule for Ni and Ni-Mo alloys

<u>Material</u>	<u>Conditions of Heat Treatment</u>	
Ni	900°C x 1 h	FC
Ni - Mo	800°C x 1.5 h	FC
Ni - 3 Mo	800°C x 1.5 h	FC
Ni - 5 Mo	800°C x 1.5 h	FC
Ni - 10 Mo	800°C x 7.5 h	FC
Ni - 15 Mo	850°C x 57 h	FC

FC - Furnace cooled

TABLE 2-4

Composition of the hot-rolled Ni-13 Mo alloy

<u>Element</u>	<u>Analysis in wt %</u>
Al	0.11
Co	0.01
Cr	<0.10
Fe	0.12
Mg	0.001
Mn	<0.01
Mo	13.03
Ni	86.68
P	<0.004
S	<0.002

The materials were used as electrodes of the plate type with a surface area 0.5 - 2.5 cm<sup>2</sup>. The sample used for the dissolution measurements was rectangular with a surface area of 14.0 cm<sup>2</sup>.

The Ni-13Mo was used as received, without a heat treatment. The grain size was 150 - 300 μm, as shown on the Fig. 2+2.

A standard polishing technique to 1 μm diamond was adopted.

Polished samples were ultrasonically degreased in acetone.

The electropolishing technique (0.1 A/cm<sup>2</sup>, 1 min, 60 vol % H<sub>2</sub>SO<sub>4</sub>) followed by cathodic reduction in the cell was employed in the course of preliminary experiments. The influence of such sample preparation will be discussed in the section devoted to the experimental results. As a consequence, mechanical polishing was adopted as the final step before the cathodic reduction.

Fig. 2-2

Microstructure of Ni-13 Mo (hot rolled)



## 2.2 ELECTROLYTIC SOLUTION

All experiments were performed in 0.15 N  $\text{Na}_2\text{SO}_4$  solution prepared from ultrapure  $\text{Na}_2\text{SO}_4$ \* and double distilled deionized water. The pH of the solution was adjusted with concentrated  $\text{H}_2\text{SO}_4$  to pH 2.7 - 2.8

The studies of formation and removal of oxide films on Ni in  $\text{Na}_2\text{SO}_4$  solutions (pH 8.4 - 2.0) [73], have shown that complete removal of all oxide films was possible in solutions of pH < 2.8 with moderate cathodic treatments. On the other hand the study of the nature of anodic oxide film on Ni in  $1\text{NH}_2\text{SO}_4$  (pH 0.4) [142] revealed a large amount of anodic dissolution of Ni and very fast removal of the passive film. Therefore it was decided to perform the experiments on Ni-Mo alloys in a less aggressive solution of pH 2.8.

All measurements were performed under deaeration and stirring conditions maintained by continuous bubbling of purified nitrogen.

The temperature of the electrolyte was  $23 \pm 1^\circ\text{C}$ .

\* Alfa Division of the Ventron Corporation, Danvers, Ma., U.S.A:

### 2.3 DESCRIPTION OF APPARATUS FOR ELECTROCHEMICAL MEASUREMENTS

A single compartment electrochemical cell, with a capacity of 600 ml was used for the electrochemical measurements (see fig. 2-3). The two Pt-gauze counter electrodes were set symmetrically to the plate type working electrode. The reference electrode was a saturated calomel electrode (SCE) with an agar/ $\text{Na}_2\text{SO}_4$  salt bridge and Luggin capillary. All potentials quoted as results of this work refer to the saturated calomel electrode (+243 mV vs SHE).

The electrochemical setup consisted of a potentiostat (Wenking 70HC3), a galvanostat, and a two pen potentiometric recorder with an integrator on the current channel, Fig. 2-4.

The electrical circuit is shown on Fig. 2-5. It provided the possibility of switching the working electrode from the potentiostatic to galvanostatic mode of control and vice versa without leaving it on the open circuit at any instant of time.

Fig. 2-3

The electrochemical cell



c - counter electrodes

w - working electrode

LC - Luggin Capillary

Fig. 2-4

The electrochemical setup





The electrical circuit

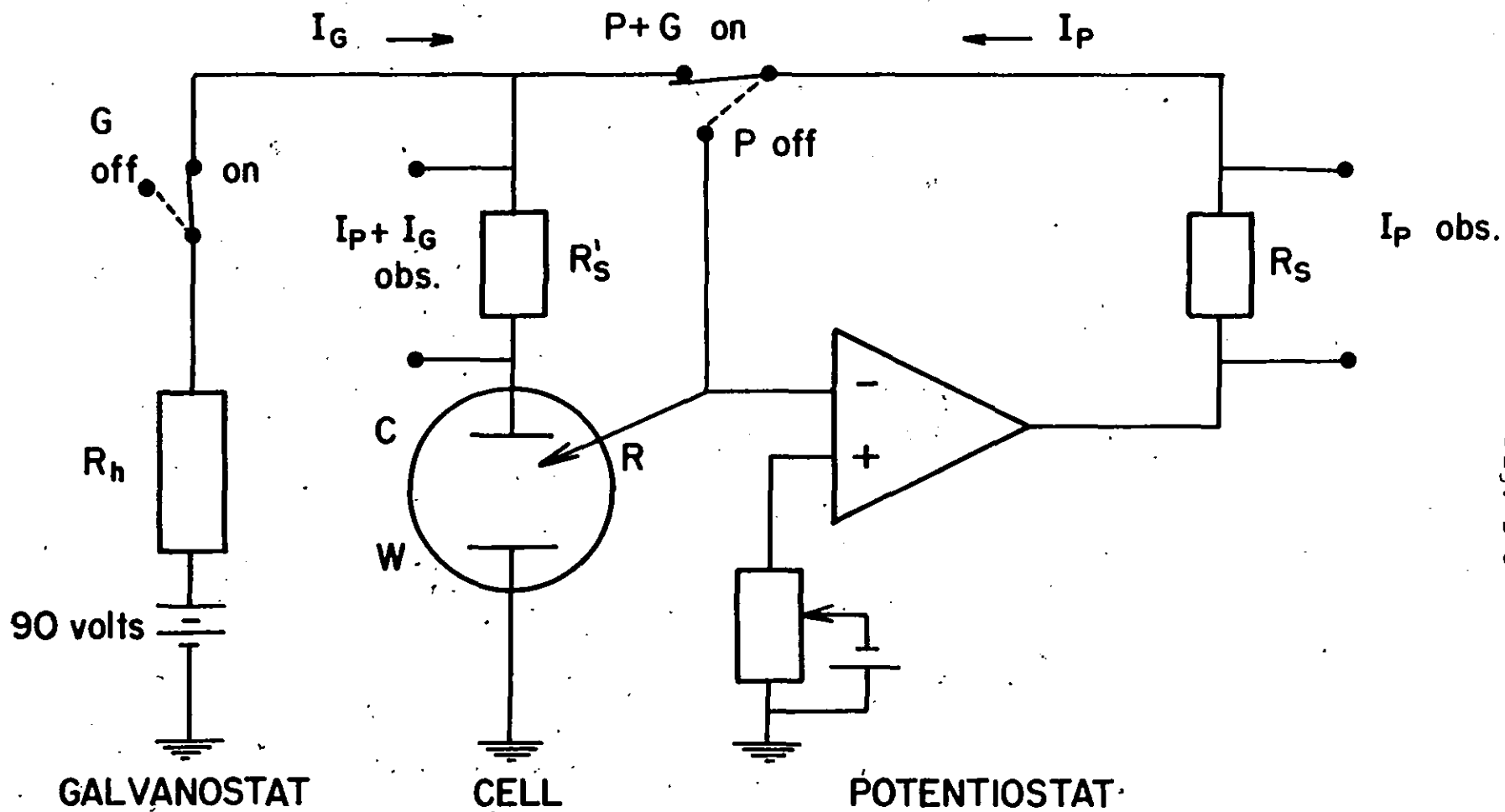


Fig. 2-5

**W - WORKING ELECTRODE**  
**C - COUNTER ELECTRODE**  
**R - REFERENCE ELECTRODE**  
 **$I_P$  - POTENTIOSTATIC CURRENT**  
 **$I_G$  - GALVANOSTATIC CURRENT**

## 2.4. ELECTROCHEMICAL TECHNIQUES

### 2.4.1 POTENTIOSTATIC POLARIZATION

After polishing the electrodes were cathodically polarized at  $-2.0$  V for 10 min without  $N_2$  bubbling. The conditions for the cathodic reduction were established on the basis of the current maximum in the region of active passive transition, which was found to be strongly influenced by the potential and time of cathodic treatment [142].

The anodic potentiostatic polarization curves were obtained in 50 mV steps, made at 2 min intervals, starting from  $-600$ mV or the rest potential established after the cathodic reduction.

Polarization at fixed potentials in the passive region was performed by the potential step from a cathodic or the rest potential to a desired value in the passive region. Corresponding anodic current transients followed by a slow change of current with time were recorded.

### 2.4.2 OPEN CIRCUIT POTENTIAL DECAY, GALVANOSTATIC CHARGING AND SURFACE REACTIVITY MEASUREMENTS

The potential decay curves were recorded by switching the potentiostat off after the sample was potentiostatically polarized for a desired period of time at a potential in the passive region.

Galvanostatic charging of an anodized sample was performed by switching a constant cathodic current on without leaving the sample on the open circuit. The change of potential with time was recorded (see Fig. 2-5).

Surface reactivity measurements [72] were performed in order to determine relative activity of the surface after a time on the open circuit or after the passage of a certain amount of cathodic charge.

When a film free metal electrode is directly subjected to a potential in the passive region, the amount of charge consumed during the formation of a steady state film,  $Q_0$ , can be considered as the amount of charge needed for film formation on a "clean" surface. If, however, the film were formed under the same conditions (potential and time of anodization) but starting with a surface not completely film free, the charge consumed,  $Q$ , would be less than in the former case. The ratio  $(Q/Q_0) \times 100\%$  can be defined as surface reactivity,  $R_s$ , since a film free surface would be 100% active.

The surface reactivity was measured after different elapsed times on open circuit by stepping the potential back to the value at which the film had been previously grown.

The same procedure was performed after a partial removal of the anodic film by galvanostatic cathodic reduction.

Conclusions on the stability of film coverages on the open circuit and efficiency of their removal by galvanostatic

cathodic reduction could be made on the basis of surface reactivity measurements.

For all experiments the data presented here are the record of particular experimental runs but are typical for the given conditions. Potentiostatic polarization measurements were reproducible to within  $\pm 5\%$ . The maximum scatter in the potential decay measurements was  $\pm 10$  mV.

## 2.5 SURFACE ANALYSIS

The surface analysis techniques that have been employed in this investigation are Auger electron spectroscopy (AES) and X-ray photoelectron spectroscopy (XPS or ESCA). Both are based on emission and subsequent energy analysis of secondary electrons produced by high energy electrons in the case of AES and by soft X-ray bombardment in XPS.

### 2.5.1 AUGER ELECTRON SPECTROSCOPY AND ION SPUTTERING

In an Auger process an atom is initially ionized in an inner level  $x$  and Auger emission results in an atom with two final state holes in levels  $y$  and  $z$  and an Auger electron of energy  $E(xyz)$ .

The energy of Auger electrons in principle can be determined by the difference in total energies before and after the transition.

The AES technique involves energy analysis of Auger

electrons. It employs primary electrons in the 2-10 keV range to cause primary excitation. The energy analysis of secondary electrons is usually accomplished with a cylindrical mirror analyzer [143].

The Auger spectra are most often presented as the derivative of the energy distribution,  $dN(E)/dE$ , as a function of kinetic energy  $E$ . Elements are identified by the energy positions of peaks in the spectrum. Peak heights are related to the atomic concentrations and quantitative information can be, in principle, obtained from the spectrum. The problem of quantitative analysis is described in detail by Powell [144]. The suitability of this technique to the application in the field of thin films is due to three reasons:

- (i) The analysis depth is typically less than 20 Å and corresponds to the escape depth of Auger electrons.
- (ii) The technique is capable of obtaining compositional information from the areas of the same size as the incident electron beam (submicron range).
- (iii) High sensitivity for light and heavy elements.

Other important assets include rapid data acquisition and depth composition analysis in conjunction with sputter etching.

The instrument used for the AES analysis was a Physical Electronics Industries (PEI) 590 System, which employs a cylindrical mirror analyser (CMA) with a concentric electron gun. The samples were positioned so that their surface normal was 30°

to the axis of the CMA. The electron gun was operated at 5 keV with a current  $\sim 5 \times 10^{-7}$  A. The beam diameter was  $3 \times 10^{-4}$  cm and it was rastered 300-400 times over the surface area of  $9 \times 10^{-4}$  cm<sup>2</sup>.

The ion gun, operated for sputtering with Xe<sup>+</sup> at 1 keV, was positioned so that the ion beam struck the specimen surface at an angle of  $\sim 52^\circ$  to the surface normal and  $\sim 80^\circ$  to the axis of the electron spectrometer. The beam current was  $4 \times 10^{-9}$  A and it was rastered over  $4 \times 10^{-2}$  cm<sup>2</sup>.

The gas pressure in the ionization chamber was  $< 5 \times 10^{-5}$  torr, while the pressure in the vicinity of the sample was in the mid  $10^{-9}$  torr range.

The common method of converting derivative-mode Auger signals to atomic percent (at%) concentration, based on the equation of Davis et al. [145], was employed for the analysis:

$$C_x = \frac{\frac{I_x}{S_x} \times 100}{\sum_n \frac{I_n}{S_n}}$$

where  $C_x$  (at%) is the concentration of element X,  $S_x$  is the relative sensitivity of element X and  $I_x$  the magnitude of Auger derivative mode signal (Auger peak-to-peak height - APPH). The sum is over one peak from each element present in the surface.

The relative sensitivity factors for Ni and Mo were determined from thick film standards: NiO on pure Ni and Mo-oxide (assumed to be MoO<sub>3</sub>) on Mo-foil. There are several

inherent errors in this semi-quantitative approach. These are:

- (i) Matrix effects on electron transport properties. The dependence of Auger electron escape depth on the electronic structure of the host material may alter the depth of measurement in the specimen relative to that in the standard [146-148].
- (ii) Chemical effects on peak shapes may lead to error when using APPH in the differentiated spectrum [149,150].
- (iii) Surface topography affects the magnitude of the signal [157-152].

Therefore, the analysis is considered to be semi-quantitative with an accuracy of 30 - 50%. On the other hand it is recognized that the process of ion sputtering can induce changes in the surface composition of a multicomponent system. A number of papers [153-158], mainly on binary alloys, have considered the quantitative aspects of AES combined with ion sputtering.

### 2.5.2 X-RAY PHOTOELECTRON SPECTROSCOPY

X-ray photoelectron spectroscopy (XPS or ESCA) is similar to AES. The main difference is that in XPS the electrons originate directly from the core and valence levels. The energy spectrum of core level electrons uniquely identifies the emitting atom. The chemical information is obtained from the core level energy shifts that are associated with the degree of ionic or covalent binding [159]. The analysis consists of irradiation of



a sample by monoenergetic X-rays (usually  $K_{\alpha\text{Al}}$  or  $K_{\alpha\text{Mg}}$ ) and measurement of the number of photoelectrons as a function of their energy.

The major advantages of XPS are its surface sensitivity (sampling depths 5-25 Å for metals) and minimum radiation damage of the surface.

On metal-oxygen systems an appreciable amount of work has been published. Shifts in elemental binding energies are usually sufficiently large to permit clear differentiation of metal and oxide phases. The quantitative aspects of the technique for metal and oxide surfaces have been discussed extensively by McIntyre [160,161].

XPS was used in this work in a qualitative sense only, in order to characterize the species present on Ni-Mo alloys after the different conditions of sample pretreatment in the electrochemical cell.

X-ray photoelectron spectra were recorded using a Mg X-ray source ( $K_{\alpha\text{Mg}} = 1253.6 \text{ eV}$ ) and a PHI 15-255G double pass cylindrical mirror analyzer attachment, which was operated with 50 eV pass energy. The data have been collected at 0.1 V/step and 100 msec/step.

All the data reported are referenced to Au (4f 7/2) level, at  $83.8 \pm 5 \text{ eV}$ .

## 2.6 DISSOLUTION MEASUREMENTS BY ATOMIC ABSORPTION

### SPECTROSCOPY (AAS)

Absorption of energy by ground state atoms in the

gaseous state is the basis for the atomic absorption process. Ground state atoms are produced by evaporation of solvent and decomposition of molecular species into neutral atoms. A hollow cathode is usually used as a source of radiation of the proper wavelength. The magnitude of the atomic absorption signal is directly related to the number of ground state atoms in the optical path of the spectrometer. The signal is the difference between the intensity of the source in the absence of analyzed atoms and the decreased intensity obtained when those atoms are present in the optical path. The absorption of radiant energy is related to the path length,  $l$ , and the concentration of atomic vapour,  $c$ , by the Beer-Lambert relation:

$$P_{\lambda} = P_{0\lambda} e^{-k_{\lambda} l c}$$

where  $P_{\lambda}$  and  $P_{0\lambda}$  are the power of the source at wavelength  $\lambda$  and the power of radiation at the same wavelength after passage through the sample, respectively. By definition, absorbance,  $A$ , is given as  $\log (P_{0\lambda}/P_{\lambda})$  and hence

$$A = a l c$$

where  $a$  is a constant, called absorptivity. Therefore the measurement consists of the construction of a calibration curve -  $A$  vs  $c$  - which is a straight line from the origin in the absence of interference effects, and determining the values of concentration of the sample for each absorbance measured.

Interferences in AAS, in general, could be spectral, ionization and chemical. General background radiation from the solvent, the emission lines of other elements, radicals or molecules belong to the first group of interferences. The ionization interferences result from the fact that production of ground state atoms also involves the production of some excited state atoms, ions and electrons. However, at temperatures commonly used for evaporation, the population of atoms in the ground state is much larger than those in the lowest excited state, except when the particular element ionizes easily. Whenever some chemical reaction changes the concentration of the ground state element a chemical interference occurs (e.g., if stable oxides, hydroxides or carbides are formed).

The AAS analysis was performed by a flameless atomic absorption spectrometer (Perkin Elmer HGA-2100), graphite furnace). The HGA-2100 uses a graphite tube, about 28 mm long and 8 mm in diameter placed so that the sample beam of the spectrometer passes along its axis. Solution samples (5-100  $\mu\text{l}$ ) are pipetted through a sample introduction hole in the centre of the tube. The tube is heated in three stages by passing an electrical current through its walls: a low current is used for drying the sample, an intermediate one for charring and a high current for atomizing. The signals are read from a strip chart recorder.

A deuterium background corrector, which automatically

corrects for non atomic absorption was used because of the relatively high concentration of the electrolyte (0.15 N  $\text{Na}_2\text{SO}_4$ ).

Sensitivity for the HGA is defined as the mass of the element giving a peak absorbance of 0.0044. The wavelength and the detection limit for each element are as follows:

Mo: 313.3 nm 90 pg/0.0044 abs

Ni: 232.0 nm 140 pg/0.0044 abs

The electrolyte was analyzed for Ni and Mo dissolved during the potentiostatic polarization of a Ni-13Mo sample at a constant potential. Samples of solution for analysis were removed in 10 ml aliquots at various times using a metal-free extractor. The concentration of each component in the aliquot was determined by AAS not later than 24 hours after the sample solution had been taken from the cell.

Although the spectrophotometer showed comparatively good reproducibility, the concentration of sample solution was determined from the average of seven samples of each solution.

## CHAPTER III

### RESULTS AND DISCUSSION

#### 3.1.1 POLARIZATION CHARACTERISTICS OF Ni and Mo

The anodic polarization curves for Ni (Fig. 3-1) and Mo (Fig. 3-2) were obtained in 50 mV/2 min steps after cathodic pretreatment in the same cell.

On the basis of the results obtained from applying different regimes of cathodic pretreatment [142] the following conditions were adopted:  $E = -2.0$  V,  $t = 10$  min.

The passive current densities obtained were not the true steady-state values and would be expected to decrease in magnitude with time. The 50 mV/2 min. step polarization was adopted to reduce the time required to cover the active-passive-transpassive potential range. At the same time it provided a reasonable approximation to steady state values although the obtained polarization curves should be considered only qualitative because of the influence of time.

The potentiostatic polarization of Ni (Fig. 3-1) shows a typical active-passive transition. Passive Ni does not show a potential range of constant passive current density. In the transpassive region a change of slope around 1.2 V can be observed, probably due to oxygen evolution. The potential dependent current density might be related to a corresponding change in the degree of oxidation, in agreement with the literature data [50, 54-56].

Potentiostatic polarization of Ni

Figure 3-1

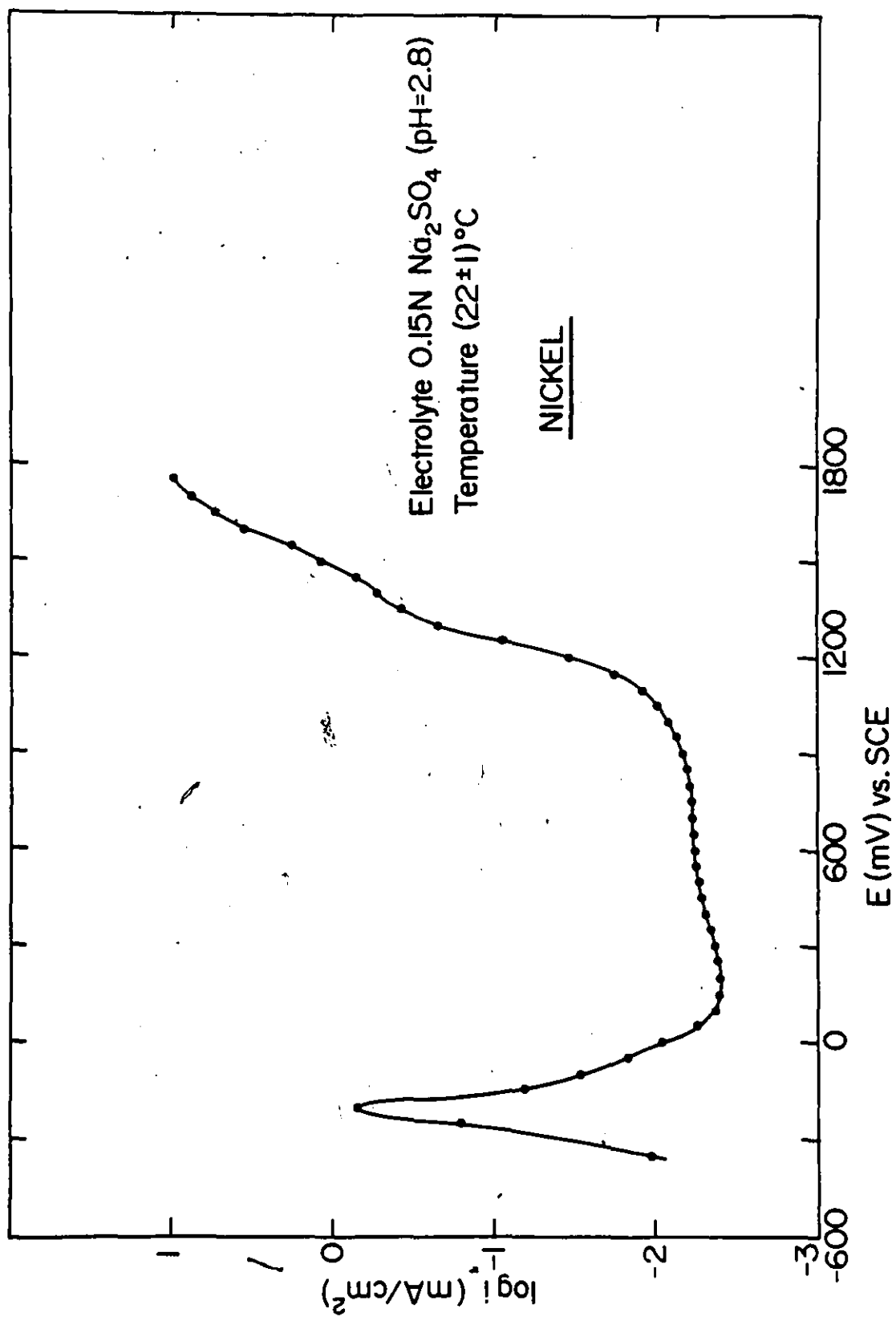
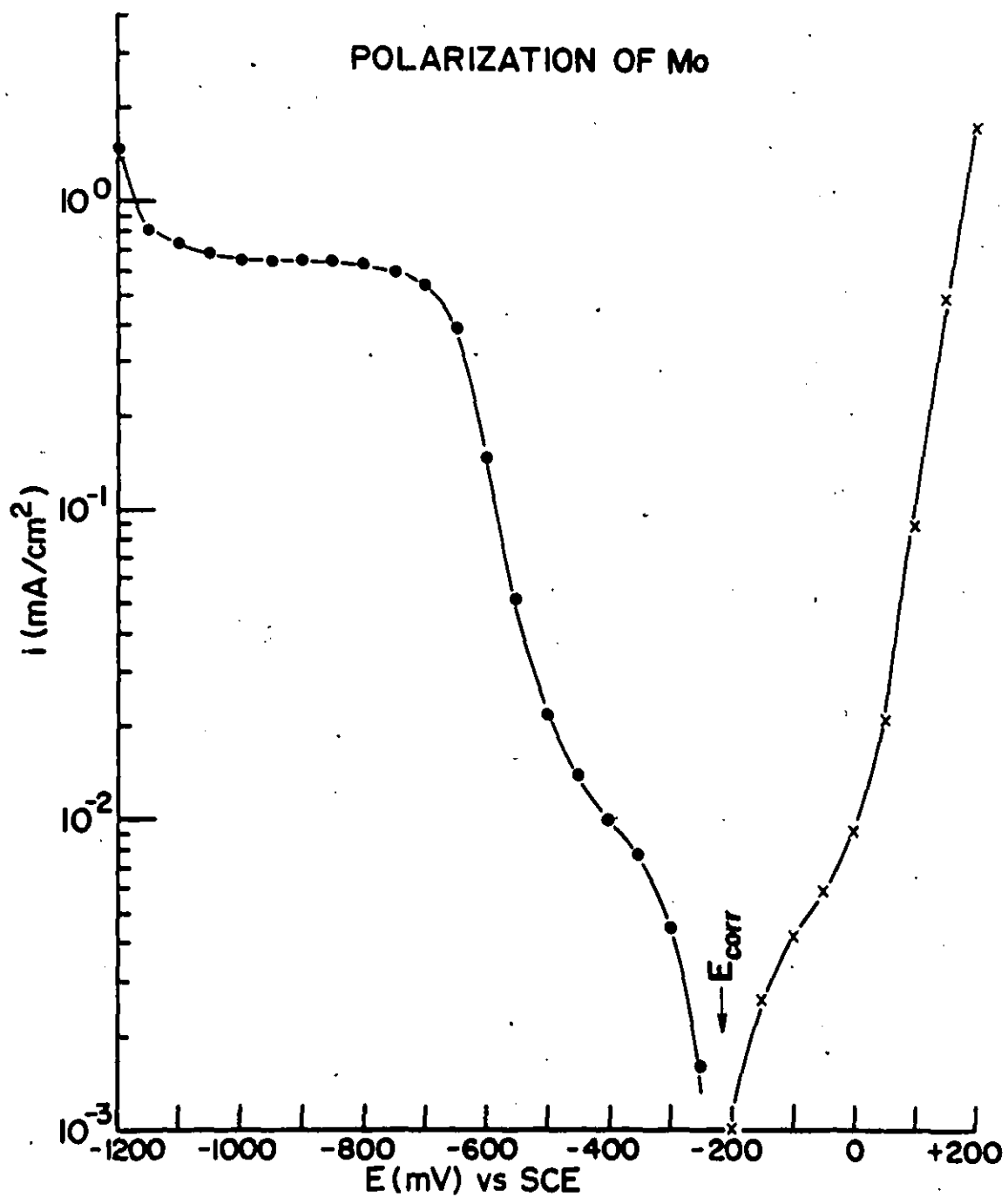


Fig. 3-2





Polarization of Mo (commercial sheet 99.99%) from -1200 mV to +200 mV is given on Fig. 3-2. The limiting current plateau in the range -1100 to -800 mV is probably due to evolution of hydrogen adsorbed on the surface [93]. A change of slope observed in the range ~ -500 to ~ -300 mV could be associated with a small current plateau. According to the potential - pH equilibrium diagram [3] and some reports on the electrochemical behaviour of Mo [95-97] it is possible that in the above potential range the surface of Mo is covered by  $\text{MoO}_2$  which undergoes oxidation and dissolution ( $\text{Mo}^{6+}$  state) on further anodic polarization. Therefore polarization beyond ~ -300 mV leads to the transpassive dissolution of Mo. On the basis of thermodynamic considerations the product of transpassive dissolution of Mo depends on the pH of the solution, i.e.,  $\text{MoO}_3$  is expected to be formed in solutions with  $\text{pH} < 3.5$  and  $\text{MoO}_4^{2-}$  (on  $\text{HMoO}_4^-$ ) in solutions  $\text{pH} > 3.5$ . Oxidation states between +4 and +6 and mixed oxide phases have also been proposed [93].

Polarization characteristics of Ni and Mo in the sulphate electrolyte of pH 2.8 show that the passive range of Ni corresponds to the potential range of transpassive dissolution of Mo.

### 3.1.2 ANODIC POTENTIOSTATIC POLARIZATION OF Ni-Mo ALLOYS

The polarization curves for all Ni-Mo alloys were obtained by the potential step method, at 50 mV/2 min after the cathodic pretreatment at -2.0 V for 10 min.

Fig. 3-3 gives the anodic polarization behaviour of Ni and Ni-Mo alloys low in Mo (1.2, 3.7, 5 wt% Mo). Samples with 1.2% and 3.7% Mo do not show typical active-passive transition behaviour, exhibiting two regions of active dissolution and subsequently two narrow "passive" regions approximately in the range of passivity of pure Ni. It is possible that initial formation of one type of surface coverage which undergoes dissolution at higher anodic potentials is replaced by another type of surface film formed upon further anodic polarization.

Fig. 3-4 shows that the typical anodic polarization of Ni is retained in the case of alloys with 5, 10 and 15 wt% Mo. The alloy with 22 wt% Mo, which is a two-phase alloy, does not show the characteristic active-passive behaviour of Ni. The same figure shows the polarization behaviour of Mo in the potential range of interest.

The polarization parameters are summarized in Table 3-1.

The passivation potential shows no trend with Mo content, being shifted for 200 mV in the more noble direction with respect to pure Ni. The critical passivation current density does not show any dependence on Mo content for the alloys with Mo content higher than 5%, i.e., it increases and then decreases with increasing Mo content. Similar observations were reported by Greene [118]. The current density increases monotonically with Mo content for the alloys higher in Mo (> 5 wt% Mo).

Potentiostatic polarization of Ni and  
Ni-Mo alloys (1%, 3%, 5% Mo)

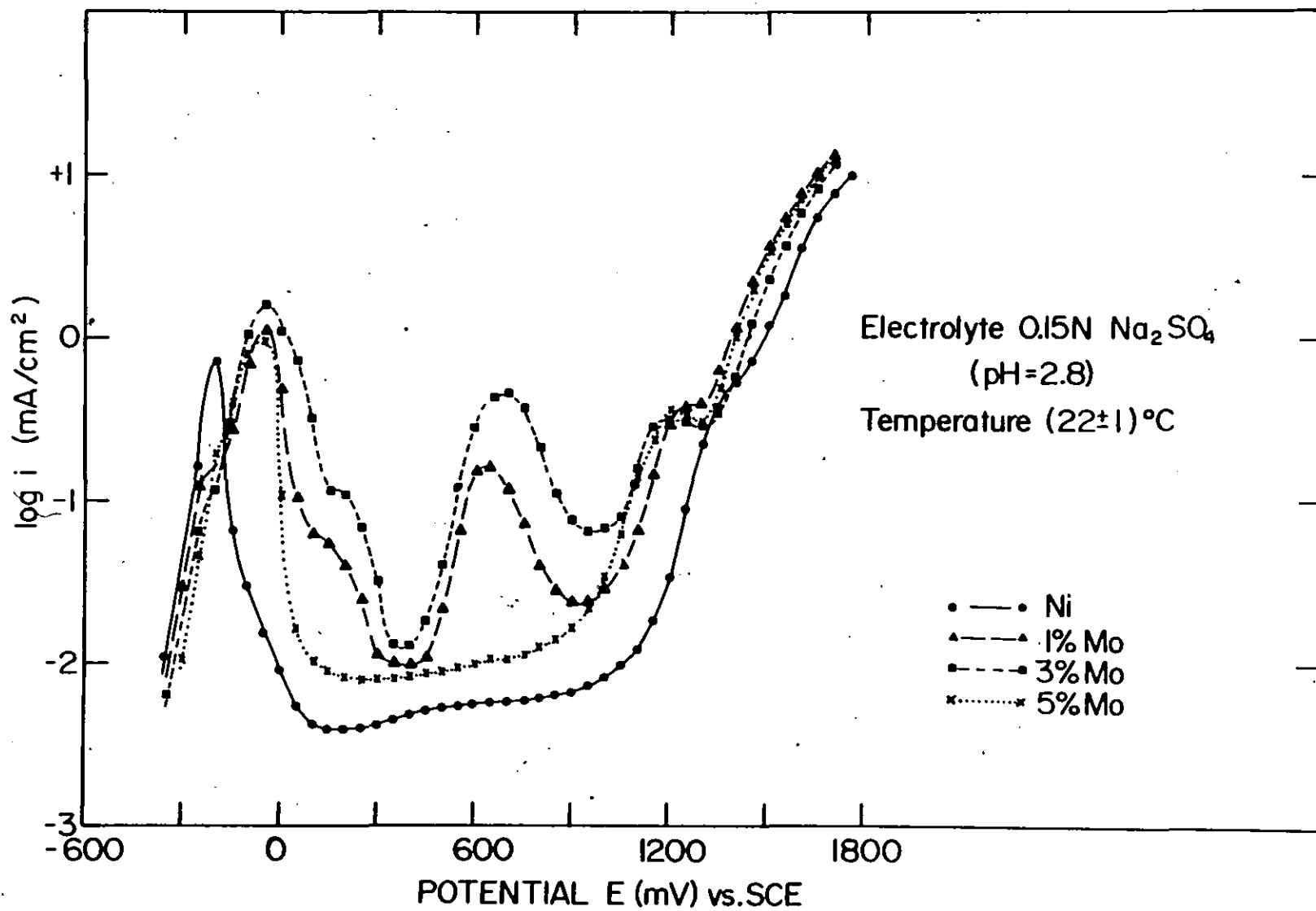


Figure 3-3

Potentiostatic polarization of Ni, Mo and  
Ni-Mo alloys (5%, 10%, 15%, 22% Mo)

Fig. 3-4

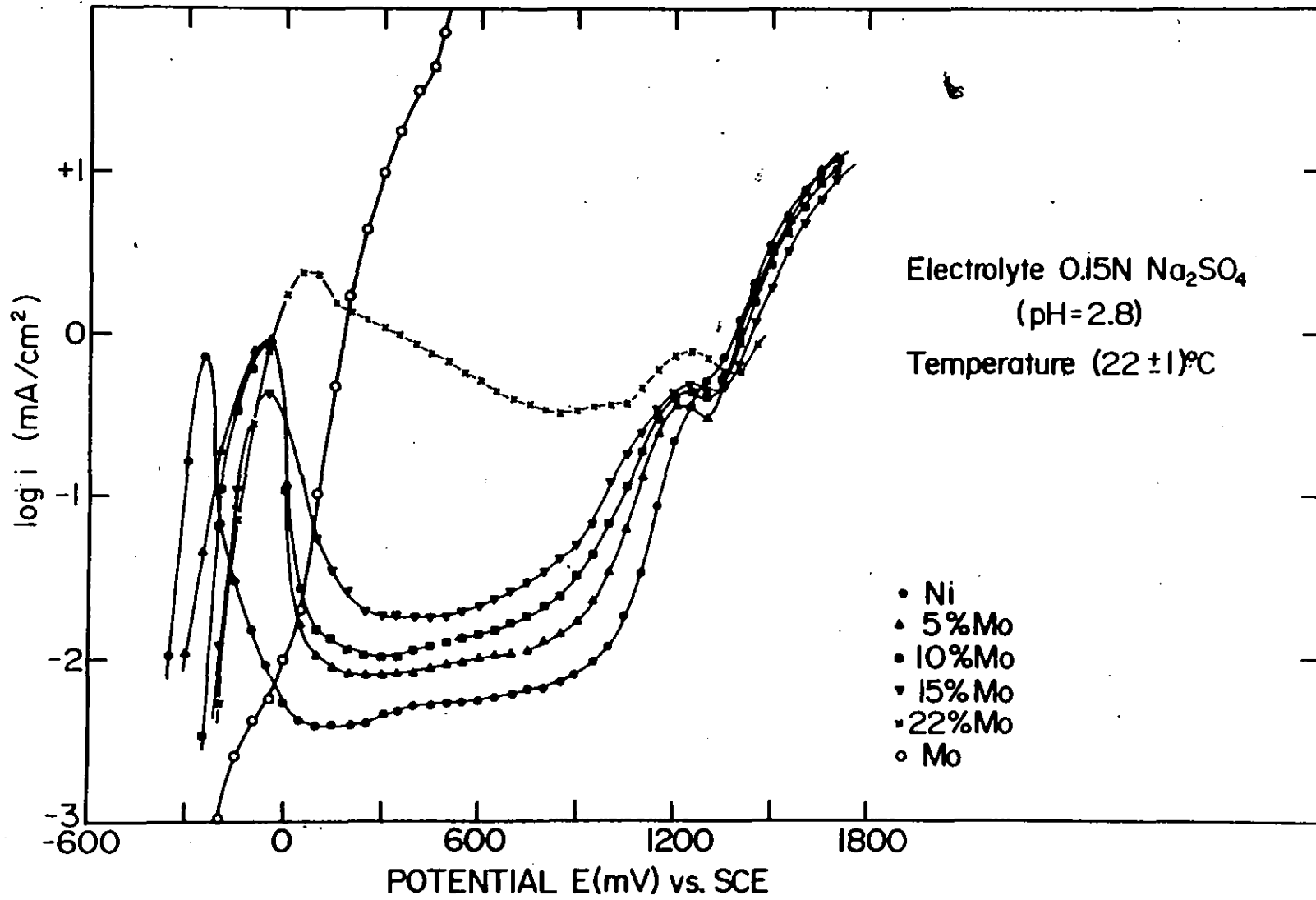


TABLE 3-1

Effect of Mo Content on Characteristic  
Polarization Parameters

% Mo	$E_p$ [mV]	$i_p$ [ $\frac{\text{mA}}{\text{cm}^2}$ ]	$i_{ps}$ [ $\frac{\text{mA}}{\text{cm}^2}$ ]
0	-250	0.72	0.004
1.2	- 50	1.22	(0.010)
3.7	- 50	1.58	(0.013)
5	- 50	0.93	0.008
10	- 50	0.89	0.010
15	- 50	0.43	0.018
22	+ 50	2.40	0.330

$E_p$  - passivation potential

$i_p$  - passivation current

$i_{ps}$  - the lowest value of current in the passive range

From the polarization characteristics of Ni, Mo and single phase Ni-Mo alloys it appears that Mo as an alloying element decreases the corrosion resistance of the passive film on Ni. This effect could be caused by a transpassive dissolution of alloyed Mo, as judged by the fact that pure Mo undergoes transpassive dissolution in the potential range of passivity of pure Ni.

Small amounts of Mo (1.2 and 3.7 wt%) have a strong effect on the passivation behaviour of Ni, modifying the passive state of Ni more than the higher Mo contents in the single phase region of Ni-Mo alloys. It might suggest an inhibitive action of Mo dissolved in the active region which requires a certain critical concentration to be effective. On the other hand small amounts of Mo could be incorporated in the passive film on Ni thereby increasing the defectiveness of the film and decreasing its protective properties. A higher amount of Mo ( $3.7 < \text{Mo} \leq 5$ ) might be required for the formation of another type of oxide coverage, less protective than the passive film on pure Ni but more than the film formed in low Mo alloys.

Low Mo alloys were not further studied in the course of this work.

### 3.1.3 POTENTIOSTATIC FILM FORMATION

The kinetics of passive film growth on metals is often investigated by following the change of the anodic current with time upon polarization into the passive potential region.



Anodic current transients, i.e., change of anodic current with time, recorded by switching the potential to the passive range, plotted on a log-log scale, are shown on figures 3-5 and 3-6 for Ni and Ni-10Mo alloy respectively.

In electrochemical oxidation the amount of charge for oxide film formation ( $Q_f$ ) is proportional to the weight gain (or film thickness) if the anodic current efficiency for film formation is unity. In that case, parabolic, cubic and logarithmic rate laws are expressed as a function of time, as follows\*:

$$\text{parabolic} \quad Q_f = At^{1/2} \quad (3-1)$$

$$\text{cubic} \quad Q_f = At^{1/3} \quad (3-2)$$

$$\text{logarithmic} \quad Q_f = A \ln t + B \quad (3-3)$$

where A and B are constants. Since the derivative, with respect to time, of  $Q_f$  gives anodic current, equations 3-1 to 3-3 give equations 3-4 to 3-6 respectively:

$$i_f = \frac{dQ_f}{dt} = \frac{1}{2} At^{-1/2} \quad (3-4)$$

$$i_f = \frac{1}{3} At^{-2/3} \quad (3-5)$$

$$i_f = At^{-1} \quad (3-6)$$

\* Inverse logarithmic\* law (i.e.,  $\frac{1}{Q_f} = C - D \ln t$ ) is also sometimes observed.

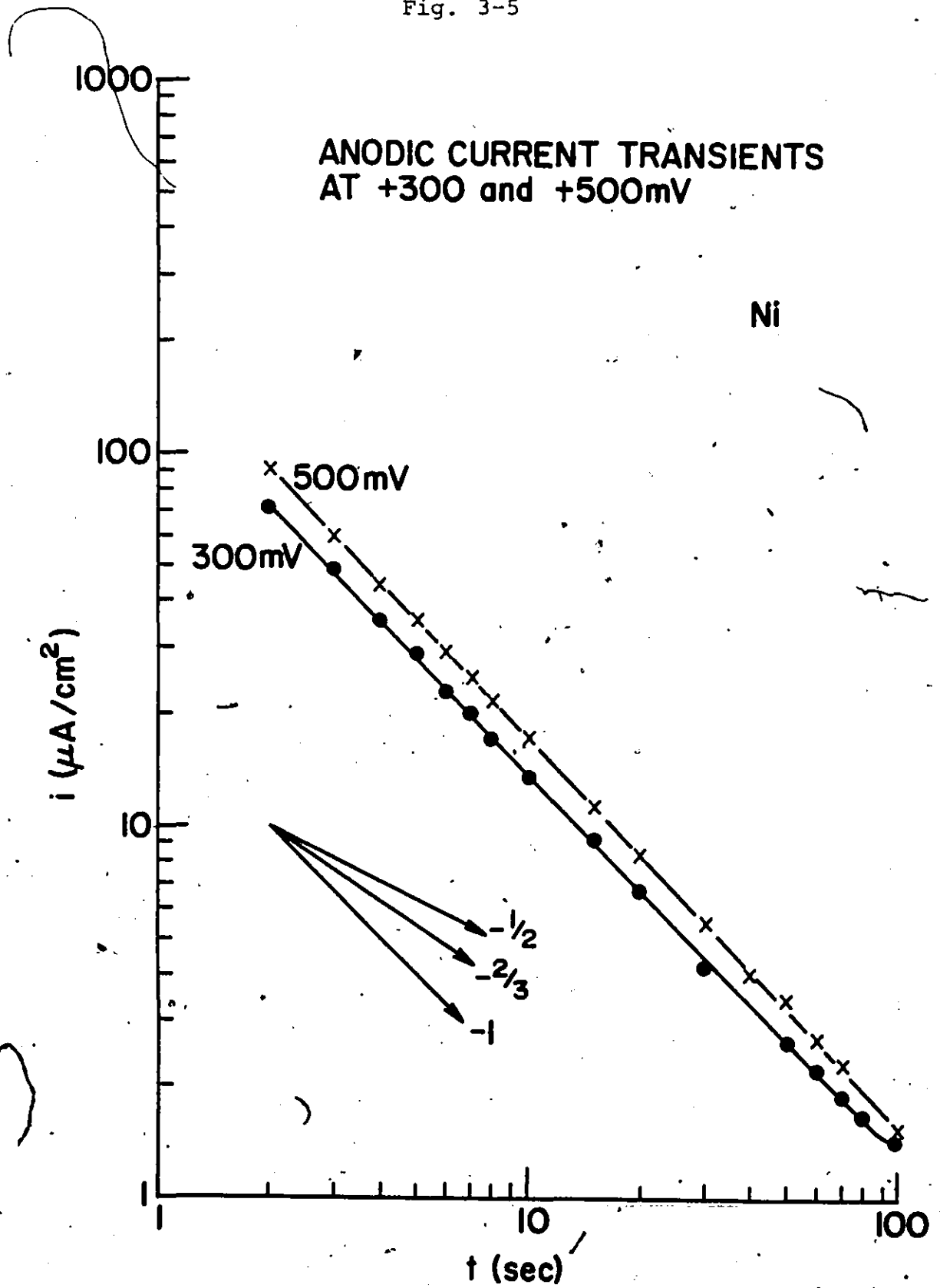
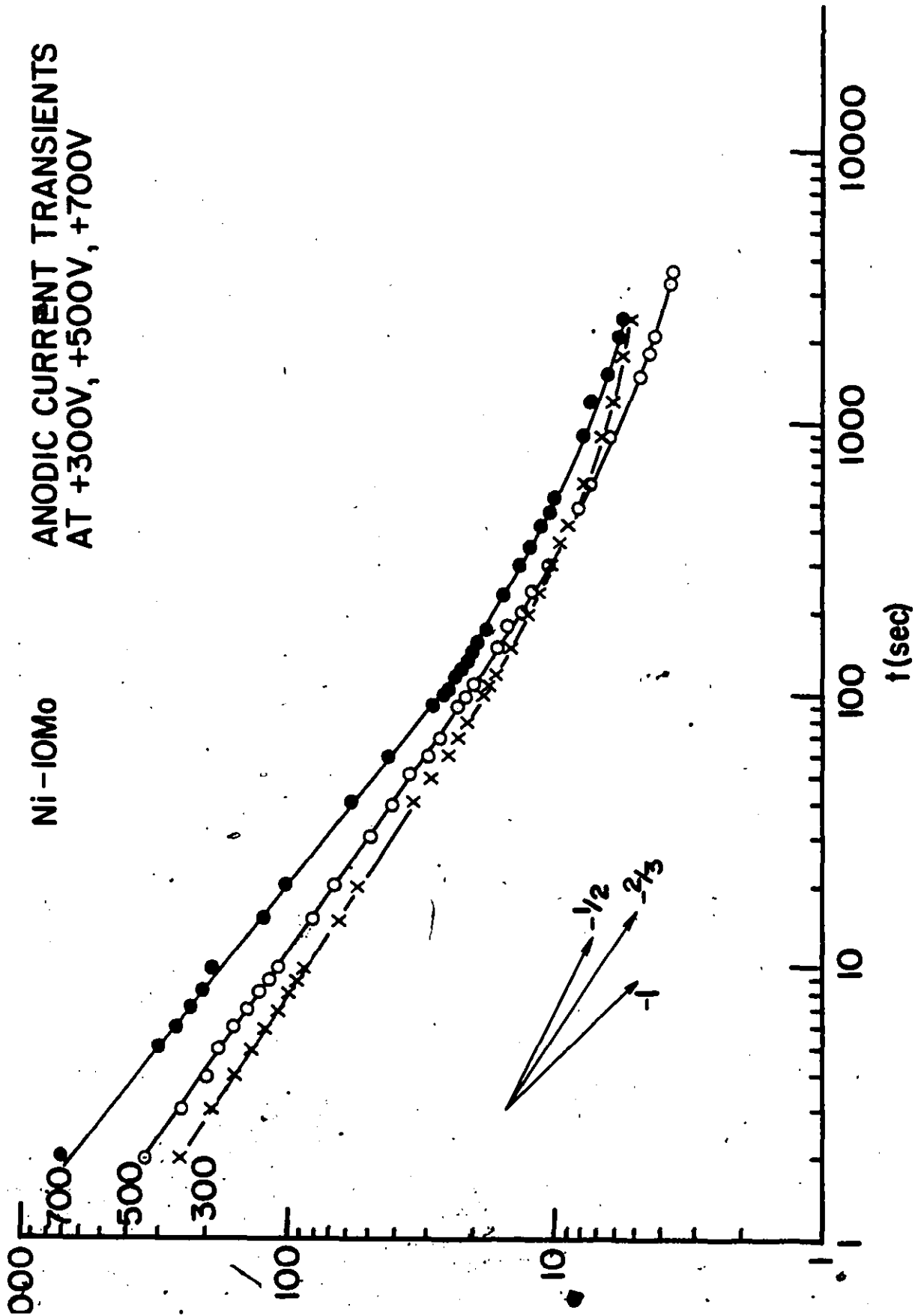


Fig. 3-6



The exponent of  $t$  gives the slope ( $m$ ) in the logi-log $t$  plot. Thus, one can obtain the following results for the growth rate laws:

$$\begin{aligned} m &= -1/2 && \text{for parabolic} \\ m &= -2/3 && \text{for cubic} \\ m &= -1 && \text{for logarithmic.} \end{aligned}$$

Conventionally, the time of the current maxima appearing on the current decay curve when applying a potential step method, is used as the start of film growth ( $t=0$ ). However, the current maxima were not reproducible and the attention was therefore placed only on the relative change of anodic current with time.

It can be seen from Fig. 3-6 that the passive film on Ni-10Mo alloy grows approximately in accordance with either the cubic rate law (at +300 mV and +500 mV) or with a slope in between -1 and -2/3 (at +700 mV).

Approximate logarithmic growth of the passive film on Ni is shown on Fig. 3-5 in agreement with the literature data [84].

The dependence  $i-t$  for the potentiostatic passivation of metals has been derived theoretically by Schwabe et al. [86]. It follows from the considerations that for conditions distant from stationary state, i.e., for the initial period of passivation, the direct logarithmic law is obeyed for very thin layers. It has been assumed that the slowest step in the oxidation process is electron transfer across the phase boundary. The migration of

ions through a thin layer is rapid and exponentially dependent on the gradient of electric field in the layer.

The laws of cubic and parabolic build-up kinetics have been derived under the following conditions:

- the rate controlling step is the lattice defect migration through the film.
- the driving force for the lattice defect migration is concentration and/or electric field gradient.
- migration rate is directly proportional to the gradient of concentration or potential.

Consequently, these laws are obeyed for relatively thicker films [6].

Accordingly, from the results shown on figures 3-5 and 3-6, it appears that the film on Ni-10Mo could be somewhat thicker than that on pure Ni under the same potentiostatic conditions.

The fact that  $i-t$  dependence is changed after  $\sim 100$  sec and the density of anodic current is considerable suggests a rapid dissolution and/or poor protective properties of the film on Ni-10Mo alloy.

### 3.2 OPEN CIRCUIT POTENTIAL DECAY AND SURFACE REACTIVITY

#### MEASUREMENTS

In order to investigate the nature and relative stability of the passive film on Ni and Ni-Mo alloys, open circuit potential decay (OCPD) and surface reactivity measurements were

performed on Ni and single phase Ni-Mo alloys.

When an electrode is polarized in the passive region and then the regulating circuit is opened, the electrode potential changes spontaneously towards its rest potential exhibiting one or more potential arrests.

It is well known that the observed potential of a metal immersed in a solution represents either an equilibrium potential of a single redox reaction or a mixed potential of several redox reactions. Even if the hydrogen and oxygen-electrode reactions can exist thermodynamically in the solution within the experimentally observed potential range, they will not proceed if there is no dissolved hydrogen and oxygen in the solution. In such a case, it may be assumed that the potential of a metal is determined by some redox reactions concerning either the metal itself or the surface film. It has widely been accepted that the arrest potential of a metal anode is closely related to the equilibrium potential of the surface oxide on the metal, which was verified in some cases with the negligible dissolution of the oxide film [162, 163]. An approximate coincidence of the two may be expected if the rate of dissolution is small. Then the potential arrest should occur near the equilibrium redox potential of a metal anode and the oxide composing the passive film,  $\text{MeO}_n/\text{Me}$  or at some equilibrium potential of two oxides  $\text{MeO}_n/\text{MeO}_m$ . A number of investigators [58, 60, 62, 119, 164] have employed the OCPD technique for studying passivity, the work of Flade [196] being probably one of the first.

The interpretation of potential plateaux on an open circuit potential decay curve of a passive metal, in terms of an equilibrium redox potential of a metal/oxide or the two different oxide species, has difficulties in explaining a slow change of potential during an arrest. The argument could be explained by introducing a nonstoichiometric nature of the oxide film, in which case an equilibrium potential is not necessarily well-defined. Relatively recently, MacDougall and Cohen [72-74] applied the OCPD technique in order to determine the stability of the steady-state oxide on anodized Ni. The observed potential arrests did not correspond to the redox potentials of Ni-oxides. It follows from their conclusions that potential arrest may also be associated with the presence of a defective oxide of the same oxide species, not necessarily with the stoichiometric oxide and its equilibrium redox potential.

### 3.2.1 OPEN CIRCUIT POTENTIAL DECAY OF PASSIVE Ni

The OCPD was studied as a function of anodization time and potential. The potentials of anodization were chosen within the passive potential region, i.e., +300, +500 and +800 mV. The passive film was formed by stepping the potential from the cathodic region to the desired value. The specimen was held at the chosen potential 5, 10 or 30 min. After that, the circuit was opened and the spontaneous change of potential with time was recorded.

For all the anodization conditions, the surface reactivity (see page 40) was estimated immediately after the appearance of the potential spike,  $R_s$ , and 10 min. later,  $R_s'$ . The time elapsed before the spike has been termed the induction time.

Figures 3-7 and 3-8 show the effect of anodization time and potential, respectively.

The results of surface reactivity measurements are given in Table 3-2.

TABLE 3-2  
Results of the Surface Reactivity Measurements  
for Pure Ni

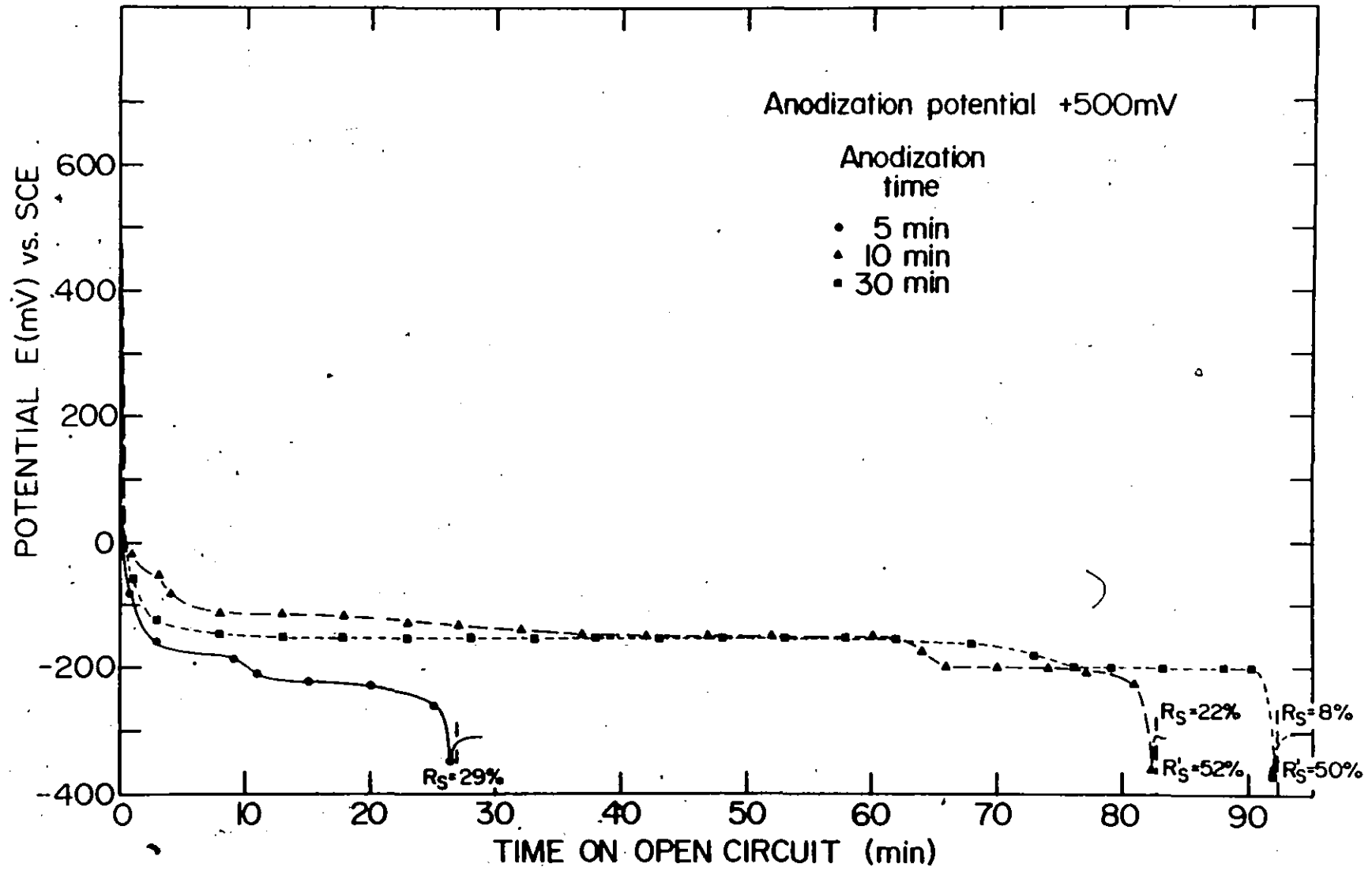
Anodization Potential [mV]	Anodization Time [min.]	Induction Time [min.]	$R_s$ %	$R_s'$ %
+300	5	21	48	91
	10	56	28	77
	30	71	10	67
+500	5	27	29	59
	10	83	22	52
	30	92	8	50
+800	30	324	9	



Open circuit decay of potential as a  
function of anodization time (Ni)

11.

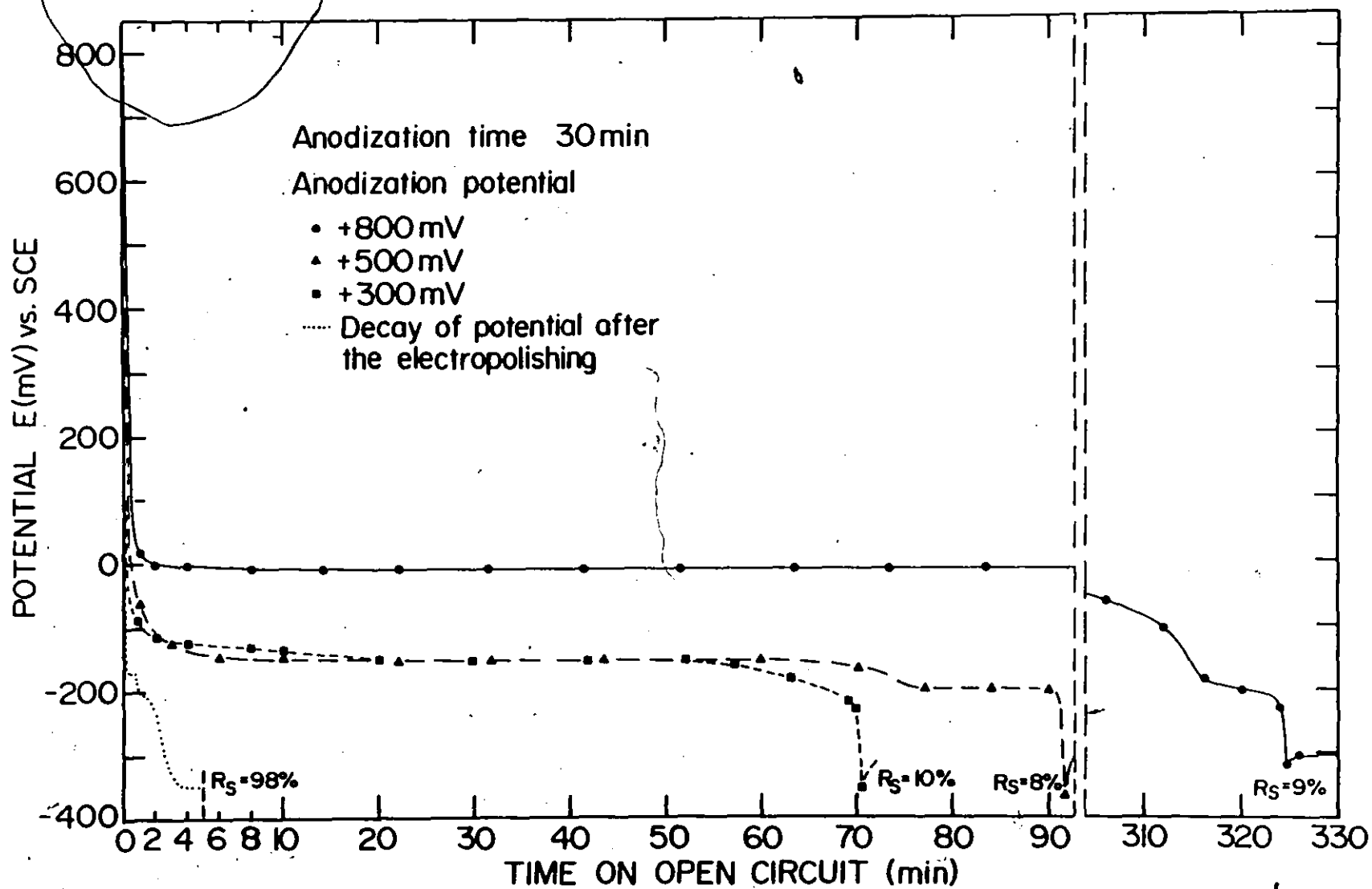
Figure 3-7



Open circuit decay of potential as a  
function of anodization potential (Ni)



Figure 3-8



All decay curves exhibit well resolved potential arrests, even in the case of electropolished Ni (Fig. 3-8). It can be seen that higher anodization potential and longer anodization time give rise to longer duration of the arrests. It is also evident that polarization at +800 mV brings out an additional potential plateau at  $\sim 0$  mV which does not appear on the potential decay from the lower polarization potentials.

The abrupt change of potential occurs always at  $\sim -300$  mV. Characteristic potential plateau appears at  $\sim -150$  mV and  $\sim -200$  mV. The observed potential arrests do not correspond to the equilibrium potentials for the oxides of Ni in the electrolyte of pH 2.8, which are given in Table 3-3. These are calculated on the basis of thermodynamic data [3, 91, 165].

TABLE 3-3

Equilibrium	E [mV] vs SCE (pH = 2.8)
$\text{NiO}_2/\text{Ni}_2\text{O}_3$	+ 1026.5
$\text{Ni}_2\text{O}_3/\text{Ni}_3\text{O}_4$	+ 897.5
$\text{Ni}_2\text{O}_3/\text{NiO}$	+ 624.5
$\text{Ni}_3\text{O}_4/\text{NiO}$	+ 489.5
$\text{NiO}/\text{Ni}$	- 299.5
$\text{Ni}_3\text{O}_4/\text{Ni}$	- 97.5
$\text{Ni}_2\text{O}_3/\text{Ni}$	+ 12.52

The abrupt change of potential at  $\sim -300$  mV corresponds to the redox potential of Ni/NiO electrode in the given solution and the arrest at  $\sim 0$  mV could be due to the Ni/Ni<sub>2</sub>O<sub>3</sub> equilibrium.

From the values of surface reactivity, it appears that the major part of Ni surface remains covered with the passive film during the induction time ( $8\% < R_s < 22\%$ ) but is removed relatively quickly at longer times, in agreement with the findings of McDougall and Cohen [71-76].

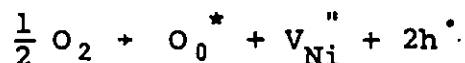
Considering the behaviour of anodized Ni, one could suppose that each observed potential arrest corresponds to a particular degree of imperfection of NiO. NiO is a metal deficit oxide with certain concentration of Ni vacancies. Therefore, each potential plateau might be thought of as the equilibrium potential of Ni/(NiO)<sub>def</sub>. The difference in potential,  $\Delta E$ , between an arrest and the Ni/NiO equilibrium potential would give an estimate of the excess free energy,  $\Delta G$ , associated with the concentration of defects, from the simple relationship  $\Delta G = 2F\Delta E$ , where  $F$  is Faraday constant. The estimated concentrations of Ni-vacancies which could contribute to the observed

$$\Delta E = E_{\text{Ni}/(\text{NiO})_{\text{def}}} - E_{\text{Ni}/\text{NiO}}$$

are however extremely large and difficult to rationalize.

It is interesting to note that polarization of Ni at the end of the passive region ( $+800$  mV) brings out the plateau  $\sim 0$  mV, which might correspond to Ni/Ni<sub>2</sub>O<sub>3</sub> equilibrium. Ni<sub>2</sub>O<sub>3</sub> could, be

considered to be NiO with sufficiently high concentration of point defects (Ni-vacancies). The defect equation



implies that concentration of vacancies,  $[V_{Ni}'']$ , increases with increasing partial pressure of oxygen. Since the condition of electroneutrality requires that

$$[V_{Ni}'' ] = \frac{1}{2} [h^\bullet]$$

where  $[h^\bullet]$  denotes the concentration of positive holes (Ni<sup>3+</sup> ions) in the structure of NiO, then

$$[V_{Ni}'' ] = \frac{k}{4} P_{O_2}^{1/3}$$

Polarization potential of +800 mV might be sufficiently close to the oxygen evolution region and high enough to produce the higher valence state of Ni, i.e., Ni<sup>3+</sup> ions. Therefore the long potential arrest at ~ 0 mV could be due to the presence of highly defective NiO or Ni<sub>2</sub>O<sub>3</sub>.

A further speculation on estimated values of ΔG from observed ΔE is possible assuming other types of imperfections (the film could be strained, cracked or porous) so that the excess free energy could represent strain and/or surface energy but these would also be excessive.

### 3.2.2 OPEN CIRCUIT POTENTIAL DECAY OF Ni-Mo ALLOYS

The effect of the amount of Mo on the relative stability of the passive film, with respect to that formed on pure Ni, was investigated by means of open circuit potential decay and surface reactivity measurements. The results obtained on Ni-5-15Mo alloys are shown on Fig. 3-9. The same figure contains the values of

surface reactivity at different times on open circuit. Each value was estimated for an anodized sample which was then left on the open circuit for a desired period of time, i.e., the measurements do not correspond to successive polarization and opening of the circuit for the same sample.

The potential arrests are not resolved well enough to indicate any definite trend with Mo content.

The equilibrium potentials of Mo-species possibly present, calculated from thermodynamic data [3] are given in table 3-4. These data do not include the equilibrium potentials of the species that depend on the concentration of Mo-ions in the solution.

TABLE 3-4

Equilibrium	E (mV) vs SCE (pH - 2.8)
$\text{MoO}_4/\text{Mo}$	- 13
$\text{MoO}_3/\text{Mo}$	- 350
$\text{MoO}_2/\text{Mo}$	- 479 (- 487)
$\text{H}_2\text{MoO}_4/\text{Mo}$	- 407 (- 409)
$\text{MoO}_4/\text{MoO}_3$	+ 994
$\text{MoO}_4/\text{MoO}_2$	+ 454
$\text{MoO}_3/\text{MoO}_2$	- 67 (- 87)
$\text{H}_2\text{MoO}_4/\text{MoO}_2$	- 258 (- 269)
$\text{MoO}_4/\text{H}_2\text{MoO}_4$	+ 1190



During the first 5 min on open circuit the rates of potential decay in in the order

$$\frac{dE}{dt}_{15Mo} > \frac{dE}{dt}_{10Mo} > \frac{dE}{dt}_{5Mo} > \frac{dE}{dt}_{Ni}$$

with the corresponding surface reactivities (5 min)

$$R_s(15Mo) > R_s(10Mo) > R_s(5Mo) > R_s(Ni)$$

indicating that the film on alloys breaks down faster than the passive film on Ni, the rate of breakdown being proportional to the Mo content.

The surface reactivity data obtained at various times suggest that up to the abrupt change of potential of Ni-electrode the oxide film on Ni is the most stable one. After that the situation is reversed: at longer times (17 min after the appearance of potential spike of Ni) the surface reactivity values are in the order

$$R_s(Ni) > R_s(5Mo) > R_s(10Mo) > R_s(15Mo).$$

It appears that the rate of film breakdown on open circuit increases monotonically with Mo content while the rate of its removal at longer times is inversely proportional to the Mo content. No sharp change of potential was observed for the alloys even after 24 h on the open circuit, except slight fluctuations of potential ( $\pm 20$  mV).

Open circuit decay of potential as a function  
of Mo content (5%, 10%, 15% Mo)

20

Figure 3-9

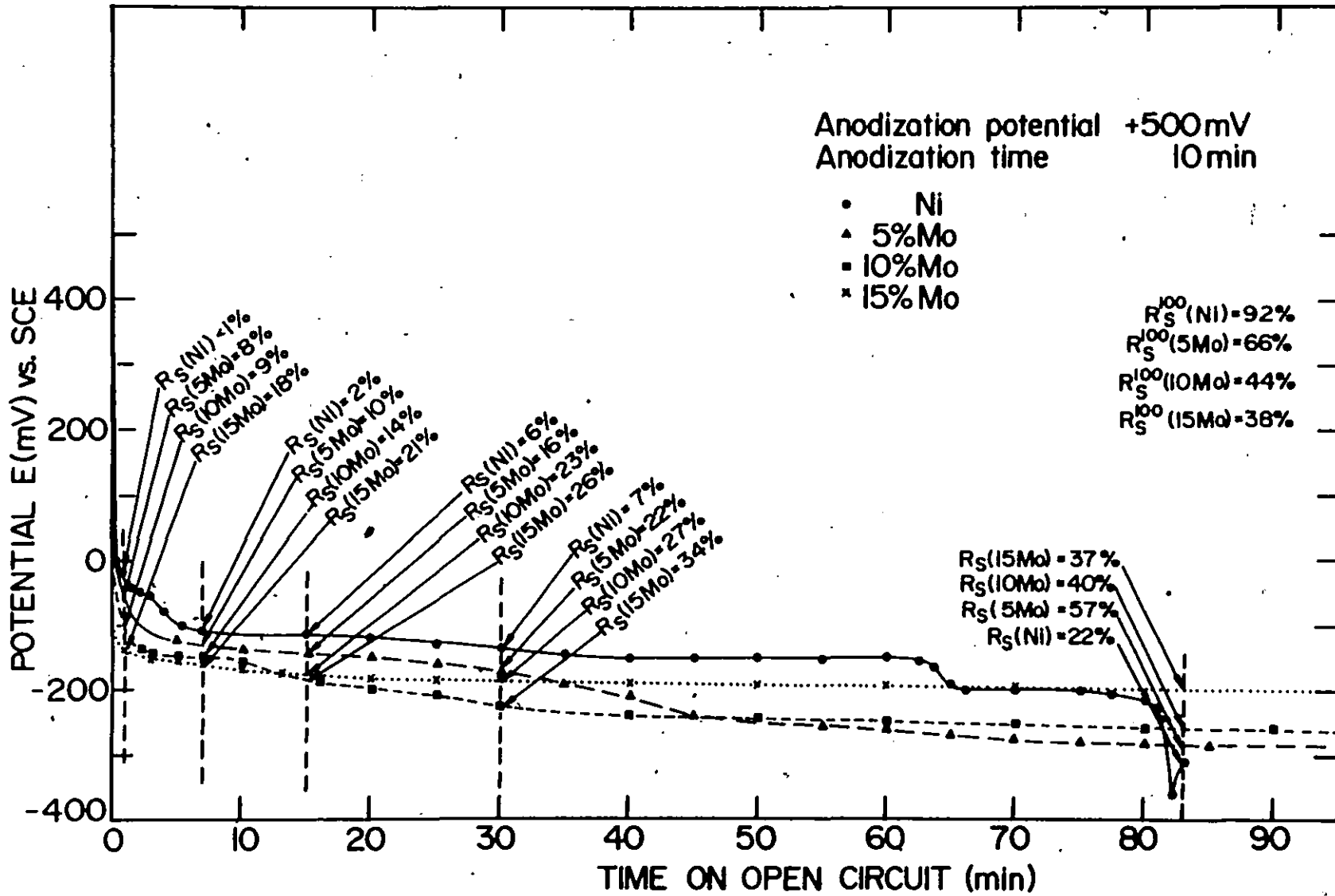
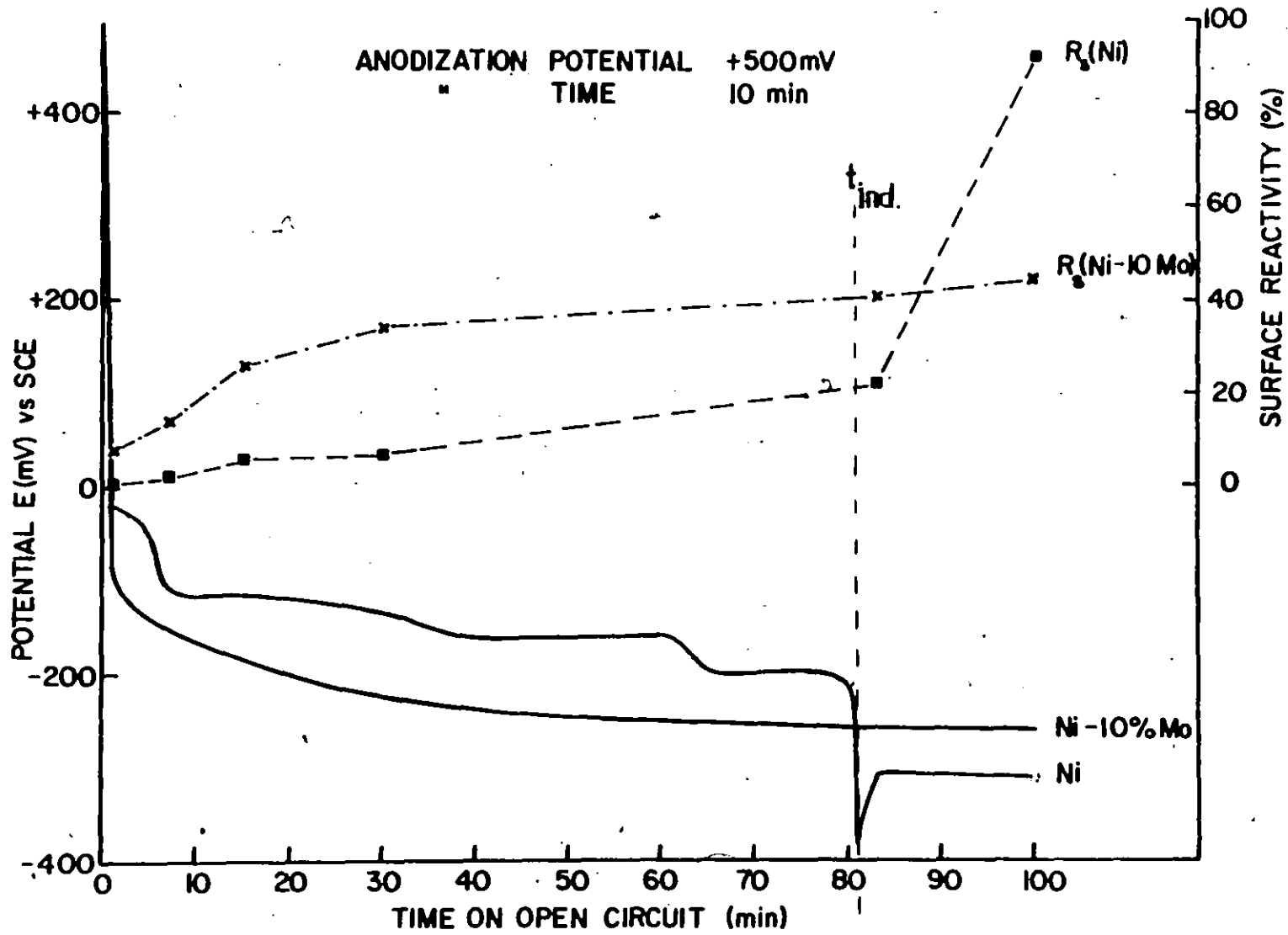


Fig. 3-9

Open circuit decay profile and change of  
surface reactivity for Ni and Ni-10Mo alloy

Figure 3-10



The change of potential and surface reactivity of Ni and Ni-10Mo alloys with time is given on Fig. 3-10 indicating a gradual removal of surface film on the alloy and almost completely covered surface of Ni during the induction time. Only the film on Ni is removed rapidly from the surface at longer times.

If the destruction of the passive state is defined in terms of the time required for the potential to decay from the passivating potential to the active potential then it could be concluded that the passive film on Ni provides better corrosion resistance than the film formed on Ni-Mo alloys. The fact that surface reactivity for these alloys increases faster than that for Ni at  $t < t_{ind}$  also indicates a faster breakdown of the film on alloys at open circuit. Once the film breaks down its removal involves active metal dissolution from oxide free or defective areas and a cathodic reduction (such as  $H_2$  evolution) on the remaining film-covered surface. A slower removal of the film from alloys than that from Ni at  $t > t_{ind}$  could be explained in terms of the effect of Mo being such that

- (i) it increases the polarization associated with the active dissolution (by decreasing the exchange current density) which leads to slower oxide undermining at  $t > t_{ind}$  and/or
- (ii) the cathodic reaction might be slowed down with resulting decrease of metal dissolution and corresponding lower rate of reactivation.

### 3.3 CATHODIC REDUCTION OF ANODIZED Ni-Mo ALLOY

An open circuit potential decay (OCPD) experiment is

fundamentally equivalent to the cathodic reduction of the passive film at which the externally imposed current is zero, thus a small and unknown time-dependent reduction current is used for the reduction of the passive film. Since the charge stored in the film is a measure of the film thickness, the charge consumed for the galvanostatic reduction of a passive film could provide information on the film thickness, provided that the reduction proceeds with sufficiently high current efficiency and that proper assumptions are made about the valence state of the components in the film as well as about the uniformity of the film removal.

### 3.3.1 CATHODIC REDUCTION OF Ni-13Mo ALLOY

Fig. 3-11 shows the cathodic galvanostatic charging curves and the open circuit potential decay of Ni-13Mo alloy that had been previously anodized at +500 mV for 1 hour.

When a cathodic current was used for the film reduction, the sample was cathodically charged for 30 min, left on open circuit for 2 min and then the potential was stepped back to the value at which the film had been previously formed, i.e., +500 mV. Therefore, the surface reactivities given on Fig. 3-11 were obtained after 32 min of potential decay in each case.

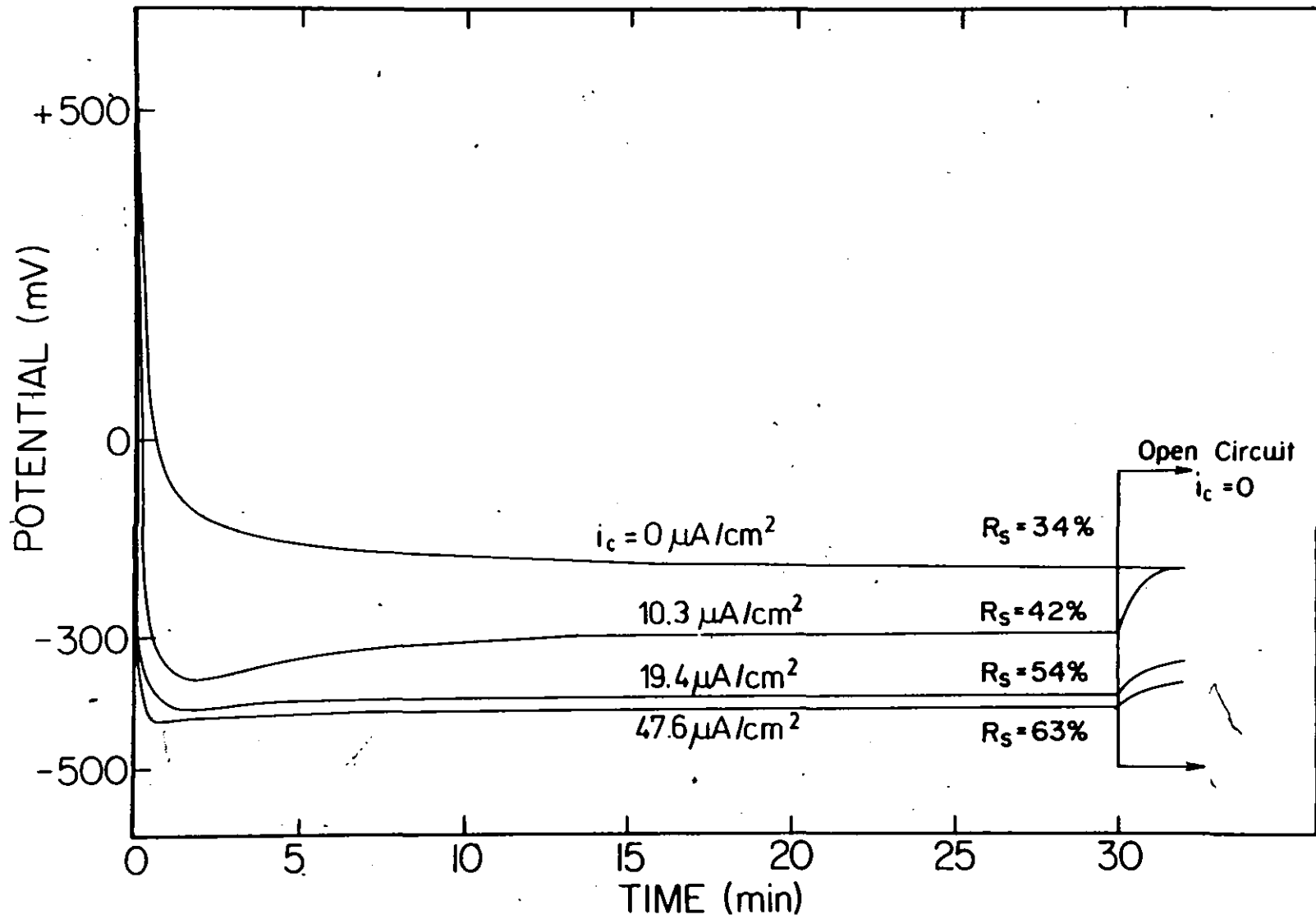
It is evident that both the rate of potential decay and the surface reactivity increase by increasing the cathodic current.

The values of surface reactivity as well as a potential

Galvanostatic cathodic charging of  
anodized Ni-13Mo



Fig. 3-11



shift towards more positive values on open circuit after the cathodic reduction indicate that 30 min of cathodic charging does not remove the surface film. The values of surface reactivity also show that the current efficiency for the film removal is relatively low, e.g.,  $\sim 86 \text{ mC/cm}^2$  leads to a less than 30% increase of surface reactivity with respect to the value obtained after the same time on open circuit.

The possible side processes during cathodic reduction are: reduction of oxygen adsorbed on the surface during anodic passivation, hydrogen evolution and self-dissolution of the layer.

Overestimation results from the first two effects, underestimation from the last one.

By comparing the values of surface reactivity after OCPD and those obtained after cathodic reduction it can be concluded that current efficiency for the film removal is very low and the side reactions could not be neglected here. Therefore conversion of the cathodic charge into the film thickness would have no meaning.

### 3.4 DISSOLUTION DURING ANODIC POLARIZATION AT

#### A FIXED POTENTIAL IN THE PASSIVE REGION

In order to elucidate the role played by alloying components in the formation and growth of passive layers on alloys it is essential to know the dissolution behaviour of an alloy and its individual components under the conditions of passivation.

### 3.4.1 DISSOLUTION OF Ni-13Mo ALLOY DURING POLARIZATION AT +500 mV.

Fig. 3-12 gives the time dependence of the dissolution rates of Ni and Mo during polarization of Ni-13Mo alloy at +500 mV. The results were obtained by atomic absorption spectroscopy of the solution aliquots obtained during potentiostatic polarization. It is evident that both dissolution rates change significantly with time during the first 2 hours of passivation.

Fig. 3-13 shows the selectivity coefficient of Mo,  $Z_{Mo}$ , calculated from the amounts of Ni and Mo in the solution, i.e.,

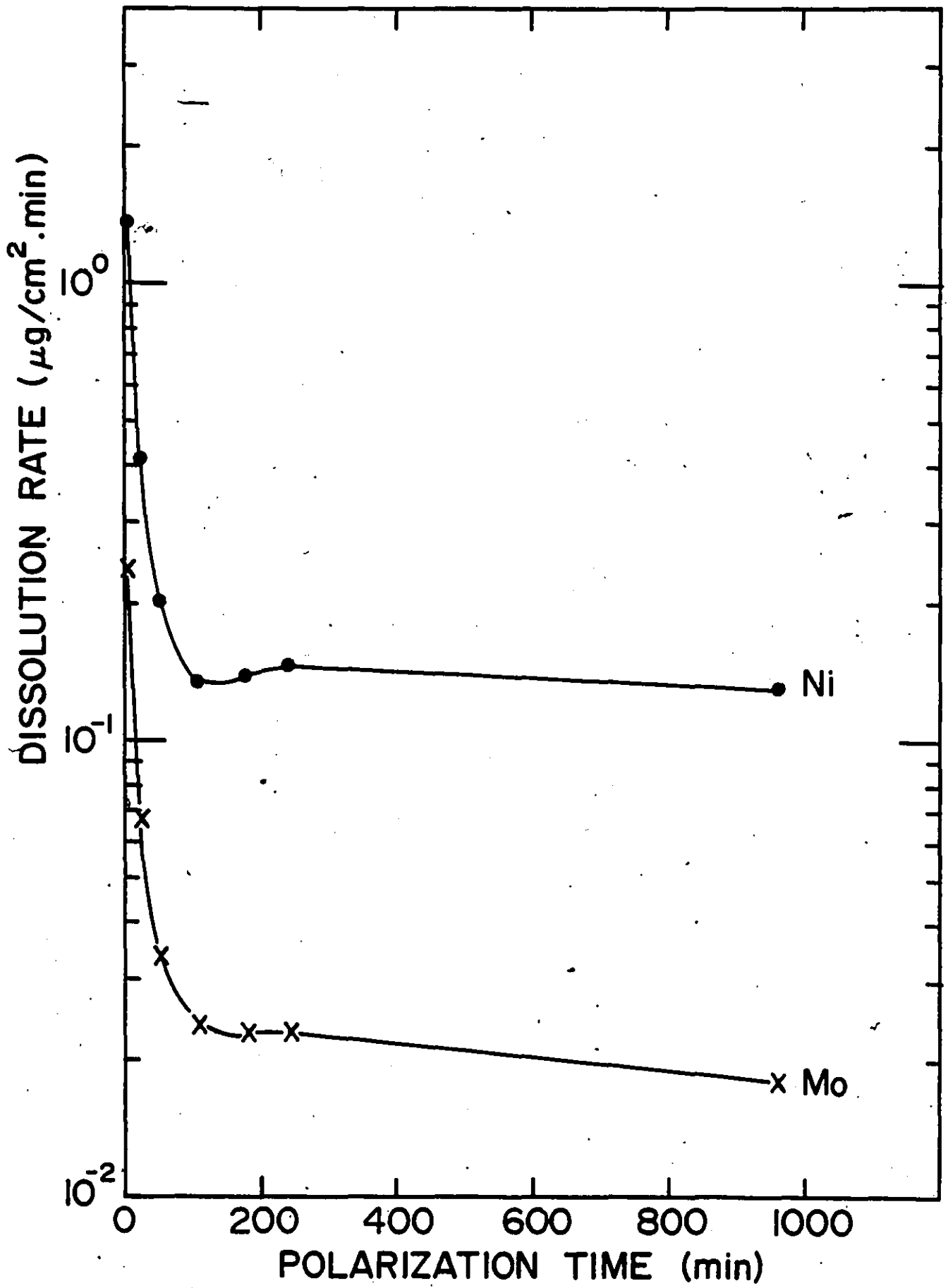
$$Z_{Mo} = \frac{\frac{Mo}{Ni} \text{ solution}}{\frac{Mo}{Ni} \text{ alloy}}$$

The selectivity coefficient of Mo shows by what factor the ratio of the concentrations of Mo to Ni in dissolution products differs from the actual ratio in the alloy. When  $Z_{Mo} = 1$  the components of the alloy dissolve uniformly. When  $Z_{Mo} > 1$  the solution is enriched in Mo, indicating its preferential dissolution. At  $Z_{Mo} < 1$  the solution is impoverished in Mo.

Table 3-5 summarizes the results obtained from the dissolution analysis and the charge measurements during potentiostatic passivation of Ni-13Mo alloy.

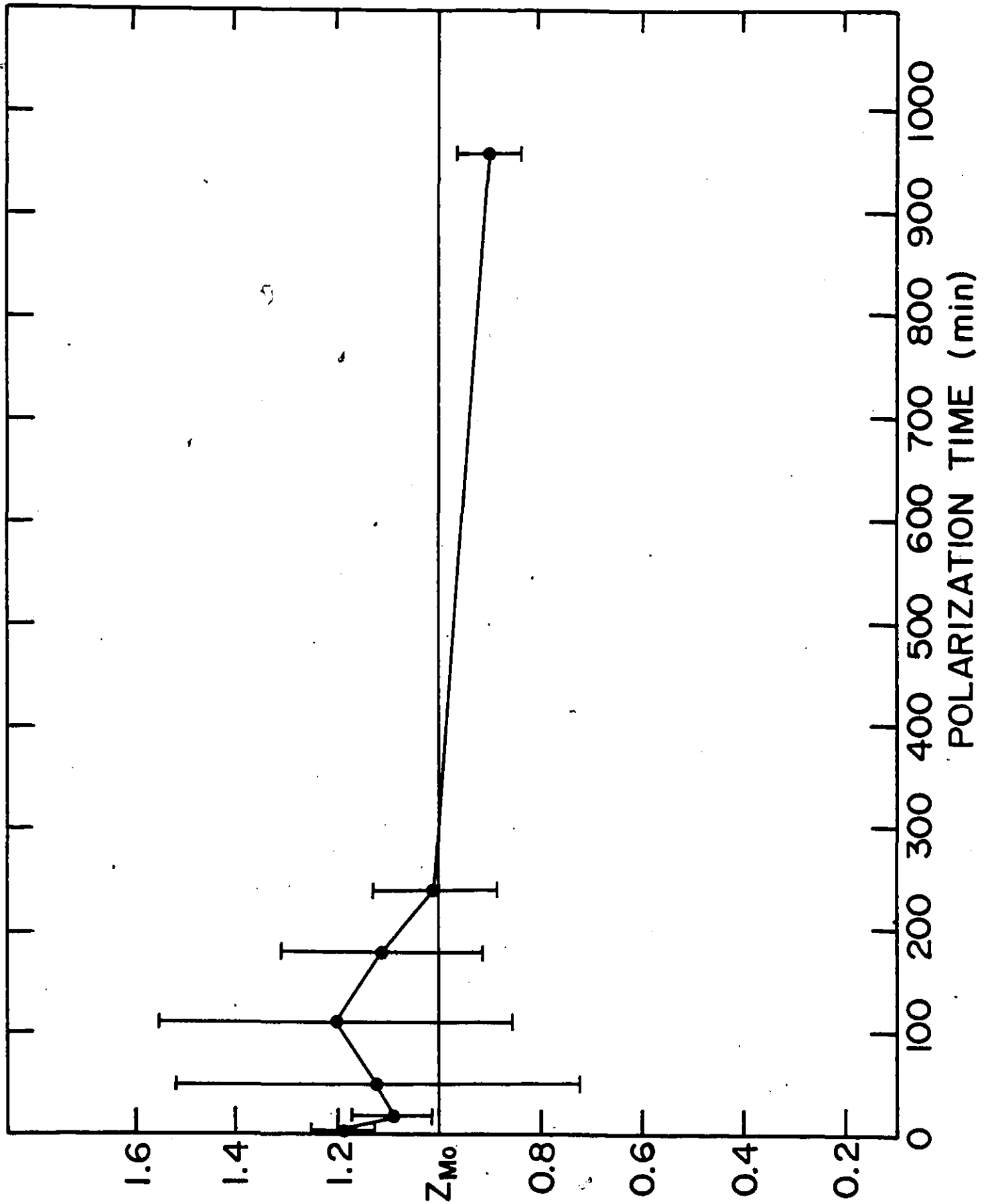
It is not evident from fig. 3-13 that  $Z_{Mo}$  changes with time. The sharp changes are clearly correlated with the changes of the partial dissolution rates of the alloy. Although the error that comes from the standard deviation in atomic absorption data

Dissolution rate of Ni and Mo as a function  
of anodization time (Ni-13Mo)



Selectivity coefficient of Mo as a function  
of anodization time (Ni-13Mo)

Fig. 3-13



Calculated and measured dissolved amounts  
of Ni and Mo as a function of anodization time



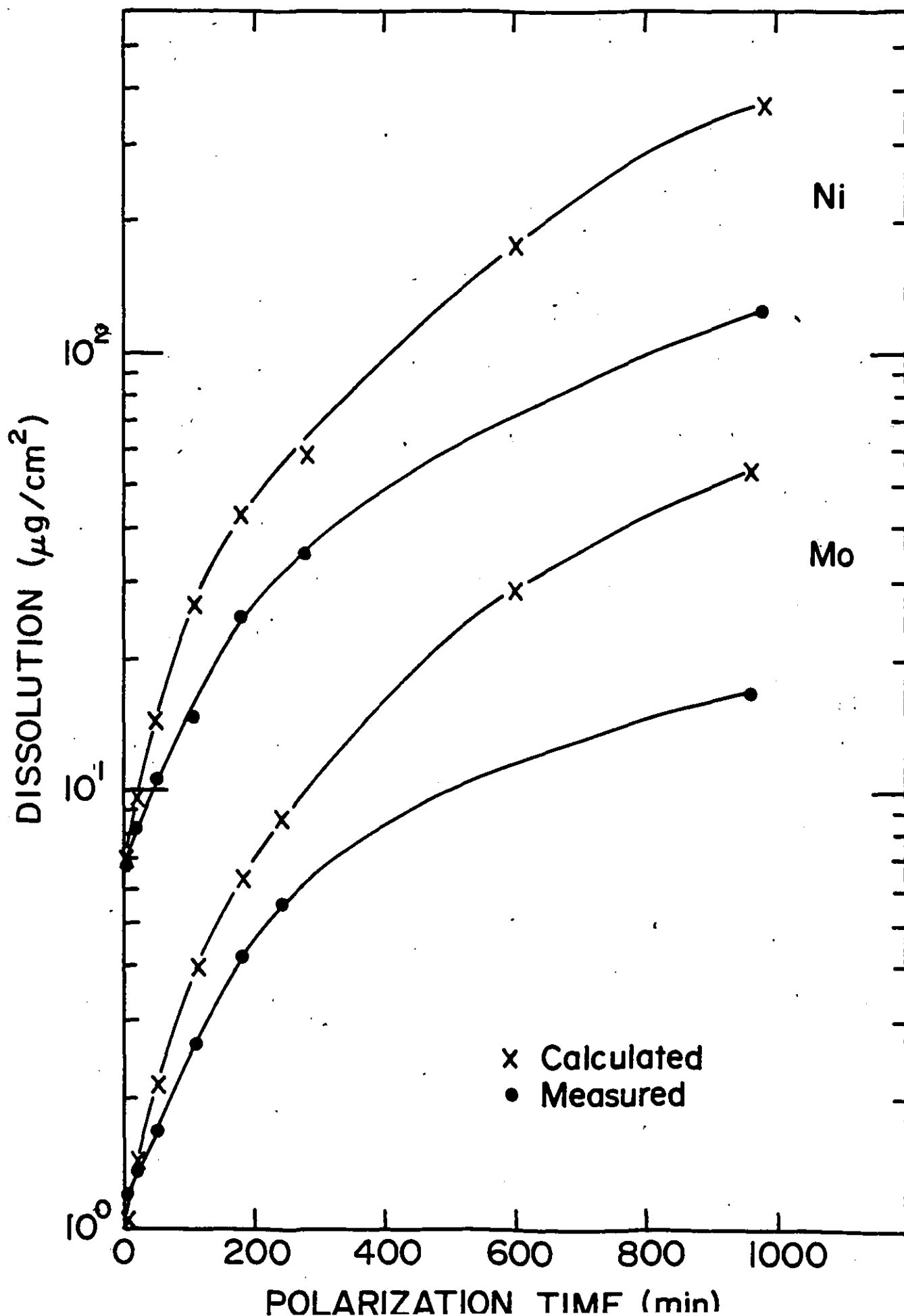


TABLE 3-5

DISSOLUTION OF NI AND Mo FROM NI-13 Mo ALLOY DURING POTENTIOSTATIC POLARIZATION AT +500 mV

Polarization Time [min]	Charge Q $\pm$ [C/cm <sup>2</sup> ]	Ni-Dissolved [ $\mu$ g/cm <sup>2</sup> ]	Ni-Calculated From Q [ $\mu$ g/cm <sup>2</sup> ]	$\Delta$ Ni = N <sub>film</sub> [ $\mu$ g/cm <sup>2</sup> ]	Mo-Dissolved [ $\mu$ g/cm <sup>2</sup> ]	Mo-Calculated From Q [ $\mu$ g/cm <sup>2</sup> ]	$\Delta$ Mo = M <sub>film</sub> [ $\mu$ g/cm <sup>2</sup> ]	$\left(\frac{Mo}{Ni}\right)_{sol.}$	$\left(\frac{Mo}{Ni}\right)_{film}$	$\frac{\left(\frac{Mo}{Ni}\right)_{sol}}{\left(\frac{Mo}{Ni}\right)_{alloy}}$	$\frac{\left(\frac{Mo}{Ni}\right)_{film}}{\left(\frac{Mo}{Ni}\right)_{alloy}}$	ESTIMATED ACCUMULATION RATE IN THE FILM			
												Ni [ $\frac{\mu g}{cm^2 \cdot min}$ ]	Mo [ $\frac{\mu g}{cm^2 \cdot min}$ ]	Ni Layers of NiO/min	Mo Layers of MoO <sub>3</sub> /min
5	0.0187	6.72 $\pm 0.14$	6.854 $\pm 0.968$	0.134 $\pm 0.208$	1.19 $\pm 0.049$	1.022 $\pm 0.010$	-	0.18 $\pm 0.010$	-	1.19 $\pm 0.07$	-	0.027 $\pm 0.042$	-	0.24	-
20	0.0403	8.23 $\pm 0.34$	9.624 $\pm 0.096$	1.394 $\pm 0.436$	1.35 $\pm 0.05$	1.434 $\pm 0.014$	0.084 $\pm 0.064$	0.16 $\pm 0.012$	0.06 $\pm 0.06$	1.09 $\pm 0.08$	0.40 $\pm 0.40$	0.070 $\pm 0.002$	0.004 $\pm 0.0032$	0.64	0.046
50	0.0597	10.07 $\pm 2.26$	14.256 $\pm 0.142$	4.186 $\pm 3.502$	1.68 $\pm 0.05$	2.125 $\pm 0.021$	0.445 $\pm 0.071$	0.17 $\pm 0.060$	0.10 $\pm 0.10$	1.12 $\pm 0.40$	0.71 $\pm 0.67$	0.084 $\pm 0.070$	0.009 $\pm 0.014$	0.77	0.097
110	0.1110	14.78 $\pm 3.28$	26.506 $\pm 9.265$	17.726 $\pm 3.545$	2.66 $\pm 0.06$	3.952 $\pm 0.040$	1.292 $\pm 0.100$	0.18 $\pm 0.053$	0.11 $\pm 0.04$	1.20 $\pm 0.35$	0.74 $\pm 0.26$	0.107 $\pm 0.032$	0.012 $\pm 0.0009$	0.97	0.128
180	0.1780	24.91 $\pm 4.02$	42.506 $\pm 0.425$	17.596 $\pm 4.445$	4.18 $\pm 0.09$	6.366 $\pm 0.063$	2.186 $\pm 0.153$	0.17 $\pm 0.030$	0.12 $\pm 0.04$	1.12 $\pm 0.20$	0.83 $\pm 0.03$	0.098 $\pm 0.024$	0.012 $\pm 0.0008$	0.89	0.130
240	0.2420	34.57 $\pm 3.14$	57.789 $\pm 0.578$	23.219 $\pm 12.086$	5.50 $\pm 0.13$	8.615 $\pm 0.086$	3.115 $\pm 0.216$	0.16 $\pm 0.018$	0.13 $\pm 0.03$	1.06 $\pm 0.12$	0.90 $\pm 0.20$	0.097 $\pm 0.015$	0.013 $\pm 0.0009$	0.88	0.140
960	1.527	125.16 $\pm 8.44$	364.648 $\pm 3.646$	239.488 $\pm 12.086$	16.89 $\pm 0.19$	54.361 $\pm 0.544$	37.471 $\pm 0.734$	0.13 $\pm 0.010$	0.16 $\pm 0.01$	0.90 $\pm 0.07$	1.05 $\pm 0.44$	0.249 $\pm 0.012$	0.040 $\pm 0.0008$	2.28	0.420

introduces a fairly large error in  $Z_{Mo}$ , it is possible that during the initial period of polarization there is a tendency of preferential dissolution of Mo. At longer anodization times  $Z_{Mo}$  falls below 1 indicating an enrichment of the surface film by Mo.

From the charge,  $Q$ , consumed during polarization, it is possible to estimate the amounts of Ni and Mo that would be present in the solution under the following assumptions:

- the total charge is consumed only by the dissolution of both components,
- the dissolution ratio of the components corresponds to their ratio in the alloy, i.e., there is no preferential dissolution,
- Ni and Mo enter the solution as  $Ni^{2+}$  and  $Mo^{6+}$ .

Figure 3-14 gives the dissolved amounts of Ni and Mo experimentally observed and the corresponding calculated values.

From the observed total charge and the amount of each component dissolved during polarization at a fixed potential, the amount of Ni and Mo accumulating on the surface can be estimated. The difference between the estimated and observed dissolved amount is a measure of surface accumulation. Table 3-5 gives the accumulation rates of Ni and Mo on the surface as  $\mu g/cm^2$  min. The accumulation rates are also expressed in terms of layers/min of  $MoO_3$  and  $NiO$ , where the layer growth rates have been estimated using the interatomic spacings of  $NiO$  and  $MoO_3$ . These results suggest much thicker films on Ni-13 Mo alloy than the values reported for pure Ni, i.e., 6 - 20 Å, in the same solution [71-75].

The process of dissolution at initial stages of passivation is governed by the dissolution properties of the components in the alloys and the mechanism of film formation. The mechanism of growth and the properties of the film are the factors that control the dissolution of the components at later stages of anodization.

The question that naturally arises in the cases when  $Z_{Mo} < 1$  (depletion of dissolution products in Mo) is whether it is the result of the adsorption of Mo ions from the solution onto the active areas of the surface (the defects in the passive film) or a consequence of the slowing down of the passage of Mo into the solution from the film. At initial stages of passivation there is a selective dissolution of Mo which might be expected since Mo undergoes transpassive dissolution at the anodization potential applied (+500 mV). The values of  $Z_{Mo} > 1$  are maintained probably until the film is fully formed on the alloy surface. During that period of time Mo can to a certain extent display its individual properties, one of which is a high dissolution rate. This would further suggest that the composition and structure of the passive layer on Ni-Mo alloys depend on the time of its formation.

### 3.5 AUGER ELECTRON SPECTROSCOPY AND DEPTH PROFILING

AES with depth profiling was applied to anodized Ni and Ni-13Mo alloy in order to determine the composition of the film and estimate the film thickness as a function of anodization time, the time on open circuit, and the solution pH.

The technique was also used in order to clarify the influence of the alloy sample pretreatment on the composition of the surface which is then subjected to a fixed passivation potential.

### 3.5.1 AES ANALYSIS OF THE PASSIVE FILM ON Ni

Figs. 3-15, 3-16 and 3-17 show the AES spectrum of passive Ni, anodized 48 h at +500 mV and the corresponding depth profiles as Auger peak-to-peak heights (APPH) and atomic concentrations (at %) as a function of sputtering time, respectively.

The depth profile (Figs. 3-17 and 3-18) of anodized Ni was obtained by employing a model for the quantitative analysis of thin surface layers developed by Mitchell [167]. The model combines Davis' [145] and Pons' [197] approach.

The composition profiles in depth measured by AES involve in part the composition of subsequent layers since the escape depth of Auger electrons is 5 - 30 Å. Pons et al. [166] proposed a differential method to obtain the exact composition of successive layers by eliminating the influence of subsequent layers.

According to Davis [145] the concentration of a component X in the surface,  $C_x$  (at %), can be expressed as follows:

$$C_x = \frac{\frac{I_x}{S_x} \times 100}{\sum_n \frac{I_n}{S_n}} \quad (3-7)$$

where  $S_x$  - relative sensitivity factor

$I_x$  - magnitude of the Auger derivative mode signal from element  $x$  (Auger peak-to-peak height APPH)

The APPH for a component  $x$ ,  $I_x$ , as given by Pons [197] is

$$I_x = \sum_{i=0}^{\infty} \alpha_x k_x^i N(x, i) \quad (3-8)$$

where  $\alpha_x$  - sensitivity coefficient (a function of ionization cross section for the particular transition, of the probability that the ionized atom will decay through that transition and of the geometry of the system

$k_x^i$  - attenuation or absorption coefficient (reflects the probability of production and escape of Auger electron from the layer  $i$  compared to that for the topmost layer ( $i=0$ ))

$N(x, i)$  - fraction of element  $x$  in the layer  $i$ .

The relation between  $S_x$  and  $\alpha_x$  can be obtained by combining equations (3-7) and (3-8) and by assuming a homogeneous sample, in which case  $N(x, i)$  becomes independent of  $i$  and equal to  $C_x$ . It follows that

$$S_x = \frac{\alpha_x}{1 - k_x} \quad (3-9)$$

and consequently (3-8) becomes

$$I_x = S_x (1 - k_x) \sum_{i=0}^{\infty} k_x^i N(i, x). \quad (3-10)$$

The attenuation coefficient,  $k_x$ , is a function of the mean free path (mfp) of primary electrons,  $\Lambda_p$ , and the escape depth of Auger electrons,  $\Lambda_s$ :

$$k_x = \exp\left[-\frac{1}{\Lambda_p \cos \theta_p} + \frac{1}{\Lambda_s \cos \theta_s}\right] \quad (3-11)$$

Where  $\theta_p$  and  $\theta_s$  are the primary electron beam angle off normal ( $30^\circ$ ) and the emitted Auger electron beam angle ( $42^\circ$ ) respectively.

$\Lambda_p$  and  $\Lambda_s$  are the electron absorption path lengths (mean free paths, mfp) for the primary and secondary (Auger) electrons. The mfp of Auger electrons may be approximated [147,148] to  $\Lambda_s = K\sqrt{E_s}$  where  $E_s$  is their energy and  $K$  is a constant. While appropriate values of  $\Lambda_p$  are not available [147], for the large ratio of the primary beam energy to the Auger energies used in this work,  $\Lambda_p \gg \Lambda_s$ , and thus the term  $\frac{1}{\Lambda_p \cos \theta_p}$  may be dropped from equation (3-11), approximating

$$k_x = \exp\left[-\frac{1}{K\sqrt{E_s} \cos 42^\circ}\right] \quad (3-12)$$

Fig. 3-15

AES spectrum of passive film on Ni (+500 mV, 48 h.  
pH 2.8)

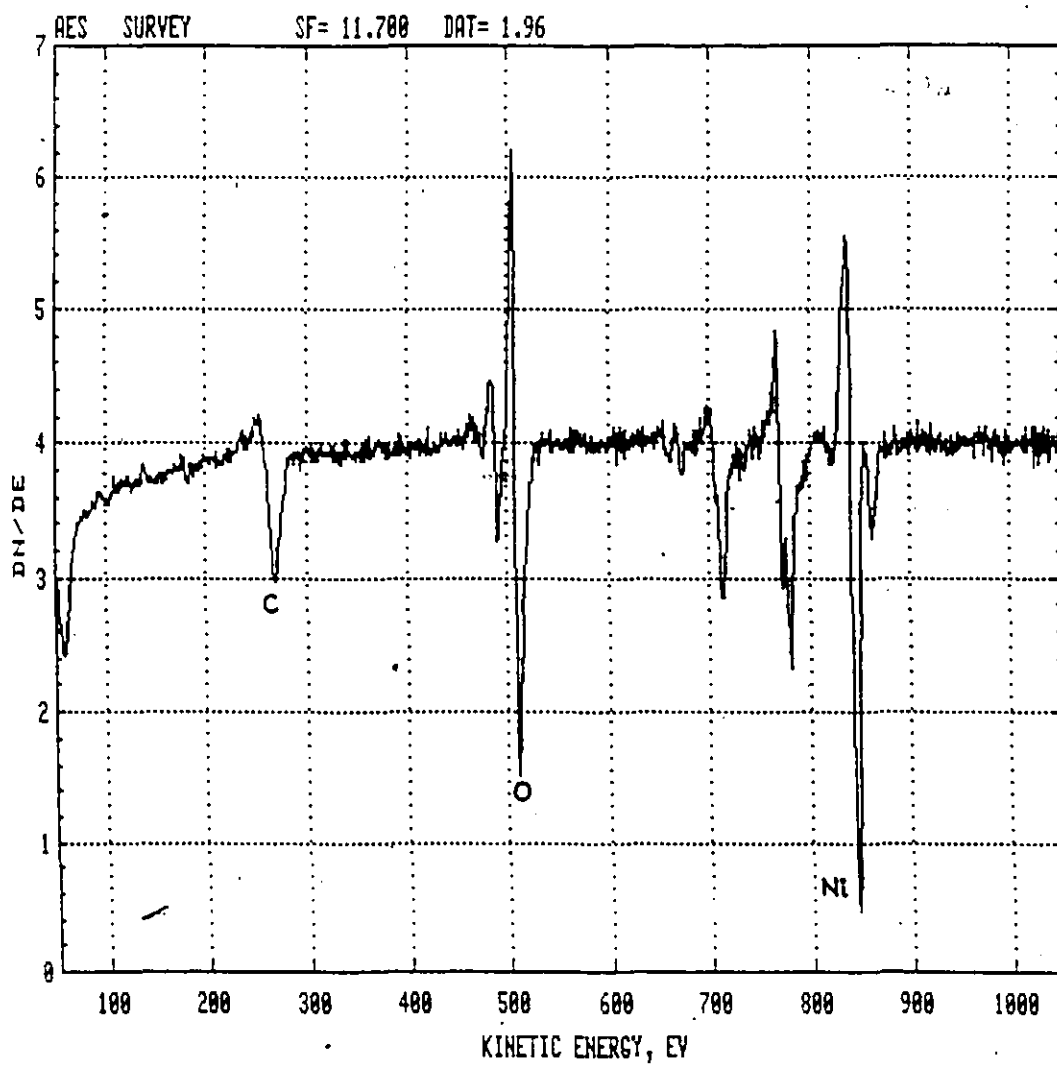




Fig. 3-16

AES profile of passive film on Ni (+500 mV), 4h h.,  
pH 2.8)

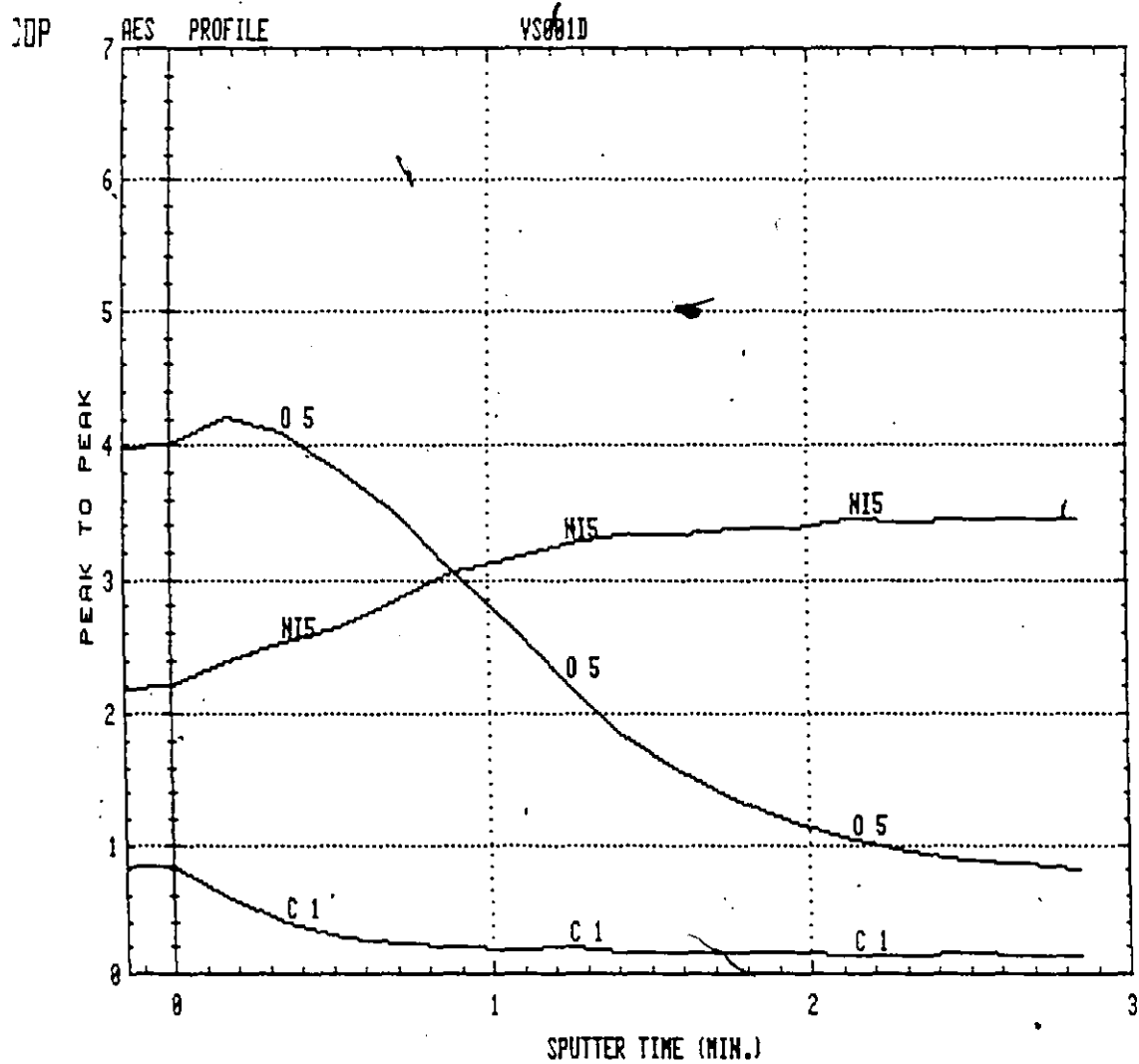


Fig. 3-17

AES profile of passive film on Ni (+500 mV, 48 h.  
pH 2.8)

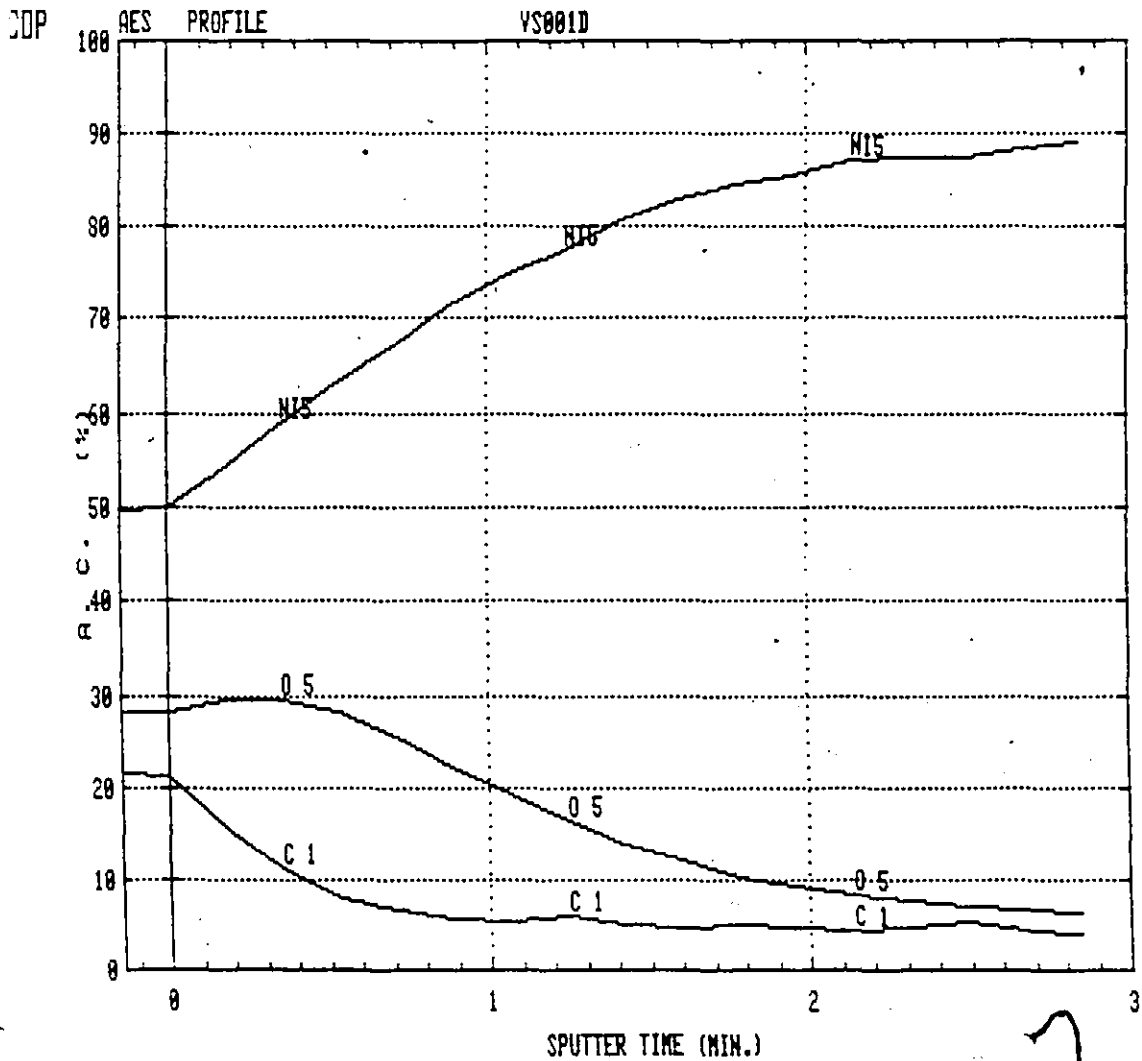
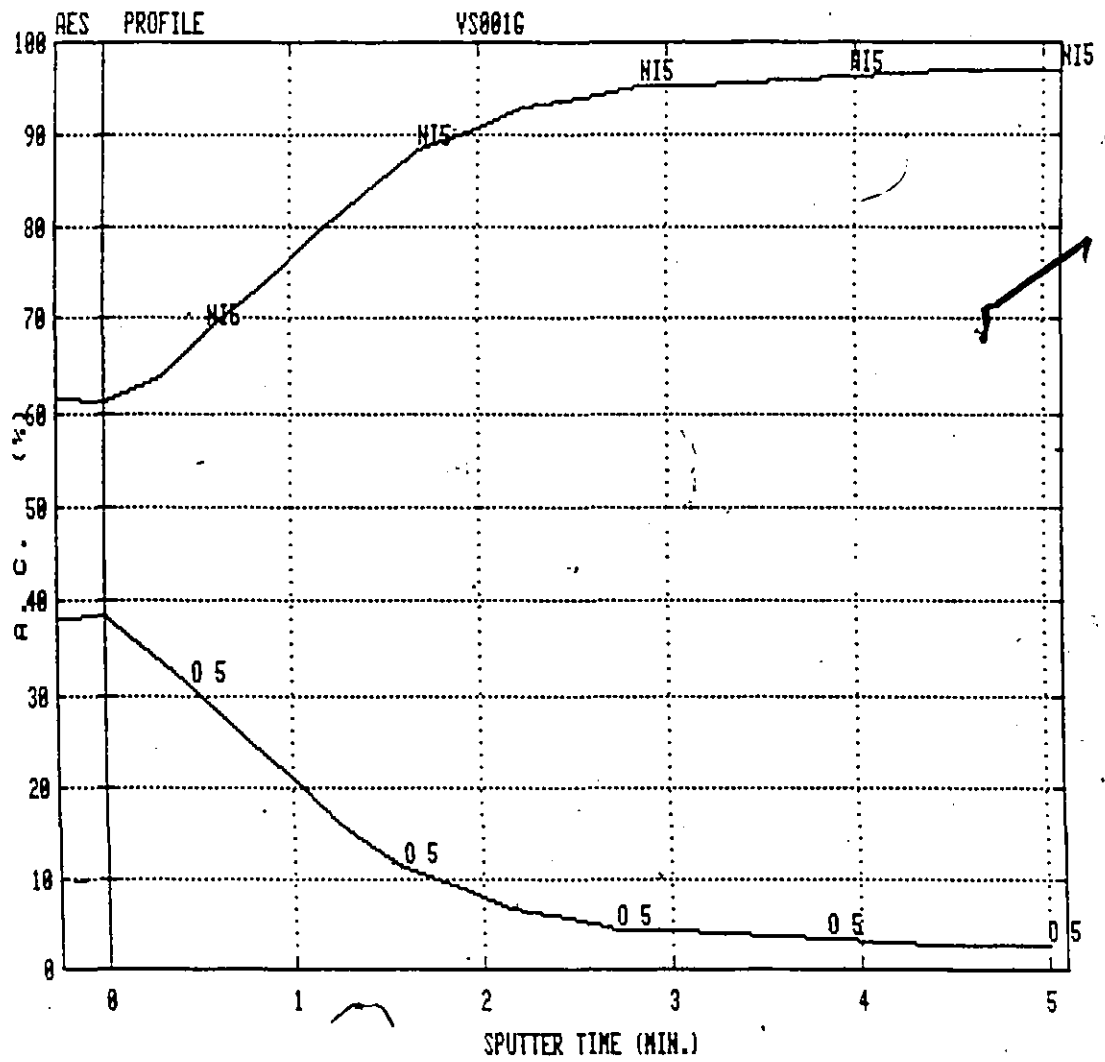


Fig. 3-18

AES profile of passive film on Ni (+500 mV, 48 h.  
pH 2.8) - carbon line removed



Knowing independently the oxide thickness, equation (3-10) can be used to determine  $k_x$  and then equation (3-12) to determine  $K$ . For Ni-oxide, the value of  $K$  is 0.19, when  $A_s$  is expressed in terms of atomic monolayers and  $E_s$  in eV. (The value of 0.19 for  $K$  could be used for other oxide systems if 1 monolayer in a {100} plane =  $1.6 \times 10^{15}$  atoms/cm<sup>2</sup> corresponds to  $\sim 2.1$  Å). By using equations (3-10) and (3-12) and the relative sensitivity factors obtained from thick film standards, it is possible to calculate relative signal intensities for a thin film system, assuming uniform layer by layer sputtering.

The analysis performed on anodized Ni (Fig. 3-17 and 3-18) with the sputtering rate of 2 layers/min, shows that 48 h of anodization at +500 mV produces a 12 - 16 Å film, assuming NiO with 2.1 Å/layer.

The carbon profile shown on Fig. 3-17 could be removed by ignoring the carbon signal and considering the presence of Ni and O only. In doing so C is effectively distributed proportionally to the other elements present, i.e., Ni and O. The composition profile obtained in this manner is given in Fig. 3-18.

It is evident that the passive film on Ni does not thicken with anodization time, i.e., the films formed under the same conditions of the solution pH and the potential for short periods of time were reported to be less than 20 Å thick [71-76].

### 3.5.2 AES ANALYSIS OF THE FILMS ON Ni-13 Mo ALLOY

The model applied for the quantitative analysis of the

passive film on Ni was not applicable for Ni-Mo alloys for several reasons. The experimental determination of the relative sensitivity factor,  $S_x$ , was not possible since the composition of the film to be used as a standard was not known. Instead of using elemental sensitivity factors for Ni and Mo [145], the sensitivity factor for Mo was determined from a thick, air-formed film on pure Mo, which was assumed to be composed of a layer of  $\text{MoO}_2$  at the metal/film interface and a layer of  $\text{MoO}_3$  covering it. The sensitivity factor for Ni was taken to be the same one used for the analysis of the passive film on Ni ( $\text{NiO}$ ). Two other important factors that prevented a quantitative analysis in the case of Ni-Mo alloys are a significant preferential sputtering of Ni and changes of Mo Auger peak (a peak shift and shape change) during the sputtering process. Therefore, the results presented should not be considered as quantitative, although a number of conclusions could be drawn by comparison of different AES profiles obtained under the same experimental conditions. The sputtering rate was estimated to be approximately 2 layers/min.

#### 3.5.2.1 THE EFFECT OF SAMPLE PREPARATION ON THE COMPOSITION OF THE SURFACE OF Ni-13Mo

Although a mechanical polishing followed by cathodic reduction in the cell had been adopted as a pretreatment procedure for the alloy samples, the influence of electropolishing and cathodic reduction on the composition of the 'starting' surface was examined by AES.

The AES profiles given on Figs. 3-19, 3-20 and 3-21 correspond to an electropolished surface, electropolished and cathodically reduced surface and the one that was subjected to cathodic reduction only, in the order mentioned. In all three cases the samples were first mechanically polished to 1  $\mu\text{m}$ .

The elemental composition of the surface before sputtering is given in Table 3-6.

Using 75% reduction in the oxygen concentration profile as a measure of the film thickness, the films, (probably due to air exposure) are less than 10  $\text{\AA}$  thick in all three cases.

Table 3-6

	Ni at %	Mo at %	O at %	( $\frac{\text{Mo}}{\text{Ni}}$ ) surf.	$\left[ \frac{(\text{Mo/Ni}) \text{ surface}}{(\text{Mo/Ni}) \text{ alloy}} \right]$
Electro-pol.	55.0	3.5	41.5	0.064	~ 0.7
Electro-pol. + cath. red.	68.0	3.0	29.0	0.044	~ 0.5
Cathod. red.	63.0	6.0	31.0	0.095	~ 1.0

The ratio (Mo/Ni) surface / (Mo/Ni) alloy (Table 3-6) shows that the composition of mechanically polished surface followed by cathodic reduction corresponds to the nominal composition of Ni-13 wt % Mo (8.2 at % Mo). Electropolishing leaves the surface depleted in Mo. The effect of cathodic reduction (-2.0 V) remains unclear (it seems

Fig. 3-19

AES profile of Ni-13 Mo following electropolishing

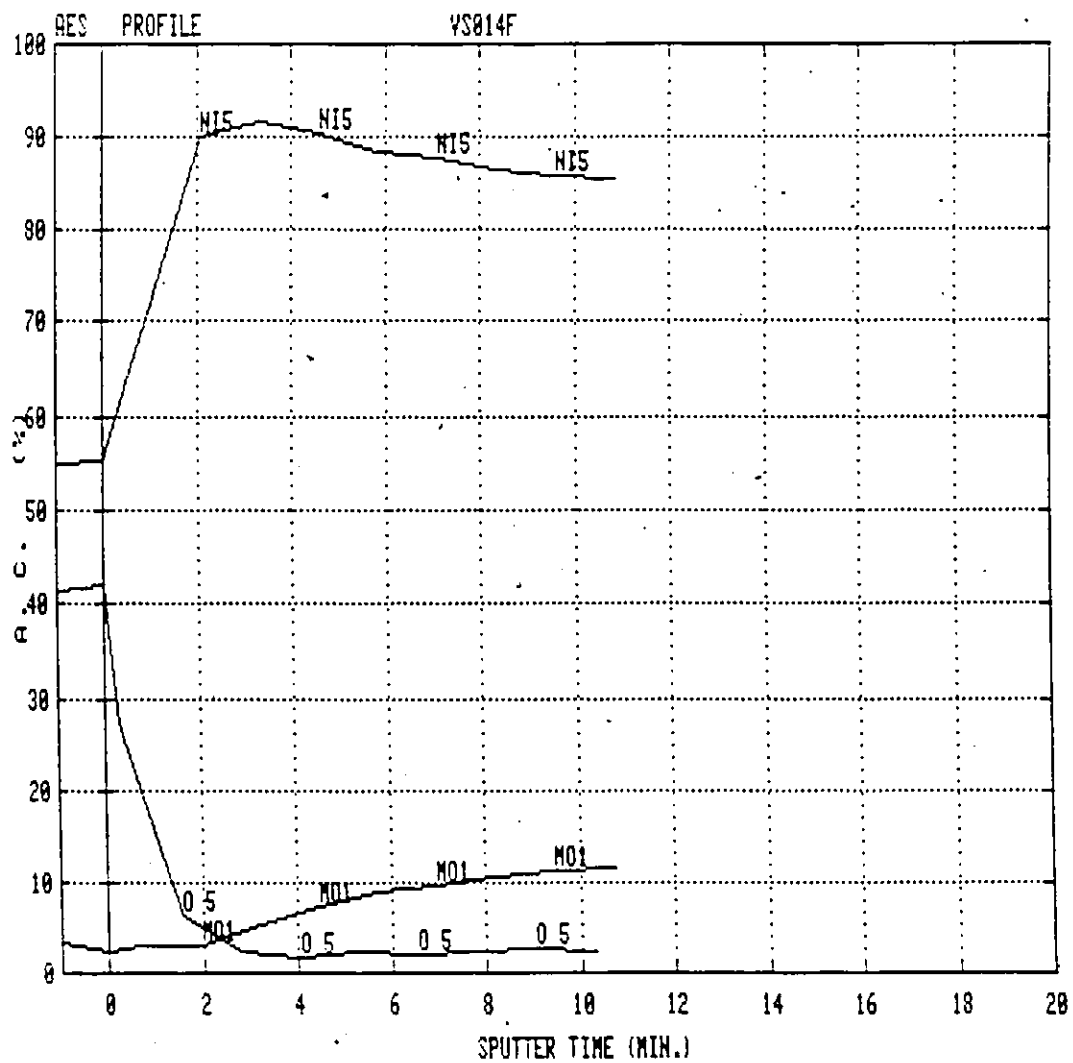


Fig. 3-20

AES profile of Ni-13 Mo following electropolishing and cathodic reduction

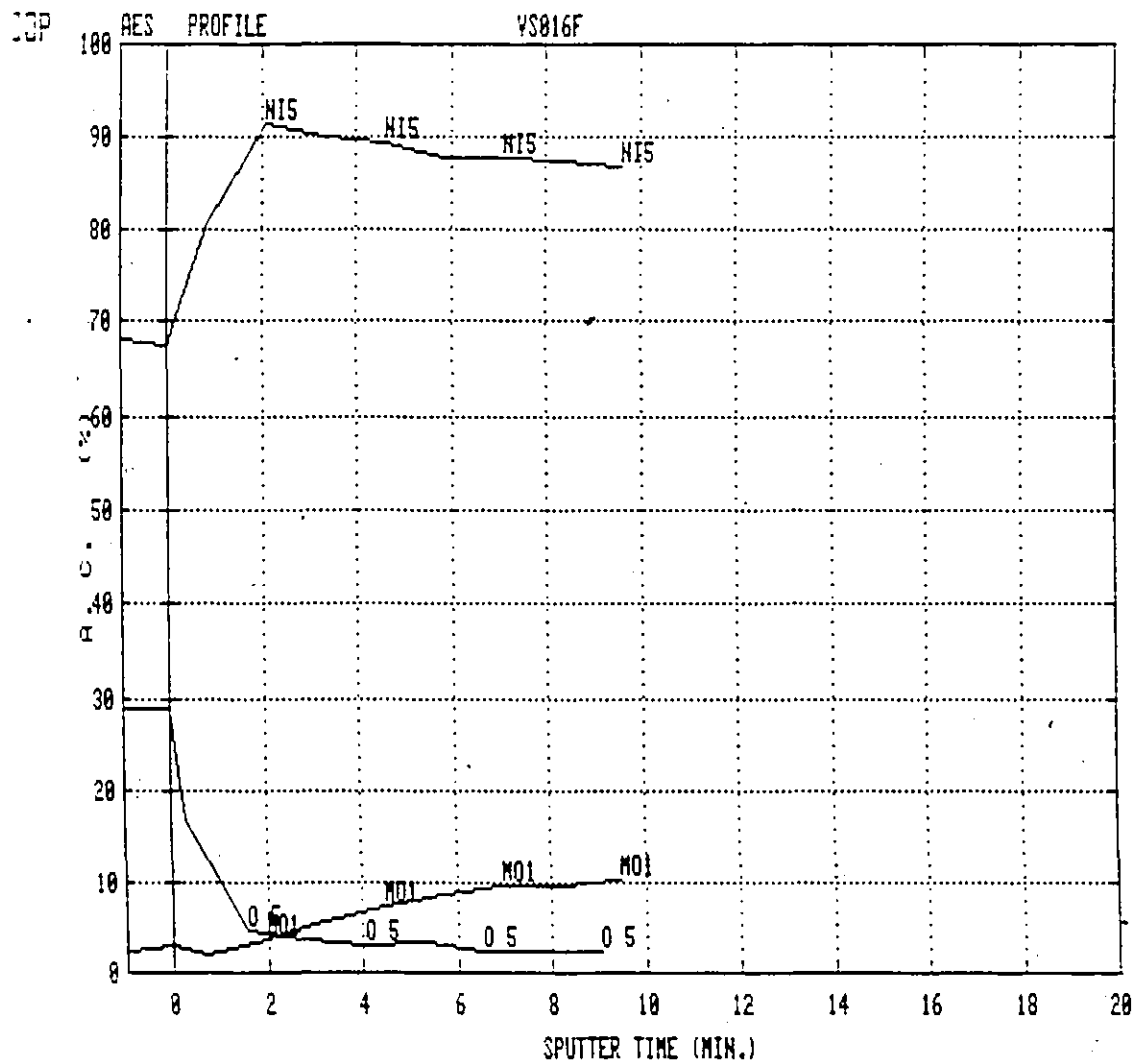
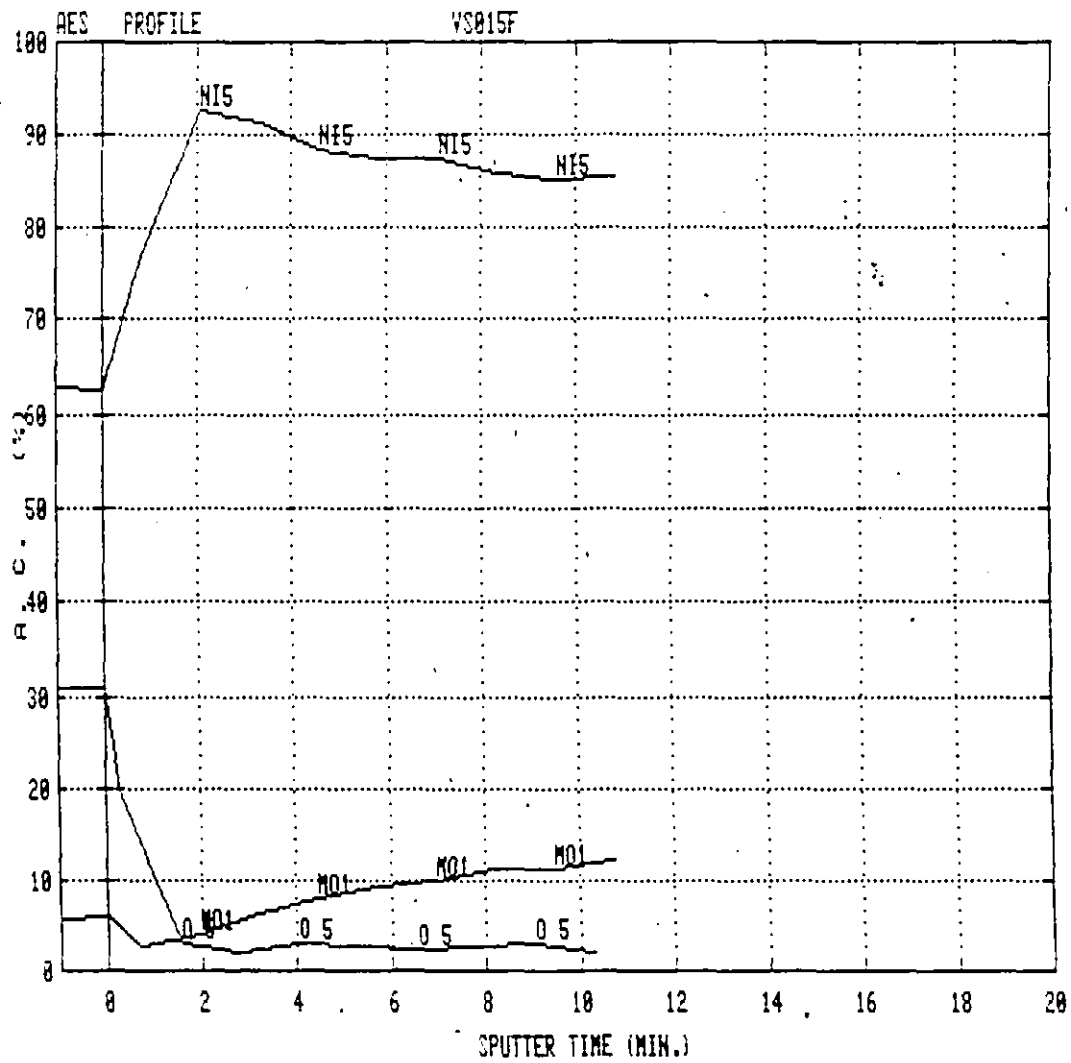




Fig. 3-21

AES profile of Ni-13 Mo following cathodic reduction



that electropolishing with subsequent cathodic reduction produces a surface with the highest degree of Ni-enrichment).

These results demonstrate that electropolishing might not be an appropriate technique in the case of alloys due to the effect of preferential dissolution and consequent change of the surface composition.

### 3.5.2.2 FILM THICKNESS AS A FUNCTION OF ANODIZATION TIME

The AES profiles obtained on Ni-13 Mo samples anodized at +500 mV for 1, 2, 4 and 48 hours are shown on Figs. 3-22 to 3-25 respectively.

The elemental composition of the surface before sputtering is given in Table 3-7.

Table 3-7

Anodization Time [h]	Ni [at %]	Mo [at %]	O [at %]	( $\frac{Mo}{Ni}$ ) surface	$\left[ \frac{(Mo/Ni) \text{ surface}}{(Mo/Ni) \text{ alloy}} \right]$
1	42.0	5.0	53.0	0.119	1.3
2	40.0	5.0	55.0	0.125	1.4
4	39.0	6.0	56.0	0.154	1.7
48	39.0	5.0	56.0	0.128	1.4

It is evident (Figs. 3-22 to 3-25) that the film thickness increases with anodization time in contrast to the passive film on pure Ni formed under the same experimental conditions (Fig. 3-26). On the basis of 75% reduction of the oxygen concentration,

Fig. 3-22

AES profile of Ni-13 Mo following anodization  
(+ 500 mV, 1 h., pH 2.8).

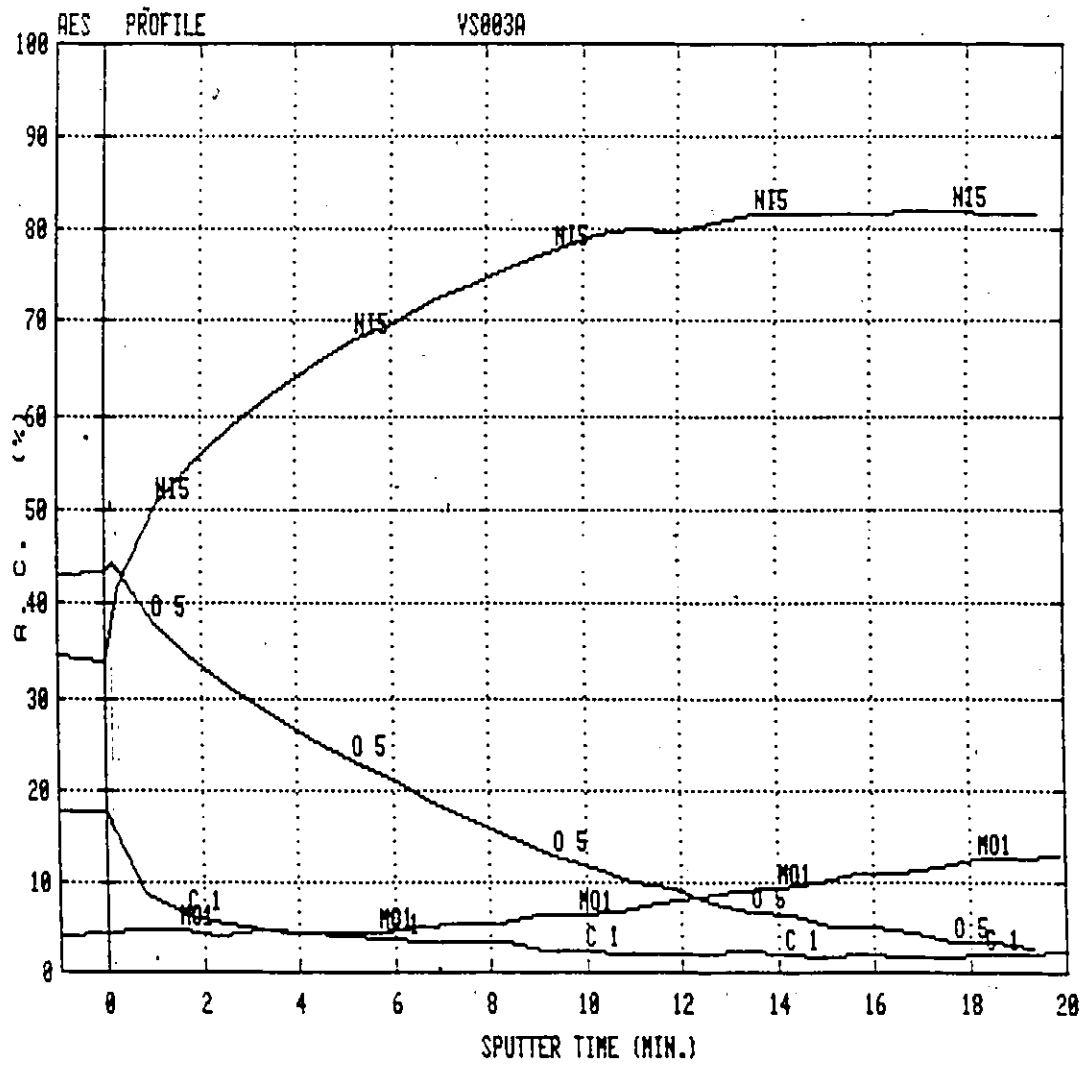


Fig. 3-23

AES profile of Ni-13 Mo following anodization  
 (+ 500 mV, 2 h., pH 2.8)

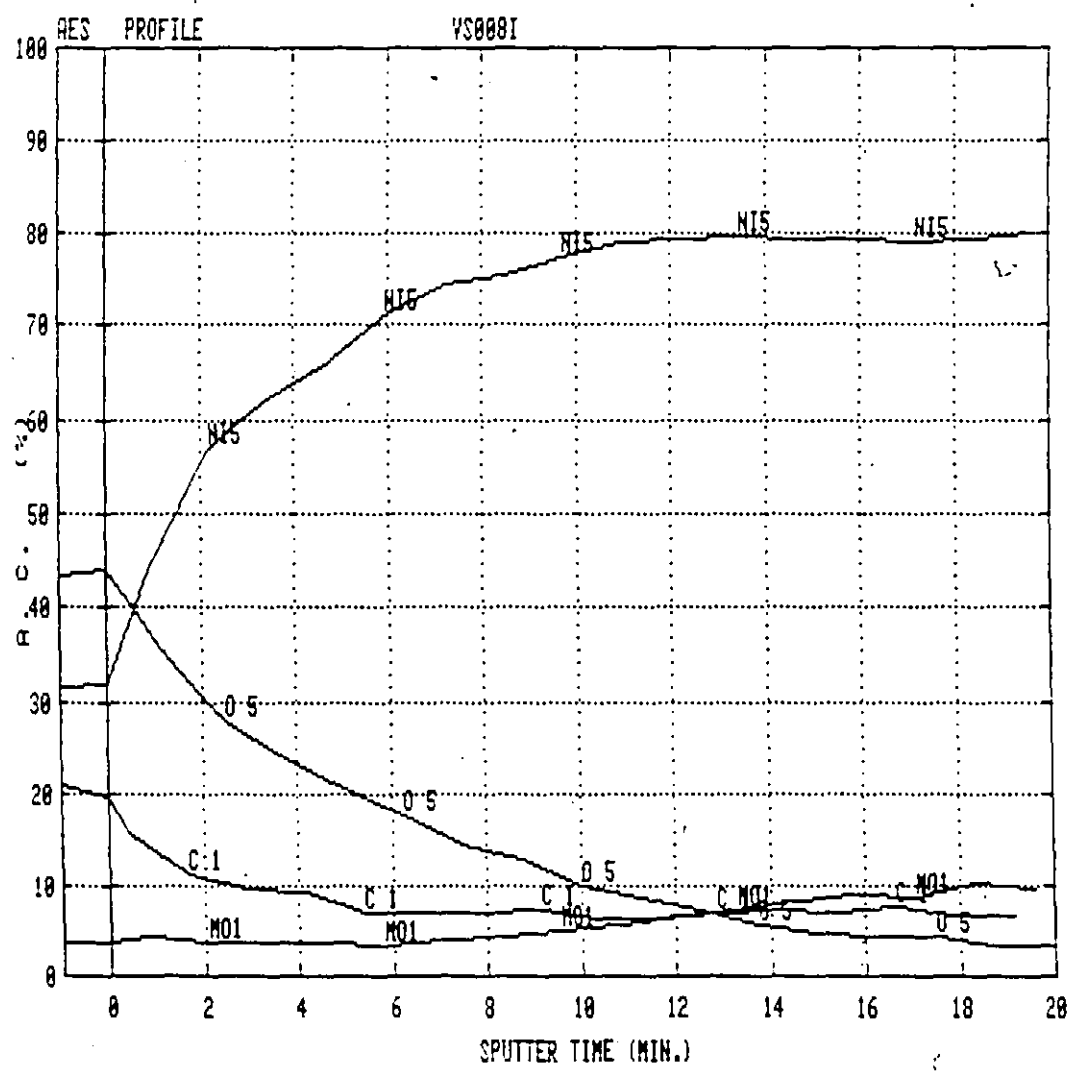


Fig. 3-24

AES profile of Ni-13 Mo following anodization  
 (+ 500 mV, 4 h., pH 2.8)

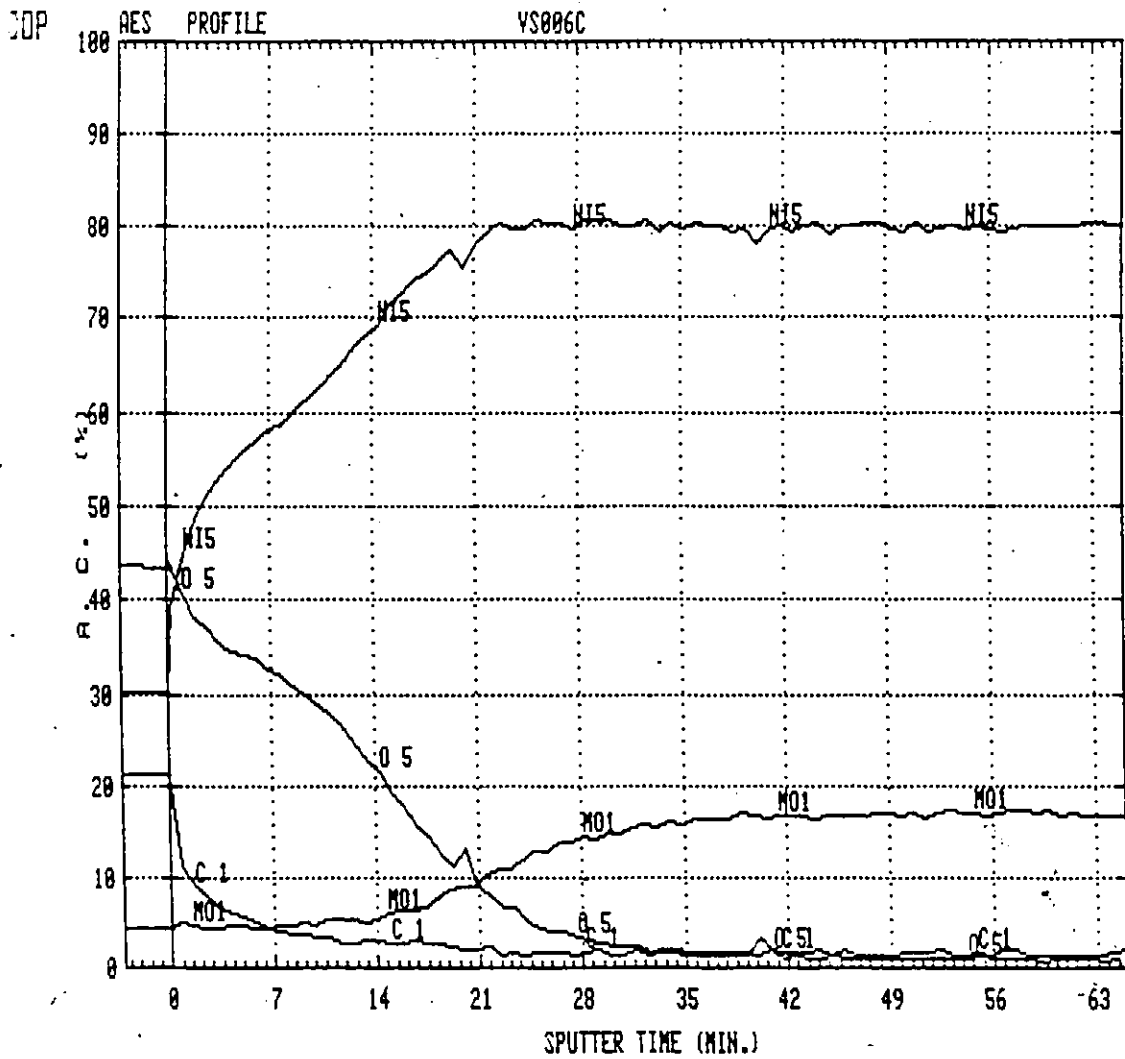


Fig. 3-25

AES profile of Ni-13 Mo following anodization  
 (+ 500 mV, 48 h., pH 2.8)

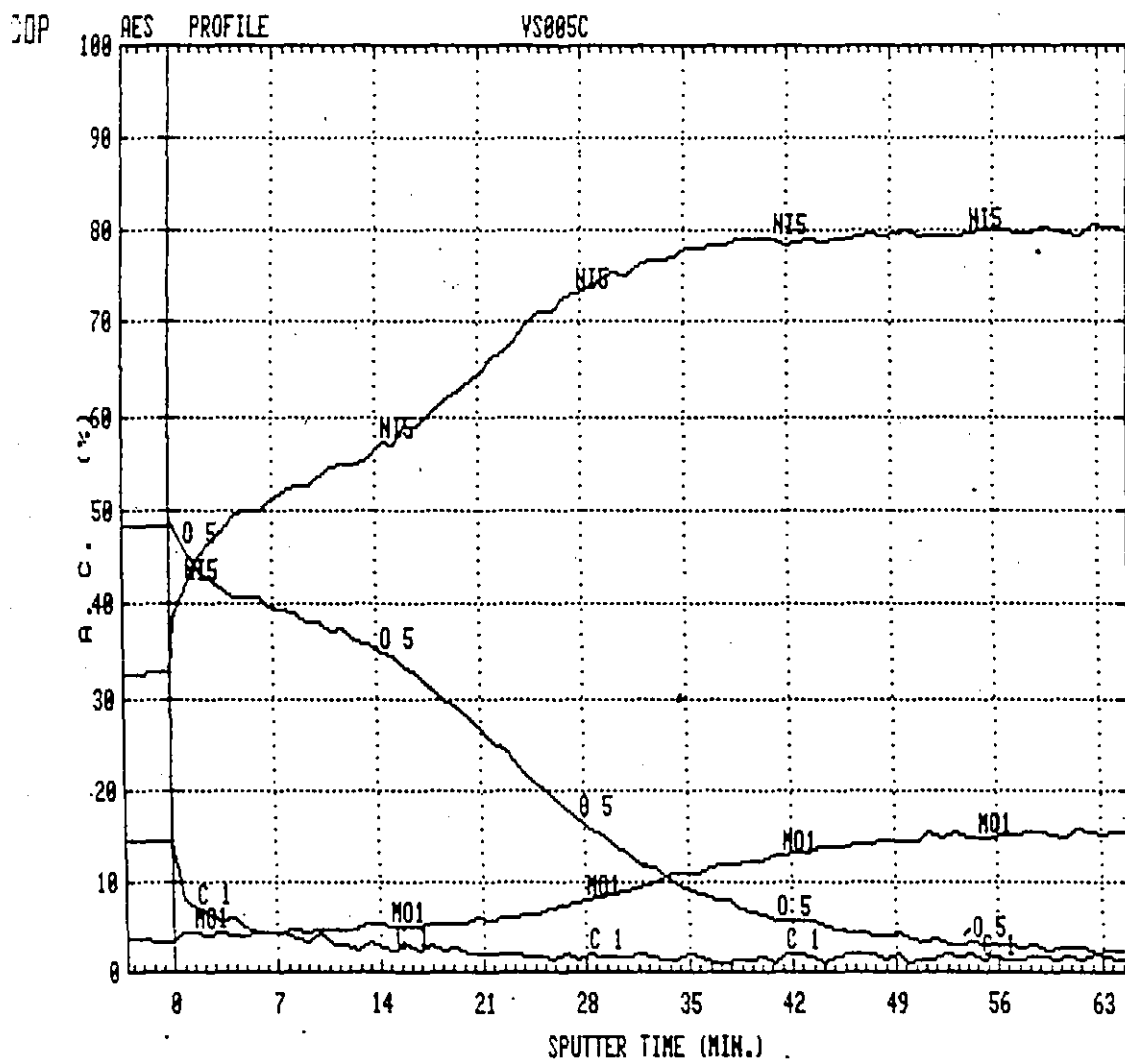
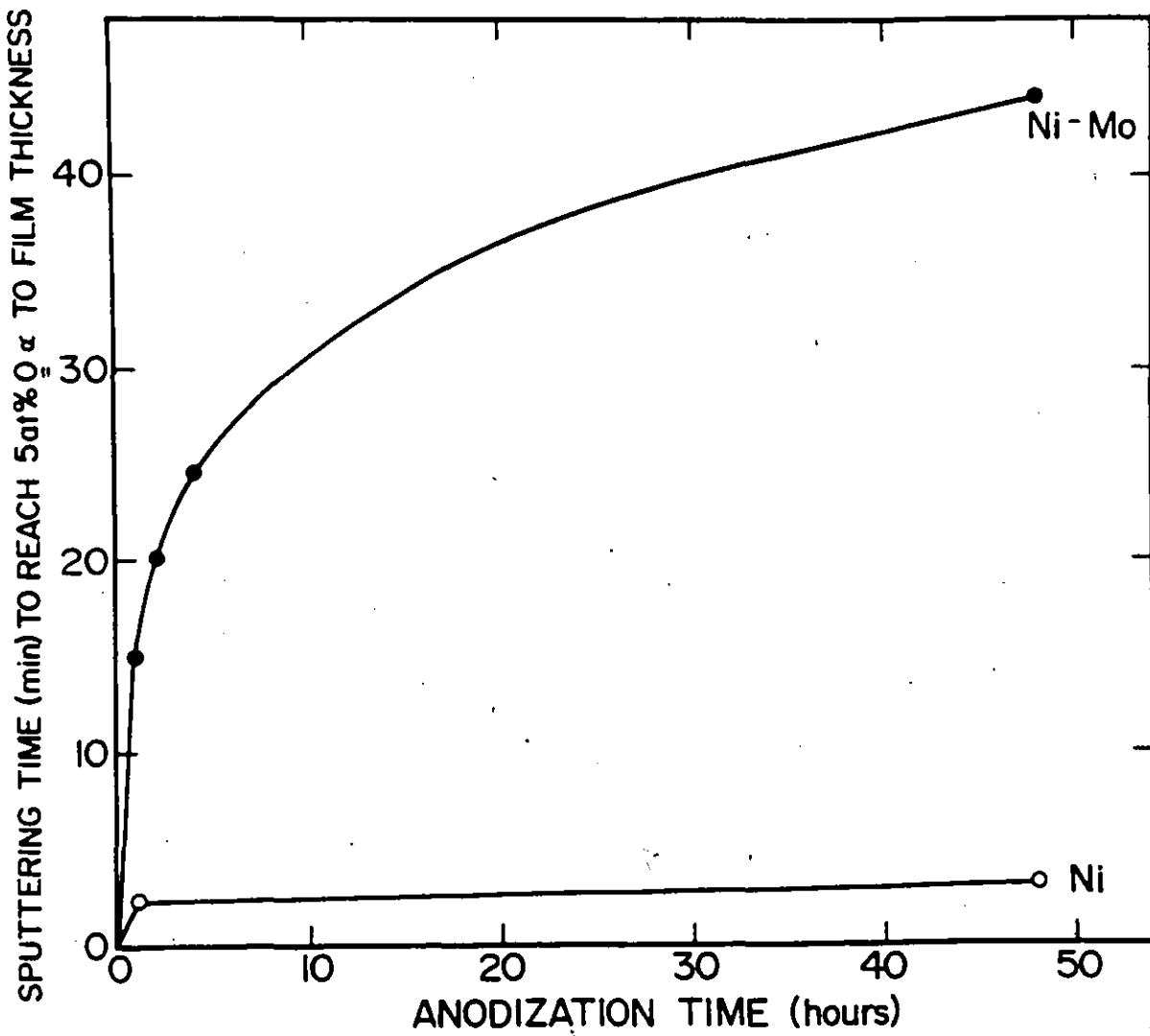


Fig. 3-25

Relative change of film thickness with anodization time



the thickness of the film on Ni-13Mo increases from  $\sim 30$  Å for 1 h of anodization to  $\sim 150$  Å for 48 h of anodization at +500 mV. Therefore the nature of the film formed on Ni-13Mo is different than the one of passive film on Ni formed under the same conditions.

It has been generally accepted that continuing anodic oxidation of an anode passivated by a slightly ion-conducting film does not occur unless

- (a) the film becomes mechanically or chemically unstable at very small thicknesses - breakdown of the outer layers of such a film can then lead to further ion transport, or
- (b) the electron conductivity of the film is especially low - when the ion current is the only important, and the film growth is the major process.

Difficult ion transport through even the thinnest film must discourage outward growth and encourage lateral growth or further nucleation on uncovered metal: in the limit, a monolayer film (often epitaxial) forms on each metal grain before any further thickening [5]. On the other hand, easy ion transport may lead to considerable outward growth from each nucleus before lateral growth links up all the small patches of film: these thicker less regular films are likely to have at least some subgrain structure or to be polycrystalline over each metal grain and hence to be structurally imperfect. Structural imperfections play their part in allowing solution to reach the metal so that electrochemical processes take



place "within" the film and lattice transport then occurs over distances much shorter than the macroscopic film thickness. Ion diffusion and migration over internal surfaces is also much easier than through the lattice. Consequently, film growth is usually an easier process with imperfect than with compact films and much greater thicknesses are possible to attain at relatively low potential differences across the film.

It is evident that the anodic film formed on Ni-13Mo is less perfect than the passive film on pure Ni.

An enrichment of the film in Mo was found for all anodization times investigated (Table 3-7); it increases monotonically with time, at least up to 4 h of anodizing.

It should be pointed out that the absolute values of the concentration ratios obtained by AES are sensitive to the values of relative sensitivity factors employed for converting APPH-s to atomic concentration units. Consequently the data given in Table 3-7 are not to be taken as accurate but rather as the results that show a trend of increasing (Mo/Ni) ratio in the film with an increase in polarization time.

The AES profiles through the film (Figs. 3-22 to 3-25) could only serve as the evidence for the presence of Mo in the film. The concentration profiles in depth could not give reliable information on change of the (Mo/Ni) ratio with depth because of quite severe changes caused by sputtering.

3.5.2.3 ANODIC FILM CHARACTERIZATION AFTER OPEN CIRCUIT POTENTIAL  
DECAY (OCPD) OF ANODIZED Ni-13Mo

A better understanding of the processes occurring on the surface of anodized Ni-13Mo on the open circuit could be achieved by analyzing the composition and relative thickness of the surface film after different times on the open circuit.

Three Ni-13Mo samples were anodized at +500 mV for 2 h. One is then left on the open circuit for 3 min (Fig. 3-28) and the other for 30 min (Fig. 3-29). Fig. 3-27 shows the AES profile of the sample that was not exposed to the open circuit after anodization.

The surface composition before sputtering (Table 3-8) shows that the ratio (Mo/Ni) decreases with time on the open circuit due to both a slight increase in Ni concentration and a decrease in Mo concentration.

TABLE 3-8

	Ni at %	Mo at %	O at %	( $\frac{Mo}{Ni}$ ) surf.	( $\frac{Mo}{Ni}$ ) surface alloy
Anodized	40.0	5.0	55.0	0.125	1.4
3 min OCPD	41.0	4.0	55.0	0.098	1.06
30 min OCPD	42.6	3.4	54.0	0.079	0.87

The film thickness, estimated from the sputtering time needed to reduce the concentration of oxygen 75%, does not change with time on the open circuit, nor does the surface concentration

Fig. 3-27

AES profile of Ni-13 Mo following anodization  
 (+ 500 mV, 2 h., pH 2-8)

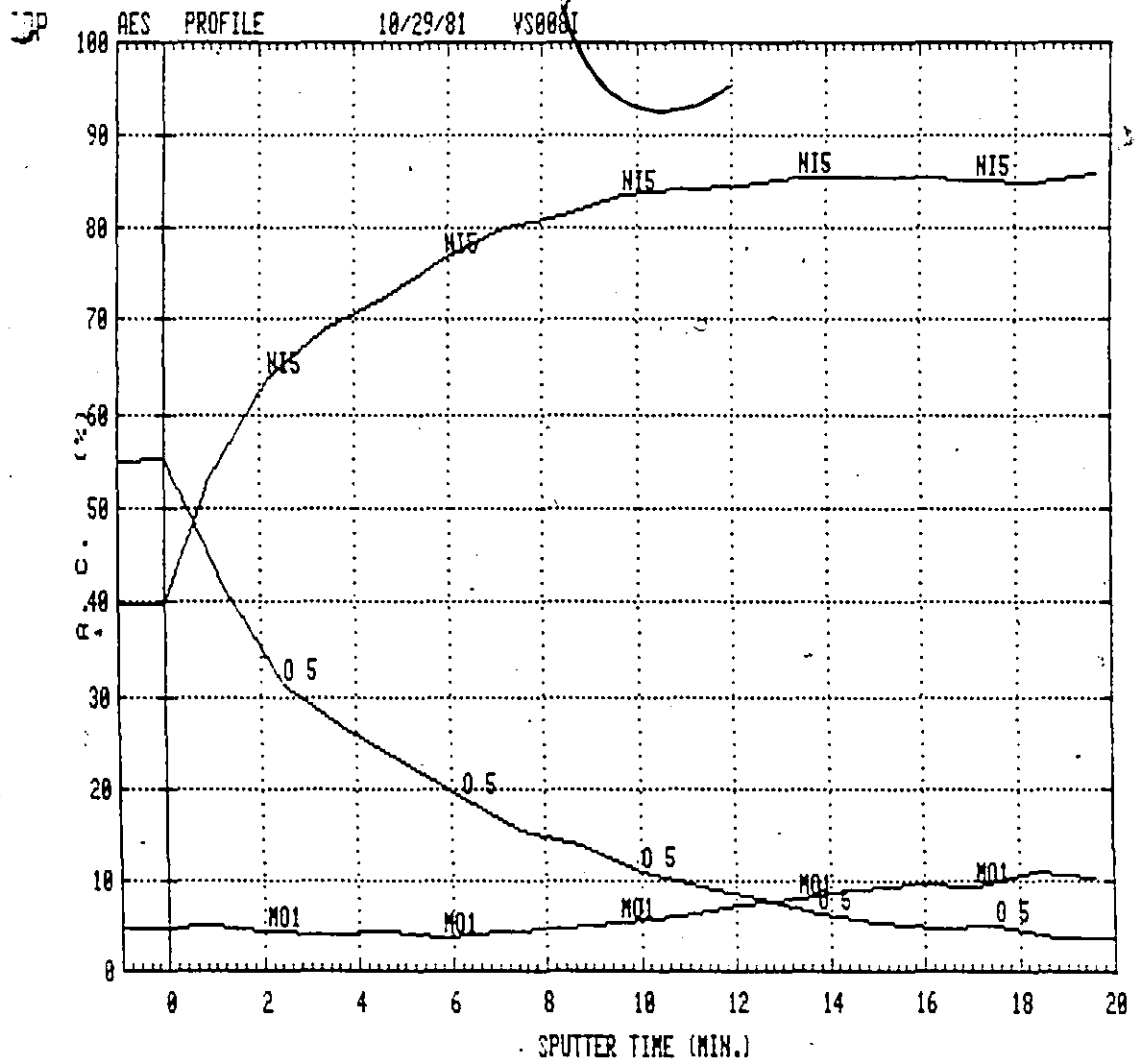


Fig. 3-28

AES profile of Ni-13 Mo following anodization  
(+ 500 mV, 2 h., pH 2.8) and OCPD (3 min)

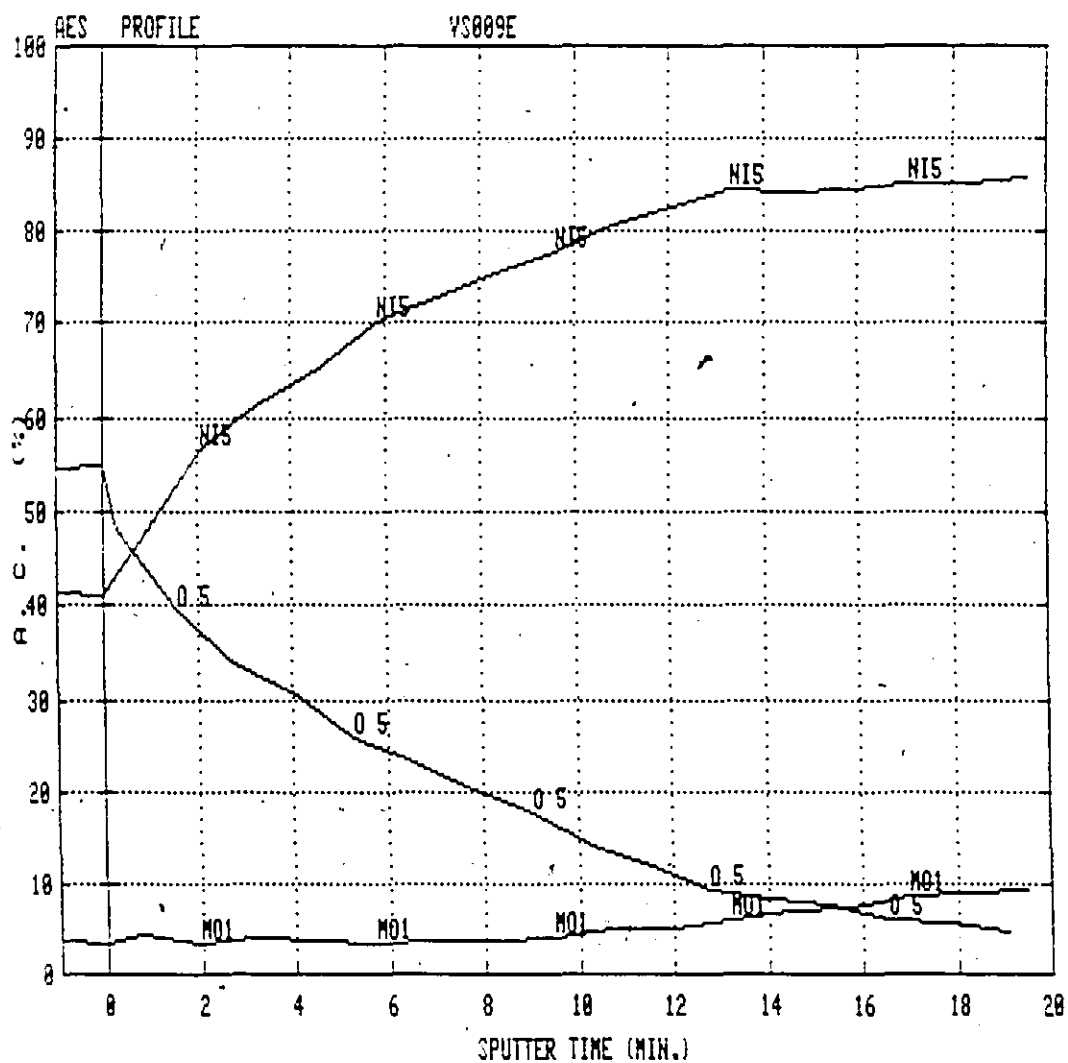
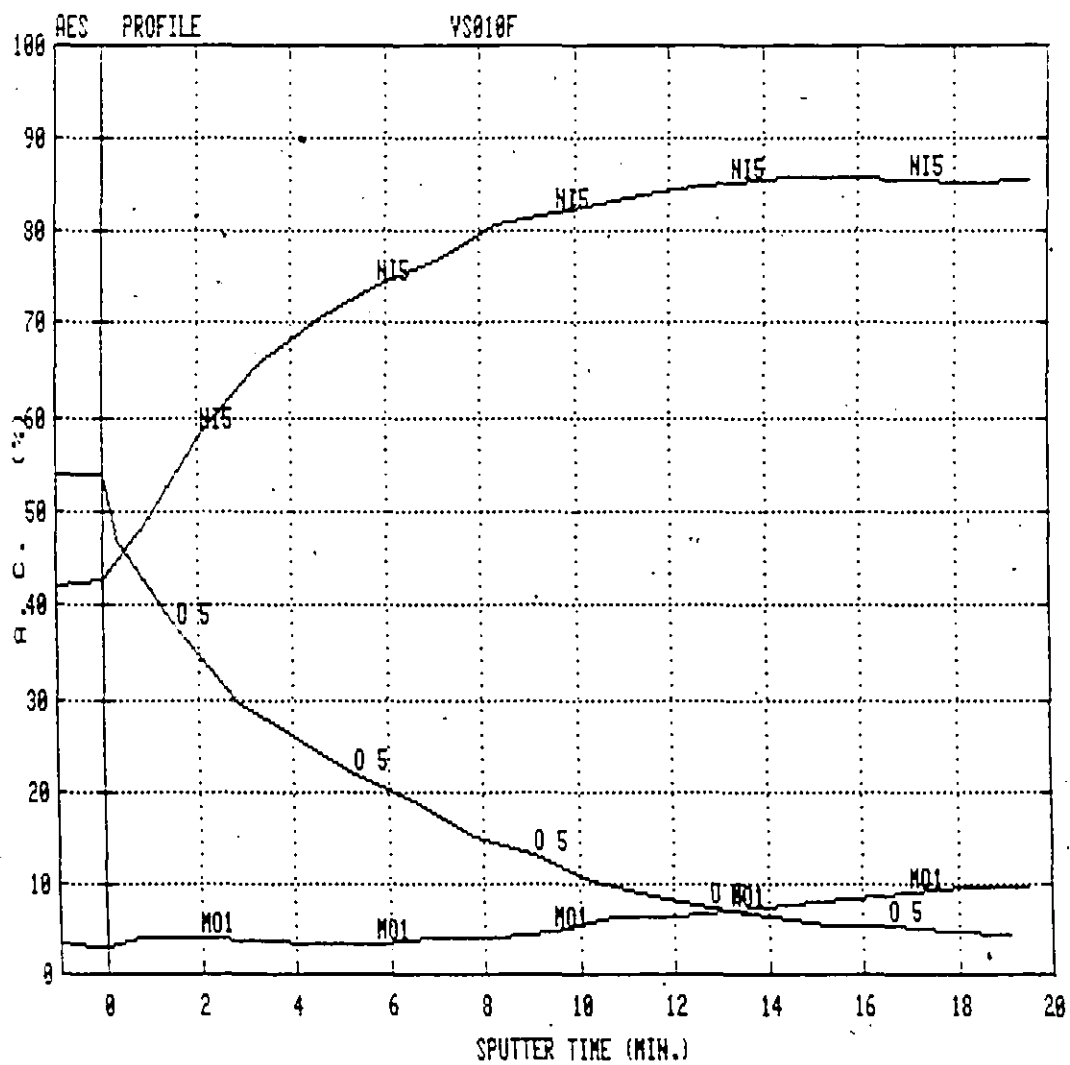


Fig. 3-29

AES profile of Ni-13 Mo following anodization  
 (+ 500 mV, 2 h., pH 2.8) and OCPD (30 min.)



of oxygen. This observation indicates that the anodic film on Ni-13Mo is not being removed from the surface on the open circuit, at least not to an extent observable by means of AES analysis. The change in Ni and Mo concentration, however, might suggest some local dissolution with preferential dissolution of Mo.

#### 3.5.2.4 SURFACE COMPOSITION OF Ni-13Mo POLARIZED IN THE ACTIVE REGION

It has been generally accepted that passivation occurs through the process of active dissolution. Even if the potential is set in the passive region an increase in concentration of soluble metal or hydroxyl ions in the vicinity of the electrode surface, i.e., active dissolution is a necessary precursor for passive film formation [168,169].

There is a view expressed by Hashimoto [131,170] that the effect of Mo as an alloying element on improving the corrosion resistance is due to an enrichment of the surface by Mo-species during the active dissolution. These species do not have high protective ability but they may decrease the activity of active surface sites prior to the passive film formation.

Consequently, it was thought to be useful to examine the surface composition of Ni-13Mo subjected to a potential in the active dissolution region.

Figs 3-30 and 3-31 give the Auger spectrum of Ni-13Mo alloy polarized at -100 mV for 30 min and the corresponding AES

Fig. 3-30

AES spectrum of Ni-13 Mo following polarization in the active region (30 min)

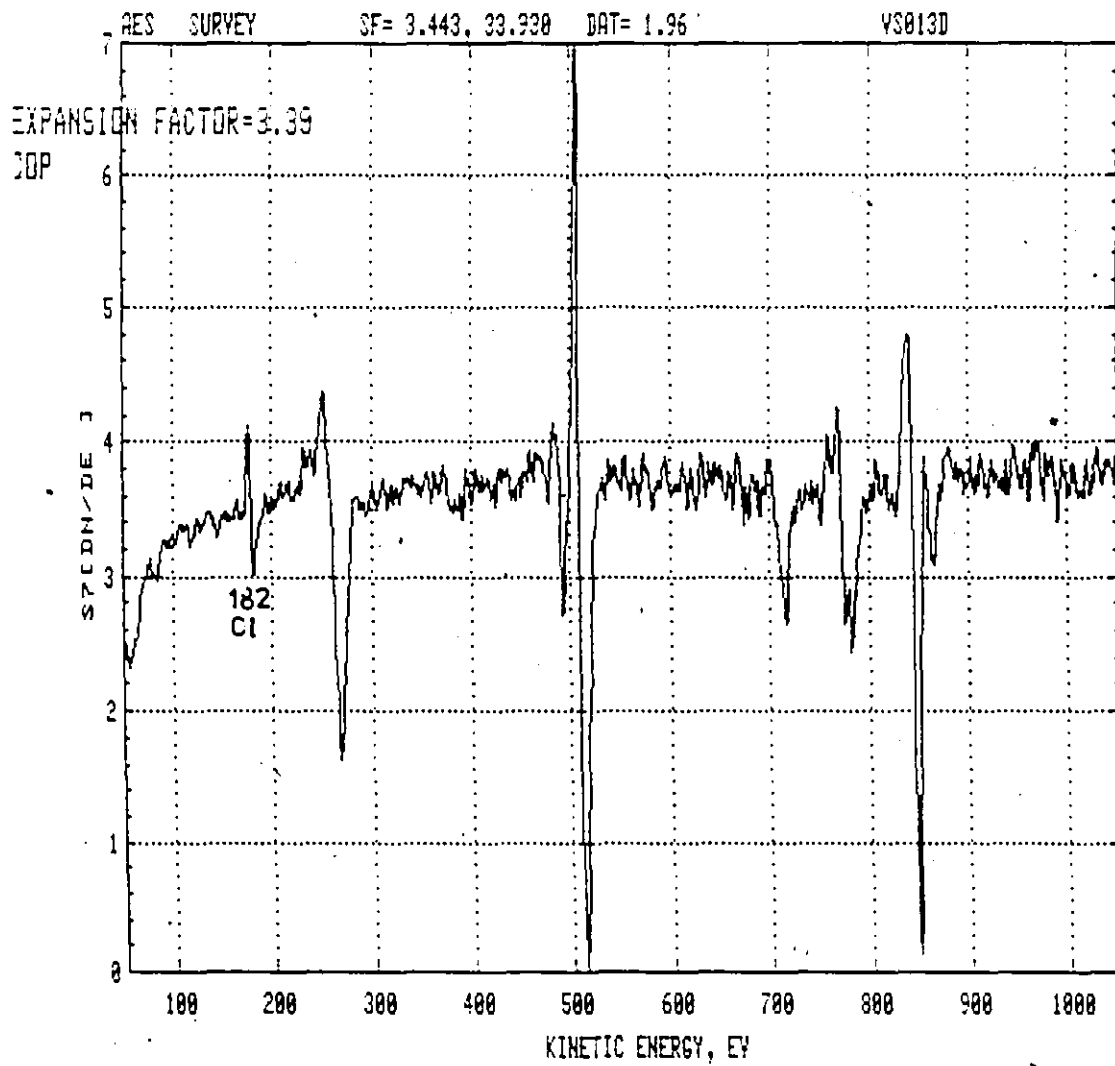
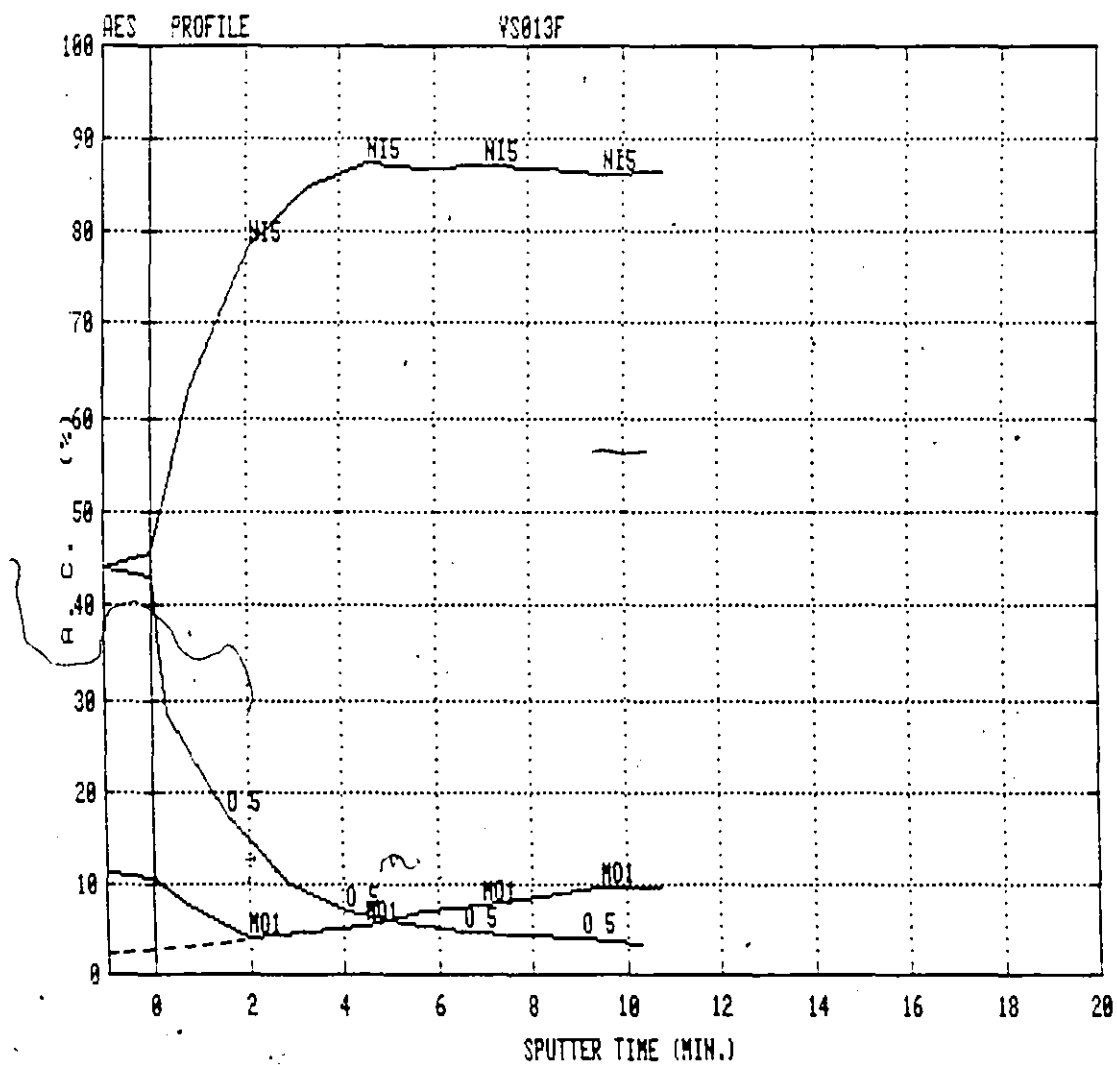


Fig. 3-31

AES profile of Ni-13 Mo following polarization in the active region (30 min)





profile, respectively. A contamination of the surface with  $\text{Cl}^-$  was detected so that the apparent surface concentration of Mo is not the true one (Mo - 186 eV, Cl - 182 eV). Since the high energy Mo peak (2040 eV) was not detected it appears that Mo dissolves preferentially leaving the surface covered with Ni. An exceedingly small amount of Mo might be present but not detected (sensitivity of 2040 eV Mo peak is very low, i.e., 0.055).

The oxide film on the surface ( $\sim 10 \text{ \AA}$ ) is probably an air formed film although it could have been formed by anodic oxidation at -100 mV (beginning of the passive range for pure Ni).

These observations exclude the possibility of enrichment of the surface by Mo species during the active dissolution before the film formation. On the other hand the presence of Mo in the passive film with (Mo/Ni) ratio greater than in the alloy suggests a different mechanism of the film formation on Ni-Mo alloys than direct oxidation, widely accepted for the passive film on Ni in acid solutions [51,52,85]. The dissolution-precipitation [64-66] could be the mechanism of the anodic film formation on single-phase Ni-Mo alloys.

#### 3.5.2.5 THE EFFECT OF SOLUTION pH ON THE COMPOSITION AND THICKNESS OF ANODIZED Ni-13Mo

The effect of the solution pH on the anodic film formed at +500 mV was examined by forming the film for 2 h in 0.15 N  $\text{Na}_2\text{SO}_4$  with pH adjusted to 10.2, 2.8 and 1.5 by either concentrated  $\text{H}_2\text{SO}_4$  or NaOH. The corresponding AES profiles are given on Figs. 3-32 to 3-34 in the order given.

It is evident that the thickness of the film increases as the solution pH increases, the film formed at pH 10.2 being almost 3 times thicker than the one formed at pH 1.5. The passive current density during polarization was  $\sim 15 \frac{\mu\text{A}}{\text{cm}^2}$  for pH 10.2 and  $\sim 1.5 \frac{\mu\text{A}}{\text{cm}^2}$  for pH 1.5.

Elemental surface composition before sputtering is given in Table 3-9.

Table 3-9

Solution pH	Ni [at %]	Mo [at %]	O [at %]	$\frac{(\text{Mo})_{\text{surf}}}{\text{Ni}}$	$\frac{(\text{Mo/Ni})_{\text{surface}}}{(\text{Mo/Ni})_{\text{surface}}}$
10.5	40.2	6.2	53.6	0.154	1.7
2.8	37.8	8.2	53.0	0.126	2.4
1.5	43.0	5.5	51.5	0.128	1.4

No trend in (Mo/Ni) ratio with pH is observed. Formation of a much thicker film and an order of magnitude higher than passive current density in the alkaline solution implies a pH dependent mechanism of the film growth on Ni-Mo alloys. According to Vetter [171], the measurable electrode current,  $i$ , in the passive state is composed of two parts, a current  $i_L$  for the layer formation or removal, and a current  $i_c$  for the corrosion process, i.e., the passing of cations into the solution at the phase boundary layer/electrolyte. Only at the stationary state

Fig. 3-32

AES profile of Ni-13 Mo following anodization  
 (+500 mV, 2 h., pH. 10.2)

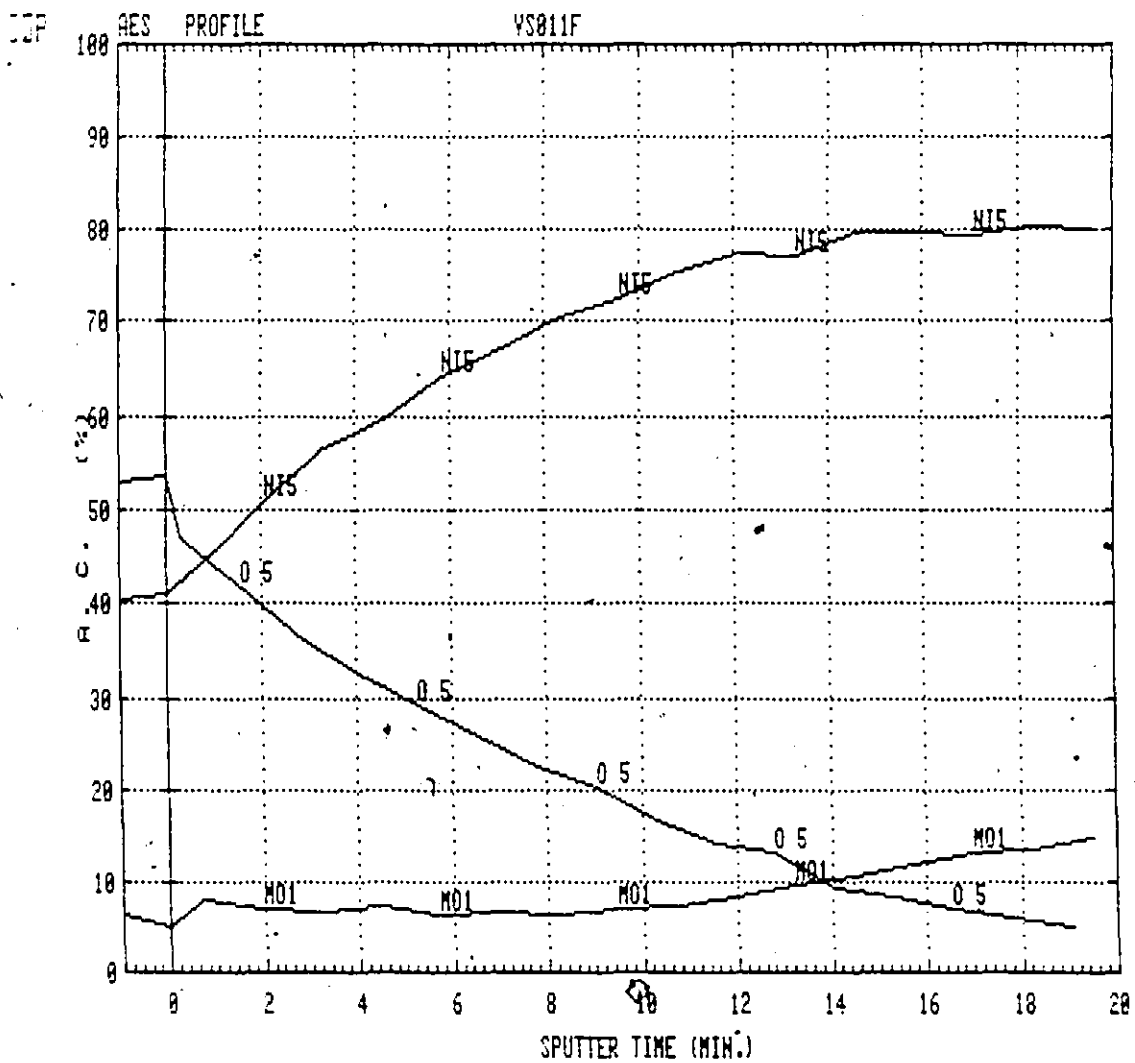


Fig. 3-33

AES profile of Ni-13 Mo following anodization  
(+ 500 mV, 2 h., pH 2.8)

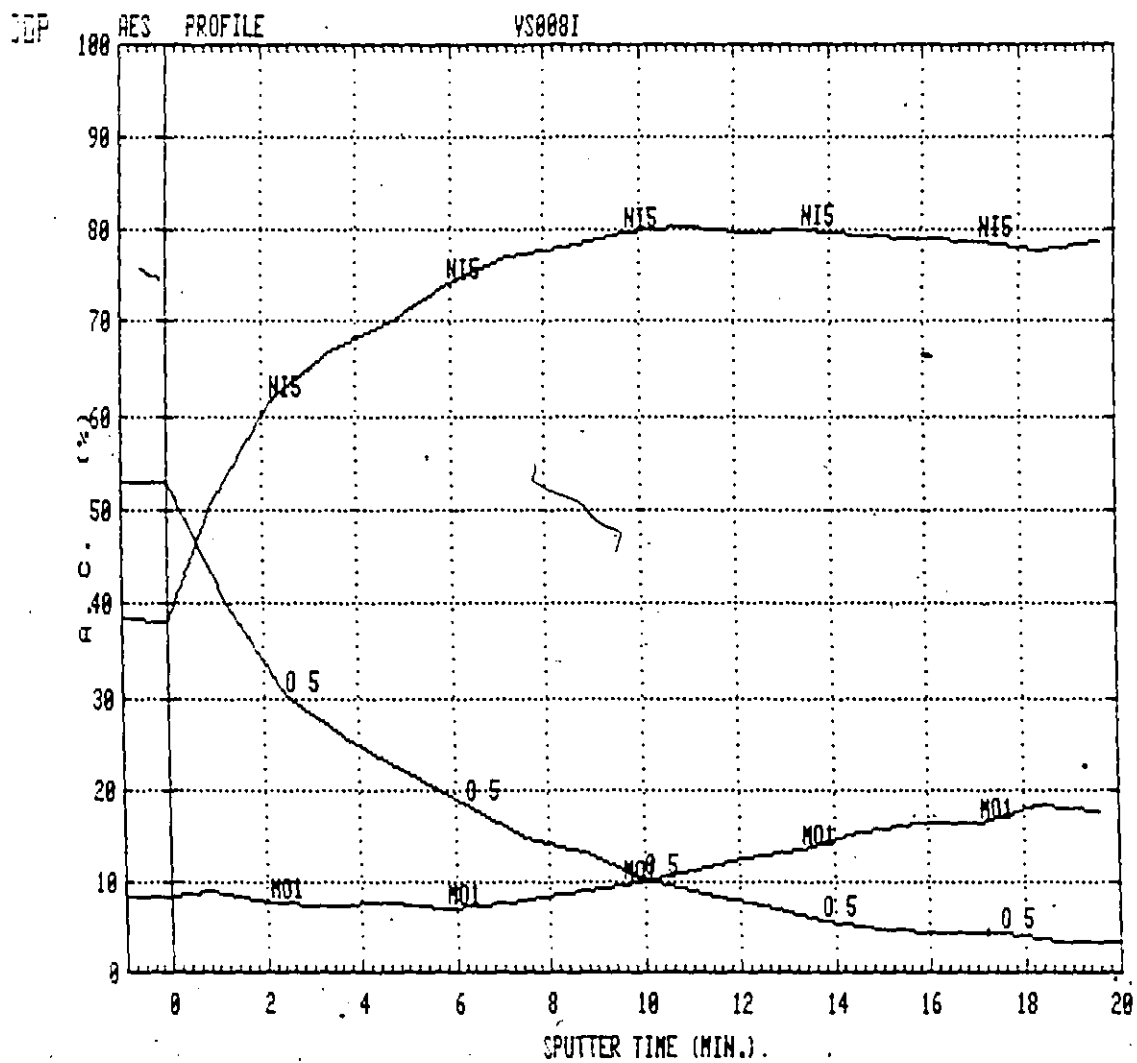
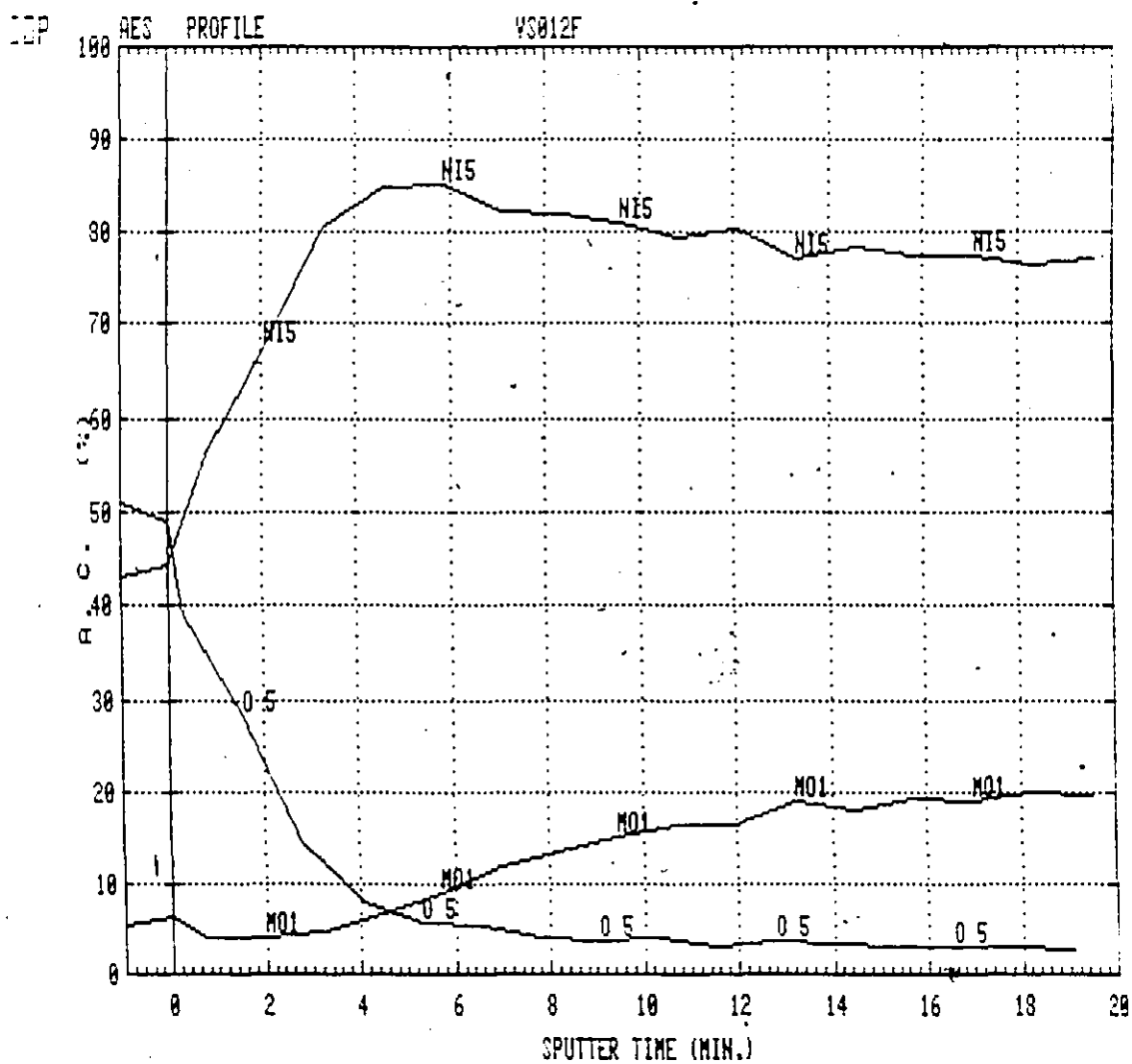


Fig. 3-34

AES profile of Ni-13 Mo following anodization  
(+ 500 mV, 2 h., pH 1.5)



which is characterized by equal rates of the layer formation and removal ( $i_L=0$ ), the measured current,  $i$ , is equal to the stationary corrosion current,  $i_c$ . For thickening of the passive layer the rate of layer formation has to be increased, which means, after Vetter, an increase of the potential difference at the layer/electrolyte phase boundary. For this reason the corrosion rate is increased too [28]. The extent of this increase is governed by the potential dependence of the corrosion reaction and the properties of the phase boundary. Consequently, a much thicker film and an order of magnitude higher current density indicate also very poor protective properties of the film formed at higher solution pH.

### 3.5.3. QUANTITATIVE ASPECTS OF AES ANALYSIS OF Ni-Mo ALLOYS

The AES data on Ni-13 Mo presented so far are to be considered as semiquantitative, i.e. the accuracy of the method is considered to be 30 - 50% [172,173].

The use of proper sensitivity factors would require a set of standards with known composition and similar surface topography. In the present case preparation of such a set of standards was impossible. Assuming the film to be composed of NiO and MoO<sub>3</sub> and using corresponding values for the sensitivity factors obviously introduces an error.

Preferential sputtering, caused by differences in sputter yields of Ni and Mo [155], leads to a transient change in the composition. Upon further sputtering a steady state composition is reached at which the concentration becomes quite different from

that in the bulk (Fig. 3-35). The effect has already been observed elsewhere [157]. Surface roughness introduces complications in relation to preferred sputtering behaviour. When surface roughness increases, the exposed surface area increases. This can promote the sputter yield and alter the Auger signal [174]. These factors can introduce a time variation of the signal not really related to selective sputtering.

Another significant effect observed during sputtering is Mo peak shift and shape change, shown on Fig. 3-36 for the air formed film on pure Mo, and on Fig. 3-37 for the anodic film on Ni-13 Mo alloy anodized at +500 mV for 2 h. This peak corresponds to the MNN Auger transition. According to the literature data [175] on AES studies of chemical shift and beam effect on molybdenum oxides, the 183 eV peak is usually assigned to  $\text{Mo}^{6+}$ , the 187 eV peak to  $\text{Mo}^{4+}$  and the 188 eV peak to  $\text{Mo}^0$ . The spectrum of the anodized alloy suggests the presence of  $\text{MoO}_3$  which is reduced to  $\text{MoO}_2$  during sputtering. The air formed film on Mo appears to be composed of both  $\text{MoO}_3$  and  $\text{MoO}_2$ . The broad peak shape also indicates the possibility of the presence of other intermediate oxides between  $\text{MoO}_2$  and  $\text{MoO}_3$ . Reduction of  $\text{MoO}_3$  to the lower valence state is observed in this case as well.

Fig. 3-38 shows the IMM spectrum of Mo obtained on the air formed film on pure Mo (2044 eV). This peak does not change as much under the ion beam as the one discussed above. However it is extremely weak (sensitivity 0.055) and was not used further in the

Fig. 3-35

AES profile of Ni-13 Mo (91.6 at % Ni, 8.4 at % Mo) following anodization

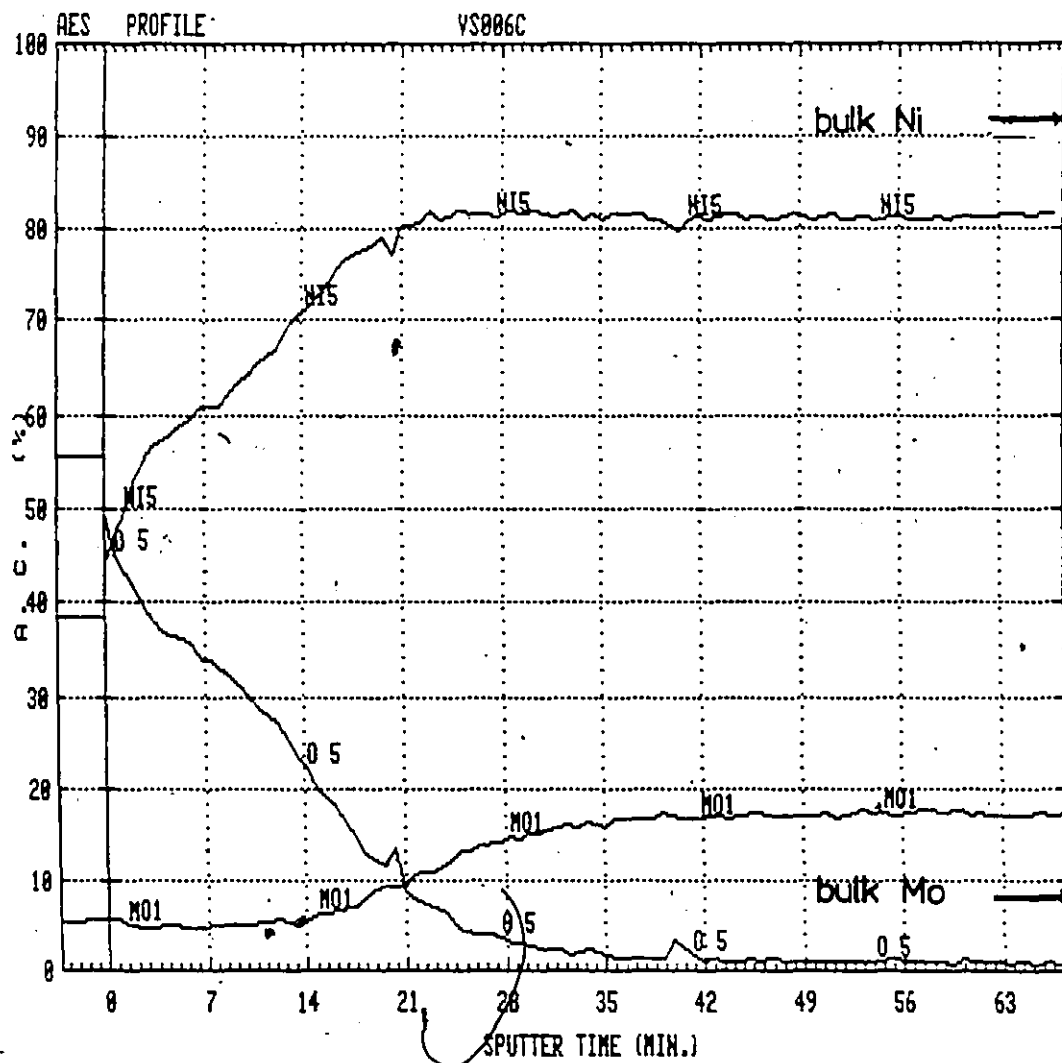




Fig. 3-36

Variation of Mo Auger MNN spectra with sputtering time (1 keV Xe<sup>+</sup>) (air formed film on Mo)

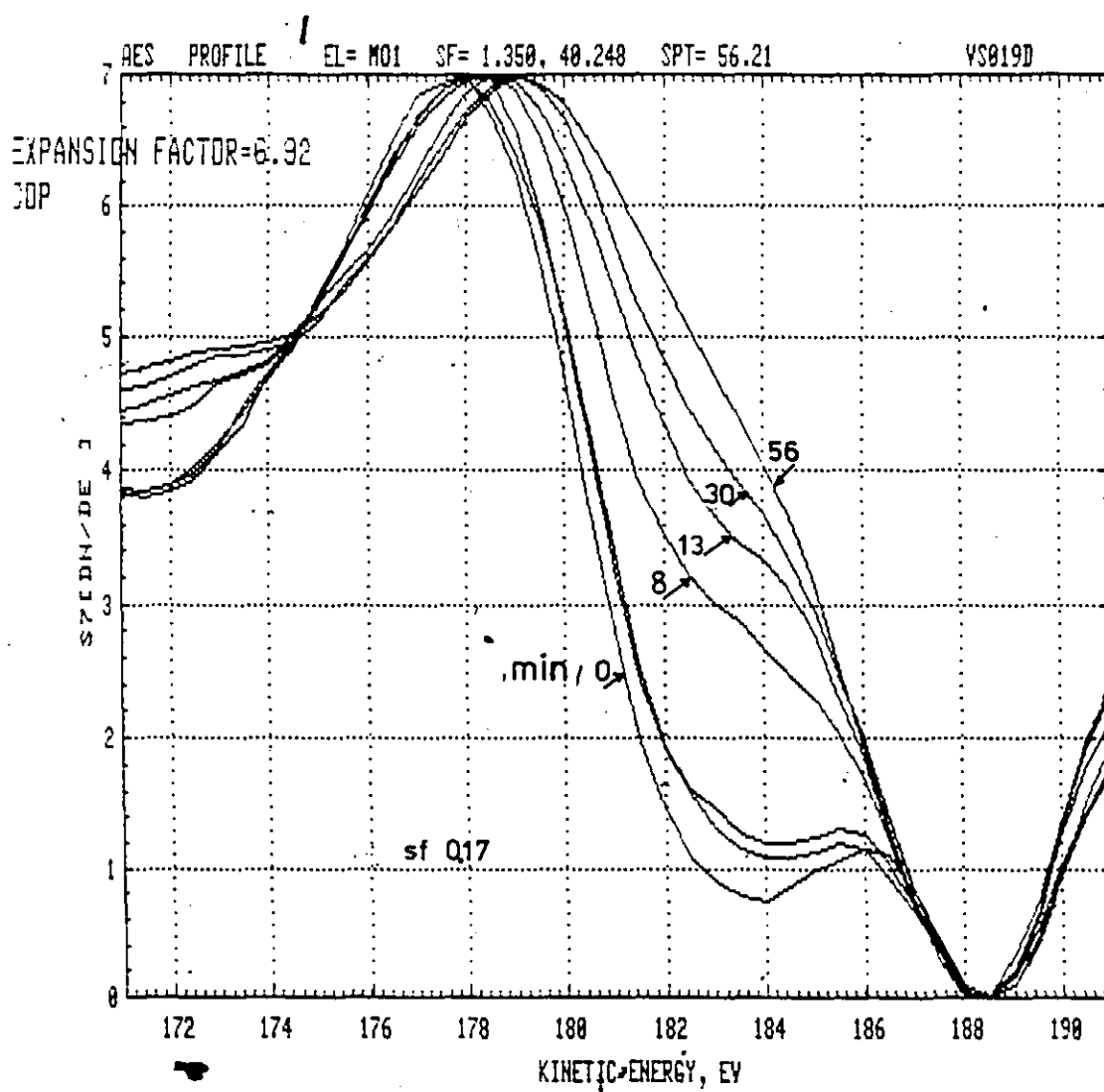


Fig. 3-37

Variation of Mo Auger MNN spectra with sputtering time (1 keV Xe<sup>+</sup>) (anodized Ni-13 Mo)

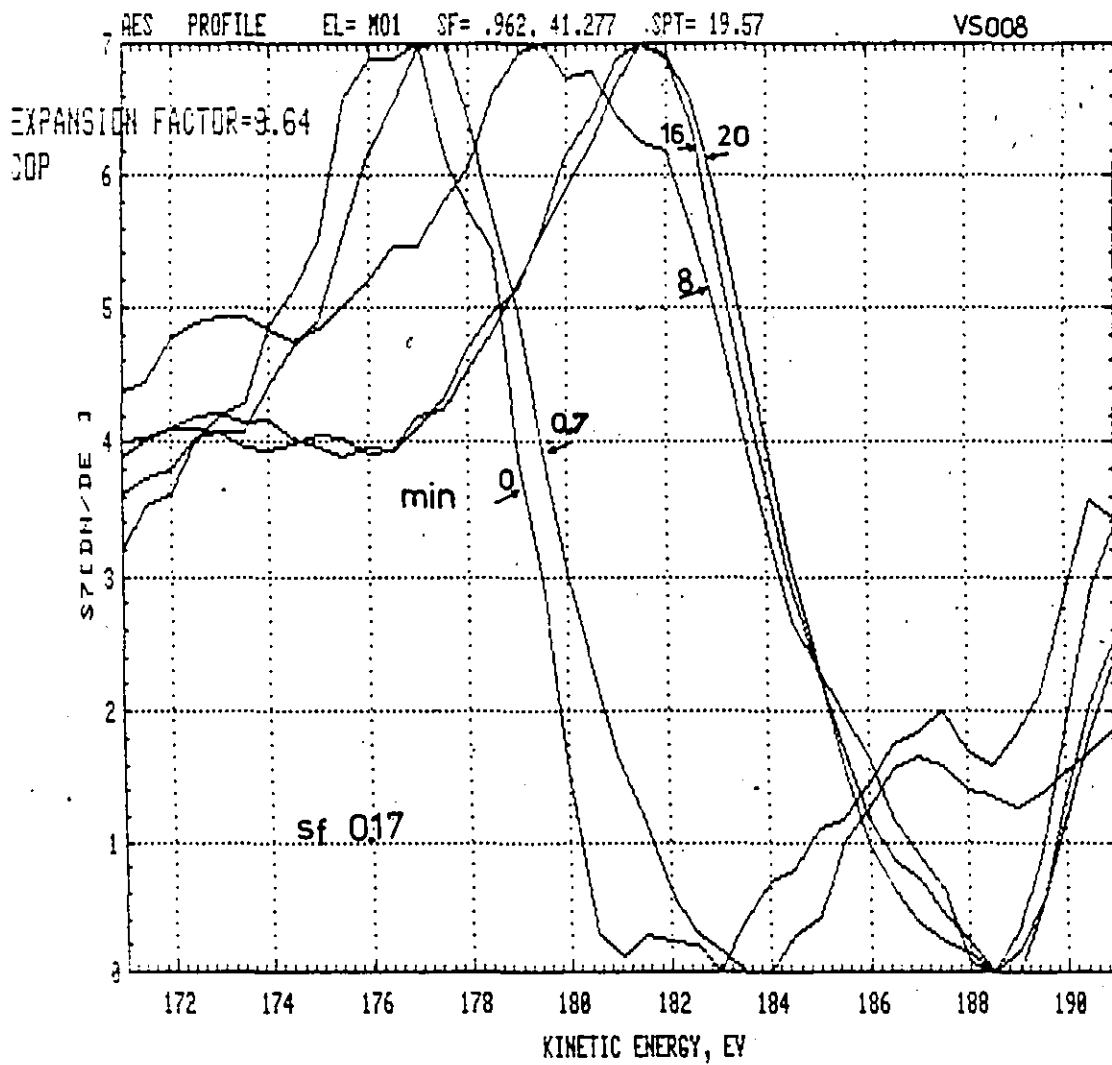


Fig. 3-38

Variation of Mo LMM Auger spectra with sputtering time (1 keV Xe<sup>+</sup>) (air formed film on Mo)

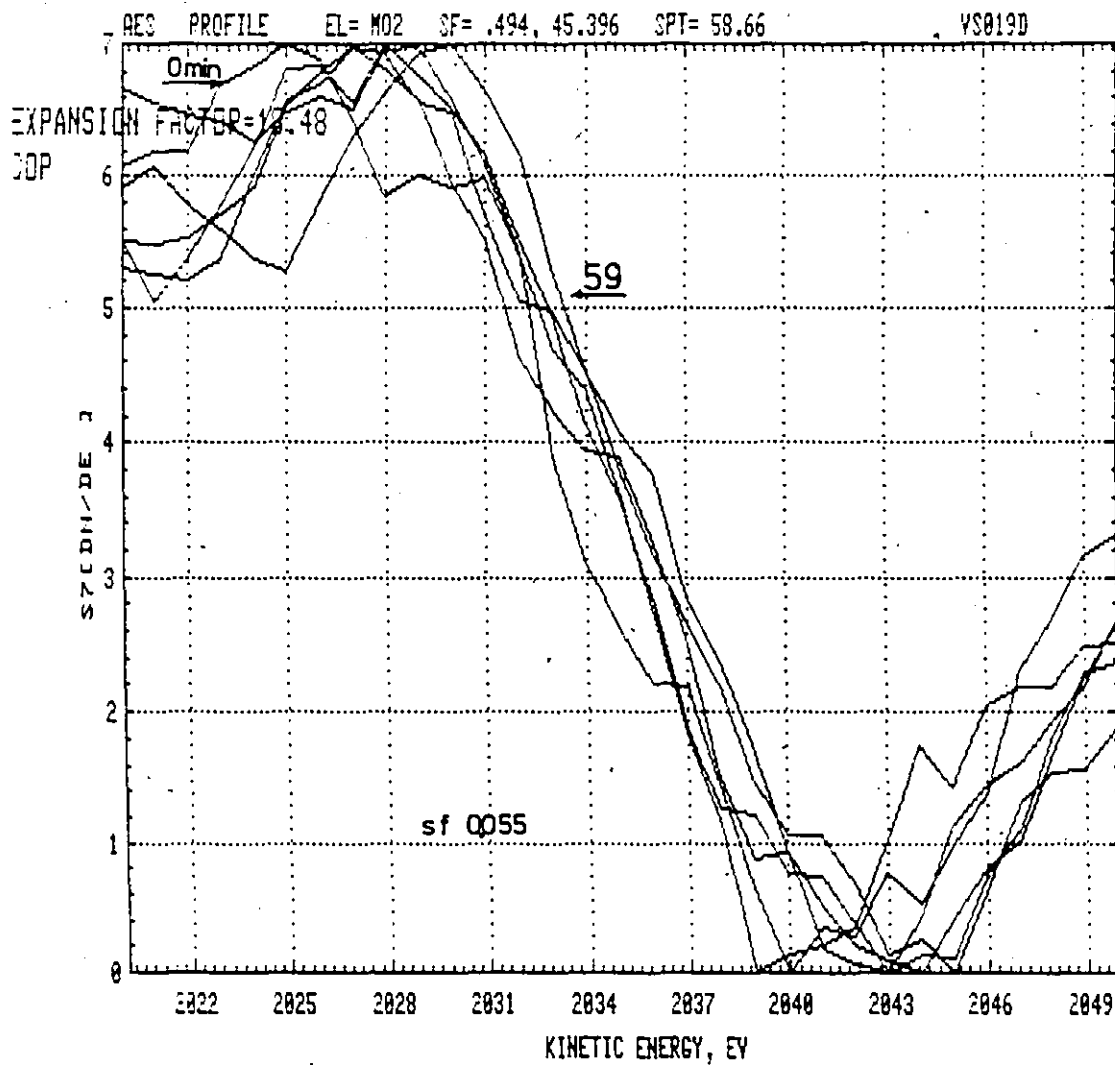


Fig. 3-39

AES profile on the air formed film on Mo. concentration change of Mo as a function of the type of Auger transition considered

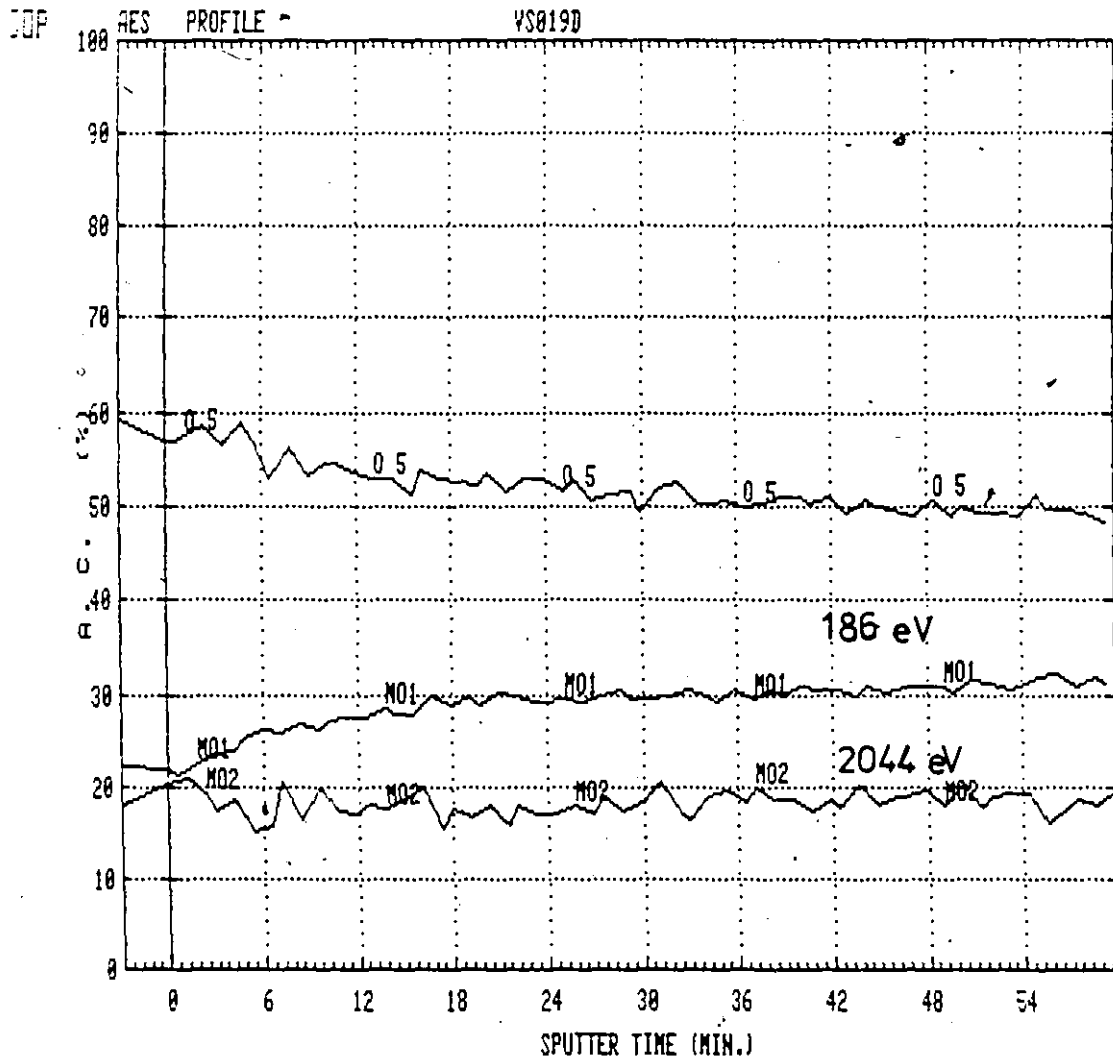


Fig. 3-40

AES spectrum of oxygen after 2.3 min of sputtering (1 keV Xe<sup>+</sup>)

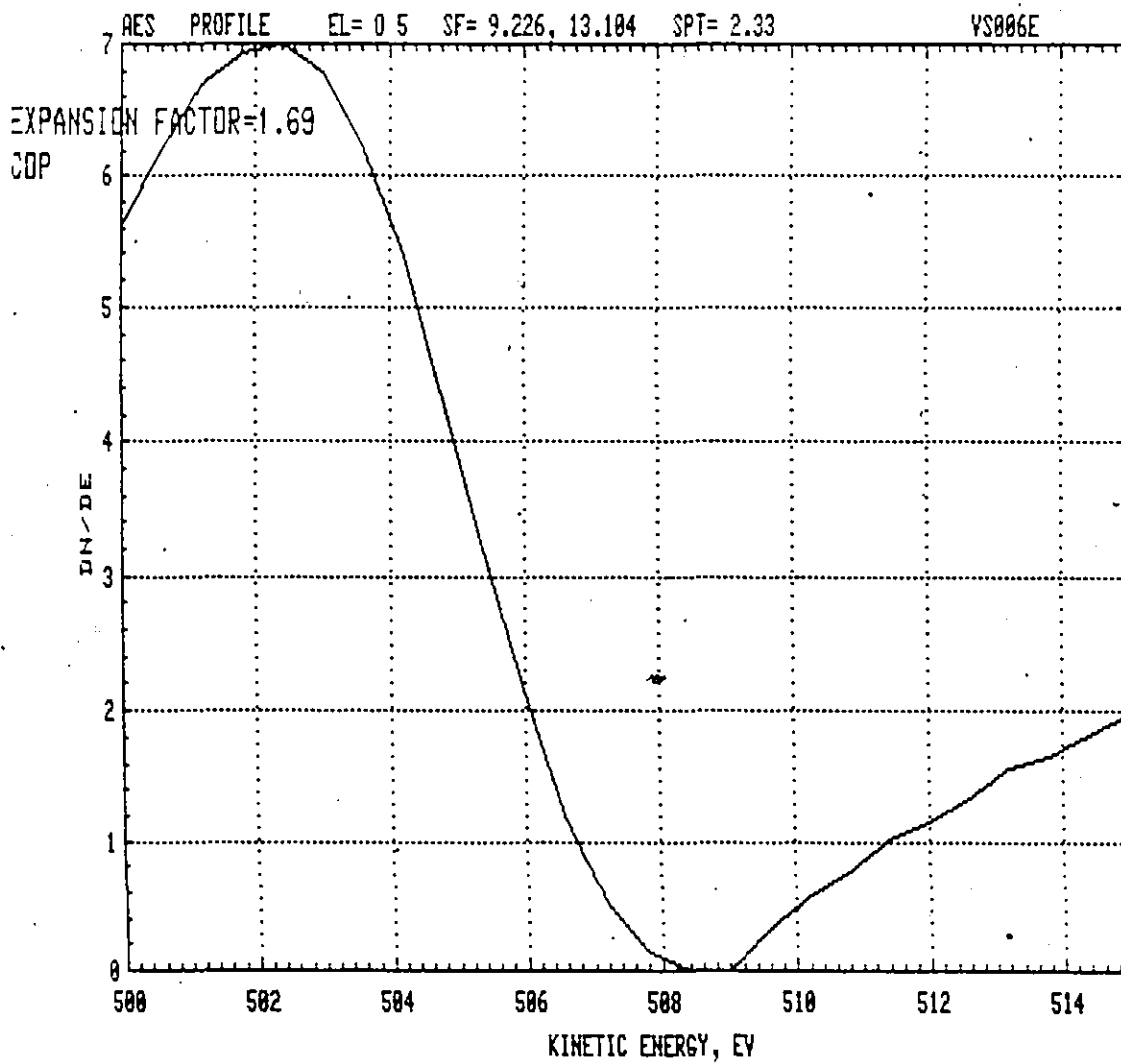


Fig. 3-41

AES spectrum of oxygen after ~ 10 min of sputtering (1 keV Xe<sup>+</sup>)

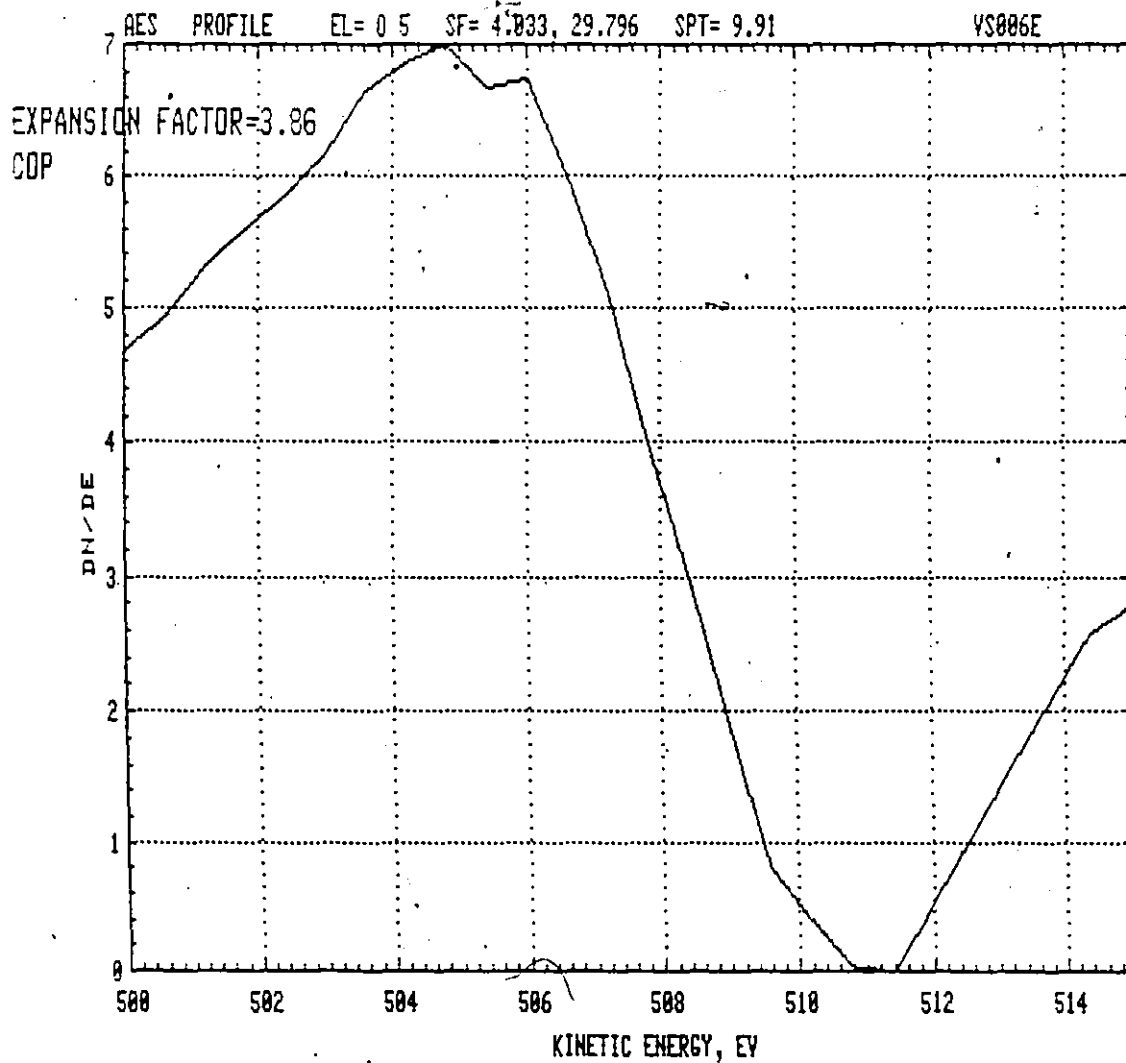
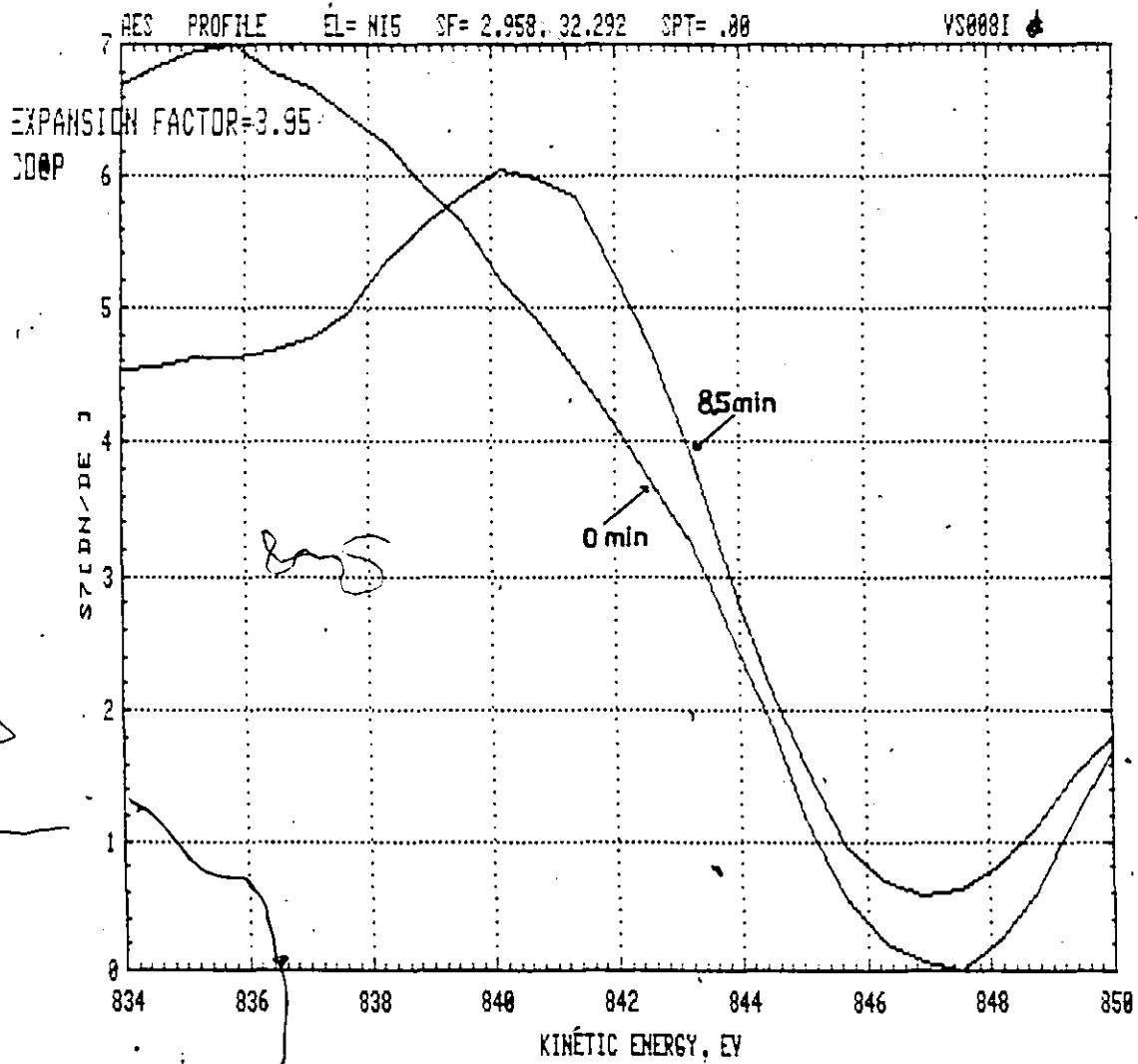


Fig. 3-42

Variation of Ni (848 eV) Auger spectrum with time of electron beam irradiation (5 keV)



analysis. AES profile of the air formed film on pure molybdenum, containing both Mo peaks, is shown on Fig. 3-39. It is clear that the 2044 eV Mo peak does not give rise to apparent increase of Mo-concentration which is due to the ion beam effect in the case of the 186 eV Mo peak.

The ion beam effect on the oxygen peak is shown on Figs. 3-40 and 3-41, after 2 min and 10 min sputtering with 1 keV Xe<sup>+</sup>.

The electron beam irradiation effect on the Ni (848 eV) peak is shown on Fig. 3-42 for an 8.5 min exposure to a 5 keV beam.

Bearing in mind that the electron beam, as well as the ion beam, energy [176-178] affect the AES depth profiling it is clear that establishing the optimum conditions with improved accuracy would involve an extensive experimental research effort which was beyond the scope of this work.

#### 3.5.4 X RAY-PHOTOELECTRON SPECTROSCOPY (XPS) OF ANODIZED Ni-13Mo

XPS was employed to characterize the species present on Ni-13 Mo electrodes after a variety of treatments including the sample preparation techniques, polarization in the active and passive ranges, the influence of the solution pH and of the time on open circuit of a previously anodized sample.

All the data reported are referenced to the Au (4f 7/2) level at  $83.8 \pm 0.5$  eV. The Mg k<sub>α</sub> X-ray line (1253.6 eV) was used for photoelectron excitation. The data have been collected at 0.01 V/sec (0.1 V/step, 100 msec/step) with the electron pass energy set to a constant 50 eV.



#### 3.5.4.1 Ni(2p) ELECTRON SPECTRUM OF Ni-13Mo

XPS Ni(2p) spectra obtained on Ni-13Mo samples after a series of different electrochemical treatments are given on Figs. 3-43 to 3-51 with the corresponding conditions of each sample prior to the XPS analysis.

Table 3-10 summarizes Ni(2P) binding energies (eV) determined visually for the set of conditions examined.

The exact kinetic energy of the photoelectron reflects the chemical environment of the element. A variety of Ni-oxygen species have been identified by a number of workers and although some controversy exists as to specific spectral components, NiO and Ni(OH)<sub>2</sub> can be clearly distinguished [179]. Various other species, such as NiO<sub>ads</sub>, Ni<sub>2</sub>O<sub>3</sub>, NiOO<sub>ads</sub>, β-NiOOH have been observed [180-182], with poor agreement of the reported values.

The electron binding energies reported range, for NiO from 854.0 ± 0.2 eV to 854.5 eV, for Ni(OH)<sub>2</sub> from 855.6 ± 0.3 eV to 856.6 eV for Ni<sub>2</sub>O<sub>3</sub> 855.8 ± 0.1 eV. Therefore from the data obtained on Ni-13 Mo (Table 3-10) it appears that NiO is not a component of the anodic oxide film. Either Ni(OH)<sub>2</sub>, Ni<sub>2</sub>O<sub>3</sub> or some mixed oxide phase with Mo could be assumed. Unanodized samples show the presence of Ni-metal (852.3 eV).

Fig. 3-43

Ni(2p) electron spectrum of Ni-13 Mo following the mechanical polishing and electropolishing procedure.

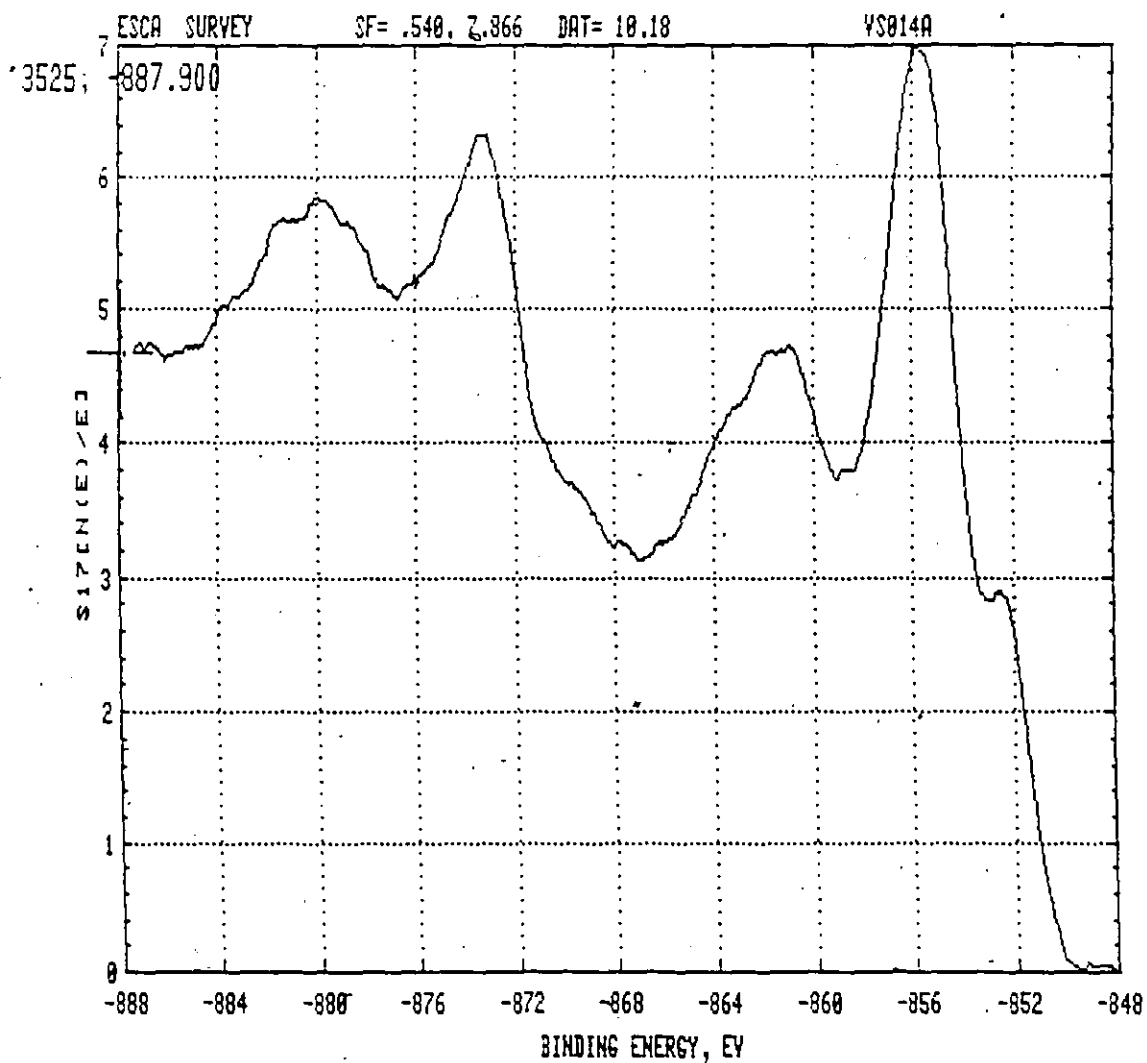


Fig. 3-44

Ni(2p) electron spectrum of Ni-13 Mo following the electropolishing and cathodic reduction procedure.

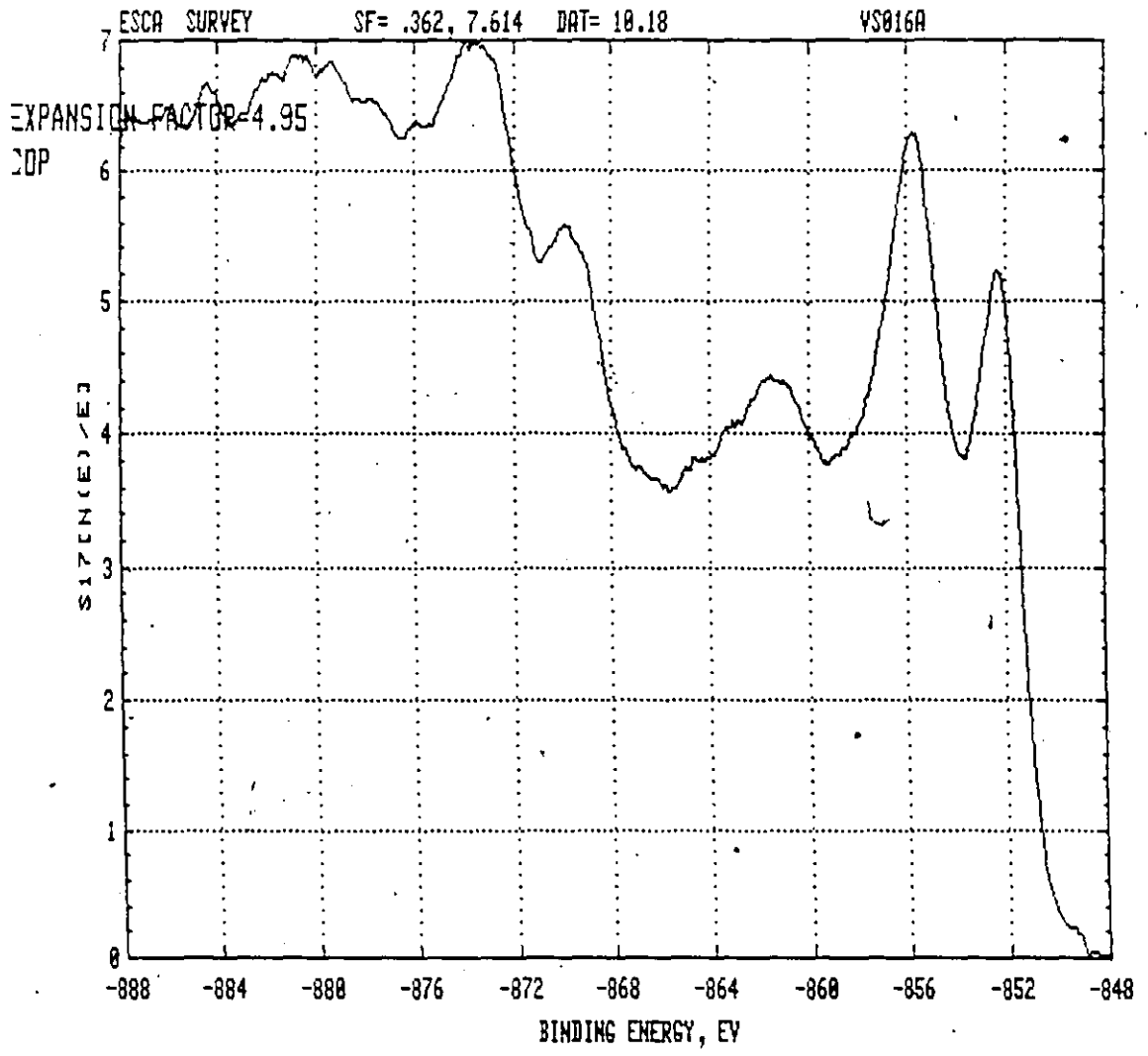


Fig. 3-45

Ni(2p) electron spectrum of Ni-13 Mo following the mechanical polishing, and cathodic reduction procedure

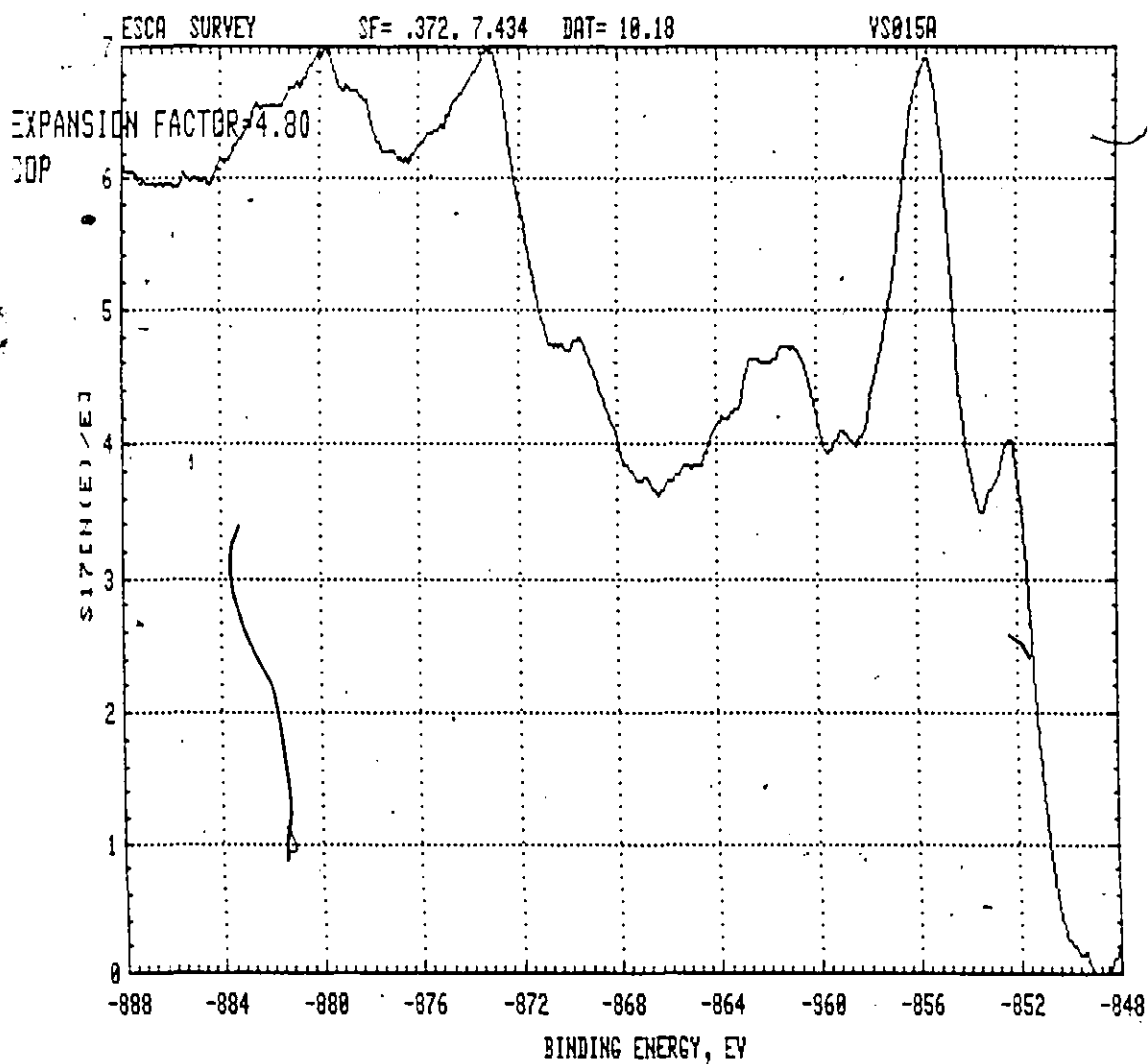


Fig. 3-46

Ni(2p) electron spectrum of Ni-13 Mo following polarization in the active potential range (30 min.)

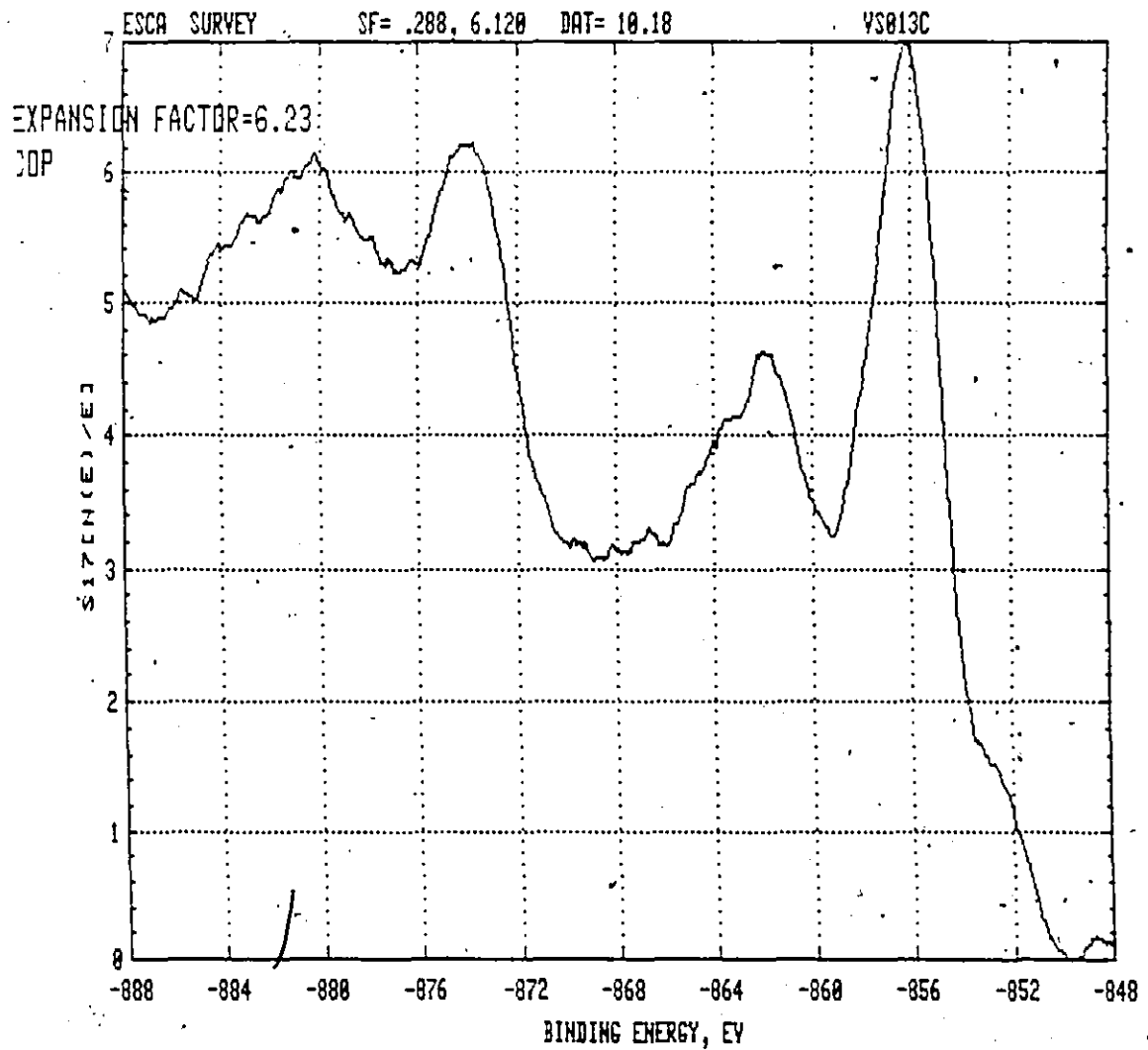


Fig. 3-47

Ni(2p) electron spectrum of Ni-13 Mo following anodization (+500 mV, 2 hr, pH 2.8).

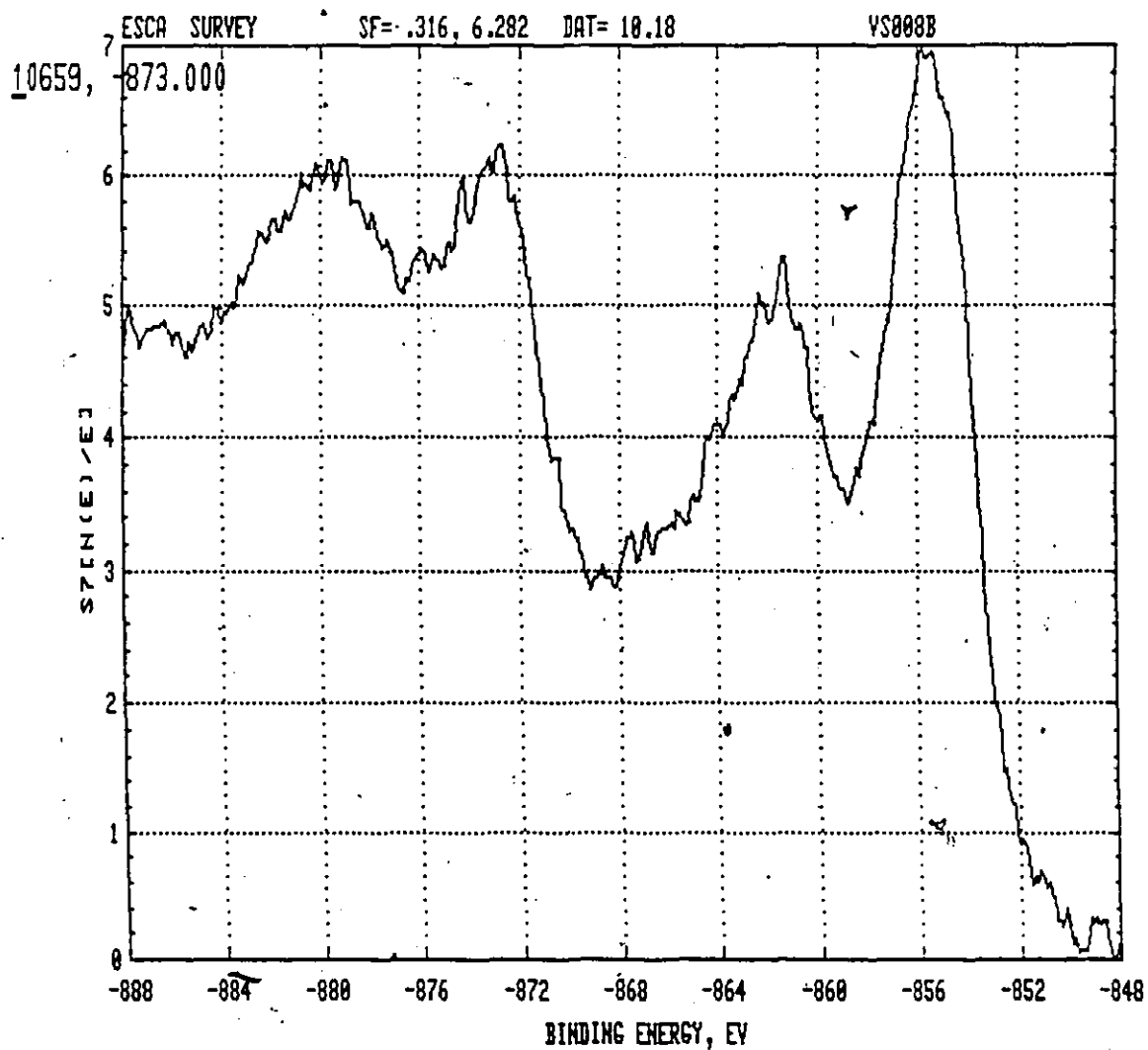


Fig. 3-48

Ni(2p) electron spectrum of Ni-13 Mo following  
anodization (+500 mV, 2 hr, pH 2.8) and OCPD  
(3 min.)

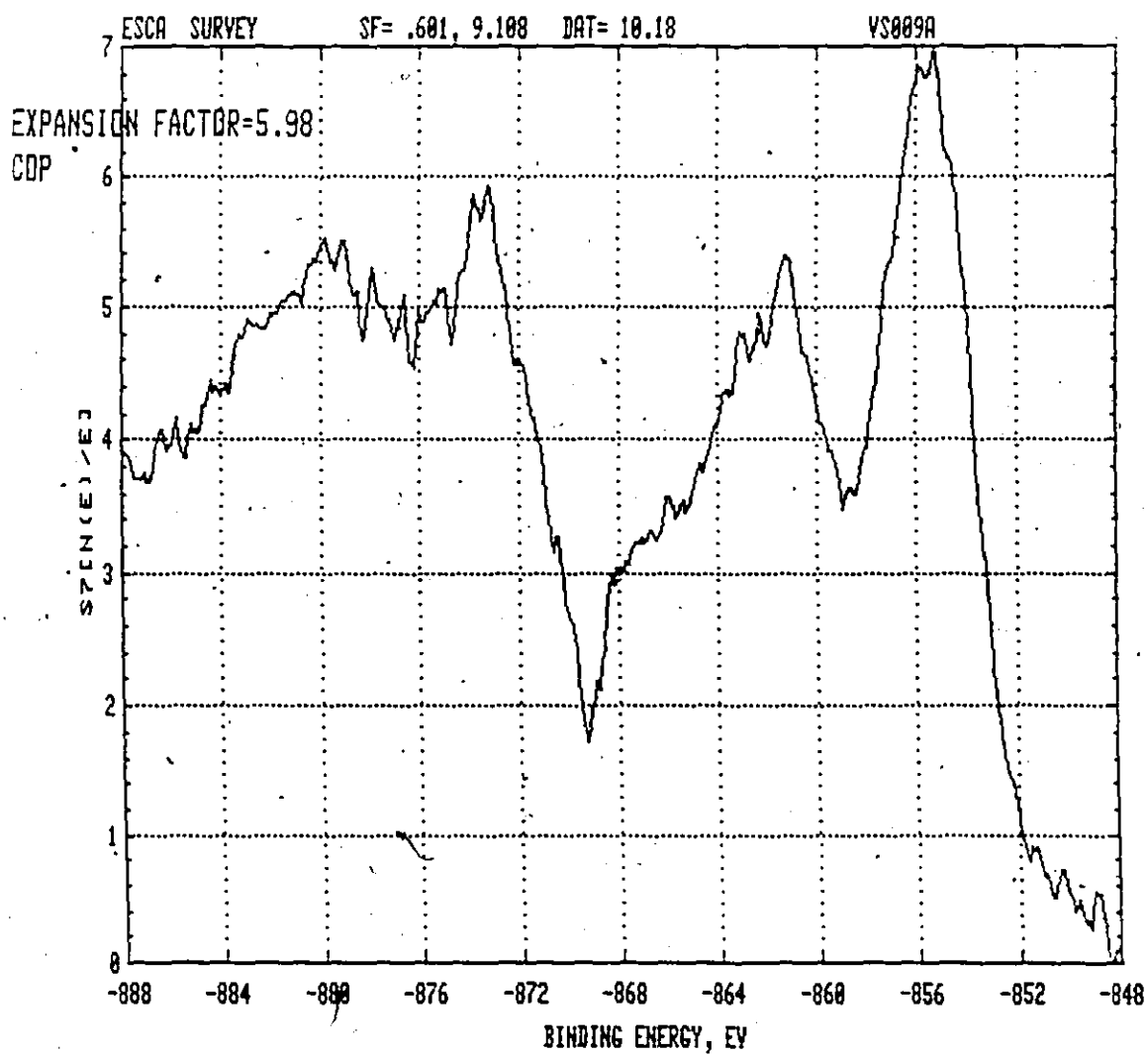


Fig. 3-49

Ni(2p) electron spectrum of Ni-13 Mo following anodization (+500 mV, 2 hr, pH 2.8) and OCPD (30 min.)

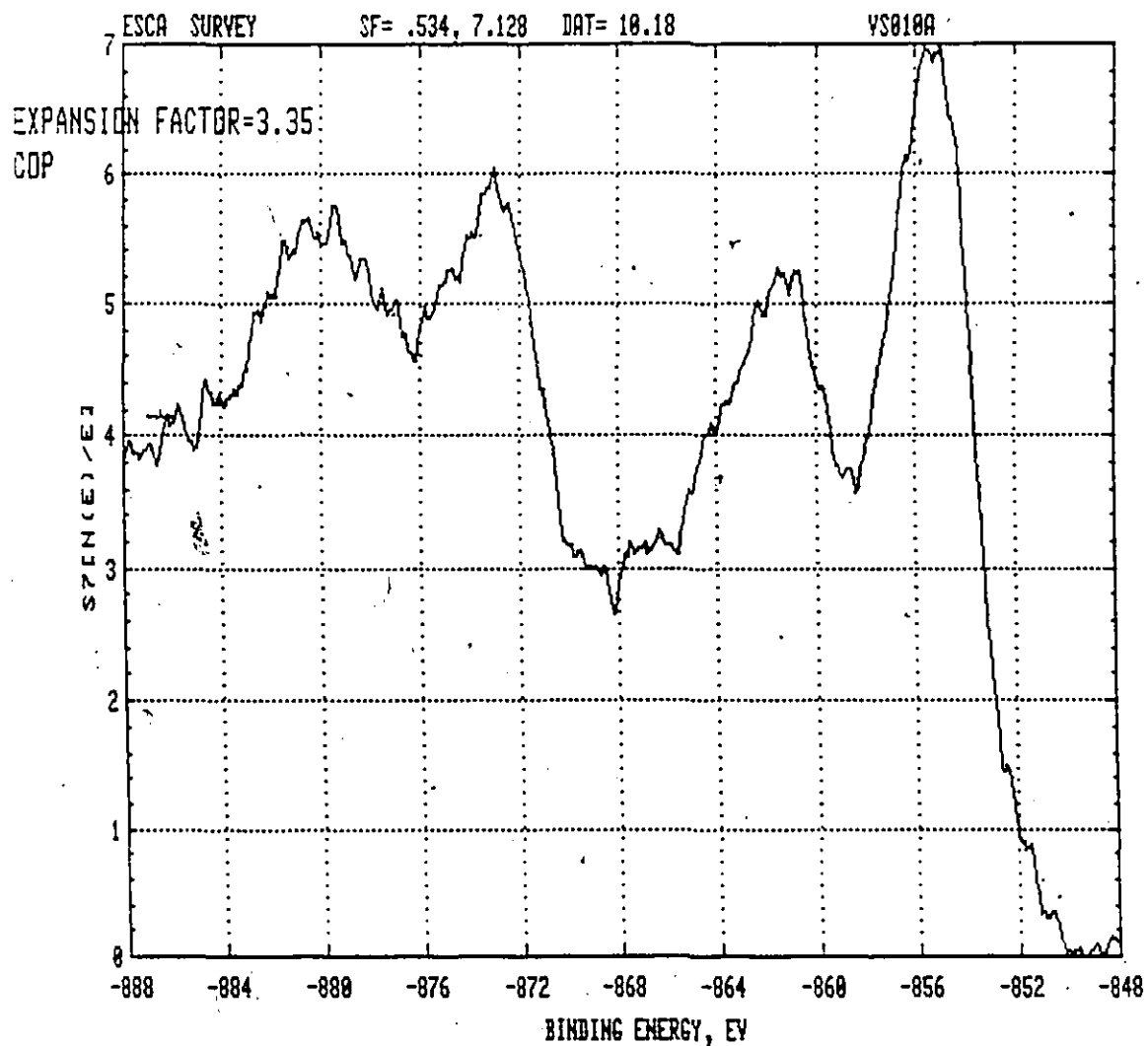




Fig. 3-50

Ni(2p) electron spectrum of Ni-13 Mo following anodization (+500 mV, 2hr, pH 10.2).

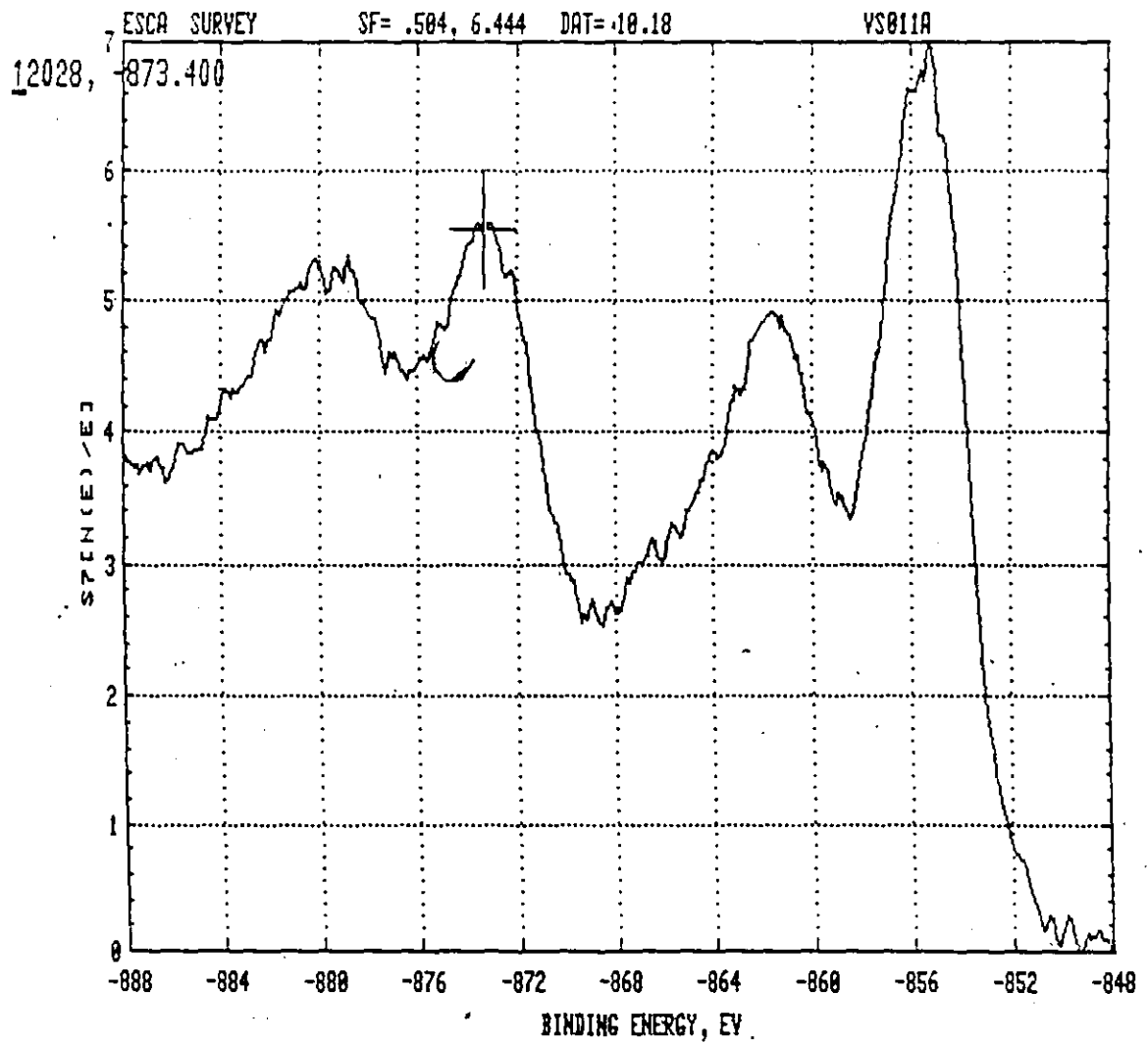


Fig. 3-51

Ni(2p) electron spectrum of Ni-13 Mo following anodization (+ 500 mV, 2 hr, pH 1.5 ).

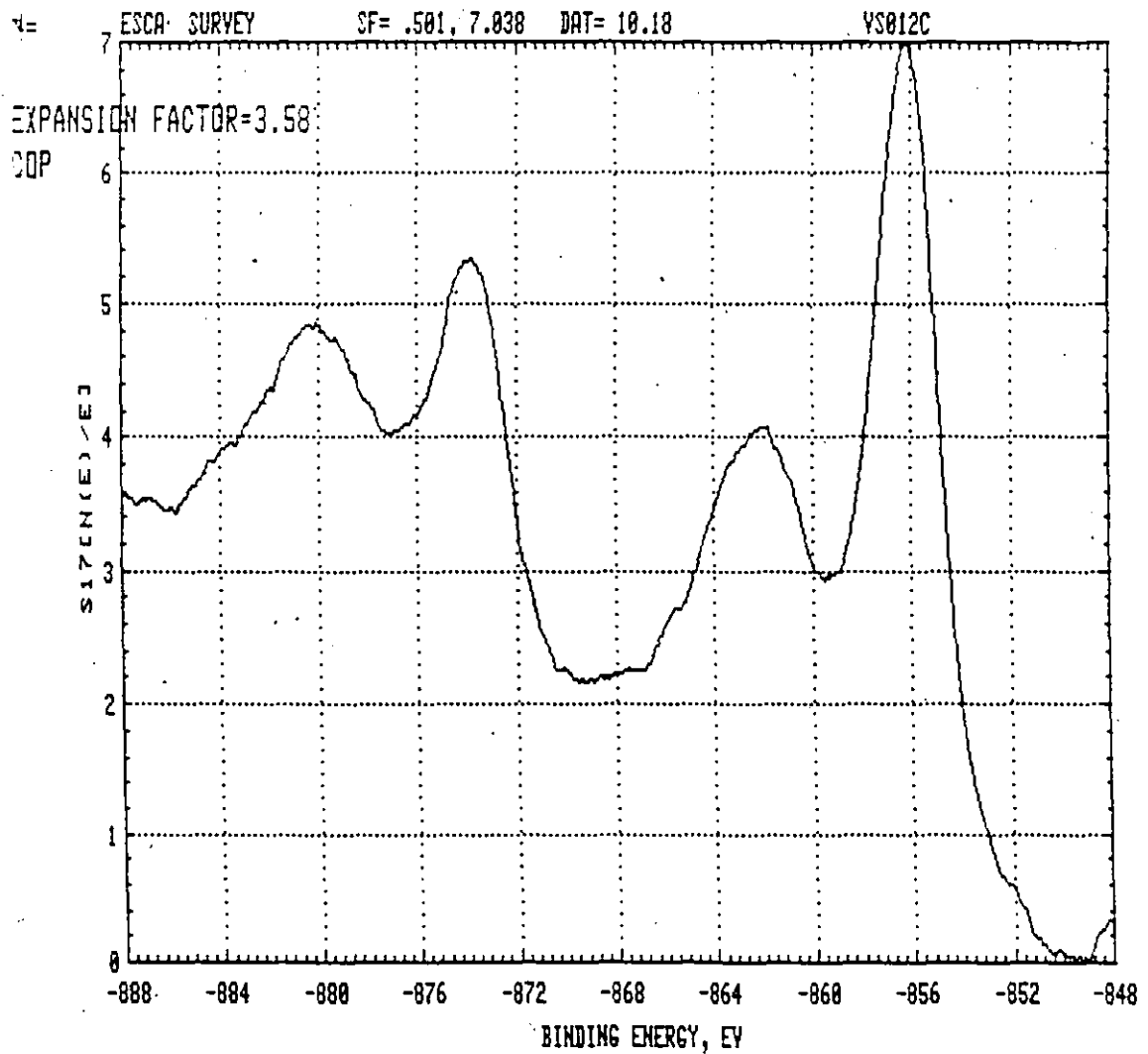


TABLE 3-10

Binding energies for the Ni(2p) observed  
in XPS spectra of Ni-13Mo.

Sample Treatment	Ni(2p) binding energy (eV)	
	NiO <sub>x</sub> 2p <sup>3/2</sup>	Ni 2p <sup>3/2</sup>
Electropolish	855.5 ± 0.2	852.5 ± 0.2
Electropol. + Cath. Red.	855.7 ± 0.2	852.3 ± 0.2
Cath. Red.	855.7 ± 0.2	852.3 ± 0.2
Active Range	856.2 ± 0.2	Shoulder 852.3
+500 mV, 2 h pH = 2.8	855.6 ± 0.2	
OCPD (3 min)	855.6 ± 0.2	
OCPD (30 min)	855.4 ± 0.2	
+500 mV, 2 h pH = 10.2	856.2 ± 0.2	
+500 mV, 2 h pH = 1.5	855.5 ± 0.2	

### 3.5.4.2 Mo(3d) ELECTRON SPECTRUM OF Ni-13 Mo

The Mo(3d) electron spectra given in Figs. 3-52 to 3-60 correspond to the results of XPS analysis of Ni-13 Mo electrodes after different electrochemical treatments (specified on each figure)., Mo(3d) electron spectrum of the air formed film on pure Mo is given on Fig. 3-61.

Table 3-11 gives X-ray photoelectron binding energies for each spectrum examined.

TABLE 3-11

Binding energies for Mo(3d) observed in XPS spectra of Ni-13 Mo

Sample Treatment	Mo(3d) Binding Energy (eV)		
	Mo 3d <sup>3/2</sup>	Mo 3d <sup>5/2</sup>	
Electropolish	235.4	232.1 ± 0.2	227.9
Electropolish and Cath. Red.	235.0	231.3 ± 0.2	227.9
Cath. Red.	235.2	231.8 ± 0.2	227.9
Active Range	235.2	232.6 ± 0.2	228.0
+500 mV, 2 h pH = 2.8	235.4	232.3 ± 0.2	-
OCPD (3 min)	235.1	232.3 ± 0.2	-
OCPD (30 min)	235.2	232.2 ± 0.2	
+500 mV, 2 h pH = 10.2	235.4	232.3 ± 0.2	
+500 mV, 2 h pH = 1.5	?	?	?
Mo Foil Air Formed Film	235.4	232.3 ± 0.2	-

Published work on the XPS analysis of Mo compounds [182-186] gives the values of the characteristic binding energies for the compounds of interest, summarized in Table 3-12.

TABLE 3-12

Compound	Mo ( $3d_{3/2}$ )	Mo ( $3d_{5/2}$ )
	235.6 ± 0.1	232.5 ± 0.1
MoO <sub>3</sub>	235.85	232.65
	235.5	232.2
		231.7
MoO <sub>x</sub> 2 < x < 3	234.3	231.2
	233.9 ± 0.1	230.9 ± 0.1
MoO <sub>2</sub>	232.5	229.4
	232.4	229.3
		231.0
Na <sub>2</sub> MoO <sub>4</sub>	235.2 ± 0.2	232.1 ± 0.2
		231.5
Na <sub>2</sub> MoO <sub>4</sub> x 2H <sub>2</sub> O		232.3
	235.3	232.2

By comparing the measured values of Mo(3d) binding energies for the Ni-13 Mo samples, oxidized Mo and the values given in Table 3-12, it appears difficult to characterize Mo-species

Fig. 3-52

Mo(3d) electron spectrum of Ni-13 Mo following mechanical polishing and electropolishing.

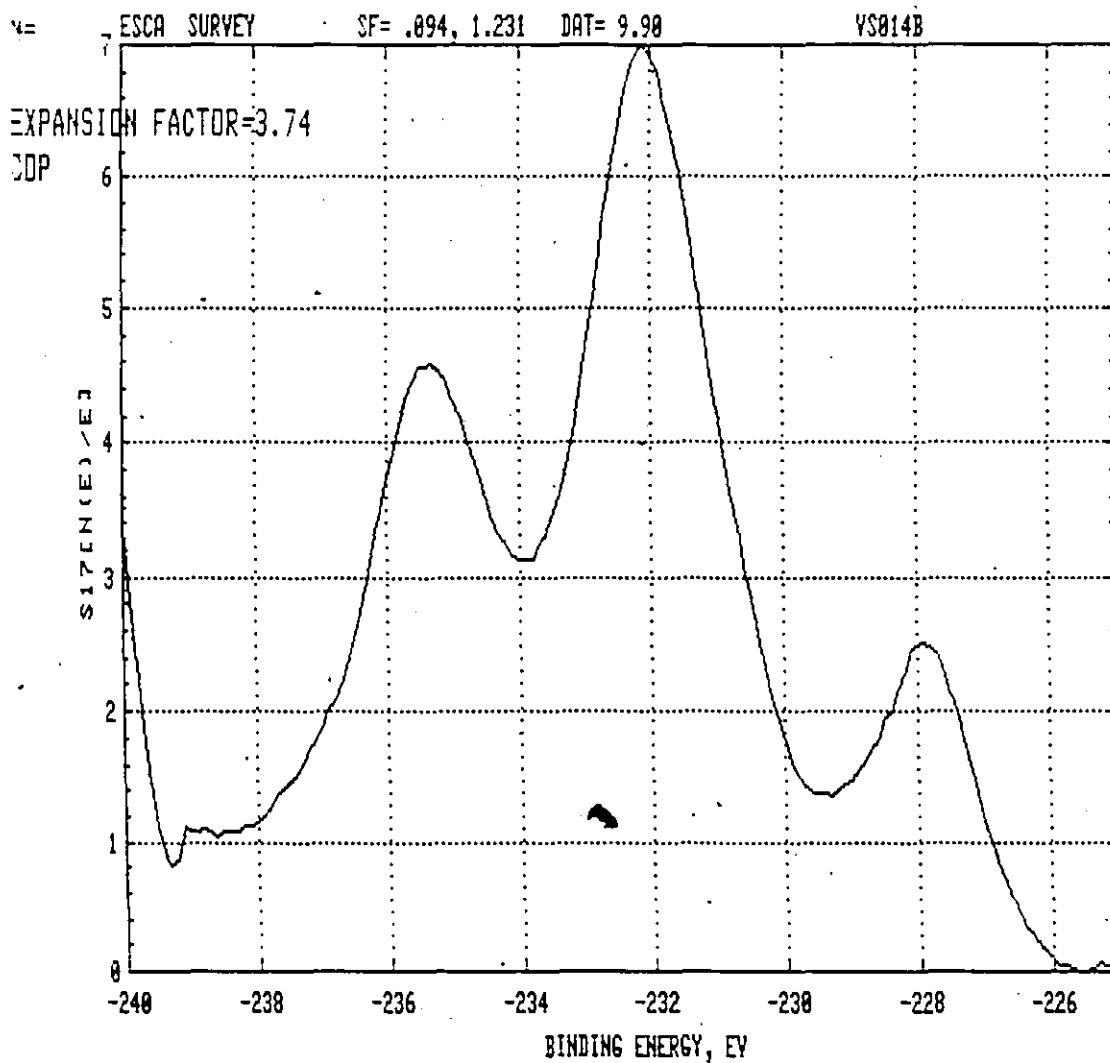


Fig. 3-53

Mo(3d) electron spectrum of Ni-13 Mo following  
electropolishing and cathodic reduction

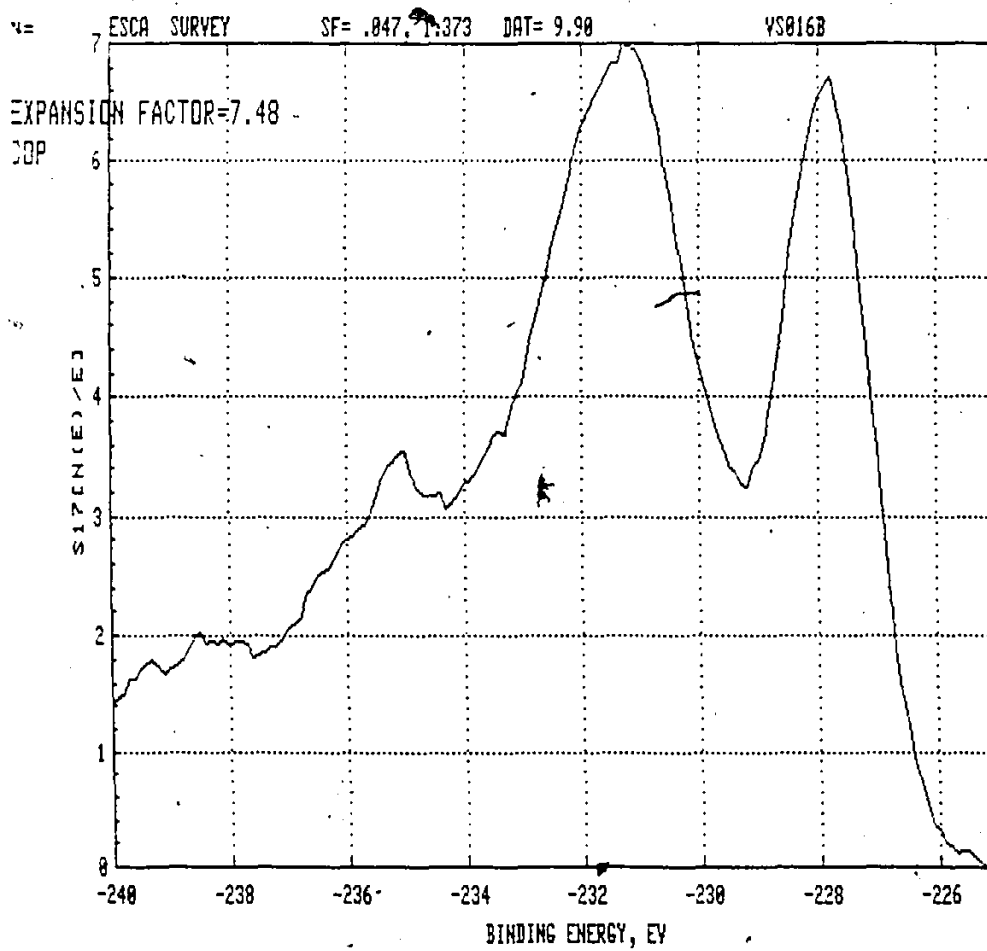


Fig. 3-54

Mo(3d) electron spectrum of Ni-13 Mo following mechanical polishing and cathodic reduction.

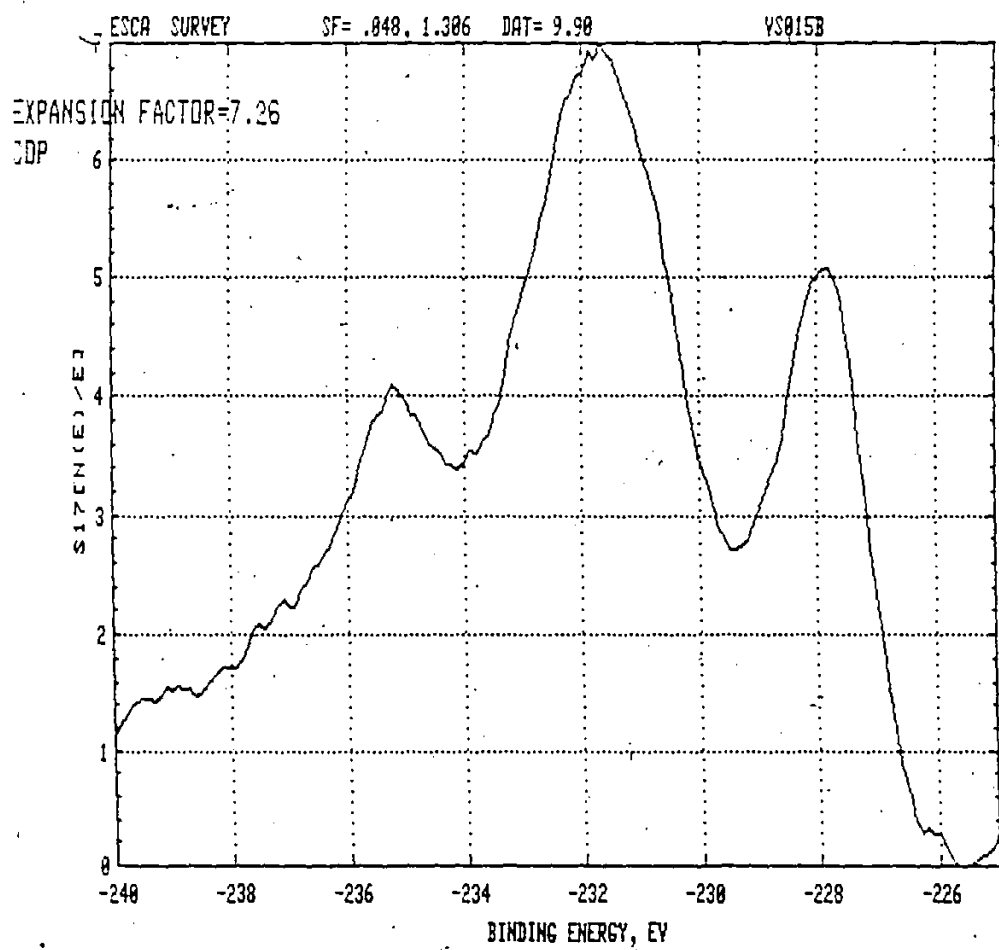




Fig. 3-55

Mo(3d) electron spectrum of Ni-13 Mo following polarization in the active range (30 min.)

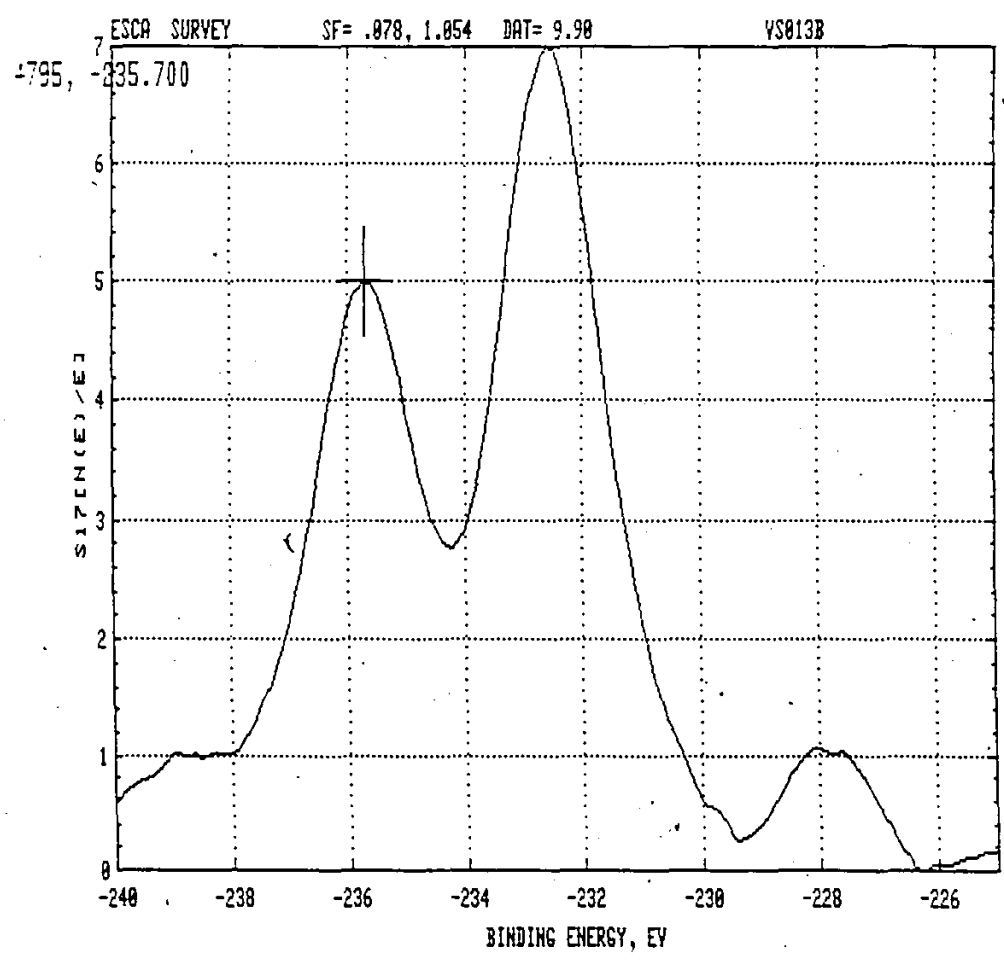


Fig. 3-56

Mo(3d) electron spectrum of Ni-13 Mo following  
anodization (+500 mV, 2h., pH 2.8)

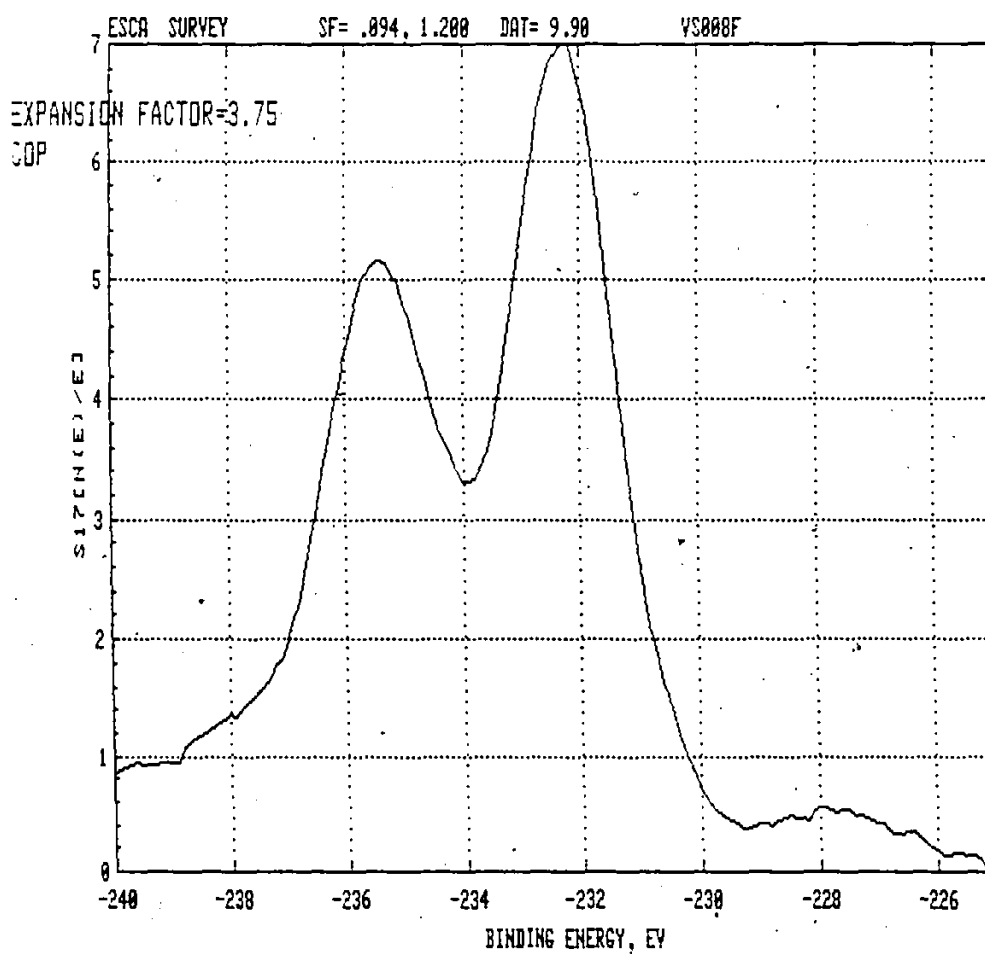


Fig. 3-57

Mo(3d) electron spectrum of Ni-13 Mo following anodization (+500 mV, 2h., pH 2.8) and OCPD (3 min).

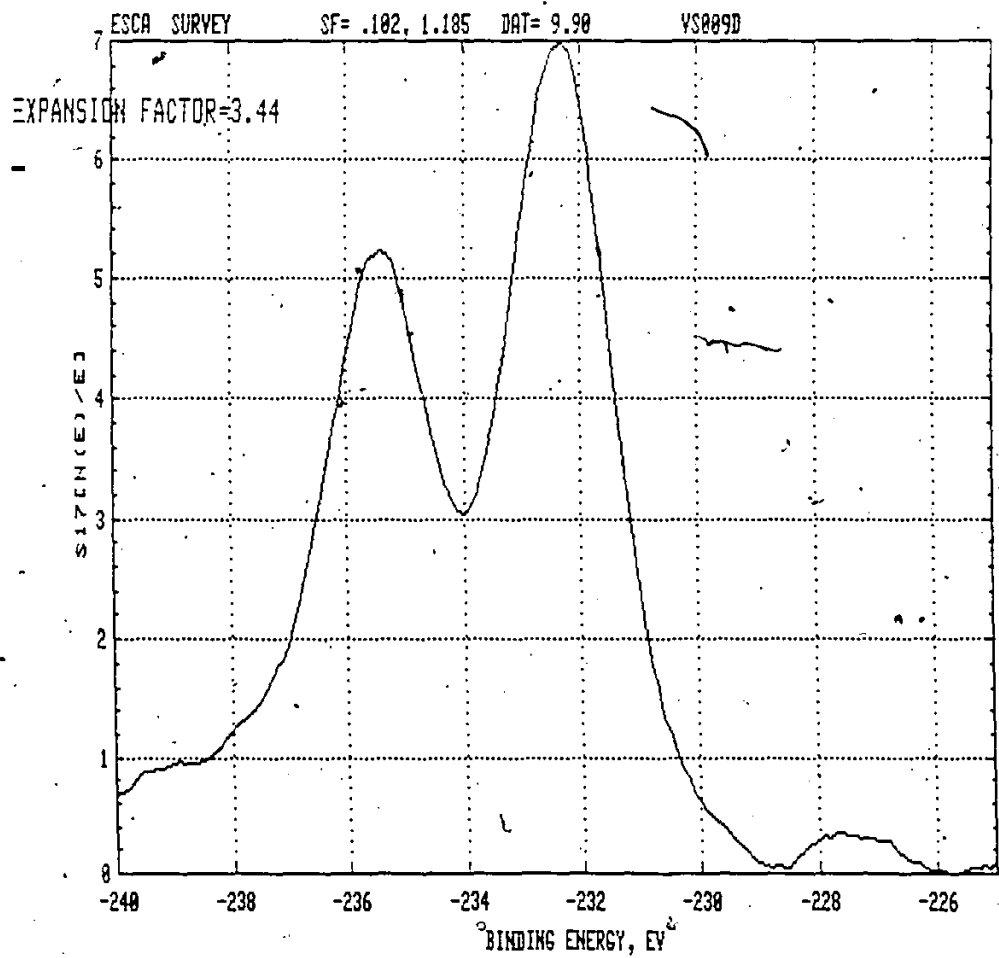


Fig. 3-58

Mo(3d) electron spectrum of Ni-13 Mo following  
anodization (+500 mV, 2h., pH 2.8) and OCPD (30 min.).

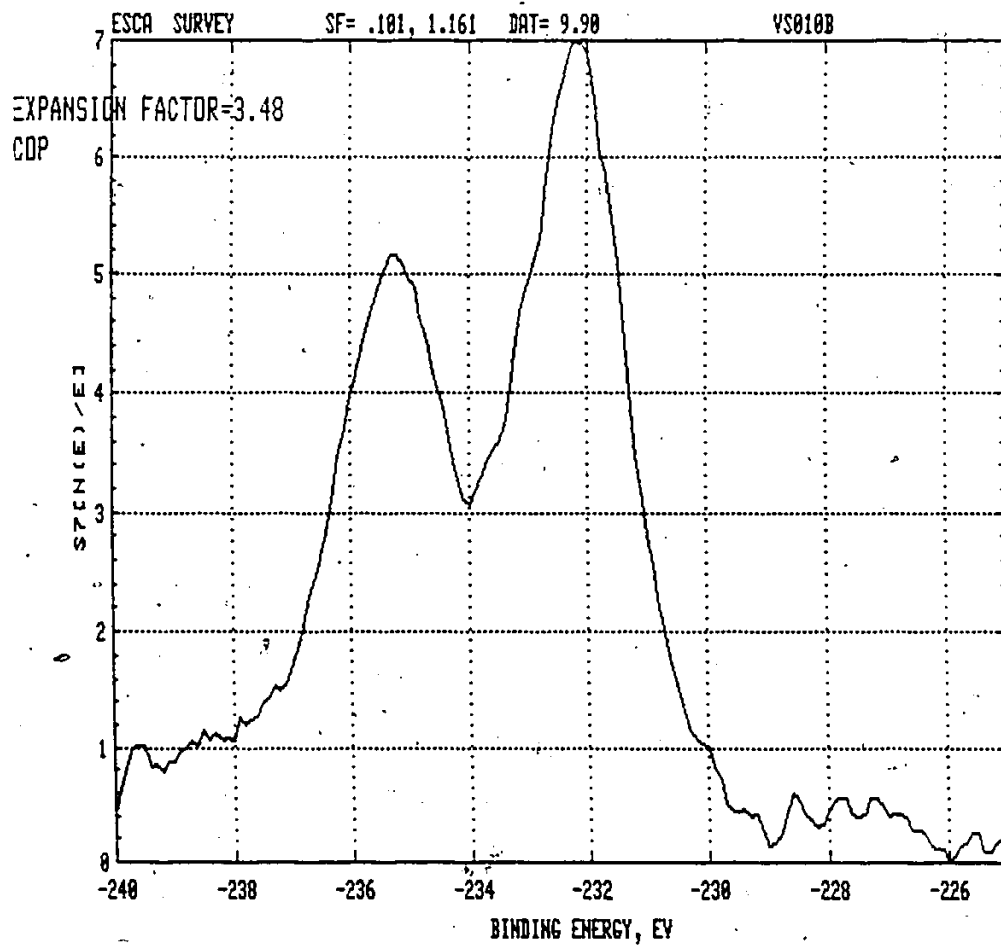


Fig. 3-59

Mo (3d) electron spectrum of Ni-13 Mo following  
anodization (+500 mV, 2h., pH 10.2).

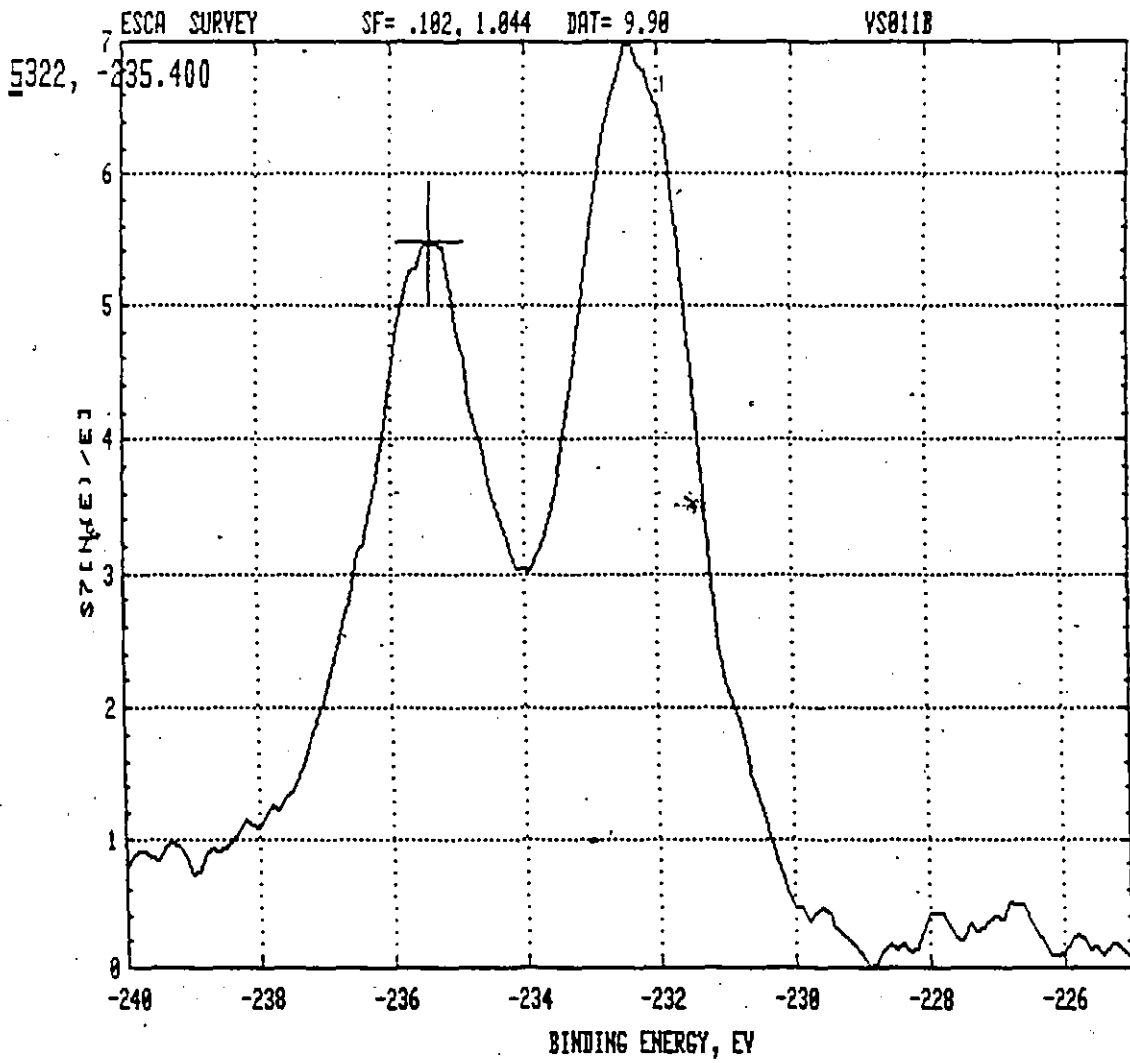


Fig. 3-60

Mo(3d) electron spectrum of Ni-13 Mo following  
anodization (+500 mV, 2h., pH 1.5).

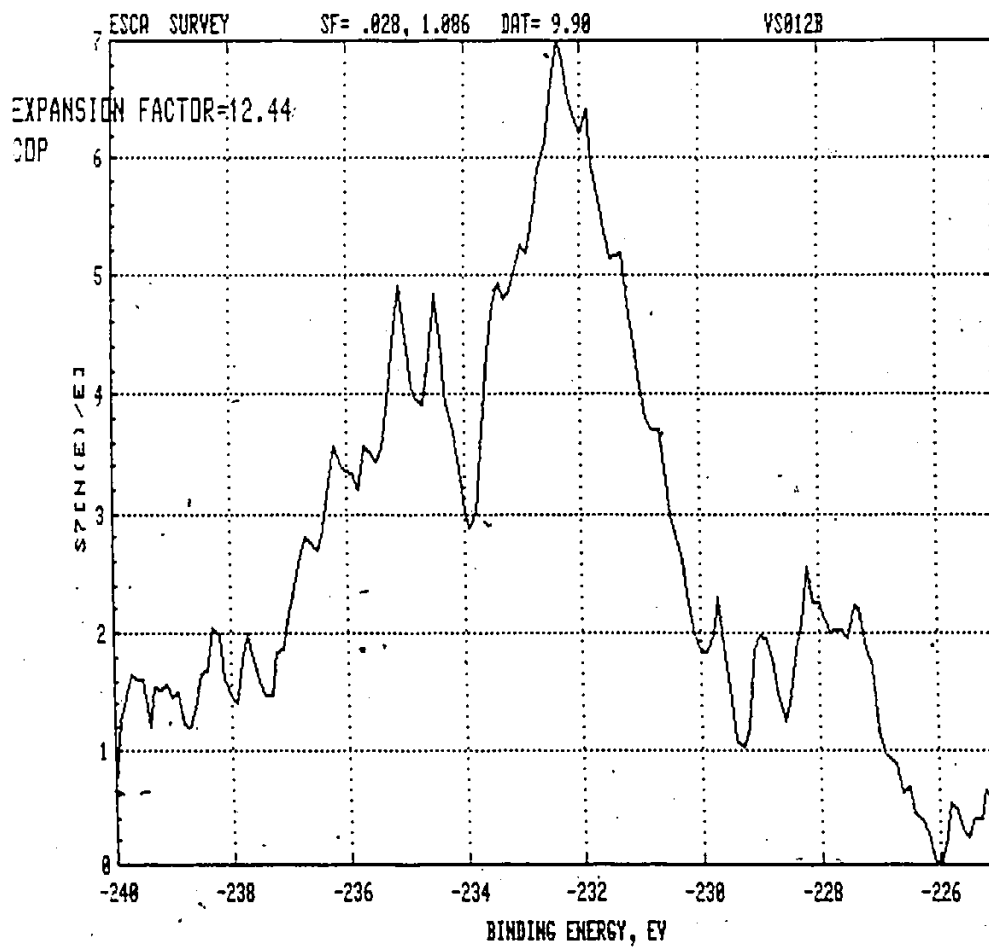


Fig. 3-61

Mo(3d) spectrum of air formed film on Mo

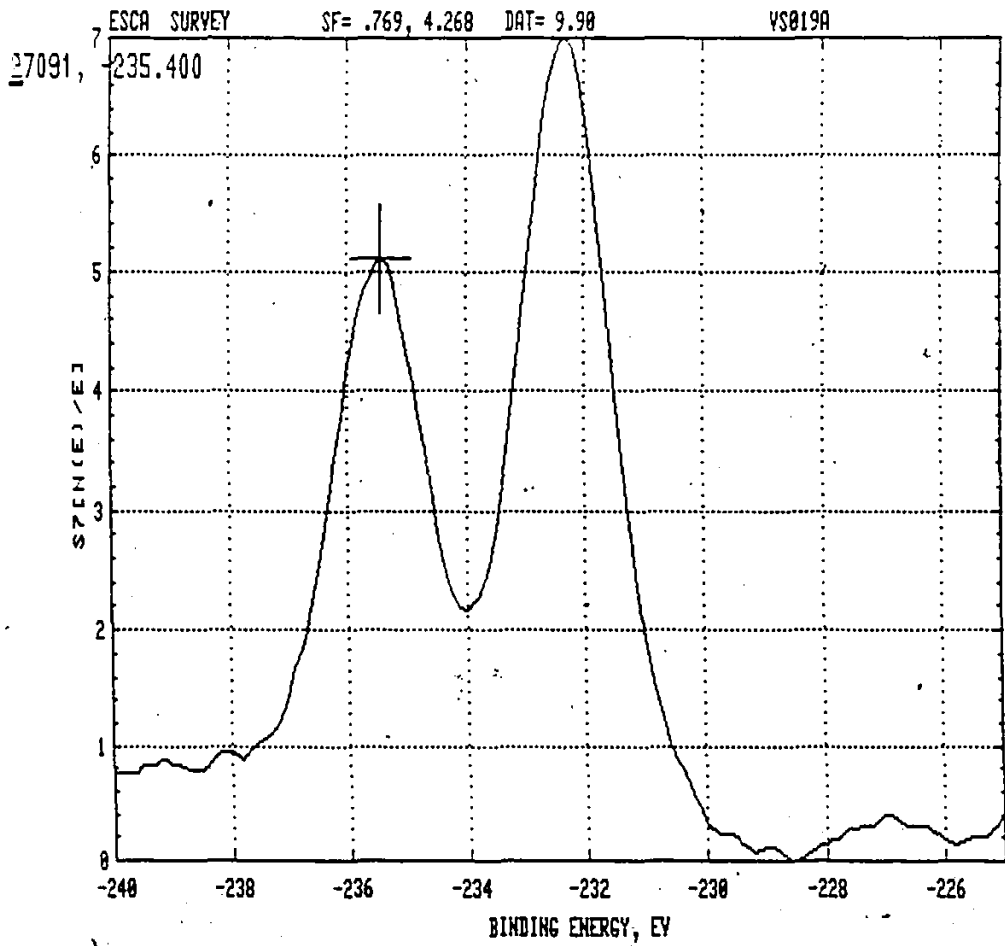
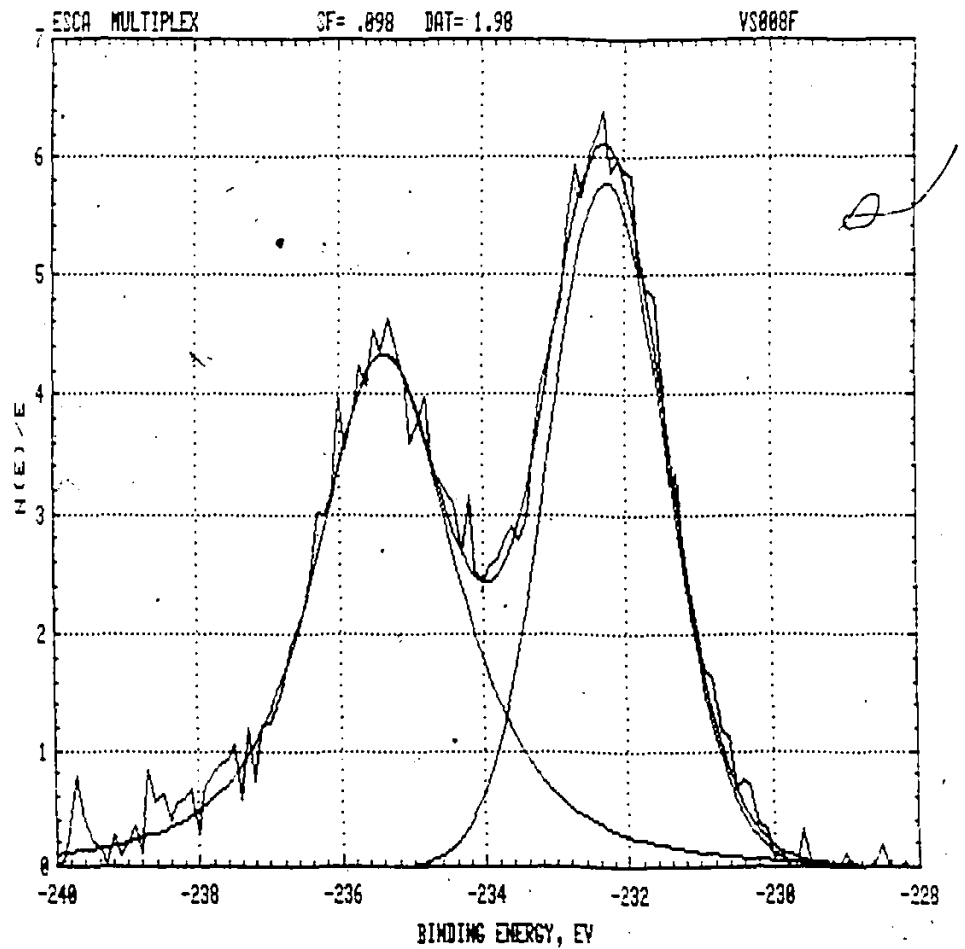


Fig. 3-62

Deconvoluted Mo(3d) peak for anodized Ni-13 Mo  
(+500 mV, 2h., pH2.8)



Band	Area	Peak Position (3V)	Intensity (counts/sec)	FWHM	Percent Gaussian
1	1186	232.26	572	1.95	100
2	1472	235.56	436	2.38	29.8



present on the surface of Ni-13Mo alloy in each case. However, certain conclusions could be drawn:

- The valence state of Mo appears to be +6 in all cases
- Mo( $3d^{5/2}$ ) peaks of the air formed film on Mo and of the anodic films formed at pH 10.2 and pH 2.8, as well as those observed on the samples after the open circuit potential decay have the same values of binding energy, suggesting the presence of  $\text{MoO}_3$  or  $\text{MoO}_4^{2-}$  in each case (Figs. 3-56 to 3-59).
- The presence of Mo-metal (227-9 eV) is evident for the samples previously subjected to all three pretreatment procedures (Figs. 3-52 to 3-54), for those polarized in the active potential range and in the solution of pH 1.5 (Figs. 3-55 and 3-60).
- The absence of Mo-metal peak in the spectra obtained on the samples after the open circuit potential decay indicates that the film is not being removed on the open circuit (Figs. 3-57 and 3-58).

Deconvolution of the Mo(3d) peak of anodized Ni-13Mo (Fig. 3-62) and the data on binding energies of Mo ( $3d^{3/2}$ ,  $3d^{5/2}$ ) [186] clearly show that the surface film produced by anodization of pH 2.8 contains Mo-species in  $\text{Mo}^{6+}$  state. It is, however, not certain whether the film is  $\text{MoO}_3$  or contains  $\text{Mo}^{6+}$  in the form of  $\text{MoO}_4^{2-}$ .

#### 3.5.4.3 O(1s) ELECTRON SPECTRUM OF Ni-13Mo

Since the O(1s) line positions of metal oxides generally provide another means for their identification, the O(1s) spectra of Ni-13Mo samples, already examined by XPS analysis of Ni(2p) and

Mo(3d) lines, is given on Figs. 3-63 to 3-71. The O(1s) spectrum of the air formed film on pure Mo is given on Fig. 3-72.

The values of binding energy are summarized in Table 3-13.

TABLE 3-13

Binding energies of O(1s) spectra of Ni-13Mo  
when fit to one peak

Sample Treatment	O(1s) Binding energy (eV)	FWHM*
Electropol.	531.3	1.85
Electropol. and Cath. Red.	531.4	1.75
Cath. Red.	531.4	1.70
Active Range	531.5	1.90
+500 mV, 2h pH = 2.8	530.9	2.35
OCPD (3 min)	530.7 (530.2 sh)	2.25
OCPD (30 min)	530.7	2.25
+500 mV, 2 h. pH = 10.2	530.9	2.30
+500 mV, 2h pH = 1.5	531.6	1.65
Mo Foil Air formed Film	530.2	1.90

\* full width at half maximum

Fig. 3-63

O(1s) electron spectrum of Ni-13 Mo following mechanical polishing and electropolishing.

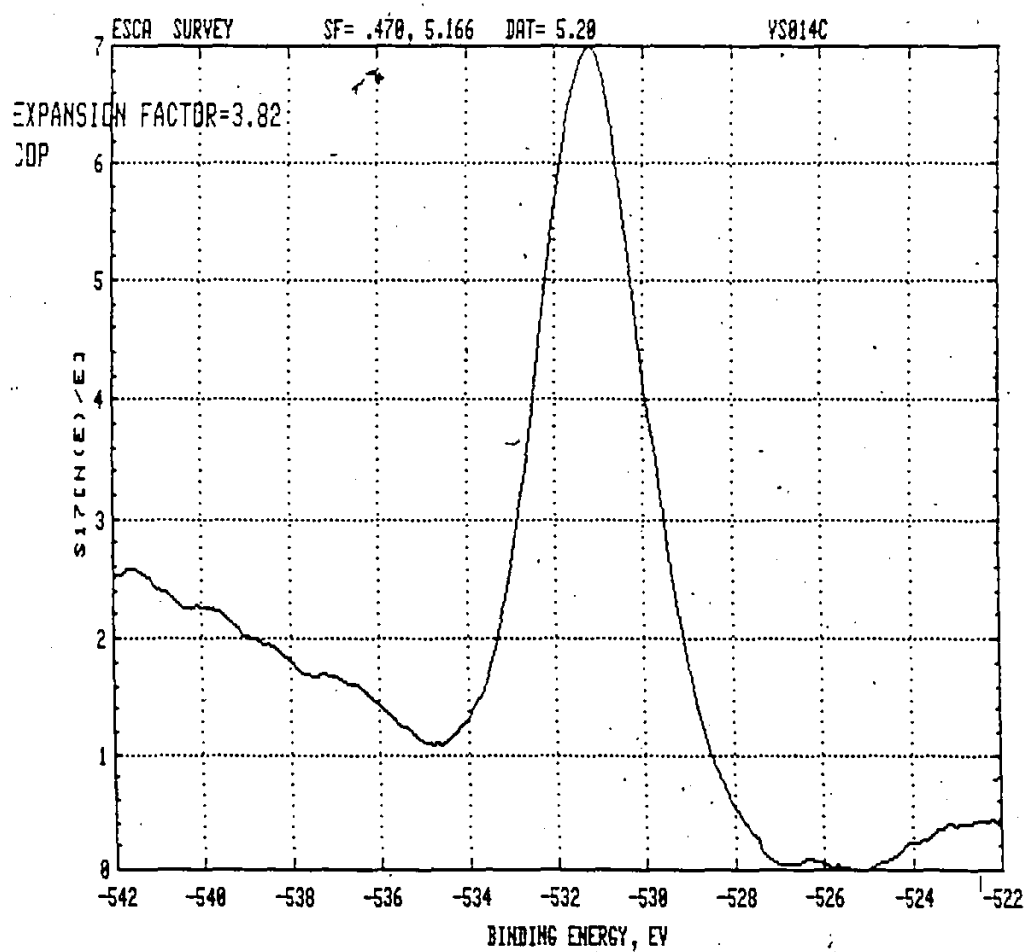


Fig. 3-64

O(1s) electron spectrum of Ni-13 Mo following  
electropolishing and cathodic reduction.

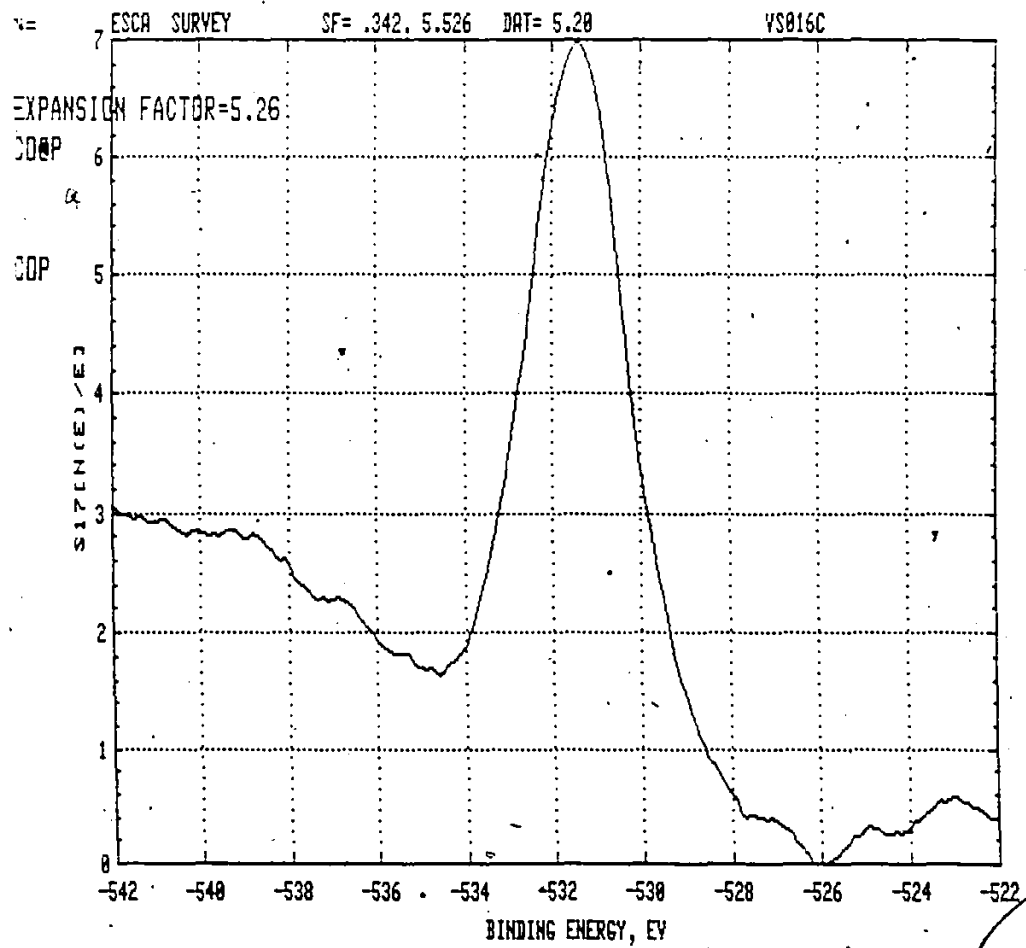


Fig. 3-65

O(1s) electron spectrum of Ni-13 Mo following  
mechanical polishing and cathodic reduction.

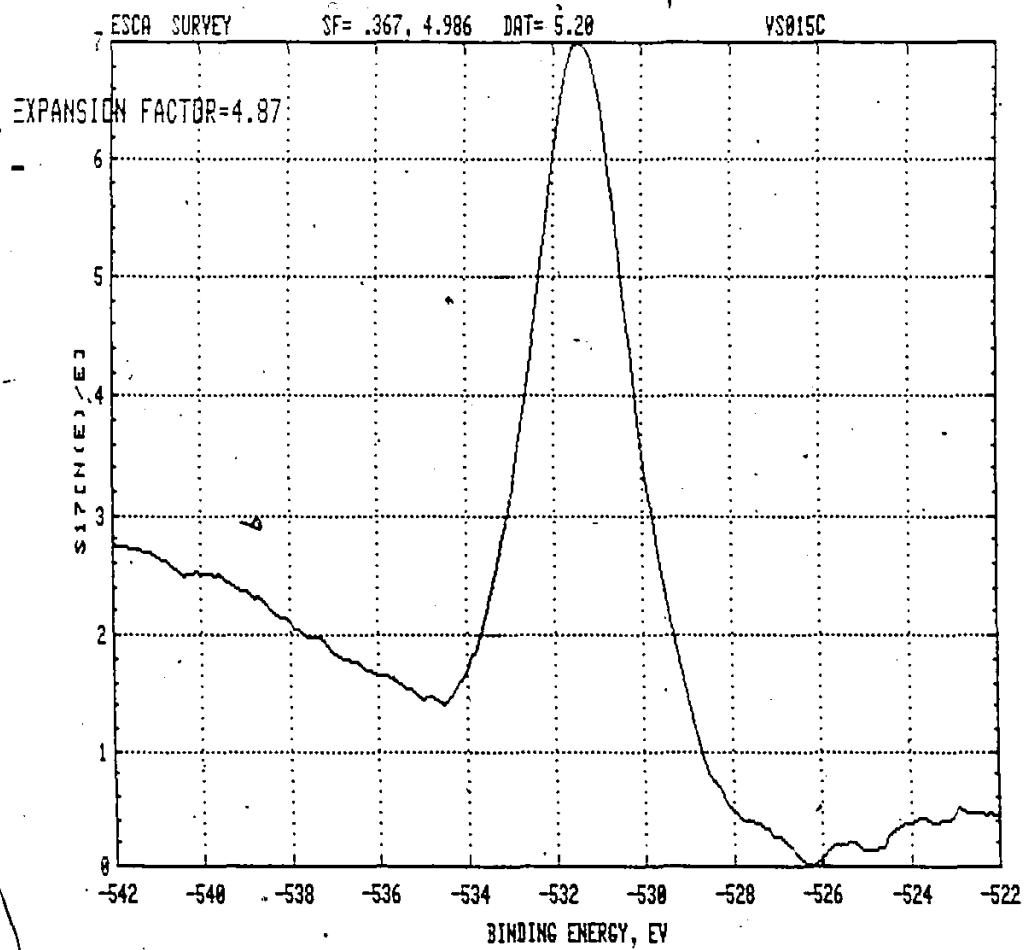


Fig. 3-66

O(1s) electron spectrum of Ni-13 Mo following polarization in the active potential range (30 min).

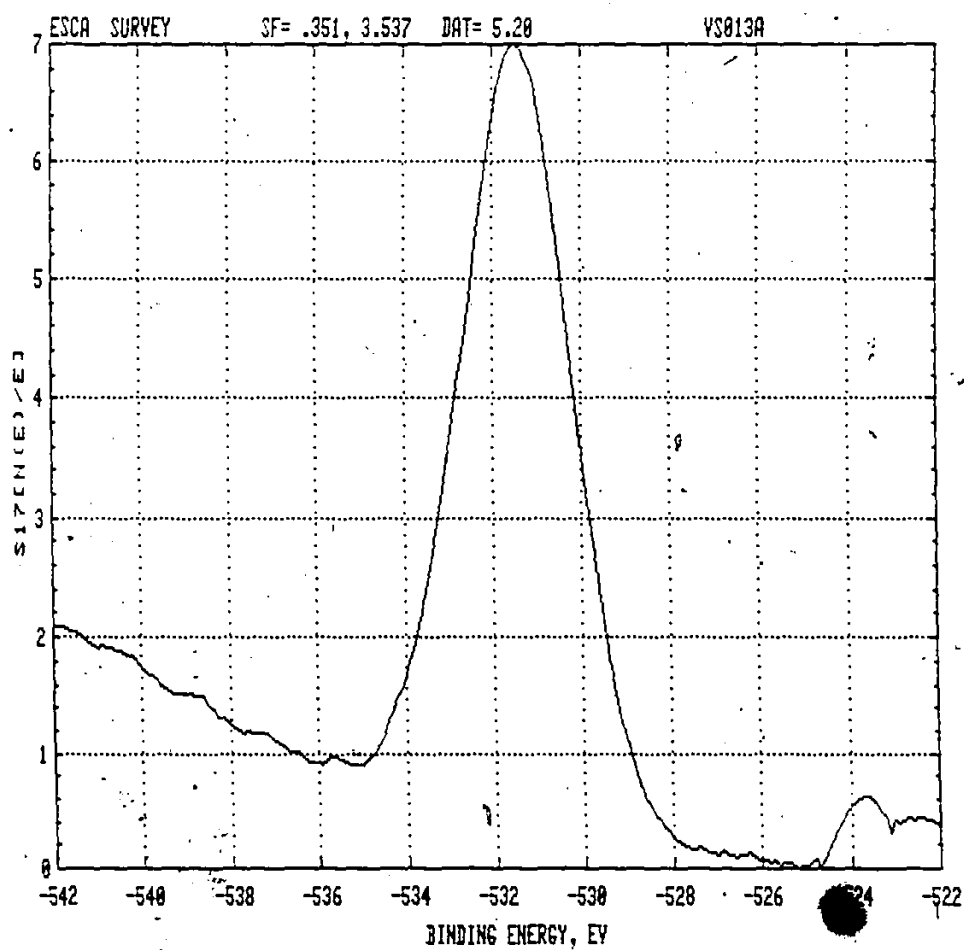


Fig. 3-67

O(1s) electron spectrum of Ni-13 Mo following anodization (+500 mV, 2 hr. pH 2.8).

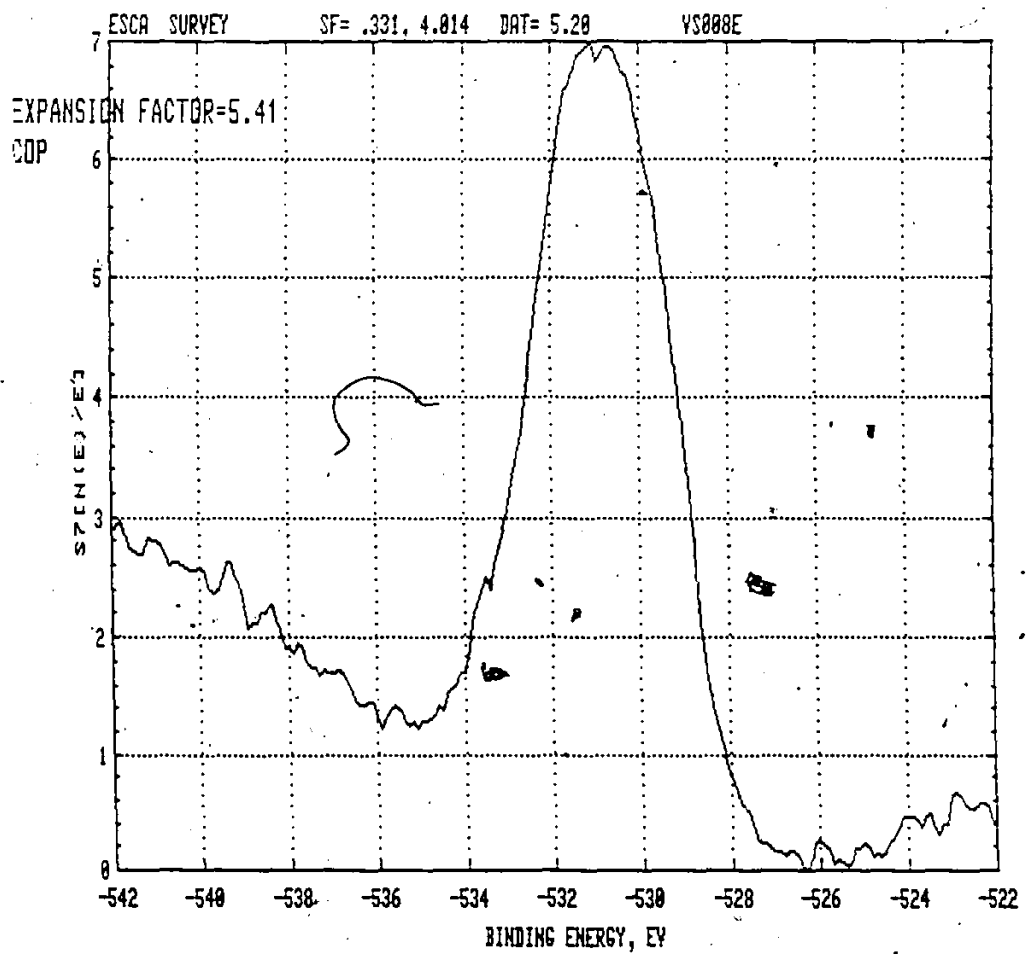


Fig. 3-68

O(1s) electron spectrum of Ni-13 Mo following anodization (+500 mV, 2 hr., pH 2.8) and OCPD (3 min).

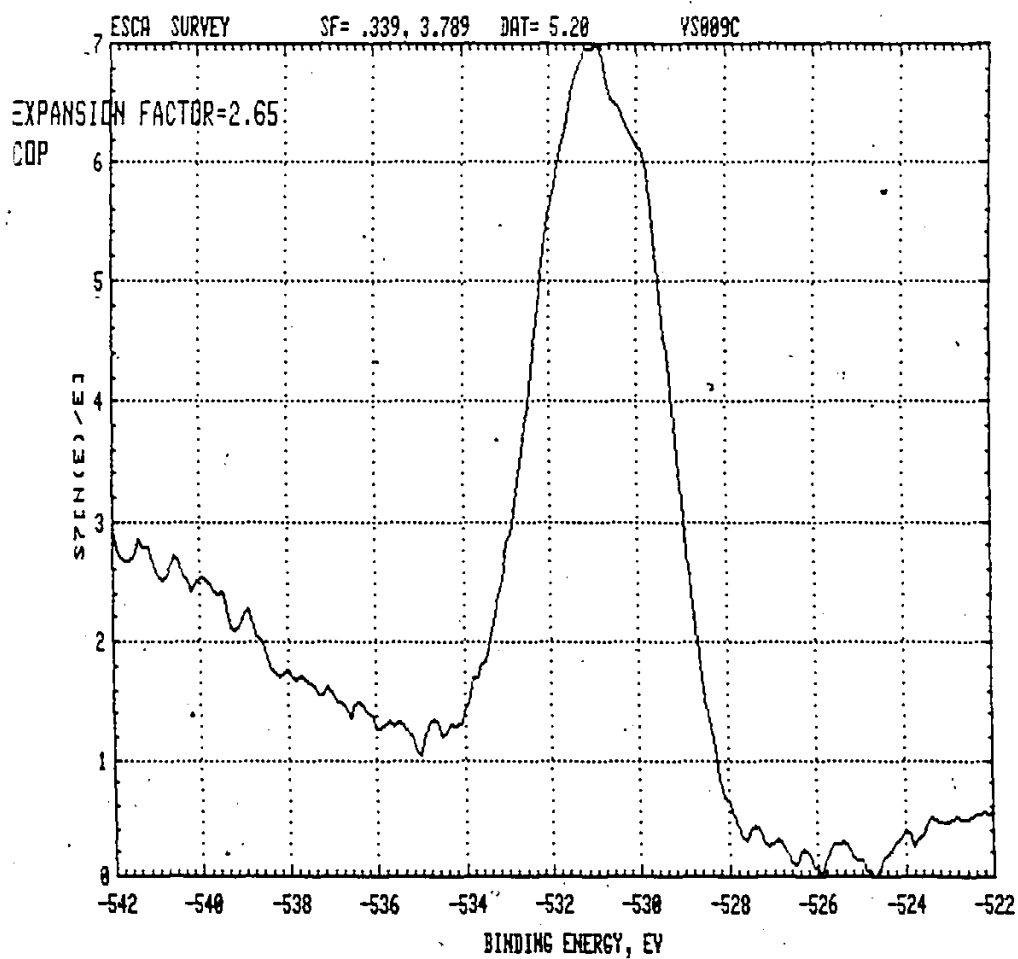




Fig. 3-69

O(1s) electron spectrum of Ni-13 Mo following anodization (+500 mV, 2h., pH 2.8) and OCPD (30 min).

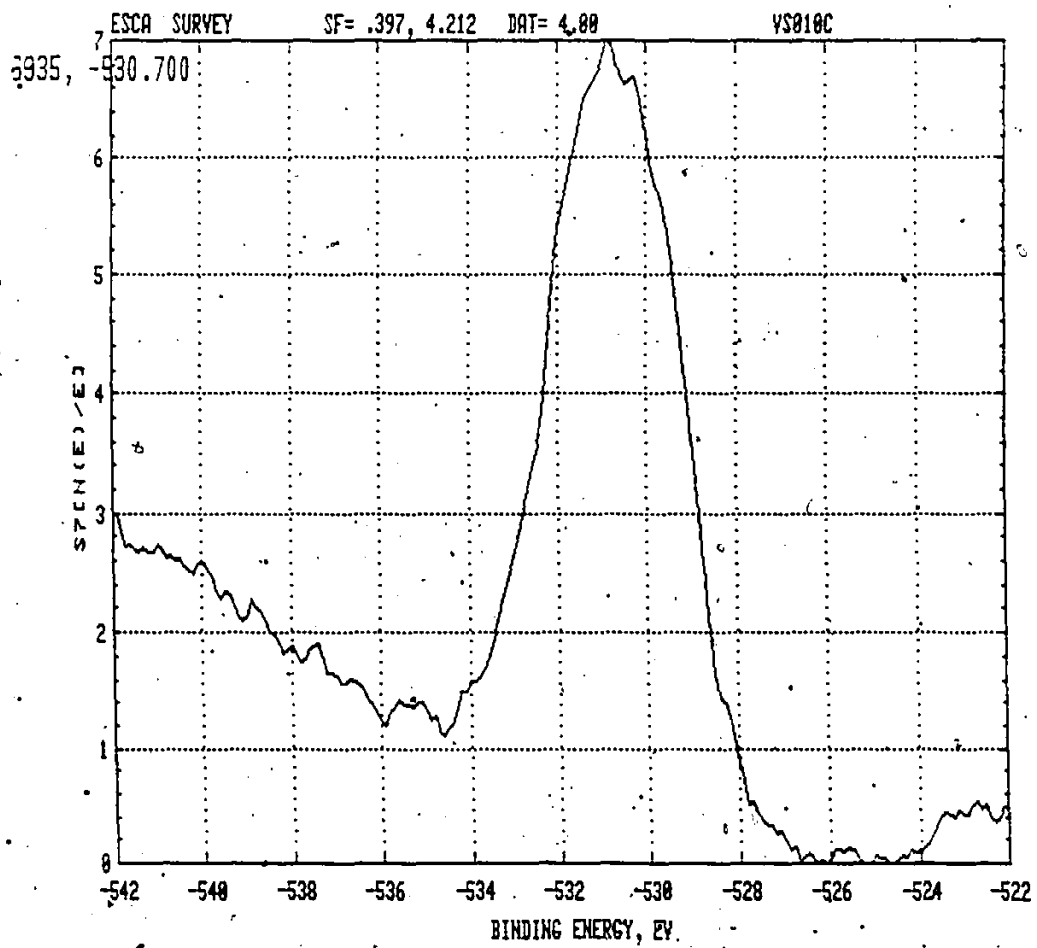


Fig. 3-70

O(1s) electron spectrum of Ni-13 Mo following  
anodization (+500 mV, 2h., pH 10.2).

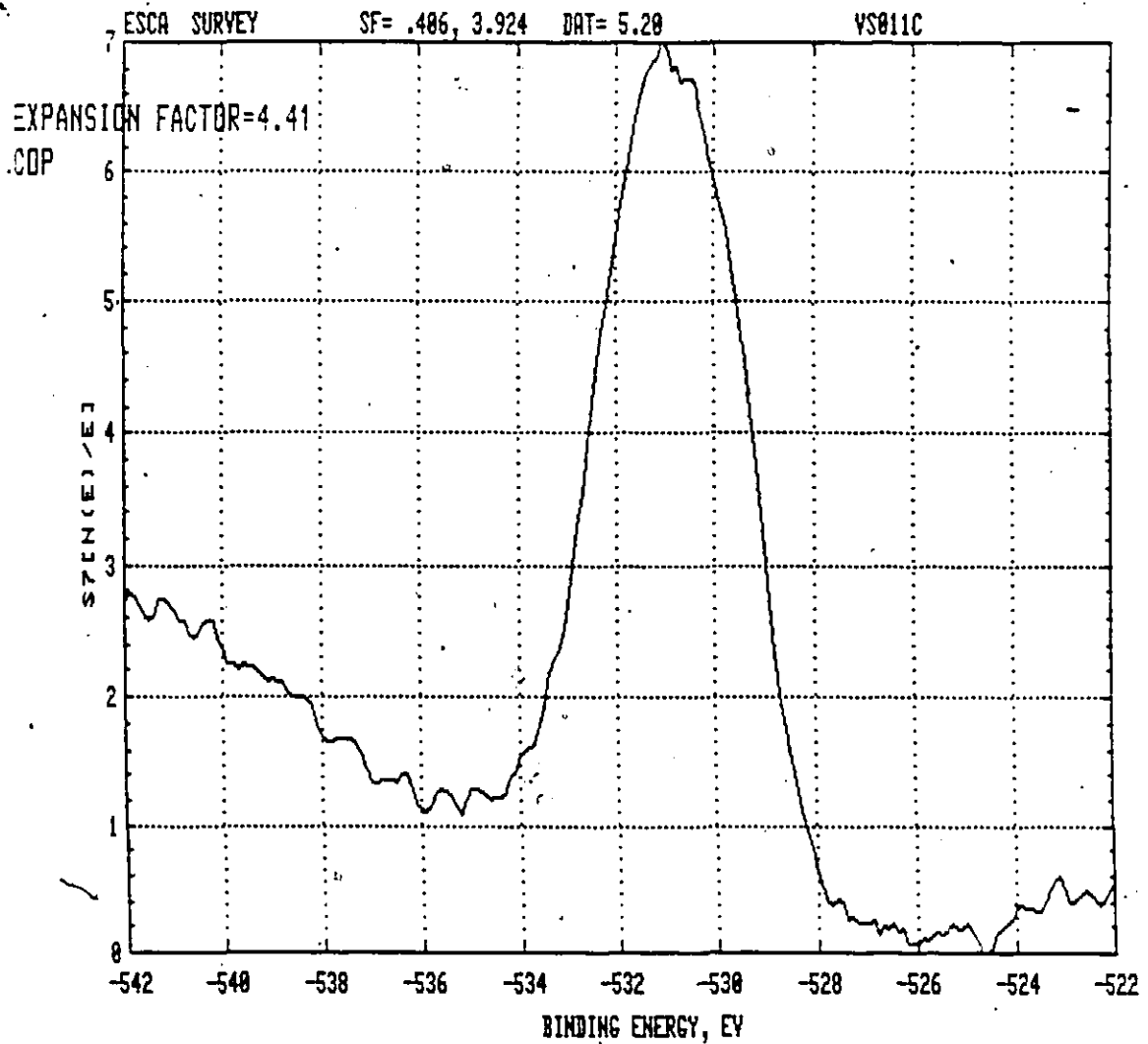


Fig. 3-71

O(1s) electron spectrum of Ni-13 Mo following  
anodization (+500 mV, 2h., pH 1.5).

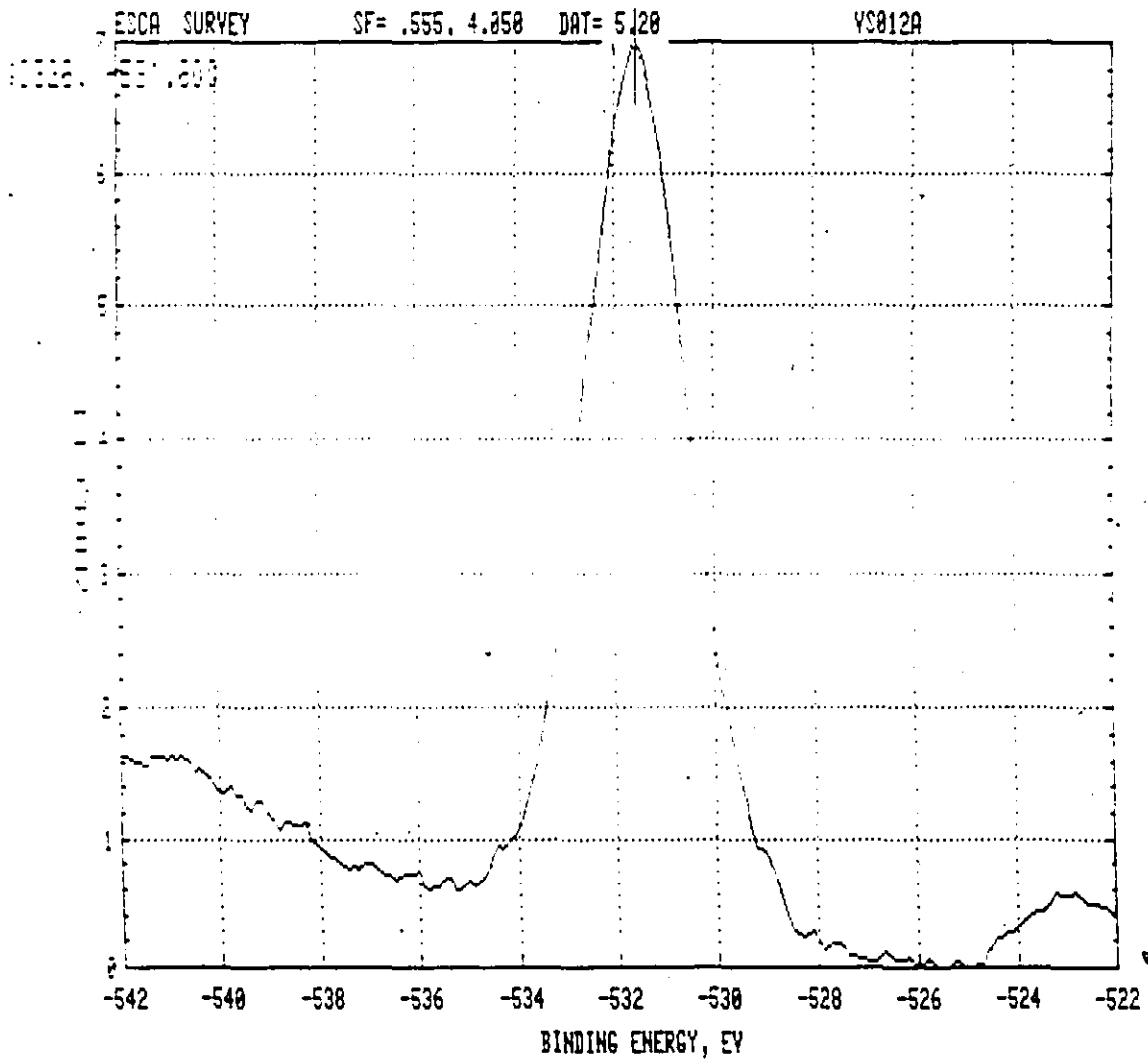
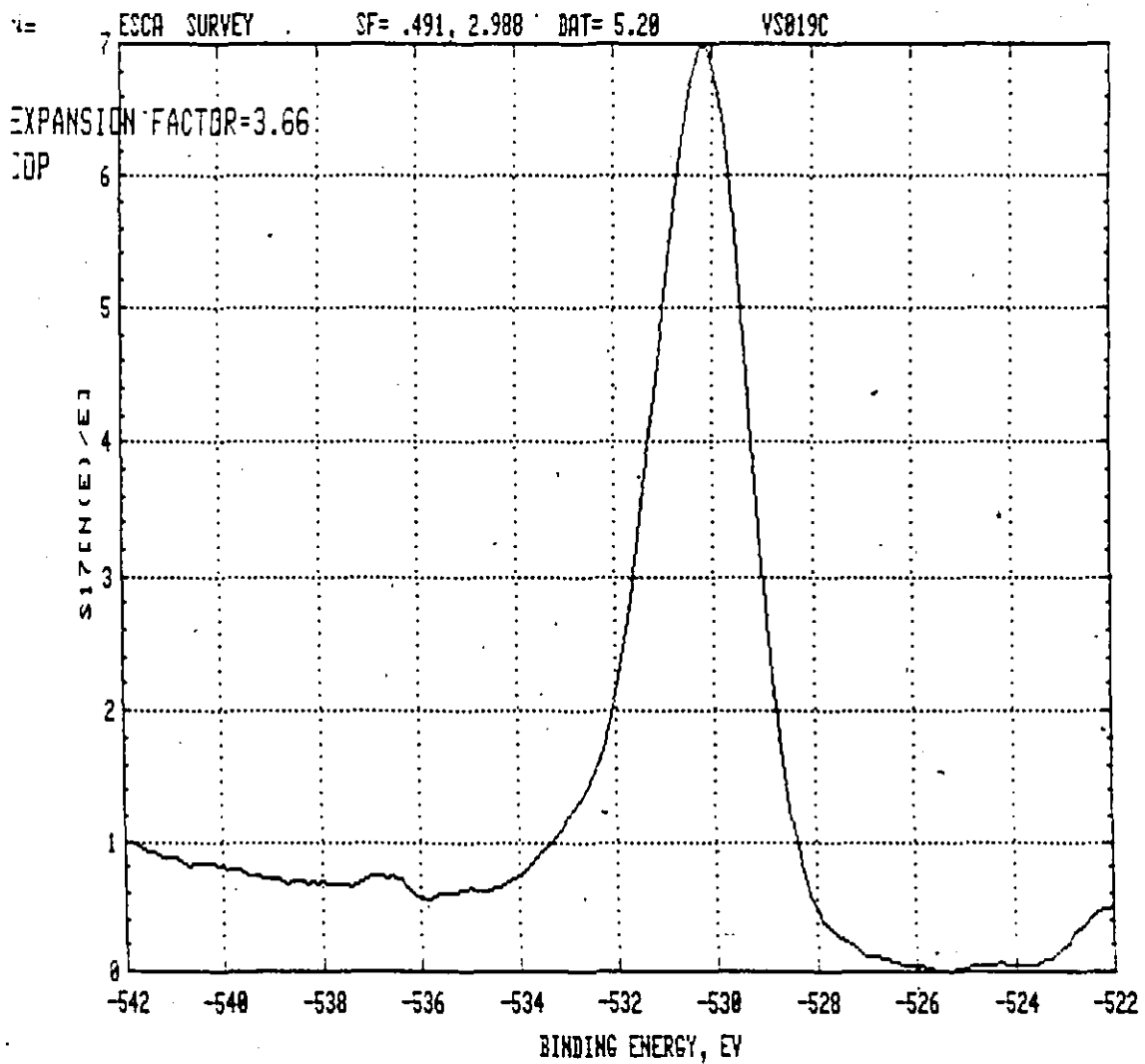


Fig. 3-72

O(1s) electron spectrum of air formed film  
on Mo.



The values for binding energy of O(1s) line given in the literature for Ni-oxygen and Mo-oxygen compounds are compiled in Table 3-14. It is clear that the air formed film on Mo is  $\text{MoO}_3$ . From the data on polarized samples it could be concluded that the

TABLE 3-14

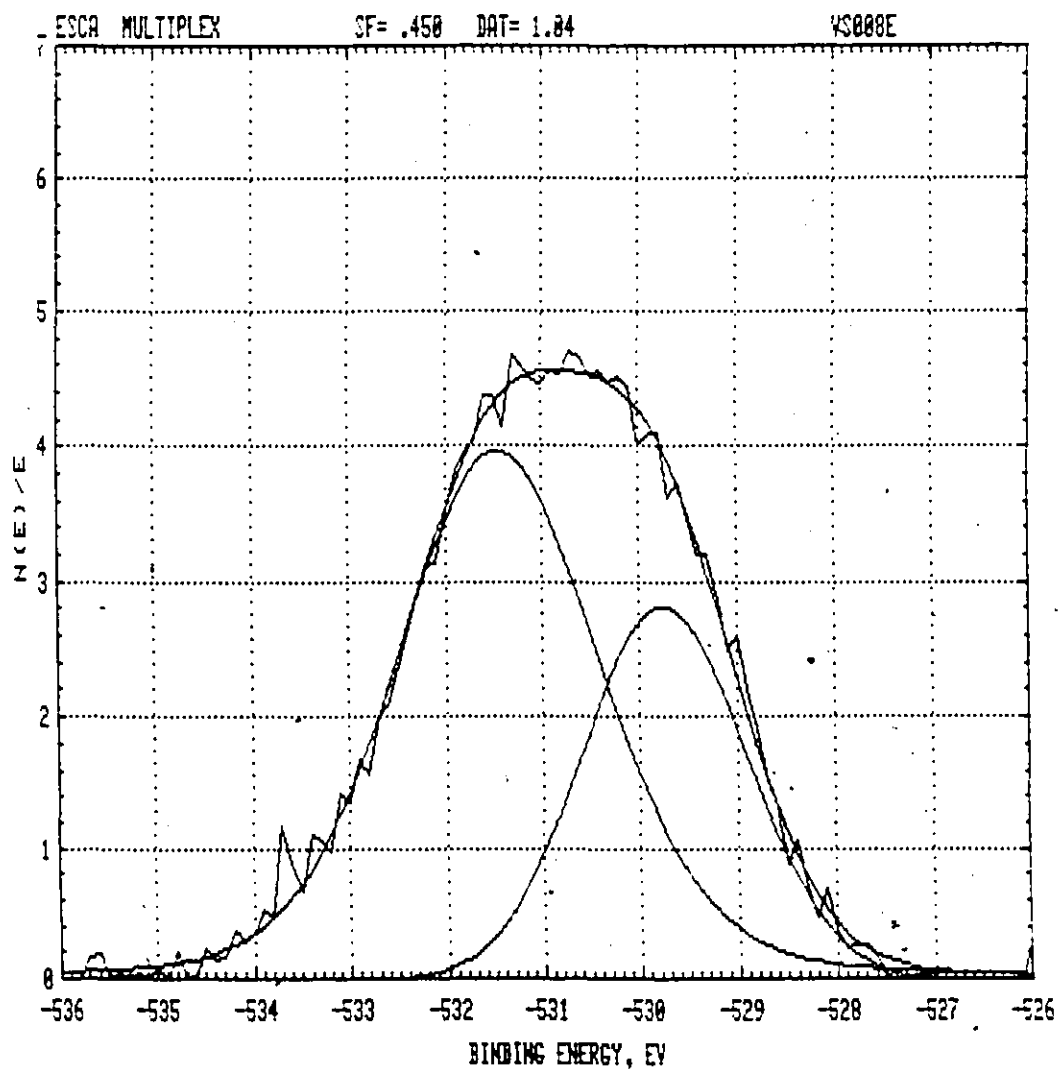
Some values of O(1s) XPS binding energies reported elsewhere [179-186]

Compound	O(1s)
NiO	529.9
	529.6 ± 0.15
	529.7
$\text{Ni}_2\text{O}_3$	531.7
	530.9
$\text{Ni(OH)}_2$	530.8 ± 0.1
	531.2 ± 0.3
$\text{MoO}_3$	530.3
$\text{MoO}_2$	530.8
	530.7

samples polarized in the active potential range and at low pH (1.5) as well as those subjected to the sample pretreatment procedures have the same type of oxygen bonding. On the other hand, anodization at pH 2.8, and 10.2 appear to have the same type of oxygen bonding, which remains unchanged for the samples left on the open circuit after anodization at pH 2.8.

Fig. 3-73

Deconvolution of O(1s) peak for anodized  
Ni-13 Mo (+500 mV, 2h., pH 2.8).



Band No.	Area	Peak (eV) Position	Intensity [counts/sec]	FWHM	Percent Gaussian
1	2709	529.76	12.73	2	100
2	5280	531.46	17.93	2.5	77.6

Deconvolution of O(1s) peak for Ni-13Mo anodized at pH 2.8 (Fig. 3-73) reveals that at least two peaks (529.76 eV and 531.46 eV) could be fitted to the broad 530.9 O(1s) peak. Therefore at least two different oxygens seem to be present in the anodic film of Ni-13Mo.

( If one of the two oxygens comes from  $\text{MoO}_3$ , and since the deconvolution of Mo(3d) suggested the presence of  $\text{MoO}_3$  or  $\text{MoO}_4^{2-}$  then it is most likely to be the 529.76 eV one. The other oxygen peak (531.46 eV) could be assigned to either  $\text{Ni}_2\text{O}_3$  (531.7 eV) or  $\text{Ni}(\text{OH})_2$  ( $531.2 \pm 0.2$  eV) (Table 3-14).

This observation can be considered to be a strong evidence for the presence of two different oxide phases in the film.

#### 3.5.4.4 REFLECTION HIGH ENERGY ELECTRON DIFFRACTION (RHEED) OF ANODIZED Ni-13Mo

Although the XPS data provided an indication that the anodic film on Ni-13Mo could be a two phase oxide coverage, it is necessary to have some structural information in order to confirm it.

A reflection high energy electron diffraction (100 keV) pattern of an anodized Ni-13Mo sample is shown on Fig. 3-74. A semicircular ring pattern, typical of a polycrystalline surface is observed. It corresponds to polycrystalline NiO [187,188]

with the mean particle size of  $\sim 20 \text{ \AA}$ <sup>\*</sup>. No Mo-containing phase could be related to the diffraction pattern observed. The absence of the reflections from the metal and the mean particle size of NiO of  $\sim 20 \text{ \AA}$  on one hand and the findings of AES analysis, i.e., Mo-enriched, 30 - 150  $\text{ \AA}$  thick film on the other, suggest either an amorphous Mo-containing phase or in the form of small crystallites ( $< 20 \text{ \AA}$ ), located in between the NiO particles.<sup>\*</sup>

---

\* RHEED gives well defined ring structure for the mean particle size, MPS, of 10 - 50  $\text{ \AA}$ . The particle size  $< 10 \text{ \AA}$  gives a diffuse reflection. The line half width is inversely proportional to MPS. As the MPS increases, the line width decreases up to  $\sim 50 \text{ \AA}$ , i.e., the lines do not become sharper for the particle size greater than 50  $\text{ \AA}$ .

\* Similar observations were obtained using dedicated STEM (scanning transmission electron microscope): both the selected area electron diffraction (beam size  $\sim 200 \text{ \AA}$ ) and micro-diffraction (beam size  $\sim 30 \text{ \AA}$ ) analysis of anodic films formed on specially thinned metal foils of Ni-13Mo have shown the presence of NiO only. However, the micro-X-ray analysis (beam size  $\sim 50 \text{ \AA}$ ) revealed not only the presence of Mo in these films but also an enrichment of the films in Mo [189].



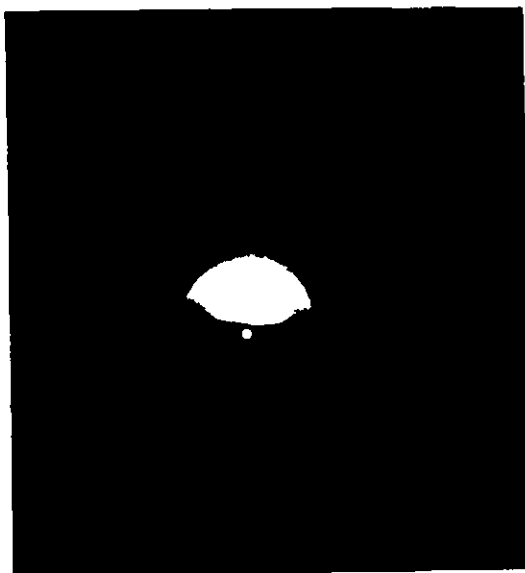
A disagreement appears in comparing the findings of RHEED analysis that reveals only NiO, and XPS analysis which indicates either  $\text{Ni}_2\text{O}_3$  or  $\text{Ni}(\text{OH})_2$  (Table 3-10) on the surface of anodized Ni-13Mo alloy. A possible explanation might be that the surface film changes under the influence of electron beam during the analysis (100 keV beam was used for the diffraction analysis). Alternatively, a defective NiO with the composition that corresponds to  $\text{Ni}_2\text{O}_3$  ( $\text{Ni}_{1-\delta}\text{O}$ ) with high enough concentration of Ni-vacancies and positive holes, i.e.,  $\text{Ni}^{3+}$  ions) would probably give a diffraction pattern not very different from that obtained for NiO, especially in the case of polycrystalline oxide films [187]. There have been no experimental evidence reported in the literature on prepared  $\text{Ni}_2\text{O}_3$  and its diffraction pattern.

The growth of thicker films on Ni can be obtained by disturbing NiO lattice [190] by incorporation of foreign elements, coming either from the solution or from the metal. Blondeau et al. [190] have shown that in spite of large chemical differences introduced by incorporation of foreign elements into NiO lattice, the crystallographic parameters of NiO remain the same as for the "real", thin compact and protective film on pure Ni, in the sense that the crystal lattice of NiO is essentially preserved but distorted. Therefore, in the present case of an anodic film on single phase Ni-Mo alloys a small amount of  $\text{Mo}^{+6}$  could be incorporated into NiO lattice, causing its reorgani-

zation and allowing the growth of a much thicker film with a crystal lattice modeled after NiO but with cation-2-anion-3 structure ( $\text{Ni}_2\text{O}_3$ ).

Fig. 3-74

Reflection high energy electron diffraction  
pattern of anodized Ni-13Mo



## CHAPTER IV

### 4.1 SUMMARY AND CONCLUSIONS

The results of this investigation can be summarized as follows:

- (a) Anodic oxide films on Ni in  $\text{Na}_2\text{SO}_4$  solution (pH 2.8) are composed of NiO. The overall film thickness is not influenced by the formation time at +500 mV (SCE) being 12 - 16 Å after 48 h of anodization. The character of the film changes with varying time and potential of anodization, as observed from the open circuit film breakdown. The film formed at the end of the passive region, e.g., +800 mV could be highly defective NiO with a composition closely corresponding to  $\text{Ni}_2\text{O}_3$ .
- (b) Mo undergoes transpassive dissolution in the range of potential where Ni is passive.
- (c) The single phase Ni-Mo alloys ( 5 - 15 wt % Mo) retain in general the polarization behaviour of Ni with a shift of the corrosion and the passivation potential in the noble direction and a monotonic increase of the passive current density with Mo content, suggesting a negative effect of Mo on the corrosion resistance of Ni.
- (d) The anodic current transients for the potentiostatic film formation indicate two different types of anodic oxide

coverage on Ni and Ni-Mo alloys, the latter being thicker but with poor protective properties.

- (e) Open circuit potential decay and surface reactivity measurements have shown that films on the alloys break down faster than those on Ni with a rate which increases with Mo content. Removal of the film proceeds gradually on open circuit with the rate inversely proportional to Mo content at  $t > t_{ind(Ni)}$ . The effect of Mo was concluded to be associated with polarization of either anodic or cathodic reaction.
- (f) Cathodic galvanostatic charging of anodized Ni-Mo alloys have shown that the cathodic current efficiency for the film removal is very low indicating that the film on the alloys is difficult to remove at pH 2.8, even with the passage of considerable cathodic charge (e.g., 86 mC/cm<sup>2</sup> led to an increase of surface reactivity of less than 30% with respect to the open circuit conditions).
- (g) A selective dissolution of Mo during the initial stages of anodization and an enrichment of the substrate in Mo at longer times indicate a time dependent nature of the film. Conversion of anodic charge into accumulation of species on the surface suggests a much thicker anodic film on the alloys than that on pure Ni.
- (h) The AES analyses of the anodic film of Ni have shown a 12 - 16 Å film, independent of the time of anodization. The

film on Ni-Mo alloys was found to be slightly enriched in Mo. The film thickness was a function of anodization time, i.e., it increased from ~ 30 Å for 1 h of anodization to ~ 150 Å for 48 h of anodization at +500 mV (SCE).

The AES analysis of the film on alloys that had been exposed to the open circuit indicated practically no change in the overall film thickness for the times examined, i.e., 5 min and 30 min. A small preferential dissolution of Mo, probably localized, confirmed a local breakdown of the film on alloys, but also very sluggish film removal.

The thickness of the film on alloys was found to be pH-dependent. An order of magnitude higher current density associated with a three times thicker film formed at pH ~ 10 than that formed at pH ~ 1.5 confirms that the thicker anodic films are less perfect and less protective.

(i) The XPS analysis of the films formed on single phase Ni-Mo alloys suggested the following:

- The anodic oxide film does not contain Ni in the form of NiO; it could be either Ni(OH)<sub>2</sub> or Ni<sub>2</sub>O<sub>3</sub>
- Mo is present in the film as Mo<sup>6+</sup>, i.e., either as MoO<sub>3</sub> or MoO<sub>4</sub><sup>2-</sup>.
- A broad O(1s) peak containing at least two different binding states of oxygen is a strong evidence of the presence of more than one oxide phase in the surface film.

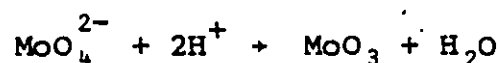
(j) Reflection high energy electron diffraction pattern of the anodic film on Ni-13Mo alloy corresponds to that of polycrystalline NiO with the average particle size of  $\sim 20$  Å. No Mo-containing phase could be related to the diffraction pattern observed. It, however, does not exclude the possibility of either the conversion of  $\text{Ni(OH)}_2$  to NiO under the influence of high energy electron beam or the presence of somewhat distorted lattice of NiO ( $\text{Ni}_{1-\delta}\text{O}$  or  $\text{Ni}_2\text{O}_3$ ) due to incorporation of a small amount of  $\text{Mo}^{+6}$  into the NiO lattice.

In view of these findings it may be concluded that the film on single-phase Ni-Mo alloys (5-15 wt % Mo) formed in 0.15 N  $\text{Na}_2\text{SO}_4$  (pH 2.8) is a two phase oxide film, possibly with a structure similar to that given on Fig. 4-1.

The nature of that film is different from the NiO film on pure Ni under the same experimental conditions, i.e., the solution pH, time and anodization potential. The oxide film formed on pure Ni does not change its thickness appreciably with prolonged anodization.

Since a thick, porous Ni-oxide ( $\text{Ni(OH)}_2$  or oxide hydroxide) can be formed on Ni in neutral and alkaline solutions [80-82] it is possible that a local pH change in the vicinity of electrode is responsible for the growth of relatively thick films on Ni-Mo alloys. A local pH increase

might be a result of Mo dissolution as  $\text{MoO}_4^{2-}$  and subsequent precipitation of Mo-oxide, since molybdate ions are not stable at pH 2.8. If molybdenum is present in the film as  $\text{MoO}_3$ , the reaction leading to a local increase in pH and precipitation of  $\text{MoO}_3$  could be:



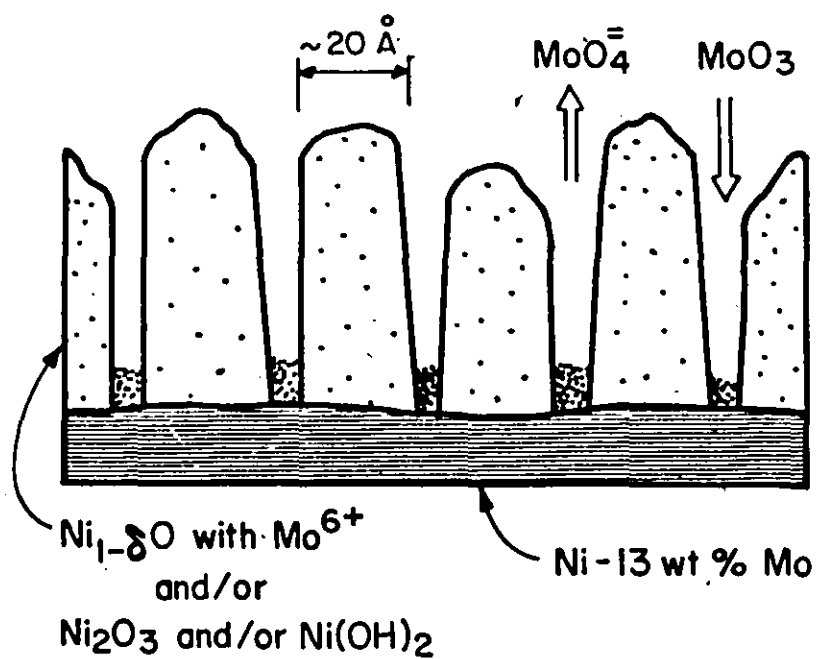
Poor protective properties of  $\text{MoO}_3$  could cause continuous dissolution and precipitation and maintenance of a higher pH which promotes the outward growth of Ni-oxide phase, probably as  $\text{Ni}(\text{OH})_2$ .

The growth of thicker films can also be obtained by disturbing the NiO lattice by incorporation of small amounts of  $\text{Mo}^{6+}$  ions. In a crystallographically perfect NiO film (which has an insulating character) ionic transport is very slow. Indeed it was shown (Fig. 3-26) that the oxide film thickness on pure Ni increases very little with anodization time. In the case of an anodic film on single phase Ni-Mo alloys small amounts of  $\text{Mo}^{6+}$  could be incorporated into the NiO lattice, causing its reorganization and allowing the growth of a much thicker film with a crystal lattice modeled after NiO but with  $\text{Ni}_2\text{O}_3$  structure.

Both mechanisms of thickening of the film on Ni-Mo

Fig. 4-1

Schematic illustration of a two phase anodic oxide film on single phase Ni-Mo alloys in acid solutions





alloys are equally well supported by the results of XPS analysis and the diffraction analysis, since  $\text{Ni}(\text{OH})_2$ , the most probable phase according to the former mechanism of film growth, could be converted to NiO during the electron diffraction analysis.

A model involving Ni-oxide with  $\text{Mo}^{6+}$  filling the cationic sites would have difficulties accounting for Mo-enrichment of the film, found by the AES analysis. It is difficult to estimate how much molybdenum can be incorporated into the NiO lattice without changing its crystallographic parameters significantly. Therefore it is most likely that the anodic film on single phase Ni-Mo alloys is a two phase oxide film with the structure given on Fig. 4-1. The Mo-containing phase is either in an amorphous state or in the form of very small particles ( $< 20 \text{ \AA}$ ) located in between the particles of Ni-oxide phase.

The fact that the anodic film on Ni-Mo alloys is much thicker than the passive film on Ni and that it breaks down faster than that on Ni indicate that the protective ability of this film is lower in spite of its relatively sluggish removal from the surface.


These results illustrate the complexity of the structure of films formed on single phase Ni-Mo alloys by an electrochemical mode of growth. The study of these films, thicker than "real" (thin, compact, protective) passive

films on Ni have shown that only an examination using several different techniques allows one to point out the structural and chemical differences between these films and NiO passive film.

## REFERENCES

- [1] N.D. Tomashov "Theory of Corrosion and Protection of Metals", The MacMillan Company, New York (1966).
- [2] H.J. Engel, *Electrochim. Acta* 22, 987 (1977).
- [3] M. Pourbaix, "Atlas of Electrochemical Equilibria in Aqueous Solutions", Pergamon Press (1966).
- [4] H.J. Engel, *Z. Phys. Chem. N.F.*7, 158 (1956).
- [5] T.P. Hoar, The Behaviour of Metals in "Modern Aspects of Electrochemistry", No. 2 pp 262-334, Ed. J. O'M Bockris, Butterworths, London (1959).
- [6] U.R. Evans, "The Corrosion and Oxidation of Metals", Arnold, London, Ch. 7, (1960).
- [7] H.H. Uhlig, *Chem. Eng. News* 24, 3154 (1946).
- [8] H.H. Uhlig, "Corrosion Handbook", H.H. Uhlig Ed., p 20, Wiley, New York (1948).
- [9] H.H. Uhlig, *Trans. Am. Inst. Min. and Met. Engrs.* 175, 710 (1948).
- [10] H.H. Uhlig, *J. Electrochem. Soc.* 97, 215c (1950).
- [11] H.H. Uhlig, *Annals N.Y. Academy of Sciences* 58, 843 (1954).
- [12] H.H. Uhlig and P. King, *J. Phys. Chem.* 63, 2026 (1959).
- [13] H.H. Uhlig, "Corrosion and Corrosion Control", 1st. Ed., p 67, Wiley, New York (1963).
- [14] H.H. Uhlig, *Corrosion Sci.*, 7, 325 (1967).
- [15] A. MacRae, *Science* 139, 379 (1963).

- [16] A. MacRae, *Surface Science* 1, 319 (1964).
- [17] A. Pignocco and G. Pellisier, *J. Electrochem. Soc.* 112, 1188 (1965).
- [18] M. Fleishman and H.R. Thirks, *J. Electrochem. Soc.* 110, 688 (1963).
- [19] N. Sato, "Passivity and Its Breakdown on Iron and Iron Base Alloys", USA-Japan Seminar, p. 1, NACE, Houston (1976).
- [20] H.H. Uhlig, *ibid.*, p. 21.
- [21] H.H. Uhlig, *Z. Elektrochem.* 62, 700 (1958).
- [22] A.T. Fromhold Jr., "Passivity and Its Breakdown on Iron and Iron Base Alloys", USA-Japan Seminar, p. 25, NACE, Houston (1976).
- [23] A.T. Fromhold Jr. and J. Kruger, *J. Electrochem. Soc.* 120, 722 (1973).
- [24] M. Sakashita and N. Sato, "Passivity of Metals", p. 479, R. P. Frankenthal and J. Kruger Ed., *The Electrochem. Soc. Inc.*, Princeton, New Jersey (1978).
- [25] M. Sakashita and N. Sato, *J. Electroanal. Chem. and Interfacial Electrochem.* 62, 127 (1975).
- [26] N. Sato, "Passivity of Metals", p. 29, R.P. Frankenthal and J. Kruger Ed., *The Electrochem. Soc. Inc.*, Princeton, New Jersey (1978).
- [27] R.P. Frankenthal, *J. Electrochem. Soc.* 116, 1646 (1969).
- [28] K.J. Vetter and F. Gorn, *Z. Phys. Chem.*, NF 86, 113 (1973).
- [29] N. Sato and K. Kudo, *Electrochim. Acta* 19, 461 (1974).

- [30] T. Ohtsuka et al., J. Jpn. Inst. Met. 40, 124 (1976).
- [31] N. Sato et al., J. Electrochem. Soc. 123, 1419 (1976).
- [32] T. Noda et al., J. Jpn. Inst. Met. 37, 951 (1973).
- [33] N.D. Tomashov et al., Proc. 5th ICMC-Tokyo, p. 245, NACE, Houston (1975).
- [34] E.K. Oshe and I.L. Rosenfeld, Proceedings of the 6th Int. Cong. on Metallic Corrosion, Vol. 2, p. 249, Sydney, Australia (1975).
- [35] K. Asami et al., Corrosion Sci. 16, 387 (1976).
- [36] M. Seo and N. Sato, Corrosion Sci. 17, 209 (1977).
- [37] H. Leckie and H.H. Uhlig, J. Electrochem. Soc. 113, 1262 (1966).
- [38] J. O'M Bockris et al., Electrochim. Acta 16, 1859 (1971).
- [39] N. Sato et al., Electrochim. Acta 16, 1909 (1971).
- [40] G. Okamoto, Proc. 5th ICMC 1972 p. 8. NACE, Houston (1974).
- [41] H. Kono and M. Nagayama, "Passivity of Metals", Ed. R. P. Frankenthal and J. Kruger, p. 585, The Electrochem. Soc., Inc., Princeton, New Jersey (1978).
- [42] G. Okamoto, Corros. Sci. 13, 471 (1973).
- [43] K.E. Heusler and M. Schultze, Electrochim. Acta 20, 237 (1975).
- [44] N. Cabrera and N. Mott, Rep. Progr. Phys. 12, 163 (1949).
- [45] N. Sato and M. Cohen, J. Electrochem. Soc. 111, 52 (1963).
- [46] C.Y. Chao, L.F. Lin, D.D. MacDonald, J. Electrochem. Soc. 128, 1187 (1981).
- 

- [47] K.J. Vetter, Z. Electrochem. 59, 67 (1955).
- [48] K.J. Vetter, J. Electrochem. Soc. 110, 597 (1963).
- [49] V.M. Novakovski and Y.A. Likhachev, Electrochim. Acta 12, 267 (1967).
- [50] G. Okamoto et al., Z. Elektrochem. 62, 775 (1958).
- [51] K. Schwabe and V. Ebersbach, Proc. 4th Int. Conf. on Met. Corros.", p. 709, Amsterdam (1969).
- [52] T.S. De Gromoboy and L.L. Shreir, Electrochim. Acta 11, 895 (1966).
- [53] R.L. Cowan and R.W. Staehle, J. Electrochem. Soc. 118, 557 (1971).
- [54] K.J. Vetter and K. Arnold, Z. Elektrochim. 64, 244 (1960).
- [55] K.J. Vetter and K. Arnold, *ibid.* 62, 664 (1958).
- [56] C. Wagner, Ber. Bunsenges Phys. Chem. 77, 1090 (1975).
- [57] H.H. Uhlig, J. Electrochem. Soc. 108, 327 (1961).
- [58] G. Okamoto and N. Sato, Trans. Jpn. Inst. Met. 1, 16 (1960).
- [59] G. Okamoto and N. Sato, *ibid.* 2, 113 (1961).
- [60] N. Sato and G. Okamoto, J. Electrochem. Soc. 110, 604 (1963).
- [61] N. Sato and G. Okamoto, *ibid.* 111, 897 (1964).
- [62] N. Sato and G. Okamoto, J. Electrochem. Soc. Japan 27, 125 (1959).
- [63] N. Sato et al., J. Jpn. Inst. Met. 35, 1007 (1971).
- [64] A.K.N. Reddy et al., J. Chem. Phys. 42, 2246 (1965).
- [65] J. O'M. Bockris et al., J. Electrochem. Soc. 113, 1133 (1966).

- [66] A.K.N. Reddy et al., J. Chem. Phys. 42, 2246 (1965).
- [67] N. Sato and K. Kudo, Boshoku Gijutsu 21, 24 (1972).
- [68] N. Sato and K. Kudo, Electrochim. Acta 19, 461 (1974).
- [69] J. Siejka et al., Electrochim. Acta 17, 161, 2371 (1972).
- [70] J. Seijka et al., J. Electrochem. Soc. 119, 991 (1972).
- [71] B. MacDougall and M. Cohen, J. Electrochem. Soc. 121, 1152 (1974).
- [72] B. MacDougall and M. Cohen, *ibid.* 123, 1783 (1976).
- [73] B. MacDougall and M. Cohen, *ibid.* 123, 191 (1976).
- [74] B. MacDougall and M. Cohen, *ibid.* 124, 1185 (1977).
- [75] B. MacDougall and M. Cohen, Passivity, Ed. R.P. Frankenthal and J. Kruger, p. 827. The Electrochemical Soc. Inc. (1978).
- [76] B. MacDougall et al., Jsr. J. Chem. 18, 125 (1979).
- [77] J.L. Ord et al., J. Electrochem. Soc. 124, 1714 (1977).
- [78] J.L. Ord, "Passivity of Metals", Ed. R.P. Frankenthal and J. Kruger, p. 273. The Electrochem. Soc. Inc. (1978).
- [79] T. Dickinson et al., J. Chem. Soc. Faraday Trans. I 73, 327 (1977).
- [80] B. MacDougall et al., J. Electrochem. Soc. 127, 1248 (1980).
- [81] B. MacDougall, "Corrosion 81", Toronto, Canada, April 1981 published by NACE.
- [82] B. MacDougall, J. Electrochem. Soc. 128, 2321 (1981).
- [83] J. Mieluch, Roczniki Chemii Ann. Soc. Chim. Polon. 40, 365 (1975).

- [84] J. Mieluch, Polish Journal of Chemistry 52, 151 (1978).
- [85] K. Schwabe, J. Electrochem. Soc. 110, 663 (1963).
- [86] K. Schwabe, Electrochim. Acta 3, 186 (1960), also *ibid.* 12, 977 (1967).
- [87] D.E. Davies and W. Barker, Corrosion 20, 47t, (1964).
- [88] V.A. Lobachev et al., Elektrokimiya 6, 1416 (1970).
- [89] H.H. Uhlig and H.G. Feller, J. Electrochem. Soc. 107, 865 (1960).
- [90] Y. Osterwald and H.G. Feller, *ibid* 107, 473 (1960).
- [91] W.M. Latimer, "Oxidation Potentials", 2nd. Ed., Prentice Hall, New York (1952).
- [92] A.A. Pozdeeva et al., Zashch. Met. 1, 15 (1965),
- [93] A.A. Pozdeeva et al., Corrosion Sci. 6, 149 (1966).
- [94] T. Markovic et al., Werkst. Korros. 17, 696 (1966).
- [95] T. Heumann and G. Hauck, Zeitschem. F. Metallkunde 56, 75 (1965).
- [96] T. Heumann and G. Hauck, Ber. Bunsenges Phys. Chem. 71, 404 (1967).
- [97] L. Wikstrom and K. Nobe, J. Electrochem. Soc. 116, 525 (1969).
- [98] L. Kis and A. Körösi, Magyar. Kem. Foly. 73, 169 (1967).
- [99] J.W. Johnson et al., Corrosion, NACE 26, 238 (1970).
- [100] T. Heumann and M. Klimmeck, Werkst. Korros. 22, 115 (1971).
- [101] T. Heumann and M. Klimmeck, Proceedings of the 6th Int. Cong. on Metallic Corrosion, Vol. 2, p. 155, Sydney, Australia (1975).



- [102] V.V. Andreeva and T.P. Stepanova, *Korroz. Met. Splavov* 44 (1963).
- [103] S. Ikonopisov, *Electrodeposition and Surface Treatment* 1, 305 (1972/73).
- [104] C.M. Day and R.G. Keil, *J. Electrochem. Soc.* 122, 350 (1975).
- [105] J.W. Hicreman and E.A. Gulbransen, AIMME Tech. Pub. No. 2144 (1947).
- [106] H.M. Kennett and A.E. Lee, *Surf. Sci.* 48, 663 (1975).
- [107] D.K. Murti et al., unpublished work at McMaster University, Hamilton, Canada.
- [108] A.M. Arora and R. Kelly, *J. Materials Sci.* 12, 1673 (1977).
- [109] H.H. Uhlig, "Corrosion and Corrosion Control", p. 353, Wiley, New York (1963).
- [110] M. Moriya et al., *Bulletin of the Faculty of Engineering, Hokkaido University*, No. 86 (1978).
- [111] M. Moriya et al., *Jpn. Corrosion Engineering* 27, 653 (1978).
- [112] D. Stout et al., *Extended Abstracts, Fall Meeting of the Electrochem. Soc.* (1976) p. 243.
- [113] J.B. Lumsden, *Corrosion* 77, NACE, San Francisco 1977, paper no. 15.
- [114] K. Sugimoto and Y. Sawada, *Corros. Sci.* 17, 425 (1977).
- [115] M. Seo et al., *Trans. Jpn. Inst. Met.* 20, 501 (1979).
- [116] T. Kodama and J.R. Ambrose, *Corrosion* 33(5), 155 (1977).
- [117] J.R. Ambrose, *Corrosion* 34(1), 27 (1978).

- [118] N.D. Greene, Proc. 1st. Int. Conf. Met. Corros., p. 113, Butterworths, London (1962).
- [119] H.H. Uhlig et al., J. Electrochem. Soc. 110, 650 (1953).
- [120] M. Zamin, Ph.D. Thesis, McMaster University (1976).
- [121] K. Tachibana and M.B. Ives, Proc. 4th Int. Symp. Passivity, p. 878, Electrochem. Soc. Inc., (1978).
- [122] V. Scepanovic and M.B. Ives, J. Electrochem. Soc. 127, 1903 (1980).
- [123] M. Prazak and V. Cihal, Corrosion Sci. 2, 71 (1962).
- [124] M.B. Rockel, Corrosion 29, 393 (1973).
- [125] E.A. Lizlovs, Corrosion 22, 297 (1966).
- [126] E.A. Lizlovs and A.P. Bond, J. Electrochem. Soc. 118, 221 (1971).
- [127] N.D. Tomashov et al., Corrosion 20, 166t (1964).
- [128] E.A. Lizlovs and A.P. Bond, J. Electrochem. Soc. 116, 574 (1969).
- [129] J. Horvath and H.H. Uhlig, J. Electrochem. Soc. 115, 791 (1968).
- [130] J.B. Lumsden and R.W. Staehle, Sci. Met. 6, 1205 (1972).
- [131] K. Hashimoto et al., "Passivity and Its Breakdown on Iron and Iron Base Alloys", NACE (1976), p. 34.
- [132] J. Kruger and J.R. Ambrose, NBS Report No. NBS;R74-583. Technical Summary Report No. 5 (1974).
- [133] K. Sugimoto and Y. Sawada, Corrosion 32, 347 (1976).
- [134] M. Klimmeck, Electrochim. Acta 25, 1375 (1980).

- [135] M. Naka et al., *J. Non-Cryst. Solids* 29, 61 (1978).
- [136] K. Hashimoto, *Sci. Rep. RITU, A-Vol.* 27, No. 2 (1979).
- [137] H. Ogawa et al., *Corrosion* 37, 52 (1978).
- [138] M. Seo and N. Sato, *Transaction ISIJ*, Vol. 19 (1979).
- [139] E.A. Yaniv et al., *J. Electrochem. Soc.* 124, 490 (1977).
- [140] M. da Cunha Bello et al., *J. Electrochem. Soc.* 124, 1317.
- [141] G. Grube and O. Winkler, *Z. Elektrochem.* 44, 427 (1938).
- [142] V. Scepanovic, M.Eng. Thesis, McMaster University (1978).
- [143] P.W. Palmberg et al., *Appl. Phys. Lett.* 15, 254 (1969).
- [144] C.J. Powell, "Quantitative Surface Analysis of Materials", pp. 5-31, ASTM stp. 543 (1978).
- [145] L.E. Davis et al., "Handbook of Auger Electron Spectroscopy", 2nd. edition (Physical Electronics Industries, Inc., Eden Prairie, Minnesota), 1976.
- [146] H. Hach, "Topics in Current Physics" Series, Vol. 4, p. 7, Ed. H. Hach, Springer-Verlag (1977).
- [147] C.J. Powell, *Surf. Sci.* 44, 29 (1974).
- [148] D.R. Penn, *J. Electr. Spectr. Rel. Phen.* 9, 29 (1976).
- [149] J.S. Solomon and V. Meyers, *American Lab.* 8, 31 (1976).
- [150] J.S. Johannessen et al., *Appl. Phys. Lett.* 27, 452 (1975).
- [151] C.A. Fadley in "Progress in Solid State Chemistry", Vol. 11, p. 265. Eds. G. Somorjan and J. McCaldin, Pergamon Press, New York (1976).
- [152] R.J. Baird et al., *Analytical Chemistry* 48, 843 (1976).

- [153] M.L. Tang and G.K. Wehner, J. Appl. Phys. 42(6), 2449 (1971).
- [154] H.W. Pickering, J. Vac. Sci. Technol. 13(2), 618 (1976).
- [155] H. Oechsner, Appl. Phys. 8, 185 (1975).
- [156] K.S. Kim et al., Surf. Sci. 55, 285 (1976).
- [157] P.S. Ho and J.E. Lewis, Surf. Sci. 57, 393 (1976).
- [158] P.M. Hall and J.M. Morabito, Surf. Sci. 62, 1 (1977).
- [159] K. Seigbahn et al., "ESCA, Atomic, Molecular and Solid State Structure Studied by Means of Electron Spectroscopy", Almquist and Wiksells, Upsalla, (1967).
- [160] N.S. McIntyre and M.G. Cook in "Surface Analysis Techniques", p. 18, ASTM (1976).
- [161] N.S. McIntyre and D.G. Zetaruk, J. Vac. Sci. Techn. 14, 181 (1977).
- [162] K.J. Vetter and G. Klein, Z. Phys. Chem. N.F. 31, 405 (1962).
- [163] H. Gohr and E. Lange, Z. Phys. Chem. 17, 100 (1958).
- [164] B. Droste and H.G. Feller, Proc. 4th Int. Symp. Passivity, Ed. R.P. Frankenthal and J. Kruger, The Electrochemical Soc. Inc., Princeton, New Jersey (1978).
- [165] F. Flade, Z. Phys. Chem. 76, 513 (1911).
- [166] F. Pons et al., Surface Sci. 69, 565 (1977), also 69, 547 (1977).
- [167] D.F. Mitchell, Division of Chemistry, NRC Canada, private communication.

- [168] N. Sato and G. Okamoto, *Trans. Japan Inst. Metals* 2, 113 (1961).
- [169] J. Kruger and J.P. Calvert, *J. Electrochem. Soc.* 114, 43 (1967).
- [170] K. Hashimoto et al., *Corrosion Science* 19, 3 (1979).
- [171] K.J. Vetter, *Electrochim. Acta* 16, 1923 (1971).
- [172] A. Joshi et al., in "Methods of Surface Analysis", ed. A.W. Czanderna, p. 159.
- [173] P.W. Palmberg, *J. Vac. Sci. Technol.* 13, 214 (1976).
- [174] P.H. Holloway, *Surf. Sci.* 66, 479 (1977).
- [175] D.R. Penn, *Phys. Rev. Lett.* 38, 1429 (1977).
- [176] G.T. Burstein and T.P. Hoar, *Corros. Sci.* 17, 939 (1977).
- [177] G.T. Burstein, *Mat. Sci. Eng.* 42, 207 (1980).
- [178] T.T. Lin and D. Lichtman, *J. Vac. Sci. Technol.* 15, 1689 (1978).
- [179] N.S. McIntyre and M. Cook, *Anal. Chem.* 47, 2208 (1975).
- [180] K.S. Kim and R.E. Davis, *J. Electron Spectrosc.* 1, 251 (1972/73).
- [181] T. Dickinson et al, *J. Chem. Soc. (Faraday Trans 1)* 73(2), 327 (1977).
- [182] K.S. Kim et al., *J. Electron Spectrosc.* 5, 351 (1974).
- [183] W.E. Swartz and D.M. Hercules, *Analyt. Chem.* 43 (13), 1774 (1975).
- [184] S. Grim and L.J. Matienzo, *Inorg. Chem.* 14 (5), 1014 (1975).
- [185] T. Patterson et al., *J. Phys. Chem.* 80 (15), 1700 (1976).

- [186] Handbook of Photoelectron Spectroscopy, Physical Electronics Instruments Inc., (1976).
- [187] P.B. Sewell et al., Proceedings of the 5th Inter. Congr. on Met. Corr., Sydney, Australia, (1975).
- [188] P.B. Sewell et al., Canadian Journal of Chemistry 37, 1813 (1959).
- [189] M. Moriya and M.B. Ives, to be published.
- [190] G. Blondeau et al., Proc. 4th Intern. Symp. on Passivity, pp. 844-859, Ed. R.P. Frankenthal, The Electrochem. Soc. Inc., Princeton, New Jersey (1978).
- 